

California AHMCT Program
University of California at Davis
California Department of Transportation

**DEVELOPMENT OF THE OPERATOR
CONTROLLED CRACK SEALING MACHINE -
THE LONG REACH ARM AND CONTROL UNIT**

Todd L. Baker
Brian D. Hemmerlin
Xin Feng
Duane Bennett
Steven A. Velinsky, Principal Investigator

AHMCT Research Report
UCD-ARR-99-06-30-02

Final Report of Contract
IA 65X875 T.O. 95-12

June 30, 1999

*This report has been prepared in cooperation with the State of California, Business and Transportation Agency, Department of Transportation and is based on work supported by Contract Number IA 65X875 T.O. 95-12 through the Advanced Highway Maintenance and Construction Technology Research Center at the University of California at Davis.

ABSTRACT

Annually, governments spend millions of taxpayers' dollars maintaining a highway infrastructure that is continually growing as we near the 21st century. In order to maintain this vast infrastructure, highway workers put their lives on the line each day, subjecting themselves to the ever-present threat of inattentive drivers. The Advanced Highway Maintenance and Technology (AHMCT) Center, of the University of California, Davis, has developed numerous machines aimed at increasing the productivity, quality and safety of highway maintenance operations.

This report presents work leading towards the development of the first prototype Operator Controlled Crack Sealing Machine (OCCSM). This has included component subsystems as well as numerous critical machine components. The R- θ telescopic manipulator arm is discussed in detail from its concept phase through its detailed design, testing and test conclusions. Additionally, the camera boom system and the hose retraction systems' designs are presented in detail. The machine's controller is also presented in detail, and the R- θ telescopic manipulator arm is integrated with the controller to provide a complete system operational in the AHMCT Robotics Laboratory. This system will be moved to the OCCSM support vehicle for use on actual highways in the next phase of the project.

The most important aspects of this phase were the design and fabrication of the R- θ Telescopic Manipulator, the development of the controller, and the integration of the two systems. Through extensive research, conceptual design, detailed design, and testing, the first-generation full-scale R- θ telescopic manipulator arm has been successfully lab tested and proven to meet or exceed all critical project specifications, and the laboratory system has a dexterous workspace of 3.6 m by 3.6 m.

EXECUTIVE SUMMARY

Annually, governments spend millions of taxpayers' dollars maintaining a highway infrastructure that is continually growing as we near the 21st century. In order to maintain this vast infrastructure, highway workers put their lives on the line each day, subjecting themselves to the ever-present threat of inattentive drivers. The Advanced Highway Maintenance and Technology (AHMCT) Center, of the University of California, Davis, has developed numerous machines aimed at increasing the productivity, quality and safety of highway maintenance operations.

One specific highway maintenance task that is receiving major attention at the AHMCT Center is crack sealing. Cracks often form as a result of cyclic loading, faulty material compositions, subgrade failures, and environmental conditions including temperature and moisture fluctuations. After a crack is formed, harsh environments and heavy traffic perpetuate the crack axially along the road surface and downward toward the sublayer of the road. If left untreated, moisture will flow into the sublayer and further accelerate the degradation of the roadway. Therefore, crack sealing is crucial in preventing the high cost of complete rehabilitation of a crack-damaged highway.

Crack sealing is a tedious task requiring Caltrans to spend about \$10 million dollars annually. Of this budget, 66% is used to maintain a crew of eight individuals which can typically seal from one to two lane-miles per day. This lack of productivity leads to extended lane closures, causing traffic congestion and increased exposure of highway workers to a very harsh environment. Since crack sealing can only be performed when the roadway is dry, sealing is often limited, regionally, to the late spring through summer months when the temperatures can soar to above 43°C (110° F) on the road surface. In addition, the workers are often forced to work only feet away from traffic flowing at speeds up to 100 kph (62 mph), subjecting their safety to an increasing number of inattentive drivers.

To alleviate these problems, the AHMCT Center has developed a number of machines aimed at automating the crack sealing procedures to increase productivity, quality and safety. The latest of these machines is the Operator Controlled Crack Sealing Machine (OCCSM). The OCCSM prototype is designed to be a general crack sealing machine capable of sealing random transverse and small longitudinal cracks. The prototype uses a telescoping manipulator arm, located under the rear of the vehicle, to manipulate a pressurized sealant head over the roadway. The robotic arm is controlled from the cab of the vehicle by using a virtual interface. A computer shows a real captured image depicting the full workspace on the screen, from which the operator locates any cracks suitable for sealing. Using a digitizing device, such as a mouse or touch screen, the operator follows the crack to be sealed. The computer interprets this motion on the screen, and relays commands to the main control program. The control program then actuates the telescopic arm to mimic the operator's motion.

The telescopic manipulator arm operates as an R- θ manipulator to encompass a 3.6 m (12 ft) square workspace and is arguably the most crucial component of the OCCSM. The manipulator arm is mechanically capable of attaining positioning accuracy within 1.5 mm (1/16 in) throughout the workspace with a maximum end-effector velocity of 0.91 m/s (3 ft/s). Actuation of the manipulator arm is achieved through two subsystems, the rotational actuator and the telescopic actuator. The rotational actuator incorporates a servo motor and harmonic drive gear reducer to obtain a peak torque of over 1782 N-m (1320 ft-lb). This torque is capable of

accelerating the arm, at maximum extension, to a speed of 0.91 m/s (3ft/sec) in less than 0.5 seconds. The telescopic actuation system uses a novel prismatic ball screw actuator to provide high positioning accuracy and high-speed actuation over the entire workspace. A servo motor and custom planetary gearbox drive the ball screw actuator to attain positioning accuracy within 1.5 mm (1/16 in) with accelerations to 0.91 m/s (3 ft/s) in less than 0.5 seconds.

This report presents work leading towards the development of the first prototype OCCSM. This has included component subsystems as well as numerous critical machine components. The R- θ telescopic manipulator arm is discussed in detail from its concept phase through its detailed design, testing and test conclusions. Additionally, the camera boom system and the hose retraction systems' designs are presented in detail. The machine's controller is also presented in detail, and the R- θ telescopic manipulator arm is integrated with the controller to provide a complete system operational in the AHMCT Robotics Laboratory. This system will be moved to the OCCSM support vehicle for use on actual highways in the next phase of the project.

The most important aspects of this phase were the design and fabrication of the R- θ Telescopic Manipulator, the development of the controller, and the integration of the two systems. Through extensive research, conceptual design, detailed design, and testing, the first-generation full-scale R- θ telescopic manipulator arm has been successfully lab tested and proven to meet or exceed all critical project specifications, including its 3.6 m x 3.6 m dexterous workspace.

TABLE OF CONTENTS

ABSTRACT	III
EXECUTIVE SUMMARY	V
TABLE OF CONTENTS	VII
TABLE OF FIGURES	XV
TABLE OF TABLES	XVII
DISCLAIMER/DISCLOSURE	XIX
CHAPTER 1: INTRODUCTION	1
1.1 Current Methods of Crack Sealing	2
1.1.1 Crack Identification	2
1.1.2 Crack Preparation	2
1.1.3 Crack Sealing	3
1.2 The Automated Crack Sealing Machine (ACSM)	3
1.2.1 ACSM Drawbacks	4
1.3 The OCCSM Prototype	4
1.4 Problem Description and Objective	6
CHAPTER 2: MACHINE CONCEPT SELECTION	9
2.1 Project Specifications	9
2.1.1 Crack Definition	9
2.1.2 Workspace Definition	10
2.1.3 Sealing Specifications	10
2.1.3.1 Manipulator Speed	10
2.1.3.2 Manipulator Loading	11
2.1.3.3 Positioning Accuracy	11
2.1.3.4 Control Specifications	11
2.1.4 Environmental Conditions	11
2.1.5 Life Expectancy	12
2.1.6 Vehicular Requirements	12
2.1.7 Safety Requirements	12
2.2 Conceptual Design	12
2.2.1 Preliminary Concepts	13

2.2.1.1	X-Y Table	13
2.2.1.2	Horizontal and Vertical Articulating Manipulators	14
2.2.1.3	Wheeled Cart	15
2.2.1.4	Telescopic R- θ Arm	16
2.2.2	Trade-Off Analysis	17
2.3	Summary	17
 CHAPTER 3: TELESCOPIC R-q ARM CONCEPTUAL DESIGN		 21
3.1	Telescopic Arm Structural Concept	21
3.1.1	Telescopic Arm Structural Specifications	21
3.1.2	Telescopic Arm Structural Design Concepts	22
3.1.2.1	Custom Aluminum Extrusions	22
3.1.2.2	Steel Rectangular Extrusions	22
3.1.2.3	Thin Wall Steel Composite	22
3.1.2.4	Fiber Composites	23
3.1.3	Trade-Off Analysis	23
3.1.4	Summary	23
3.2	Telescopic Actuation Concept Selection	25
3.2.1	Telescopic Actuation Specifications	25
3.2.2	Preliminary Concepts	25
3.2.2.1	Cable-Pulley Configurations	25
3.2.2.2	Parallel Screw Configurations	26
3.2.2.3	Telescopic Hydraulic Cylinders	27
3.2.2.4	Telescopic Screw Actuator	28
3.2.3	Trade-Off Analysis	30
3.3	Rotational Actuation Concept Selection	32
3.3.1	Rotational Specifications	32
3.3.2	Preliminary Concepts	32
3.3.2.1	Planetary Gearbox	32
3.3.2.2	Chain/Gear Drive	33
3.3.2.3	Hydraulic Cylinder	33
3.3.2.4	Harmonic Drive	34
3.3.3	Trade-Off Analysis	35
3.3.4	Summary	36
3.4	Vehicle Integration and Stowage System	38
3.4.1	Specifications	38
3.4.2	Preliminary Concepts	38
3.4.2.1	Compound Slides	38
3.4.2.2	Support Plate/Roller	39
3.4.2.3	Curved Rail	39
3.4.3	Trade-Off Analysis	39
3.4.4	Summary	39

3.5	Summary	40
CHAPTER 4: DETAILED DESIGN		43
4.1	Telescopic Arm Structural Design	43
4.1.1	Specifications	44
4.1.2	Telescopic Sections	44
4.1.2.1.1	Base Cross Section	45
4.1.2.2	Intermediate Cross Section	47
4.1.2.3	Fly Cross Section	48
4.1.3	Vertical Support Systems	49
4.1.3.1	Primary Loading Rollers	49
4.1.3.1.1	Intermediate and Fly Sections	49
4.1.3.2	Secondary Loading Rollers	51
4.1.4	Horizontal Support Systems	52
4.1.5	Summary	52
4.2	Telescopic Actuator System	53
4.2.1	Specifications	53
4.2.2	Telescopic Ball Screw Actuator Design	54
4.2.2.1	Ball Screw Selection	54
4.2.2.2	Ball Screw Gun-Drilling	54
4.2.2.3	Drive Tube Design	55
4.2.2.4	Actuator Supports	55
4.2.2.5	Actuator / Section Integration	56
4.2.3	Concentric Output Planetary Gearbox Design	58
4.2.3.1	Kinematic Constraints	58
4.2.3.2	Detailed Design	60
4.2.3.2.1	Bevel Gear Selection	60
4.2.3.2.2	Planetary Gear Selection	61
4.2.3.2.3	Input Shaft	61
4.2.3.2.4	Outer Output Shaft	61
4.2.3.2.5	Inner Output Shaft	61
4.2.3.2.6	Bearing Selections	62
4.2.3.2.7	Gearbox Housing Design	62
4.2.3.2.8	Lubrication	63
4.2.4	Summary	64
4.3	Rotational Actuator System	64
4.3.1	Specifications	64
4.3.2	Harmonic Drive Selection	65
4.3.2.1	Torque Requirements	65
4.3.2.2	Speed Requirements	65
4.3.2.3	Accuracy Requirements	66
4.3.3	Servo Motor	66
4.3.3.1	Torque Requirements	66
4.3.3.2	Speed Requirements	67

4.3.3.3	Accuracy Requirements	67
4.3.4	Summary	67
4.4	Vehicle Integration and Stowage System Design	67
4.4.1	Specifications	68
4.4.2	Base-end Pivot Plate	68
4.4.3	Curved Rail Support System	68
4.4.4	Stowage System	69
4.4.5	Summary	70
4.5	Summary	71
CHAPTER 5: EXPERIMENTAL VERIFICATION		73
5.1	Telescopic Arm Structure	73
5.1.1	Qualitative Analysis	73
5.1.1.1	Arm Sections	73
5.1.1.2	Joint Connections	73
5.1.1.3	Qualitative Conclusions	74
5.1.2	Quantitative Analysis	74
5.1.2.1	Vertical Stiffness	74
5.1.2.2	Quantitative Conclusions	75
5.2	Telescopic Ball Screw Actuator	79
5.2.1	Qualitative Analysis	79
5.2.1.1	Qualitative Observations	79
5.2.1.2	Qualitative Conclusions	79
5.2.2	Quantitative Analysis	80
5.2.2.1	Positioning Accuracy	80
5.2.2.2	Actuator System Backlash	80
5.2.2.3	Quantitative Conclusions	80
5.3	Concentric Output Planetary Gearbox	83
5.3.1	Qualitative Analysis	83
5.3.1.1	Pre-Operation	83
5.3.1.2	Bevel Gear Noise	83
5.3.1.3	Qualitative Conclusions	83
5.3.2	Quantitative Analysis	83
5.3.2.1	Gearbox Backlash	83
5.3.2.2	Quantitative Conclusions	84
5.4	Vehicle Integration and Stowage System	84
5.4.1	Qualitative Analysis	84
5.4.1.1	Curved Rail Support	84
5.4.1.2	Stowage System	84
5.4.1.3	Rotational Pivot Plate	84
5.4.1.4	Qualitative Conclusions	85

5.4.2	Quantitative Analysis	85
5.4.2.1	Stowage Time	85
5.4.2.2	Quantitative Conclusions	85
5.5	Summary	85
CHAPTER 6: THE OCCSM CAMERA BOOM		87
6.1	Introduction	87
6.2	The Camera Boom Requirements	87
6.3	The Camera Boom Supports	88
6.4	Extension Mechanism	89
6.5	Selection of Boom Size and Material	90
6.5.1	Weight Analysis	91
6.5.2	Static End Deflection Analysis	92
6.5.3	Natural Frequency Analysis	94
6.5.4	Forced Vibration Analysis	97
6.5.5	Review of Analysis Results	99
6.6	Camera Boom Braces	100
6.6.1	Camera Boom Brace Arrangement	101
6.6.2	Brace Bracket Location	102
6.7	The Camera Housing	106
6.8	Summary and Recommendations	108
CHAPTER 7: THE SEALANT HOSE RETRACTION SYSTEM		109
7.1	Introduction	109
7.2	Design Requirements	109
7.3	Design Layout	110
7.4	Retraction Power System	111
7.4.1	Electric and Hydraulic Motor Options	112
7.4.2	Hydraulic Cylinder Options	112
7.4.3	Spring Powered Tool Balancer	113
7.5	Detailed Design	113
7.6	Summary and Recommendations	116

CHAPTER 8: THE CONTROL SYSTEM	119
8.1 Introduction	119
8.2 Control System Overview	119
8.3 Hardware	120
8.3.1 Robotic Arm and Servo Actuators	120
8.3.2 Motion Controller	122
8.3.3 I/O Controller	123
8.3.4 Digital Camera and its computer	125
8.3.5 The Main Computer	126
8.4 Software	127
8.4.1 Camera Computer Software	127
8.4.1.1 Camera Control	128
8.4.1.2 HTTP Server	129
8.4.2 Main Computer Software	130
8.4.2.1 The Motion Control Module	131
8.4.2.2 The I/O Control Module	132
8.4.2.3 The User Interface Module	133
8.5 Key Technologies	136
8.5.1 Embedded PC	136
8.5.2 Object-oriented Software	136
8.5.3 Programming with MFC	137
8.5.4 Multithreaded Programming	137
8.5.5 Real-time Control with Windows NT	139
8.5.6 Un-distortion of Camera Image	140
8.5.7 Motion Control Algorithm	141
8.5.8 Integration of Highway and Information Highway	143
8.6 Experiments	146
 CHAPTER 9: CONCLUSIONS AND RECOMMENDATIONS	 149
9.1 Conclusions and Recommendations	149
9.1.1 Project Goals	149
9.1.2 Telescopic Sections Design / Performance	149
9.1.3 Actuation Systems/Performance	150
9.1.4 Vehicle Integration / Performance	151
9.1.5 Further Testing	151
9.1.6 Camera Boom and Hose Retraction Systems	151
9.1.7 Control System	152
 CHAPTER 10: REFERENCES	 153

APPENDIX A. CALCULATIONS	155
APPENDIX B. MATLAB PROGRAM FOR CAMERA BOOM SIZE SELECTION	199
APPENDIX C. MATLAB PROGRAM FOR CAMERA BOOM BRACE LOCATION	201

TABLE OF FIGURES

FIGURE 1.1 - ACSM LONGITUDINAL AND TRANSVERSE SEALING MECHANISMS	4
FIGURE 1.2 - 3-D RENDITION OF OCCSM PROTOTYPE SEALING A TRANSVERSE CRACK.....	6
FIGURE 2.1 - 3-D RENDITION OF X-Y TABLE CONCEPT	14
FIGURE 2.2 - ADEPT 550 HORIZONTAL AND CRS ROBOTICS A255 VERTICAL ARTICULATING ROBOTS	15
FIGURE 2.3 - THE AHMCT TMRR WHEELED MOBILE ROBOT	16
FIGURE 2.4 - COMMERCIALY AVAILABLE TELESCOPIC BOOM LIFT.....	16
FIGURE 3.1 - THIN WALL STEEL COMPOSITE SECTION	23
FIGURE 3.2 - CABLE-PULLEY ACTUATION METHOD.....	26
FIGURE 3.3 - PARALLEL SCREW CONFIGURATION (U.S. PATENT: 4337868)	27
FIGURE 3.4 - TELESCOPIC HYDRAULIC CYLINDER	27
FIGURE 3.5 - “FLOATING” TELESCOPIC SCREW ACTUATOR.....	29
FIGURE 3.6 - BEVEL GEAR REDUCTION.....	33
FIGURE 3.7 - HYDRAULIC CYLINDER ROTATIONAL ACTUATOR	34
FIGURE 3.8 - CUP-TYPE HARMONIC DRIVE.....	35
FIGURE 3.9 - HARMONIC DRIVE OPERATION SKETCH.....	35
FIGURE 4.1 - OCCSM PROTOTYPE TELESCOPIC MANIPULATOR.....	44
FIGURE 4.2 - DEFLECTION ANALYSIS PROGRAM.....	46
FIGURE 4.3 - BASE CROSS SECTION	47
FIGURE 4.4 - FLY CROSS SECTION.....	48
FIGURE 4.5 - INTERMEDIATE SECTION OUTER SUPPORT SYSTEM	50
FIGURE 4.6 - INTERMEDIATE SECTION REAR SUPPORT SYSTEM	50
FIGURE 4.7 - FLY SECTION OUTER SUPPORT SYSTEM.....	51
FIGURE 4.8 - FLY SECTION REAR SUPPORT SYSTEM	51
FIGURE 4.9 - SPLIT TUBE FOR DRIVING THE INTERMEDIATE BALL SCREW	54
FIGURE 4.10 - REAR INTERMEDIATE SECTION FIXED SUPPORT (LEFT) AND INTERMEDIATE BALL SCREW ROLLING SUPPORT (RIGHT).....	56
FIGURE 4.11 DETAIL DRAWINGS OF TELESCOPIC ACTUATOR SYSTEM.....	57
FIGURE 4.12 - APEX 40 SERVO MOTOR AND CONCENTRIC DUAL OUTPUT PLANETARY GEARBOX ASSEMBLY	58
FIGURE 4.13 - CONCENTRIC OUTPUT PLANETARY GEARBOX	59
FIGURE 4.14 - TELESCOPIC GEARBOX AFTER FIVE HOURS OF OPERATION.....	63
FIGURE 4.15 - ROTATIONAL ACTUATOR SYSTEM	64
FIGURE 4.16 - END SUPPORT SYSTEM-CURVED RAIL	69
FIGURE 4.17 - ROLLER TRUCK DIRECTING LOADING INTO CURVED PLATE	70
FIGURE 4.18 - OCCSM STOWAGE SYSTEM	71
FIGURE 5.1 - FORCE VS. DEFLECTION PLOT FOR R=4.57M.....	76
FIGURE 5.2 - PLOT DEPICTING NONLINEAR STIFFNESS OF ARM.....	77
FIGURE 5.3 - PLOT OF FORCE VS. DEFLECTION DATA FOR VARIOUS BEAM EXTENSIONS.....	78
FIGURE 5.4 - END SUPPORT DEFLECTION MEASUREMENT DURING VERTICAL END DEFLECTION TEST	79
FIGURE 5.5 - CET MEASURING APPARATUS FOR VALIDATION OF POSITIONING ACCURACY	81

FIGURE 5.6 - PLOTS OF MEASURED ERROR VS. EXTENDED (TOP) AND RETRACTED (BOTTOM) BEAM LENGTH	82
FIGURE 6.1 - MODEL OF CAMERA BOOM BRACKET	88
FIGURE 6.2 - MODEL OF CAMERA BOOM CRANK ASSEMBLY	91
FIGURE 6.3 - RESULTS OF BOOM WEIGHT ANALYSIS	92
FIGURE 6.4 - FREE BODY DIAGRAM OF CAMERA BOOM	93
FIGURE 6.5 - RESULTS OF CAMERA BOOM END DEFLECTION ANALYSIS	94
FIGURE 6.6 - RESULTS OF CAMERA BOOM NATURAL FREQUENCY ANALYSIS	96
FIGURE 6.7 - RESULTS OF MAXIMUM VIBRATION AMPLITUDE ANALYSIS	99
FIGURE 6.8 - PROPOSED CAMERA BOOM CABLE SUPPORT	101
FIGURE 6.9 - SQUARE BRACKET WITH BRACE ATTACHMENT POSTS	102
FIGURE 6.10 - DIAGRAM OF CAMERA BOOM FOR BRACE LOCATION ANALYSIS	104
FIGURE 6.11 - NATURAL FREQUENCY RESULTS FOR BRACE ANALYSIS	106
FIGURE 6.12 - CROSS-SECTION OF CAMERA HOUSING	107
FIGURE 7.1 - HOSE RETRACTION SYSTEM LAYOUT	111
FIGURE 7.2 - MODEL OF CARRIAGE AND SHEAVE	114
FIGURE 7.3 - CROSS-SECTION OF HOSE RETRACTION ASSEMBLY	116
FIGURE 8.1 - CONTROL SYSTEM OVERVIEW	119
FIGURE 8.2 - ROBOTIC ARM	121
FIGURE 8.3 - MOTORS CONTROLLING THE TWO AXES	122
FIGURE 8.4 - POWER BOX WITH MOTOR DRIVERS	123
FIGURE 8.5 - OPTO 22 BRAIN BOARD FOR ANALOG/DIGITAL I/O CONTROL	124
FIGURE 8.6 - THE EMBEDDED CAMERA COMPUTER	126
FIGURE 8.7 - THE MAIN EMBEDDED COMPUTER	127
FIGURE 8.8 - USER-INTERFACE CLASSES ARCHITECTURE	135
FIGURE 8.9 - CAMERA IMAGE WITH DISTORTION	140
FIGURE 8.10 - IMAGE AFTER UN-DISTORTION	140
FIGURE 8.11 - MOTION CONTROL COORDINATES	142
FIGURE 8.12 - MOTION CONTROL ALGORITHM	143
FIGURE 8.13 - MONITORING THROUGH INTERNET	145
FIGURE 8.14 - "8" PATH FOLLOWING	146
FIGURE 8.15 - SQUARE PATH FOLLOWING	147
FIGURE 8.16 - AN "S" CURVE SIMULATING A CRACK	147
FIGURE 8.17 - A PATH OVERLAYING THE CRACK	148
FIGURE 9.1 - IMPROVED TELESCOPIC BEAM CROSS SECTION	150

TABLE OF TABLES

TABLE 2.1 - MACHINE CONCEPT TRADE-OFF ANALYSIS.....	19
TABLE 3.1 - TELESCOPIC SECTION TRADE-OFF ANALYSIS.....	24
TABLE 3.2 - TELESCOPIC ACTUATION TRADE-OFF ANALYSIS	31
TABLE 3.3 - ROTATIONAL ACTUATION TRADE-OFF ANALYSIS	37
TABLE 3.4 - END SUPPORT / STOWAGE SYSTEM TRADE-OFF ANALYSIS	41
TABLE 5.1 - FORCE VS. DEFLECTION DATA FOR R=4.57M	75
TABLE 6.1 - PROPERTIES OF POSSIBLE BOOM MATERIALS	92
TABLE 8.1 - SPECIFICATIONS OF THE MOTORS	122
TABLE 8.2 - CSERVO CLASS	131
TABLE 8.3 - CMOTION CLASS	132
TABLE 8.4 - CSNAP AND CSENSOR CLASSES.....	133

DISCLAIMER/DISCLOSURE

"The research reported herein was performed as part of the Advanced Highway Maintenance and Construction Technology Program (AHMCT), within the Department of Mechanical and Aeronautical Engineering at the University of California, Davis and New Technology and Research Program of the California Department of Transportation. It is evolutionary and voluntary. It is a cooperative venture of local, state and federal governments and universities."

"The contents of this report reflect the views of the author(s) who is (are) responsible for the facts and the accuracy of the data presented herein. The contents do not necessarily reflect the official views or policies of the STATE OF CALIFORNIA or the UNIVERSITY OF CALIFORNIA. This report does not constitute a standard, specification, or regulation."

Chapter 1: INTRODUCTION

Each year, local and federal government agencies spend millions of taxpayers' dollars maintaining our nation's immense highway infrastructure. The California state Department of Transportation (Caltrans) spends upwards of a \$100 million dollars annually preserving over 46,000 miles of California's highways against the ever-increasing threat of a soaring population (Velinsky, 1993). From 1983 to 1990, the U.S. Department of Transportation reported that the miles of vehicle travel had increased 41% (1990), a rate that is only expected to increase as we near the 21st century. The Advanced Highway Maintenance and Construction Technology (AHMCT) Center, of the University of California, Davis, has recognized this problem and has been redefining the future of highway maintenance with the aim of improving the productivity, quality and safety of highway maintenance procedures.

One specific highway maintenance task that is receiving major attention at the AHMCT Center is crack sealing. Cracks often form as a result of cyclic loading, faulty material compositions, subgrade failures, and environmental conditions including temperature and moisture fluctuations. After a crack is formed, harsh environments and heavy traffic perpetuate the crack axially along the road surface and downward toward the sublayer of the road. If left untreated, moisture will flow into the sublayer and further accelerate the degradation of the roadway. Therefore, crack sealing is crucial in preventing the high cost of complete rehabilitation of a crack-damaged highway. However, crack sealing does have its own cost, most of which is related to labor costs.

Crack sealing is a tedious task requiring Caltrans to spend about \$10 million dollars annually. Of this budget, 66% is used to maintain a crew of eight individuals which can typically seal from one to two lane-miles per day (Velinsky, 1993). This lack of productivity leads to extended lane closures, causing traffic congestion and increased exposure of highway workers to a very harsh environment. Since crack sealing can only be performed when the roadway is dry, sealing is often limited, regionally, to the late spring through summer months when the temperatures can soar to above 43°C (110° F) on the road surface. In addition, the workers are often forced to work only feet away from traffic flowing at speeds up to 100 kph (62 mph), subjecting their safety to an increasing number of inattentive drivers.

To alleviate these problems, the AHMCT Center has developed a number of machines aimed at automating the crack sealing procedures to increase productivity, quality and safety. The

latest of these machines is the Operator Controlled Crack Sealing Machine (OCCSM), a machine that has its origins tied to the first AHMCT crack sealing machine, the Automated Crack Sealing Machine (ACSM), which will be briefly discussed. The interested reader is referred to Velinsky (1993) for more detailed information.

1.1 Current Methods of Crack Sealing

Although crack sealing operations vary greatly by state, crack sealing can be generalized into three operations: crack identification, preparation, and sealing. Crack identification consists of determining whether a crack is suitable for sealing. Crack preparation methods concern cleaning, and preparing the crack to accept the sealant. Finally, sealing concerns methods used in applying the sealant to the road. It should be noted that the standards presented here are formulated by analyzing the current methods used by Caltrans.

1.1.1 Crack Identification

Crack width, depth, length and occurrence are all factors that determine whether a roadway should be sealed. Caltrans will usually seal cracks that range in width from 6-12 mm (0.23-0.47 in) for transverse cracks and up to 51 mm (2 in) for longitudinal cracks (Velinsky, 1993). Cracks that are larger than these dimensions can be indicative of a roadway that is beyond repair since crack depth usually increases proportionally to crack width. A crack that extends down to the sublayer is most likely to have already allowed erosion. This erosion may cause movement of the sublayer drastically reducing the life of any seal and causing further cracking. A roadway with this state of degradation is likely to be marked for complete renovation.

1.1.2 Crack Preparation

Crack preparation can include any of the following procedures: routing, cleaning, drying, and heating. For transverse cracks, Caltrans will usually clean cracks with compressed air or a stiff brush. Occasionally, some states will rout smaller cracks to increase the penetration of the sealant into the surface and achieve a stronger seal. However, this can be a time consuming process. Drying can be achieved by compressed air, the use of a heat gun or other means. The advantage of a heat gun or other heat source for drying is that it will also heat the interior surfaces of the crack creating improved sealant adhesion.

1.1.3 Crack Sealing

Crack sealing is currently a very low-tech operation in which sealant is applied to the roadway by a simple fill operation. Operators manually move a sealant wand over the crack that they are sealing. Sealant is forced out of the wand by a small amount of pressure exerted by an upstream sealant melter. This system relies on gravity and low sealant viscosity to obtain a solid fill in the crack.

1.2 The Automated Crack Sealing Machine (ACSM)

The ACSM was developed by AHMCT, through the Strategic Highway Research Program's H107A project at the University of California, Davis. The ACSM, Figure 1.1, is a fully automated crack sealing machine outfitted with subsystems for sealing longitudinal and transverse cracks in the roadway. The two subsystems are operated by the same support systems requiring only a single sealant melter and power supply. The machine uses separate sensing systems to locate the cracks on the roadway. This information is then processed to provide path planning for each subsystem.

A longitudinal apparatus is located on the side of the truck and incorporates a local sensing system, router, vacuum, heat source and a crack sealing head. Each of these subsystems is placed in line, such that a single hydraulic cylinder can accurately follow the crack measured by the local sensing system (Velinsky, 1993).

A side mounted GMF-A510 SCARA manipulator located at the rear of the vehicle seals transverse cracks. Path planning for this manipulator is acquired through a vision sensing system mounted on the front of the vehicle. As the vehicle travels along the roadway, a vision sensing system generates a full image of the roadway from which cracks are identified. This information is then transformed into real world coordinates through a vehicle orientation and control system. Once the path is planned and translated into relative coordinates, the SCARA robot manipulates the sealant head throughout the workspace (Velinsky, 1993).



Figure 1.1 - ACSM Longitudinal and Transverse Sealing Mechanisms

1.2.1 ACSM Drawbacks

The most prevalent drawback of the ACSM is its complexity and associated high cost of manufacturing and operation. Through a preliminary market report contracted to the Technology Development Center (1993) it was determined that the ACSM was too cost prohibitive to sell as a complete machine. Recommendations by members of focus groups were in favor of the development of advanced crack sealing technology. However, they believed that a machine with less automation would gain wider acceptance at a lower cost. For example, one member from the Nevada State Department of Transportation stated that worker comfort and acceptance was crucial. In addition, many members felt that safety of the crack sealing operation would be greatly increased through this type of automation.

This marketing report and the desire to meet the needs of the users has led to the concept of an Operator Controlled Crack Sealing Machine (OCCSM). Specifically, this machine targets the sealing of transverse cracks in the roadway with reduced automation and thus reduced machine cost.

1.3 The OCCSM Prototype

The Operator Controlled Crack Sealing Machine (OCCSM) project was undertaken with the goal of producing a machine that would better meet the needs of the end-user. To this extent, the OCCSM uses concepts developed by the ACSM project, but reduces the automation, while maintaining the increased productivity, quality and safety.

The OCCSM prototype is designed to be a general crack sealing machine capable of sealing random transverse and small longitudinal cracks. The prototype uses a telescoping manipulator arm, located under the rear of the vehicle, to manipulate a pressurized sealant head over the roadway. The robotic arm is controlled from the cab of the vehicle by using a virtual interface. A computer shows a real captured image depicting the full workspace on the screen, from which the operator locates any cracks suitable for sealing. Using a digitizing device, such as a mouse or touch screen, the operator follows the crack to be sealed. The computer interprets this motion on the screen, and relays commands to the main control program. The control program then actuates the telescopic arm to mimic the operator's motion.

The telescopic manipulator arm operates as an R- θ manipulator to encompass a 3.6 m (12 ft) square workspace and is arguably the most crucial component of the OCCSM. The manipulator arm is mechanically capable of attaining positioning accuracy within 1.5 mm (1/16 in) throughout the workspace with a maximum end-effector velocity of 0.91 m/s (3 ft/s). Actuation of the manipulator arm is achieved through two subsystems, the rotational actuator and the telescopic actuator. The rotational actuator incorporates a servo motor and harmonic drive gear reducer to obtain a peak torque of over 1782 N-m (1320 ft-lb). This torque is capable of accelerating the arm, at maximum extension, to a speed of 0.91 m/s (3ft/sec) in less than 0.5 seconds. The telescopic actuation system uses a novel prismatic ball screw actuator to provide high positioning accuracy and high-speed actuation over the entire workspace. A servo motor and custom planetary gearbox drive the ball screw actuator to attain positioning accuracy within 1.5 mm (1/16 in) with accelerations to 0.91 m/s (3 ft/s) in less than 0.5 seconds.

Structurally, the OCCSM telescopic manipulator arm is comprised of three prismatic sections that collapse to a length of 2.67 m (105 in) and extend to a total length of 6.7 m (264 in). The three prismatic sections are sized such that the base arm is the heaviest and largest, while the fly arm is the optimized smallest and lightest. In addition, each section is to have a high stiffness to weight ratio. This is accomplished by using custom-made thin wall sections made from mild steel. These thin wall sections also allow for the passage of the sealant hose as well as the telescopic actuation system within the telescopic arm.

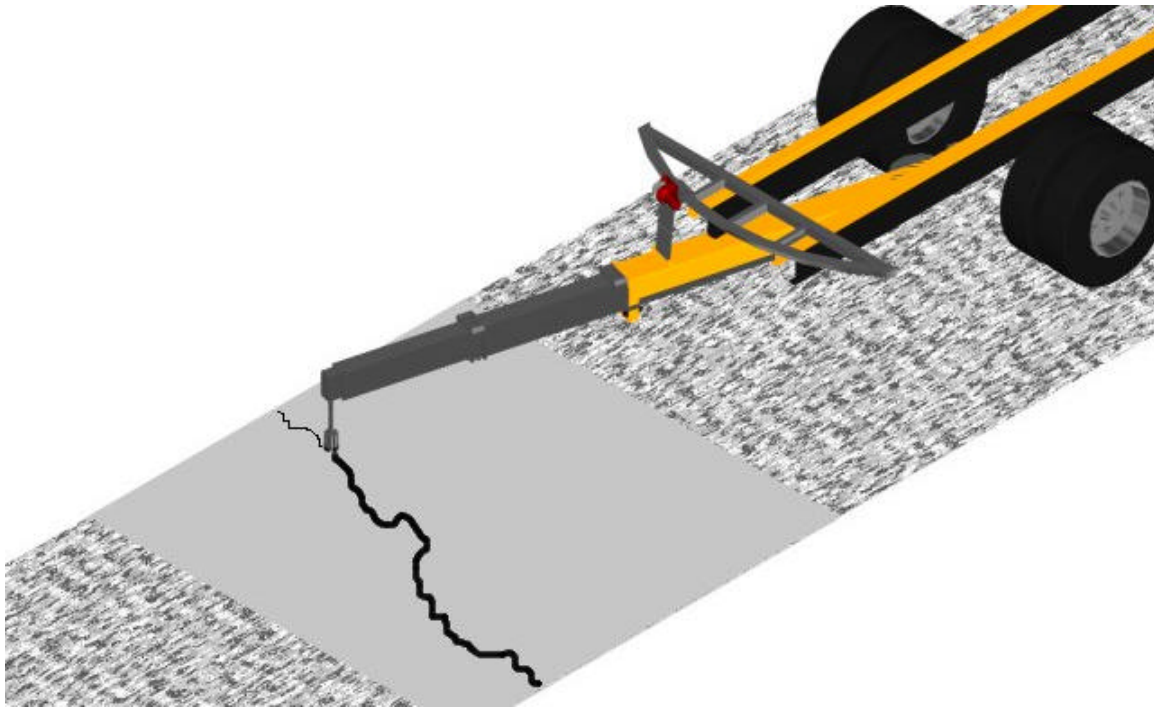


Figure 1.2 - 3-D Rendition of OCCSM Prototype Sealing a Transverse Crack

The integrated manipulator arm is then mounted onto the vehicle by using a rotating joint at the end of the base section. The rotational actuator is connected at this point to provide torque actuation of the arm. At the other end of the base section, a rotating support system further supports the arm and provides a mechanism to lift the arm into a storage position.

1.4 Problem Description and Objective

In an effort to increase the safety and productivity of highway maintenance tasks, the AHMCT research center is developing means to automate many labor-intensive tasks such as crack sealing. The ACSM was developed with the aim of fully automating the crack sealing procedures. This machine became a groundbreaking step in proving the feasibility of and need for such machines. However, in spite of the success of this first project, a marketing analysis report had shown that the machine was too costly to be pursued. This has led to the development of the OCCSM prototype. The OCCSM reduces the automation associated with the crack identification process by allowing the operator to identify and command which cracks should be sealed. This allows the OCCSM to be a more cost-effective solution while maintaining the improved productivity, quality and safety of crack sealing maintenance.

This report will present the complete mechanical design of the OCCSM robotic manipulator arm from concept formation to a first generation prototype. The project specifications and machine concept selection are discussed in Chapter 2, from which Chapter 3 proceeds with the discussion of the detailed conceptual design of the machine components. A detailed design of these components is presented in Chapter 4 with validation, through testing and qualitative analyses, following in Chapter 5. The camera boom and its retraction mechanism are discussed in Chapter 6. Vibration characteristics of the camera boom are analyzed, and braces, that were determined necessary from the vibration analysis, were designed. The hand operated crank mechanism, which extends and retracts the camera boom by means of a rack and pinion design, is examined. The design of the camera housing that attaches to the end of the boom and provides adjustments for camera alignment is also discussed. Chapter 7 focuses on the hose retraction system and several design options that were considered for powering the mechanism. The chapter also explores how the system was designed to fit in the small area beneath the truck bed and between the frame rails. Chapter 8 discusses the unique OCCSM control system. This control system integrates the state-of-the-art in personal computing and Internet technologies and provides an extremely easy to use interface for the machine operator. This report concludes with a discussion of conclusions and recommendations, aimed at directing the future OCCSM development, in Chapter 9.

Chapter 2: MACHINE CONCEPT SELECTION

The machine concept selection for the OCCSM was the most important phase in the design process. In this phase, goals and limitations regarding the machine's performance were chosen carefully in order to obtain a cost-effective and productive crack sealing machine. The first step was to determine the project specifications, such as workspace size, target crack size, life expectancy, vehicle requirements, crack sealing speeds, etc. These specifications were then used as guidelines to form and evaluate design concepts through brainstorming sessions and a trade-off analysis, respectively. Throughout this trade-off analysis, concepts were pitted against one another to ensure that the final machine concept selection would most closely fit the project specifications. This chapter presents the OCCSM concept selection process and concludes with a detailed explanation of the OCCSM machine concept.

2.1 Project Specifications

Considering factors from crack sealing procedures, control specifications and common sense developed project specifications for the OCCSM. The specifications were then studied and weighted according to their importance in the overall design process with the goal of producing a productive and cost-effective machine.

2.1.1 Crack Definition

Crack sealing procedures were used in determining the sizes and configurations of target cracks. Through research into current Caltrans methods, the target crack widths for general crack sealing were determined to be between 6 mm (0.23 in) to 12 mm (0.47 in) for transverse cracks and up to 51 mm (2 in) for longitudinal cracks. However, large longitudinal cracks presented a problem for current automated crack sealing machines. The problem was that current sealant melters were designed to operate with a manually sealing crew that was not capable of sealing at the high rates of automated sealing machines. Therefore, when an automated machine was used with these large cracks, the melter was not powerful enough to maintain a constant flow of melted sealant. To alleviate this problem, either the OCCSM machine would need to be outfitted with a larger, more expensive sealant melter, or the machine would need to be limited to smaller cracks. Through a careful cost-benefit evaluation, it was

determined that the larger melter had extra costs associated with the need for a larger vehicle and higher power consumption, all of which raised the cost-benefit ratio. Therefore, it was determined that a target crack width of 6 mm (0.23 in) to 12 mm (0.47 in) would provide the most cost-effective solution, while maintaining productivity.

2.1.2 Workspace Definition

The OCCSM workspace definition became a critical part of the conceptual design. From an early stage, it was determined that an operator-controlled machine would be very difficult to operate unless the vehicle was stationary. This necessitated a large workspace to minimize lost time required to move the vehicle ahead to the next workspace. To further increase productivity, the OCCSM workspace was required to extend through the entire lane width (3.6 m/12 ft) to eliminate the need for a second pass sealing operation. Through careful analysis it was determined that a workspace 3.6 m (12 ft) wide by 3.6 m (12 ft) long would be necessary for a productive machine.

2.1.3 Sealing Specifications

Sealing specifications were prescribed by previous experience in automated sealing as well as the operations of Caltrans. These specifications included sealing speed, manipulator load requirements, positioning accuracy and control specifications.

2.1.3.1 Manipulator Speed

Speed of the OCCSM manipulator was determined by considering situations that the operator might encounter, such as cracks at opposite ends of the workspace, as well as mechanical limitations. To improve the productivity of the machine, it was determined that the machine should operate at the highest speed possible. However, higher speeds required higher power consumption, and bulkier mechanical designs to accommodate the higher inertial loading. In addition to structural design, there was concern that the higher sealant rates would require larger, more costly sealant melters. Based on careful consideration of the preceding factors, the rapid travel speed for the OCCSM was set to 0.91 m/s (3 ft/s), with an acceleration time of 0.5 seconds, recognizing that the end-effector speed during crack sealing would lie well below this goal.

2.1.3.2 Manipulator Loading

Speed requirements were then used with sealant head data to determine the loading that the OCCSM end-effector would endure. A vertical loading requirement of 445 N (100 lb) was determined from the weight of the sealant head. In addition, the manipulator was required to handle side loading due to inertial effects and friction between the sealant head and the workspace. Specifically, the manipulator was required to handle accelerations of the sealant head to 0.91 m/s (36 in/s) in 0.5 seconds and estimated frictional forces of 89 N (20 lb) at the bottom of the sealant head. As with sealing speed, the ability to handle these loads varied greatly for each preliminary conceptual design.

2.1.3.3 Positioning Accuracy

Accuracy requirements for the OCCSM were influenced largely by target crack specifications. It was determined that the machine should be capable of placing the end-effector within the dimensions of the smallest target crack, 6 mm (0.23 in). Therefore, the target accuracy for the OCCSM was set to 3 mm (0.12 in), one-half of the smallest target crack width.

2.1.3.4 Control Specifications

Lastly, control specifications for the OCCSM were determined based on the above specifications and others. The goal of the OCCSM was to have simplified control, and as such, it was determined that the mechanical design of the OCCSM should aid in this quest. Specifically, control specifications required the mechanical design to minimize vibrations, provide maximum accuracy and minimize the complexity of the required control.

2.1.4 Environmental Conditions

Environmental conditions were determined to contribute significantly to the design of the OCCSM due to harsh operating environments. It was determined that road maintenance machinery must be designed to be robust to many environmental factors such as corrosion, caused by salt and moisture exposures. In addition, the design must be able to operate in a wide temperature range depending on geographical area. In California alone, conditions vary drastically from dessert conditions in Death Valley to the frigid Sierra Nevada. Therefore, OCCSM conceptual designs were required to be robust in any of these environmental conditions.

2.1.5 Life Expectancy

The life expectancy of any machine has a direct relation to its operating environment and as such is difficult to ascertain. For this reason, life expectancies for the OCCSM were not quantified, rather each conceptual design was compared against the robustness of current highway maintenance machinery. On a detailed mechanical design basis, component specifications were set such that the fatigue life of all components should exceed two years, operating for six hours per day and 365 days per year.

2.1.6 Vehicular Requirements

Vehicle requirements for the OCCSM project concerned the power, weight, size and specialized needs of each machine concept. Each mechanical concept was analyzed to determine the exact impact on the OCCSM vehicle in terms of vehicle size, cost, and power requirements.

2.1.7 Safety Requirements

Safety was also a major concern in the design of the OCCSM. Although the OCCSM was to be operator controlled, a computer was responsible for the physical actuation of the individual components, possibly leading to unsafe situations during power failures, software problems, etc. Therefore, safety specifications were made requiring that the OCCSM be designed with foresight into all possible scenarios. In addition, the OCCSM was required to be incapable of operating at unsafe speeds, or with unsafe forces. Parallel to the safety of the actuation systems, the structural composition was also required to be safe. Due to uncertainties in material composition, exact operating environment and other factors, all components that made up the mechanical design of the OCCSM were required to be designed with a factor of safety of at least two. Following these guidelines and developing foresight and consideration into possible unsafe operating scenarios all but guaranteed the development of a safe and productive machine.

2.2 Conceptual Design

The conceptual design phase began with a series of brainstorming sessions in which critical evaluation of the previously discussed project specifications allowed several machine design concepts to be generated. Each concept was then critically examined based on a series of weighted design specifications. The results were then tabulated in trade-off tables, from which

the designs could be compared. The results of these comparisons would ideally reveal the best conceptual design.

The development of the OCCSM began with the most general concept selection concerning the type of manipulator that would be used. Through research and brainstorming, several concepts were formulated. These concepts included an X-Y table, horizontal and vertical articulating arms, wheeled carts and an R- θ telescoping arm. Criteria were then developed considering the previous project specifications and other considerations specific to each concept. These criteria were then used in a trade-off analysis, Table 2.1, from which the most optimum design configuration could be selected. Once the optimum machine configuration was selected, subsequent designs concerning actuation and hardware design were each optimized using the same method until the entire OCCSM conceptual development was complete.

2.2.1 Preliminary Concepts

The initial brainstorming and project specifications yielded a number of competing machine concepts including an X-Y table, horizontal and vertical articulating arms, a wheeled cart, and an R- θ telescoping arm.

2.2.1.1 X-Y Table

The X-Y table concept, Figure 2.1, consists of a frame that holds two compound linear slides. In the figure shown, the Y-axis is the main slide upon which X-axis motion is obtained. The actuation requires two actuators operating simultaneously to yield compounded linear motion in any direction. The principle advantage of this design is the simplicity of the mechanical structure requiring a simple frame and commercially available actuators. The principle disadvantage is that the frame must extend beyond the active workspace. In crack sealing this would place the frame into the adjacent lanes requiring multiple lane closures.

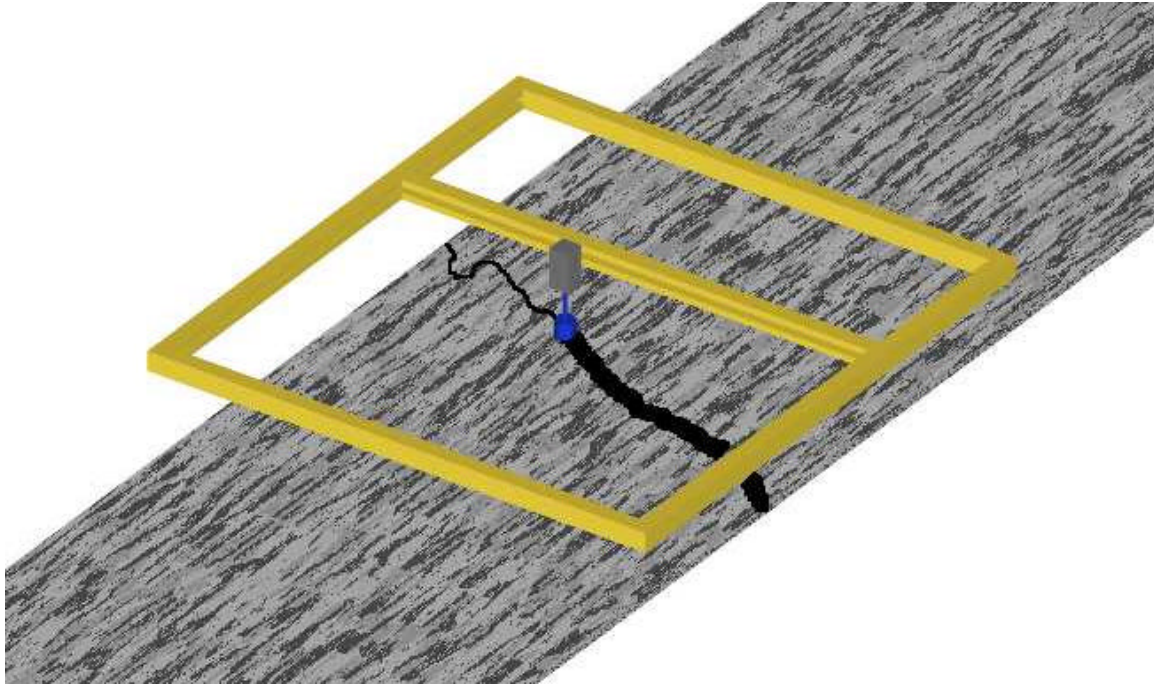


Figure 2.1 - 3-D Rendition of X-Y Table Concept

2.2.1.2 Horizontal and Vertical Articulating Manipulators

Horizontal and vertical articulating manipulators are common to many robotic applications and are becoming increasingly available on the commercial market. Figure 2.2 depicts examples of two commercially available articulating robots. Horizontal articulating robots, similar to the GMF-A510 SCARA manipulator used on the ACSM, can require as little as two actuators, depending on the number of linkages, and accurate positioning can be accomplished by solving the linkage kinematics of the articulating system.

Vertical articulating arms operate similarly to horizontal robotic manipulators with the exception that the arms are oriented vertically as in Figure 2.2. This type of robot requires four-axis control and has built in accuracy control by solving the linkage kinematics.

Both of these designs have vast applications in industry, but are rather limited for the current application due to their complexity and limited workspace.



Figure 2.2 - Adept 550 Horizontal and CRS Robotics A255 Vertical Articulating Robots

2.2.1.3 Wheeled Cart

Another form of manipulator that has applications in highway maintenance is the wheeled cart. This technology consists of a cart type vehicle that is able to manipulate the sealant head over the workspace and seal the cracks. The advantage of a wheeled cart robot is its ability to handle high tooling loads. For instance, the AHMCT Center has developed a Tethered Mobile Routing Robot (TMRR), Figure 2.3, which is designed to track, rout and seal cracks in the pavement. The cart design is necessary to handle the intense loading required by routing operations. There are two disadvantages of this type of concept. The first is that the wheels are required to track over the workspace including freshly applied sealant. This can limit the amount of cracks that can be sealed in a specific area or necessitate a drying agent to help cure the sealant surface. The second disadvantage is caused by tire slip and requires external measuring devices that relate the cart's position to the vehicle and workspace.

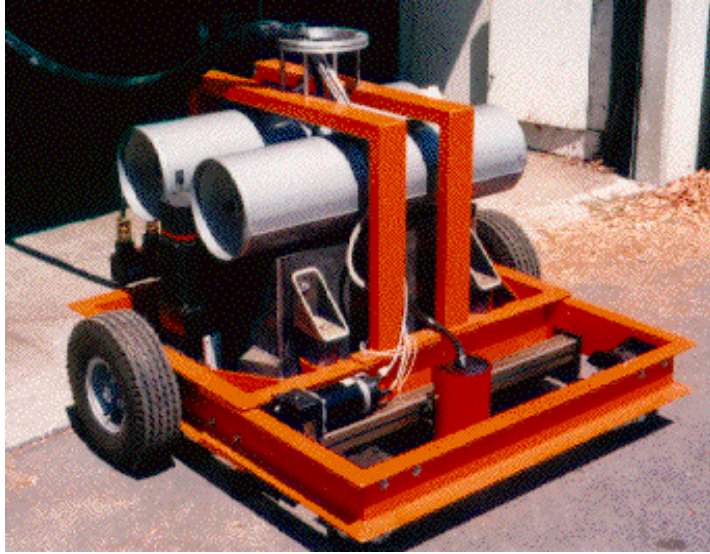


Figure 2.3 - The AHMCT TMRR Wheeled Mobile Robot



Figure 2.4 - Commercially Available Telescopic Boom Lift

2.2.1.4 Telescopic R-q Arm

The last proposed concept was an $R\theta$ telescopic manipulator arm. This design is commonly referred to as a cylindrical type robot and uses telescopic and rotational motion to manipulate throughout the workspace. This design is similar to common telescopic boom lifts, Figure 2.4, with the imposed limitation of planar motion, parallel to the workspace. The telescopic structure is accomplished through a series of prismatic sections that are rotated from the largest, base section. The sealant head would then attach to the smallest, outermost section and extend downward to seal the workspace. Rotational and telescopic actuators control the arm movement

and provide complete end-effector position measurements. The advantages of this design include the simplicity of the two-axis kinematics, compact storage size, and the vast workspace coverage. The main disadvantage is the lack of commercially available components, such as sections, actuators, etc. Although there are numerous material handling machines similar to Figure 2.4, these machines are designed for carrying much larger loads and do not incorporate accurate positioning systems.

2.2.2 Trade-Off Analysis

The next step was to determine the optimum design based on the project specifications as well as the other desired specifications. These specifications were then given weightings from one to ten based on how crucial they were in developing a productive and economical machine. Next, each of the competing conceptual designs was given a rating for each criterion in the trade-off analysis table, Table 2.1. Each rating was then converted into a numerical score from one to five, where one is the worst, five is the best. These numerical ratings were then multiplied by the weight of each criterion to determine each concept's score in that criterion. The subtotals were then summed to find the overall score for each concept. The trade-off analysis yielded two competing designs that were close enough to require extra consideration. These two designs were the X-Y table and the R- θ telescoping manipulator arm.

The X-Y table and the R- θ telescopic manipulator arm differed in only two of the comparative categories, machine boundary dimensions and mechanical complexity. Although, the mechanical complexity of the telescopic arm was high compared to that of the X-Y table, the fact that the X-Y table extended beyond lane width precluded it from being selected. It was perceived that the only solution to this problem would be to have multiple lane closures or to reduce the workspace and have the machine perform multiple passes, all of which would sacrifice the machine's productivity.

2.3 Summary

At this stage in the design process, project specifications had been developed based on the goal of producing a cost-effective and productive crack sealing machine. These specifications were then used in brainstorming sessions to develop preliminary machine concepts. To quantify the value of each of the preliminary concepts, a trade-off analysis table was formed which

numerically rated how well each concept met the specifications. As a result, the R- θ telescopic manipulator arm concept was chosen as the most ideal concept for a productive and cost-effective machine. The next step in the design process was to determine the conceptual design of the subsystems that would form the R- θ telescopic manipulator arm.

	Weighting (1-10)	X-Y Table			Vertical Articulating Arm			Horizontal Articulating Arm			Wheeled Cart			Telescopic R-Theta Arm		
		Rating	Score	Total	Rating	Score	Total	Rating	Score	Total	Rating	Score	Total	Rating	Score	Total
Controllability																
# of Actuators required(min)	5	2	5	25	2 to 3	4	20	3	1	5	2	5	25	2	5	25
kinematic complexity	7	low	5	35	high	1	7	high	1	7	high	1	7	low	5	35
Accuracy																
External measurement req'd.	7	no	5	35	no	5	35	no	5	35	yes	1	7	no	5	35
Workspace																
12'x14' attainable workspace	10	yes	5	50	yes	5	50	yes	5	50	yes	5	50	yes	5	50
Machine Boundary Dimensions																
Vertical height	4	low	5	20	high	1	4	low	5	20	low	5	20	low	5	20
Within lane width	10	no	1	10	yes	5	50	no	1	10	no	1	10	yes	5	50
Sealing																
Able to transverse over sealant	10	yes	5	50	yes	5	50	yes	5	50	no	1	10	yes	5	50
Machine Setup																
Truck stabilization required?	8	no	5	40	yes	1	8	no	5	40	no	5	40	no	5	40
Move ahead time	8	low	5	40	med	3	24	low	5	40	high	1	8	low	5	40
Cost																
commercially available	4	no	1	4	no	1	4	no	1	4	no	1	4	no	1	4
control complexity	8	low	5	40	high	1	8	high	1	8	med	3	24	low	5	40
mechanical complexity	8	low	5	40	high	1	8	high	1	8	med	3	24	high	1	8
Score				389			268			277			229			397

Table 2.1 - Machine Concept Trade-Off Analysis

Chapter 3: TELESCOPIC R-q ARM CONCEPTUAL DESIGN

The design process to this point had included the conceptual design of and optimum machine configuration using a telescopic R- θ manipulator. The next step in the design process was to determine the configurations of each of the subsystems. Specifically, the OCCSM telescopic arm was broken down into three basic subsystems: telescopic arm structural design, telescopic and rotational actuation, and vehicle integration and stowage. Within each of these subsystems, concepts were formulated and evaluated through the use of trade-off tables to determine their ability to meet the machine specifications.

3.1 Telescopic Arm Structural Concept

The conceptual design selection for the R- θ telescopic arm included section geometry, joint connections and material considerations. Research into techniques used in telescopic crane booms and material handlers was performed to gain insight into the current state of the art. This research yielded valuable information regarding commercially available beam sections and joint connections. However, it was easy to recognize that these designs were developed according to a different set of standards based on high lifting capacities. To the contrary, the OCCSM machine would require minimal tooling loads and high positioning accuracy common to robotic machines, thus eliminating the usefulness of commercially available techniques. To accommodate this, several concepts were developed ranging from custom aluminum extrusions to thin wall steel composite beam sections. These designs were then evaluated against a set of specifications in a trade-off analysis to determine the optimum structural design concept.

3.1.1 Telescopic Arm Structural Specifications

Several factors were considered in determining the optimal structural design of the telescopic arm. These factors included design considerations such as stiffness to weight ratios, overall weight, size and strength. In addition, factors concerning cost, robustness, versatility and simplicity were considered. Specifications were developed through consideration of the performance requirements set forth in the project specifications as well as consideration into the preceding factors. This analysis yielded several major design criteria that were then used to evaluate each of the competing conceptual designs.

3.1.2 Telescopic Arm Structural Design Concepts

3.1.2.1 Custom Aluminum Extrusions

Aluminum alloys are widely used in robotic applications due to their high strength to weight ratios and manufacturing versatility. However, the usefulness of these aluminum alloys for the OCCSM project was limited due to the lack of commercially available sections. The principle drawback is the high cost of large, custom, closed form extrusions which become cost-prohibitive in prototype design. Alternative methods using aluminum alloys have been considered for future prototypes. These methods include a particular design that combines two half-extrusions by adhesive or fasteners to form a custom closed section. This has a lower initial cost due to the open extrusions and offers the benefit of geometric versatility.

3.1.2.2 Steel Rectangular Extrusions

Steel rectangular extrusions were investigated because of their low cost and commercial availability. In addition, steel extrusions offer increased robustness and stiffness over aluminum alloys. The principle disadvantages of these extrusions include the lack of close fit sizes and thin wall sections. These disadvantages cause the arm sections to be larger than required, adding excessive weight to the machine which causes increases in the total beam deflection, rotational inertia, and machine power.

3.1.2.3 Thin Wall Steel Composite

Thin wall steel composite sections were developed to address the drawbacks of the previous steel rectangular sections. From research into the steel rectangular sections, it was found that the excessive wall thickness was the principle cause of all of the major drawbacks. To remedy this, it was proposed to design a steel section out of a formed light gauge material. The idea was to form a dimensionally large section to gain high stiffness, but with thin walls to maintain low weight. The proposed design would need to maintain a thicker bottom surface to which all of the high contact loading from the section joints could be directed. While increasing the stiffness to weight ratio, the formed section also offered the advantage of low cost. Associated drawbacks of the section included questionable robustness, low dimensional accuracy, and the possibility of localized buckling in the thin sidewalls. However, these drawbacks would prove to be manageable when dealing with a prototype machine.

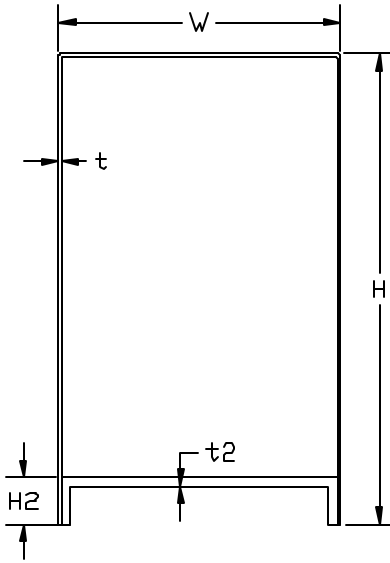


Figure 3.1 -Thin wall Steel Composite Section

3.1.2.4 Fiber Composites

Fiber composites were also considered for the OCCSM telescopic arm. These composites offered many advantages including the highest stiffness to weight ratios, low section weight and manufacturing versatility. However, fiber composites have similar drawbacks to aluminum alloys in that they are very costly and hard to procure. These drawbacks precluded the use of fiber composites in the OCCSM prototype design, where rapid prototyping is crucial.

3.1.3 Trade-Off Analysis

To help quantify the selection of the best telescopic section design, a trade-off table, Table 3.1, was formed. Each of the competing conceptual designs was rated against a set of weighted specifications. Each concept's individual score for each criterion was then summed to form a total "value" of the design. The criteria used were simplicity, manufacturing versatility, stiffness to weight ratio, robustness, size, overall weight, commercial availability and cost.

3.1.4 Summary

The results of the trade-off analysis clearly showed that the thin wall steel composite section was the most appropriate design for the proof-of-concept machine. Although the mechanical complexity is higher for these sections due to the limitation on the geometric shapes, the low cost, high stiffness to weight ratio, and high commercial availability outweigh this disadvantage.

	Weighting (1-10)	Aluminum Alloy Extrusions			Steel Rectangular Tubing			Thin-Wall Steel Composite			Fiber Composite		
		Rating	Score	Total	Rating	Score	Total	Rating	Score	Total	Rating	Score	Total
Simplicity	7	high	5	35	med	3	21	med-high	4	28	high	5	35
Manufacturing Versatility	6	high	5	30	low	1	6	med-high	4	24	high	5	30
Stiffness/Weight Ratio	10	low-med	2	20	med	3	30	high	5	50	high	5	50
Robustness	5	low	1	5	high	5	25	med	3	15	low-med	2	10
Size	4	high	1	4	low-med	4	16	low	5	20	low	5	20
Overall Weight	10	low	5	50	high	1	10	low	5	50	low	5	50
Commercial Availability	9	low	1	9	high	5	45	med-high	4	36	low	1	9
Cost	10	high	1	10	low	5	50	low	5	50	low	1	10
Score				163			203			273			214

Table 3.1 - Telescopic Section Trade-Off Analysis

3.2 Telescopic Actuation Concept Selection

Determining the actuation system for the telescopic sections began with brainstorming and research into current methods used in telescoping boom cranes, material handlers, and personnel lifts. Through this research, several actuation concepts were formulated including cable-pulley configurations, parallel screw configurations, and telescoping hydraulic cylinders. However, each of these methods of actuation had associated drawbacks that encouraged development of a novel telescopic ball screw design. All of these designs were then compared against the desired project specifications in a trade-off analysis table to determine the most appropriate design.

3.2.1 Telescopic Actuation Specifications

Project specifications were examined and refined to develop a series of telescopic actuation specifications (see Table 3.2). The specifications were then used in a trade-off analysis table to evaluate the conceptual designs. The most crucial specifications concerned concept accuracy, velocity constraints, and space requirements. Specifically, each design was required to have positioning accuracy within 3 mm (0.125 in), taking system backlash into consideration. In addition, each actuator had to provide for constant velocity actuation of the sealant head throughout the workspace, and be capable of attaining the target speed of 0.91 m/s (36 in/s). Finally, space requirements were imposed to ensure that sealing hoses and control lines for the sealant head could be routed within the telescopic sections. Other less crucial constraints concerned efficiency, robustness, weight, mechanical complexity, cost, and control complexity.

3.2.2 Preliminary Concepts

3.2.2.1 Cable-Pulley Configurations

Cable-pulley configurations provide for a simple cost-effective means of actuating nested telescopic sections. The simplest design is shown for a single telescopic section in Figure 3.2. One end of a continuous drive cable is connected to the inner end of the section to be actuated. The cable is then routed outward along the inside of the outer section around a pulley located at the outer end of the outer section. The cable is then routed along the outside of the outer section and wrapped around a cable drum several times. Next, the cable is routed around a pulley and into the base end of the outer section. Finally, the cable is connected to the base end of the inner

section. A motor initiates extension and retraction by rotating the cable drum clockwise and counterclockwise, respectively. Additional telescopic sections can be actuated using the single cable drum and a more complex cable routing.

The principle advantages of this design are its simplicity, lightweight construction and corresponding low cost. The principle disadvantage is low accuracy associated with cable compliance and winding on the drum.

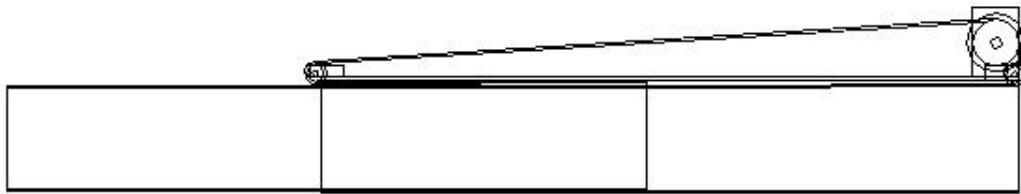


Figure 3.2 - Cable-Pulley Actuation Method

3.2.2.2 Parallel Screw Configurations

Parallel screw configurations are another common method used in telescopic applications. Figure 3.3 is a patent sketch of a parallel configuration. This design incorporates a series of ball/lead screws aligned parallel within the telescopic sections. The screws are connected such that rotation of the first screw causes rotation of the remaining screws at the same rate. To actuate the sections, each screw's nut is connected to the corresponding section, i.e. the first screw's nut to the first telescopic section. In addition the subsequent screws are connected to the previous sections such that they extend along with the sections. For example, in Figure 3.3, the first screw is rotated causing the second screw to rotate simultaneously. The first screw's nut is attached to the first telescopic section causing it to extend. The second screw is also attached to this section causing it to extend simultaneously. The second telescopic section is then extended by the second screw's nut, fixed to the second section.

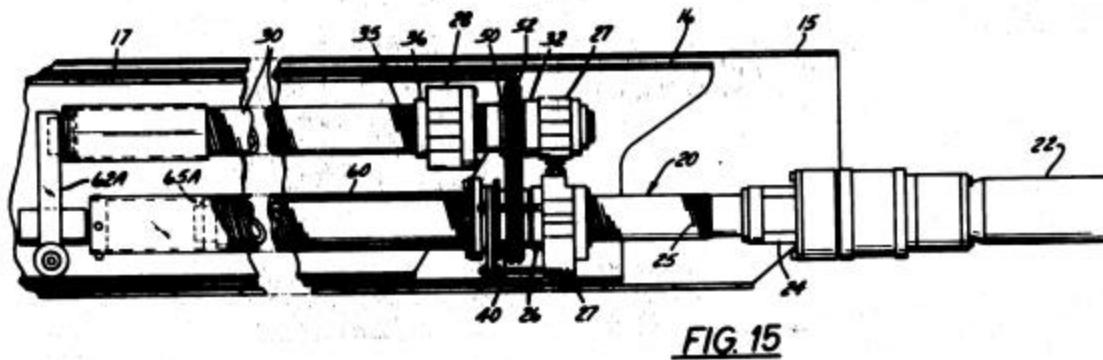


Figure 3.3 - Parallel Screw Configuration (U.S. Patent: 4337868)

This design offers advantages over cable-pulley methods in increased accuracy and robustness. However, this design includes disadvantages in large space requirements and high system backlash.

3.2.2.3 Telescopic Hydraulic Cylinders

Telescopic hydraulic cylinders, as shown in Figure 3.4, are another method commonly used in telescopic crane booms, and other industrial applications. Telescopic cylinders are composed of a series of prismatic hollow tubes concluding with a smallest solid rod. As fluid enters the cylinder, the solid rod is pushed outward, subsequently pulling the nested hollow tubes along with it.

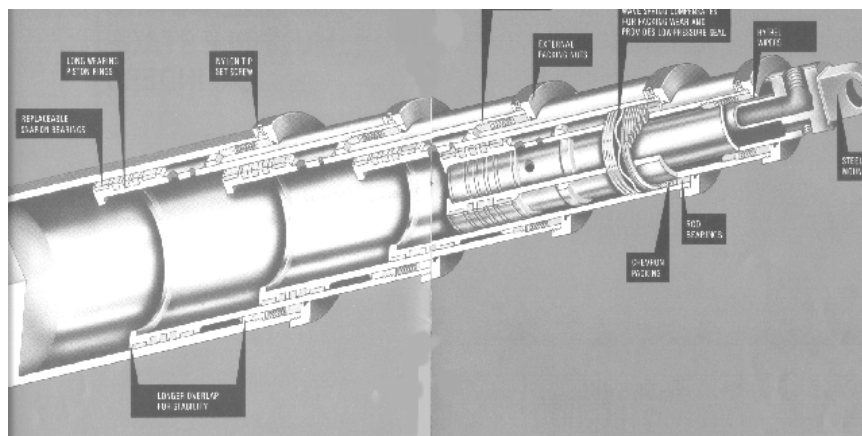


Figure 3.4 -Telescopic Hydraulic Cylinder

Advantages of this design include commercial availability, robustness and simplicity of design. However, there are associated disadvantages of telescopic hydraulic cylinders. The first

is the lack of constant velocity motion due to volumetric changes within the cylinder through extension and retraction. In addition, in order to obtain accurate positioning from the cylinder, an external measurement device and complex hydraulic control would be required.

3.2.2.4 Telescopic Screw Actuator

To alleviate many of the above problems, a novel design was invented in which a series of screws could be nested together in a prismatic manner. The idea incorporates the accurate positioning of a parallel screw mechanism with reduced backlash and the space saving features associated with telescopic hydraulic cylinders. The original conceptual design included the use of a series of nested prismatic ball screws, each of the same lead, interconnected such that rotation of the largest screw's nut would cause constant velocity translation of the smallest screw which is fixed from rotating. This is best described for a simple actuator, Figure 3.5, consisting of two ball screws. A base tube is connected to a drive motor at its base end and to the nut of the largest screw at its outer end. The largest screw is then threaded within its nut such that it resides within the base drive tube. The smaller screw's nut is then attached to the outer end of the intermediate screw and a hole is drilled throughout this screw to allow for the smaller screw to pass within. Next, the smaller screw is threaded into its nut such that its base-end resides within the larger screw. Finally, the outer end of the smallest screw is attached to the item to be actuated, thus restricting its rotation. If each of these screws are of the same lead, simply turning the base drive tube will cause three possible scenarios, all of which will result in the same constant velocity translation of the smallest screw.

The first scenario is that rotation of the base drive tube, and thus the larger nut, causes pure translation of the larger screw. Therefore, the smaller screw's nut will not rotate causing the larger screw and the smaller screw to translate as a rigid body. The actuator will continue to extend until the larger screw approaches its end-of-travel, at which point an energy absorbing stop will cause the larger screw to rotate and cease to translate. The rotation of the larger screw will then cause the smaller screw to translate with respect to the larger screw until the desired position is reached.

The next possible scenario is that the larger screw rotates with the base drive tube until the smaller screw reaches its end-of-travel. At this point, an energy absorbing stop on the smaller

screw will stop the larger screw from rotating, causing it to translate until the desired position is reached.

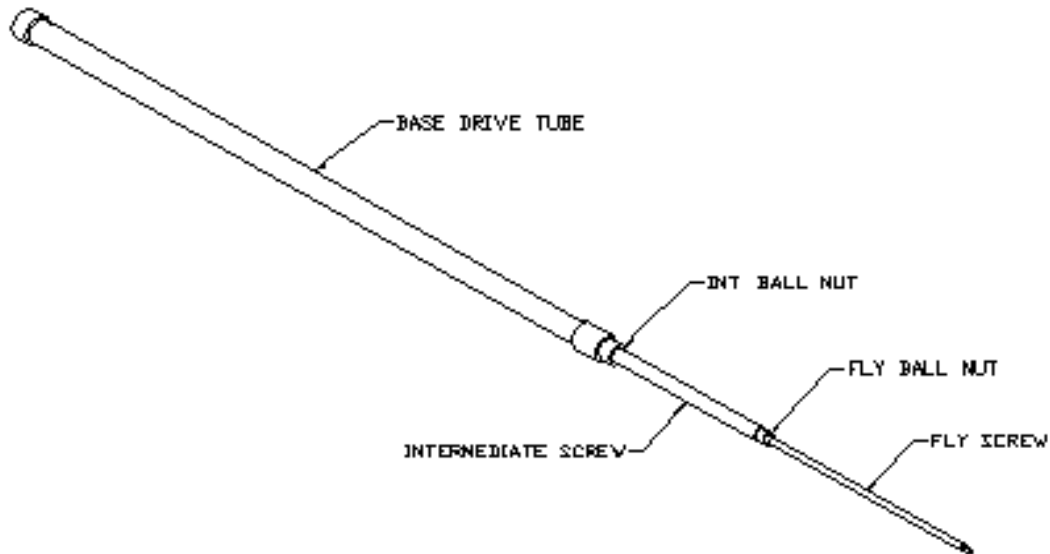


Figure 3.5 - “Floating” Telescopic Screw Actuator

The final scenario is a combination of the two absolute velocity scenarios. The larger screw rotates at a slower rate than the base drive tube such that it translates and rotates. Therefore, each screw will translate with respect to its nut until the desired position is reached.

Determination of which scenario will prevail will depend on several factors including friction, accelerations, and telescopic position. However, due to the fact that both of the screws are of the same lead, the actuation will always result in a translation proportional to the input drive tube angular velocity and the lead of the screws. This method was referred to as the floating prismatic actuator, due to the fact that the larger screw’s position is uncertain.

The advantages of this design include its simplistic, robust design that allows for accurate positioning with low backlash over an extended reach. In addition, the design offers the same space saving advantages associated with telescopic hydraulic cylinders.

There are a few disadvantages associated with the “floating” nature of the larger screw. The first is that high-speed travel is limited due to the fact that the screws are often extended to their end-of-travel limits. At these locations, a tremendous amount of energy is required in accelerating and decelerating the larger screw. This energy must be absorbed in the stops at each screw’s end-of-travel, leaving the possibility that the screw’s may jam and become locked. The

second disadvantage is that the rotational inertia of the arm varies greatly with the location of the larger screw. Since this location is uncertain, there was concern as to whether control of the arm's rotational motion would be jeopardized.

Therefore, the telescopic actuator concept was revised to include a means of "controlling" the larger screw. By placing a slotted tube inside the base drive tube, the larger screw could be rotated through a key connecting it to the slotted tube. The slotted tube could then be rotated at a prescribed rate slower than the base drive tube. The larger screw would then be forced to translate and rotate at prescribed rates proportional to the angular velocities of the base drive tube and the inner slotted tube. This allowed the actuator to be reconfigured such that each of the screws would translate with respect to their nuts at the same rate, thus eliminating the possibility of screw overrun and jamming, within the normal operating range of the actuator. The disadvantages of this design were the increased weight, complexity and the need for a gearbox to prescribe rotation of the inner and outer drive tubes at different rates.

3.2.3 Trade-Off Analysis

Through a complete trade-off analysis, Table 3.2, the conceptual designs were evaluated based on the previous weighted specifications in order to determine the most ideal design. The results of the trade-off analysis concluded that the "controlled" telescopic ball screw actuator was the most ideal with the "floating" design as the second most ideal design. It was determined that the "controlled" actuator design had benefits that outweighed its increased complexity and cost. These benefits included its improved controllability and protection against screw jamming due to overrun at high speeds.

	Weighting (1-10)	Cable Extension			Hydraulic Cylinder			Parallel Screw Configuration			"Floating" Telescopic Screw			"Controlled" Telescopic Screw		
		Rating	Score	Total	Rating	Score	Total	Rating	Score	Total	Rating	Score	Total	Rating	Score	Total
Efficiency	6	high	5	30	med	3	18	low-med	2	12	high	5	30	high	5	30
Accuracy	10	low-med	2	20	low	1	10	med	3	30	high	5	50	high	5	50
Backlash	10	med-high	2	20	high	1	10	med-high	2	20	low	5	50	low	5	50
Constant Velocity	10	yes	5	50	no	1	10	yes	5	50	yes	5	50	yes	5	50
Robustness	7	low-med	2	14	med-high	4	28	med-high	4	28	low-med	2	14	high	5	35
Max. Speed Attainable	10	ves	5	50	ves	5	50	ves	5	50	mavbe	3	30	ves	5	50
Weight	7	low	5	35	high	1	7	med	3	21	med	3	21	med-high	2	14
Mechanical Complexity	7	high	1	7	low	5	35	med	3	21	low-med	4	28	med-high	2	14
Cost	6	low	5	30	med-high	2	12	low-med	4	24	med	3	18	high	1	6
Control Complexity	8	low	5	40	high	1	8	low	5	40	med-high	2	16	low	5	40
Space Requirements	9	high	1	9	high	1	9	med-high	2	18	low-med	4	36	low-med	4	36
Commercial Availability	6	ves	5	30	ves	5	30	no	1	6	no	1	6	no	1	6
Ease of Integration into arm	6	low	1	6	high	5	30	med	3	18	high	5	30	high	5	30
Score				341			257			338			379			411

Table 3.2 - Telescopic Actuation Trade-Off Analysis

3.3 Rotational Actuation Concept Selection

Concept selection of a rotational actuation method proceeded similarly by first prescribing critical specifications. These specifications were then used as guidelines in brainstorming sessions and research to develop a number of conceptual designs. These conceptual designs were then evaluated through a trade-off analysis to determine the best conceptual design.

3.3.1 Rotational Specifications

Specifications for the rotational actuation system were developed by considering the project specifications set forth in the project conceptual design. Specifically, the rotational actuation system was to be capable of handling the maximum torque requirements, attaining the maximum speed, and maintaining the required accuracy. On a more general basis, the design should be compact, lightweight, robust, and commercially available.

3.3.2 Preliminary Concepts

3.3.2.1 Planetary Gearbox

The concept of using a planetary gearbox was formulated with consideration into the large gear reductions that are typical of planetary systems with low space requirements. In addition, planetary systems can offer high efficiency and low backlash. The planetary gearbox concept would include a set of right angle bevel gears in order to allow for the motor to be directed along the longitudinal axis of the arm. This advantage would allow significant vertical space savings. The main disadvantage of this design is the lack of commercial availability due to the stringent torque requirements arising from OCCSM performance specifications and the extreme rotational inertia of the telescopic arm. This lack of commercial availability is an especially large factor in planetary systems resulting in a cost-prohibitive design.

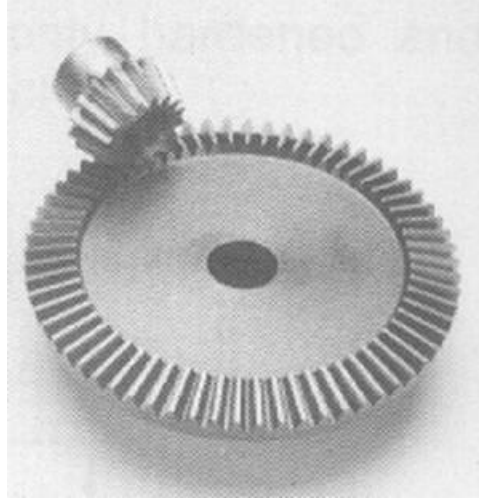


Figure 3.6 - Bevel Gear Reduction

3.3.2.2 Chain/Gear Drive

Chain and gear drives are common forms of actuation in many commercially available telescopic crane booms due to their simplistic design. Figure 3.6 shows an example of a bevel gear type drive in which the reduction ratio is about 5:1. The principle advantage of this type of design is its low mechanical complexity and associated low cost. The principle disadvantage is the large space requirements needed to achieve reduction ratios on the order of 60:1.

3.3.2.3 Hydraulic Cylinder

Hydraulic cylinders are often used in industrial machines to cause rotations. This is accomplished by placing a cylinder in a leverage position. There are a number of advantages of this design including low mechanical complexity, commercial availability and associated low cost. However, hydraulic cylinders are often difficult to use in robotics applications due to the need for external measurement devices. In addition, this type of design would require non-linear flow control to obtain constant velocity rotation of the arm.

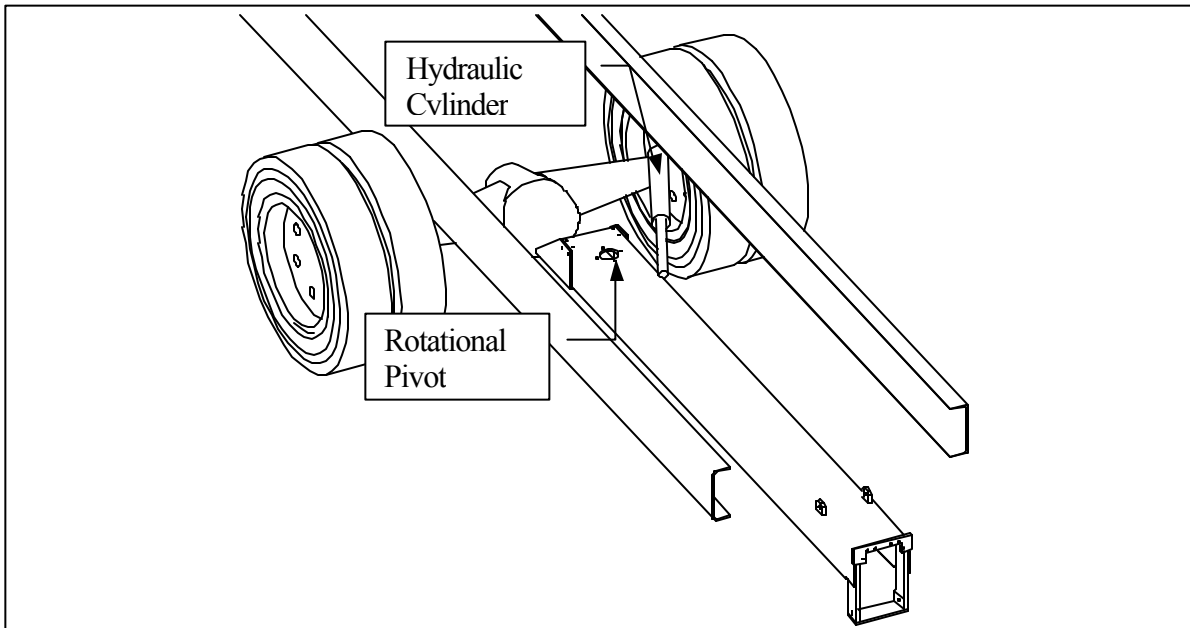


Figure 3.7 - Hydraulic Cylinder Rotational Actuator

3.3.2.4 Harmonic Drive

Harmonic drives are specialized gear reduction devices that are becoming more prevalent in robotic applications due to high reduction ratios, compact space requirements, and high torque capacities. Figure 3.8 is a detailed view of a cup type harmonic drive. The central component to the operation of a harmonic drive is an elliptical bearing known as a wave generator. The wave generator is fitted within a flexible external gear, called a flexspline. The deformed flexspline is then fitted into a rigid internal gear such that contact is only made along the major axis of the ellipse. The gear reduction is accomplished by the fact that the flexible spline contains two less teeth than the rigid internal ring gear with which it is engaged. Therefore, for each revolution of the wave generator, the flexspline will rotate slightly in the reverse direction at a ratio equal to one-half the number of teeth on the flexspline. Figure 3.9 is a sketch depicting the reduction accomplished through one-half rotation of the wave generator.

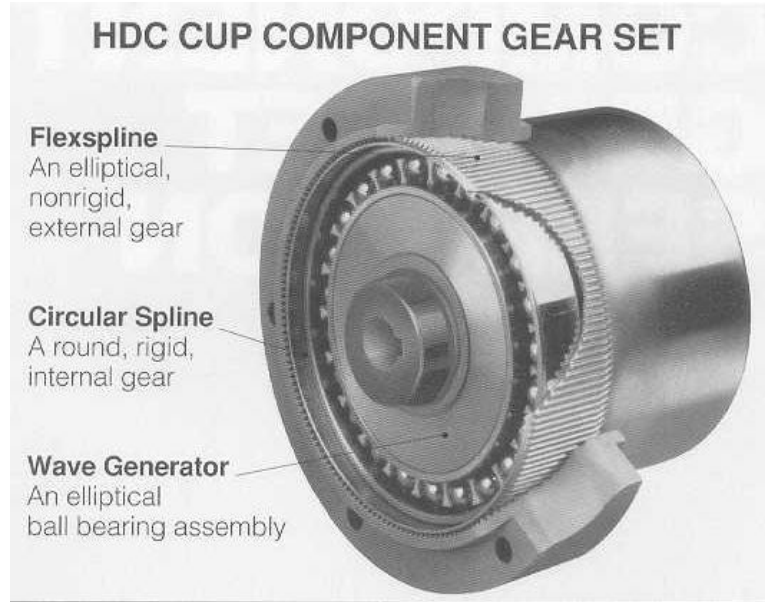


Figure 3.8 - Cup-Type Harmonic Drive

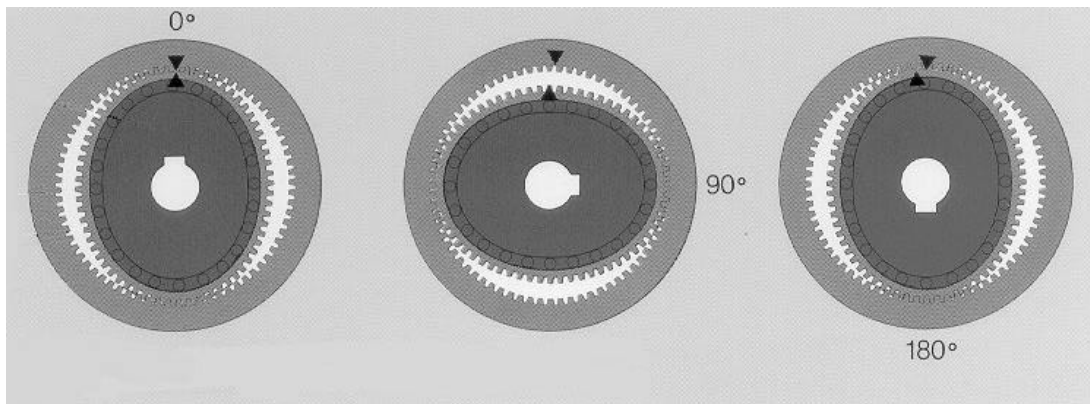


Figure 3.9 - Harmonic Drive Operation Sketch

3.3.3 Trade-Off Analysis

A complete trade-off analysis, Table 3.3, was performed in order to determine which of the above concepts would best satisfy the rotational specifications. Each of the conceptual designs was evaluated based on efficiency, accuracy, backlash, robustness weight, and a variety of other factors. The totals for each concept were summed with the totals along the bottom of the table. The highest total would reveal the best conceptual design.

3.3.4 Summary

Results of the trade-off analysis showed that the harmonic drive concept best fit the OCCSM requirements. The determining factors were the high torque capacities, low space requirements, low cost due to commercial availability, and excellent positioning accuracy. The next competing design was the chain/gear drive due to its simplicity and low weight. The major downfall of this design was its large planar space requirements.

	Weighting (1-10)	Planetary Gearbox			Chain/Gear Drive			Hydraulic Cylinder			Harmonic Drive		
		Rating	Score	Total	Rating	Score	Total	Rating	Score	Total	Rating	Score	Total
Efficiency	6	med	3	18	med/high	4	24	med	3	18	med/high	4	24
Accuracy	10	high	5	50	med/high	4	40	low	1	10	high	5	50
Backlash	10	low,med	4	40	high	1	10	high	1	10	low	5	50
Constant Velocity	10	yes	1	10	yes	5	50	no	1	10	yes	5	50
Robustness	7	med/high	4	28	med	3	21	high	5	35	low/med	2	14
Max. Speed Attainable	10	yes	5	50	yes	5	50	yes	5	50	yes	5	50
Weight	3	med/high	4	12	low	1	3	med	3	9	low/med	2	6
Mechanical Complexity	7	high	1	7	low	5	35	low	5	35	med/high	2	14
Cost	7	high	1	7	low	5	35	low	5	35	med	3	21
Control Complexity	8	low	5	40	low	5	40	med/high	2	16	low	5	40
Space Requirements	5	med	3	15	med/high	2	10	med	3	15	low	5	25
Commercial Availability	8	no	1	8	yes	5	40	yes	5	40	yes	5	40
Score				285			358			283			384

Table 3.3 - Rotational Actuation Trade-Off Analysis

3.4 Vehicle Integration and Stowage System

The conceptual design for the vehicle integration and stowage system addressed details of how the telescopic arm would be mounted onto a vehicle. This mounting would include the main pivot for the arm, an end support capable of tracking the radius generated by the end of the base section, as well as a means of stowing the arm away from the ground to aid in clearance. Specifications were developed concerning each of these subsystems, from which conceptual designs were formulated and evaluated. Using trade-off analyses, the conceptual designs were evaluated and the best concept was chosen for each subsystem.

3.4.1 Specifications

Based on the retracted length of the OCCSM telescopic arm, it was determined that the arm should mount to the rear underside of the vehicle, directly behind the wheels. When fully retracted for stowage, the arm should reside within the boundaries of the vehicle to provide for maximum protection against incidental damage. To accomplish this, it was suggested that the arm pivot up away from the road into a storage position. This would then allow sufficient ground clearance at the end of the vehicle. In addition to the stowage of the arm, the vehicle mount must also provide for an end support for the telescopic arm at all positions in the workspace. This would require a moving support that could track the radius generated by the end of the base section while providing a rigid, frictionless support. The final part of the vehicle integration system was the main pivot mount that allows the arm to rotate in the horizontal plane and the vertical plane for stowage.

3.4.2 Preliminary Concepts

3.4.2.1 Compound Slides

A simple, commercially available design was formulated which would use compounded linear slides for the end support. This idea uses multiple slides, one mounted lengthwise along the arm and a longer slide mounted transversely across the back of the vehicle. The slides are joined together such that they support the weight of the arm and provide for x - y tracking of the end radius. The advantages of this design include commercial availability, simplistic design and relatively low weight. The principle disadvantage of this design is that it does not allow for easy

lifting of the arm into a retracted position. To stow the arm using this design would require a separate system that could lift the entire slide assembly, or a system that detached the two slides to lift the arm. Another disadvantages include low robustness associated with commercially available slides.

3.4.2.2 Support Plate/Roller

Another idea that was proposed was the use of a flat plate upon which a roller, fixed on the arm, could track a radius. The plate could be located below the arm, thus allowing for stowage by simply lifting the plate upward toward the truck. Advantages of this design include high robustness, low cost and weight. Disadvantages relate to the stowage system that would require an entire separate system to lift the support plate. In addition, this support further reduces the amount of ground clearance.

3.4.2.3 Curved Rail

The last proposed idea was to use a curved rail, located on the back end of the truck. The rail would have a roller truck that would run back and forth on the rail. The roller truck would be outfitted with a set of hinged plates to connect to the arm. The system would also include a cable winch, attached to the roller truck, which would raise the arm into its stowage position. When fully dropped into its operational position, the hinged plates would extend straight and support the full load of the arm. The advantages of this design include high robustness, low cost, integrated stowage system, and no reduction in ground clearance. The disadvantages of this design are lack of commercial availability and higher mechanical complexity.

3.4.3 Trade-Off Analysis

To help evaluate the competing designs, a trade-off analysis, Table 3.4, was performed. In this analysis, the competing designs were evaluated and given numerical scores based on how well they would meet the specific design criteria. The highest scoring design was selected as the best fit based on the design criteria and weighting.

3.4.4 Summary

The trade-off analysis showed that the curved rail design best fit the specifications and weighting for the OCCSM end support and stowage system. The main benefit of this system

was the integrated, compact stowage system that provided a rigid support in the full down position. In addition, this system offered the highest ground clearance in the stowed position and the least reduction in ground clearance while in the lowered position.

The design of the rotational mount for the OCCSM telescopic arm was conceptualized to be a plate that would run between the frame rails of the vehicle. The plate would contain a hole in the center to allow for the passage of the rotational actuator system and contain a set of pivots at the interface to the frame rails to allow for stowage rotation.

3.5 Summary

This chapter has presented the conceptual design of each of the subsystems that combine to form the OCCSM telescopic manipulator. These subsystems included the telescopic arm structural design, telescopic and rotational actuation systems, and the vehicle integration and stowage system. Conceptual designs for each of these subsystems were formulated to adhere to the machine specifications through the use of trade-off analyses. These trade-off analyses helped quantify the conceptual designs to ensure the best machine design.

The next stage in the design process was to expand the conceptual designs into a fully detailed state. This will require quantifying the machine specifications on an engineering basis and localizing these constraints to each subsystem's conceptual design.

	Weighting (1-10)	Compound Slides			Support Plate/Roller			Curved Rail		
		Rating	Score	Total	Rating	Score	Total	Rating	Score	Total
Radius Tracking	10	yes	5	50	yes	5	50	yes	5	50
Commercial Availability	4	high	5	20	med	3	12	low/med	2	8
Weight	5	low/med	2	10	low	1	5	low/med	2	10
Robustness	10	low	1	10	high	5	50	high	3	30
Stowage Complexity	8	med/high	2	16	med/high	2	16	low	5	40
Maximumize Ground Clearance	8	high	5	40	low	1	8	high	5	40
Space Requirements	3	med	3	9	low/med	4	12	med	3	9
Cost	8	med	3	24	low	5	40	med	3	24
Score				179			193			211

Table 3.4 - End Support / Stowage System Trade -Off Analysis

Chapter 4: DETAILED DESIGN

The conceptual design of the OCCSM R- θ Telescopic Manipulator had been completed with formulated designs for the three main subsystems: rotational and telescopic actuation, telescopic arm structure, and vehicle integration and stowage. The next step was to elaborate these concepts and formulate a working detailed design that would meet all of the project specifications. This chapter presents this detailed prototype design in a natural progression from the conceptual design phase to form the first prototype Telescopic R- θ Manipulator, Figure 4.1.

4.1 Telescopic Arm Structural Design

The conceptual design for the telescopic arm structure was used to gain insight into the material and geometry configurations that would best meet the machine specifications. It was determined that fiber-reinforced composites would yield the highest performance, but were ruled out in this prototype design phase due to availability, cost and the need for rapid prototyping. The next best design was to use custom formed sections with properties optimized to yield the largest stiffness to weight ratio possible, and thus the smallest weight. The material and dimensions of these custom sections were selected from a detailed analysis of the beam deflection. Through this analysis, the section dimensions were optimized to yield the highest stiffness to weight ratio possible while maintaining robustness considerations. Detailed calculations for the telescopic arm structural design can be found in Appendix A, pages A-1 through A-18.

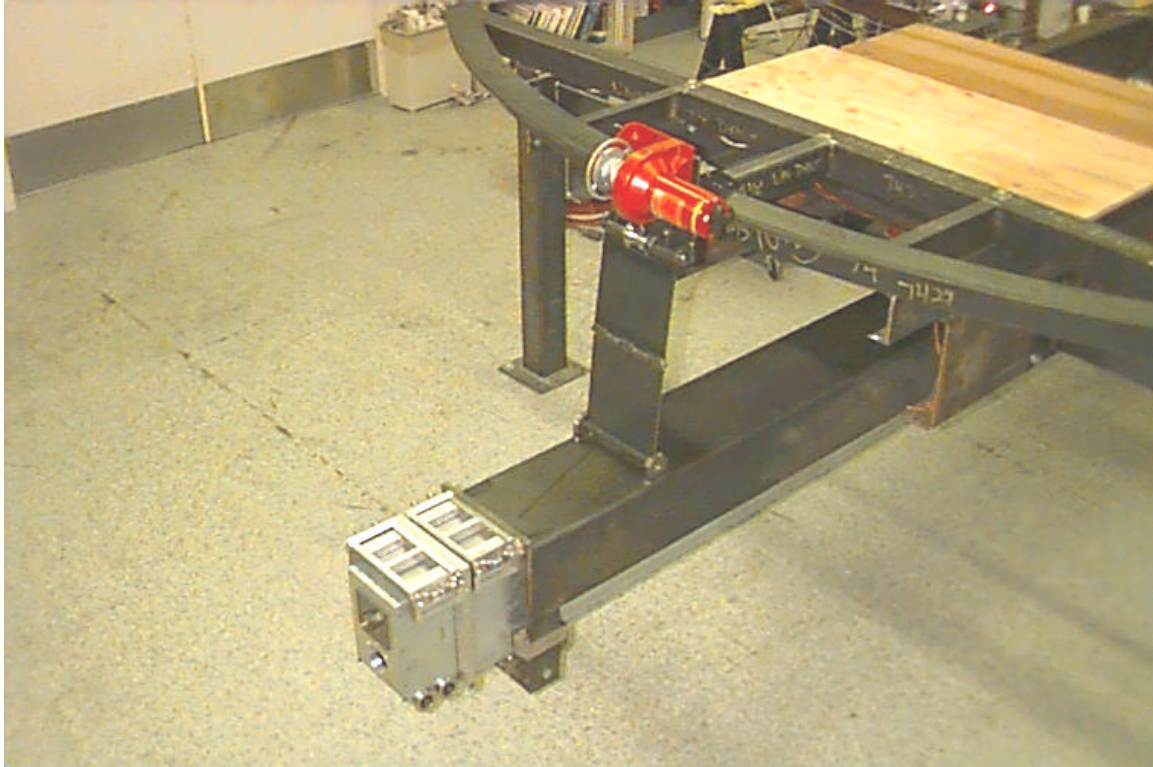


Figure 4.1 - OCCSM Prototype Telescopic Manipulator

4.1.1 Specifications

Specifications for the OCCSM telescopic arm were generated from machine and project specifications and used to determine the optimum configurations of the telescopic sections. Detailed specifications imposed constraints on the stiffness and strength of the sections such that the arm would support a 445 N (100 lb) vertical end load with less than 12.7 mm (0.50 in) deflection at maximum extension. The end loading constraint was derived from a conservative estimate of the sealant applicator weight. The deflection constraint was set in order to ensure proper actuator operation as well as ensuring high beam stiffness. Side loading was estimated to be minimal and included 89 N (20 lb) due to the frictional force of the sealant applicator and inertial loading resulting from rotational accelerations. Additional constraints on the design included robustness, controllability, and stiff joint connections between the mating sections.

4.1.2 Telescopic Sections

The design of the telescopic sections began with an examination of the detailed specifications. Through a detailed analysis of the stress and deflection of the telescopic arm, it

was determined that the critical design specification was the arm vertical deflection constraint. To optimize the design of the arm sections, a program was created in which the cross sectional and material properties could be varied. This program, Figure 4.2, used the deflection formulae, along with section properties to evaluate the end deflection of the arm. The sections' material and geometry were then iterated to determine the optimum design configuration.

After numerous iterations, the deflection behavior was generalized and several conclusions were formed. First, while limiting the material selection to aluminum, steel and titanium, it became apparent that steel would provide the highest stiffness to weight ratio, and thus produce the lightest section. This is easily seen from a comparison of the ratio of the modulus of elasticity to the density for each material. In addition, since the loading is significantly higher in the vertical plane, the sections' vertical dimensions should be larger in this direction, thus eliminating circular and square cross sections. Finally, since the beams are telescopic in nature, high wall thickness reduces the boundary dimensions of the succeeding sections and thus increases the overall deflection and weight of the arm. Therefore, it was concluded that the sections should be made of thin wall steel with vertical plane dimensions exceeding horizontal plane dimensions. In addition, examination of the section properties suggested that the heavier wall thickness at the top and bottom of the sections would further optimize the stiffness to weight ratio of the sections.

4.1.2.1.1 Base Cross Section

The design of the Base section was significantly different than that of the Intermediate and Fly sections. Low weight and high stiffness were not as crucial as the Intermediate and Fly sections due to the fact that the Base section would remain close to the pivot and be rigidly supported by the frame of the vehicle at each end. Therefore, the design of the base section was directed around the design of the Intermediate and Fly sections as well as the vehicle integration requirements.

Deflection Analysis For Beam with Varying Cross-Section									
Material: Section 1 Section 2 Section 3									
Steel Steel Steel									
Given		Reactions				Cross Sections			
End Load	P=	100	Due to P		Base(in)		Height(in)		
Dist. to Support	L0=	87	R1=	100	Lbf	Section 1:	9.375	7	
Dist. to 1st Sect.	L1=	101	M=	-26900	Lbf*in	Section 2:	6	10	
Dist. to 2nd Sect.	L2=	185	Due to w		Section 3:		5.8	8.8	
Dist. to 3rd. Sect.	L3=	269	R1=	458.0941	Lbf	lb=	41.47594	in ⁴	
Mod. of Elasticity	Eb=	3.00E+07	M=	-45917.8	Lbf*in	li=	37.825	in ⁴	
	Ei=	3.00E+07	Support		lf=		24.05475	in ⁴	
Sections	Ef=	3.00E+07	R1=	-1005.18	Lbf	X-Area1=	6.21875	in ²	
Dist. Weight	w1=	2.643688	R2=	1005.182	Lbf	X-Area2=	2.963552	in ²	
Dist. Weight	w2=	1.550722	M=	87450.84	Lbf*in	X-Area3=	2.124328	in ²	
Dist. Weight	w3=	0.72406	Net Reactions		Specific		Section 1:	0.282	
Ball Screws	Seal./Actuator		R1=	-447.088	Lbf	Weight	Section 2:	0.282	
Base Dist. Weight	w1=	0.89	R2=	1005.182	Lbf	(Lbf/in ³)	Section 3:	0.282	
Int. Dist. Weight	w2=	0.715	M=	14633.05	Lbf*in	Weight of Beam (Lbf)	314.8615		
Fly Dist. Weight	w3=	0.125			Hanging Weight(lbf)		120.5217		
Slopes and Displacements									
	Base-1 x=	87	Base-2 x=	120	Int. x=	216	Fly x=	312	
	Slope	Disp.	Slope	Disp.	Slope	Disp.	Slope	Disp.	
Due to P	-0.00158	-0.073	-0.00202	-0.13251	-0.00289	-0.37599	-0.00307	-0.67924	
Due to w(W/O SPRT)	-0.00205	-0.10433	-0.00239	-0.17803	-0.00278	-0.43267	-0.00284	-0.70429	
Support Deflect.	0.003057	0.177322	0.003057	0.278213	0.003057	0.571712	0.003057	0.865211	
Total Deflection(in.)	-0.00057	0	-0.00135	-0.03233	-0.00261	-0.23695	-0.00285	-0.51832	
Material Data									
Mat'l	Aluminum	Steel	Titanium			Constants			
E:(psi)	1.00E+07	3.00E+07	1.65E+07		C1=	194258.6	C1=	1312258	
Spec. Wt.(lbf/in ³)	0.098	0.282	0.17		C2=	-9E+06	C2=	-1E+08	

Figure 4.2 - Deflection Analysis Program

The prototype Base section design is shown in Figure 4.3. The section was made from 6.35 mm (0.25 in) thick hot roll steel plate that was formed into a C-shape, slightly closed in on the bottom surface to provide greater side wall strength as well a ledge for the rear vertical support system of the Intermediate section. The dimensions for this section were determined by iteration through the beam deflection program, as well as consideration of support constraints imposed by the Intermediate section.

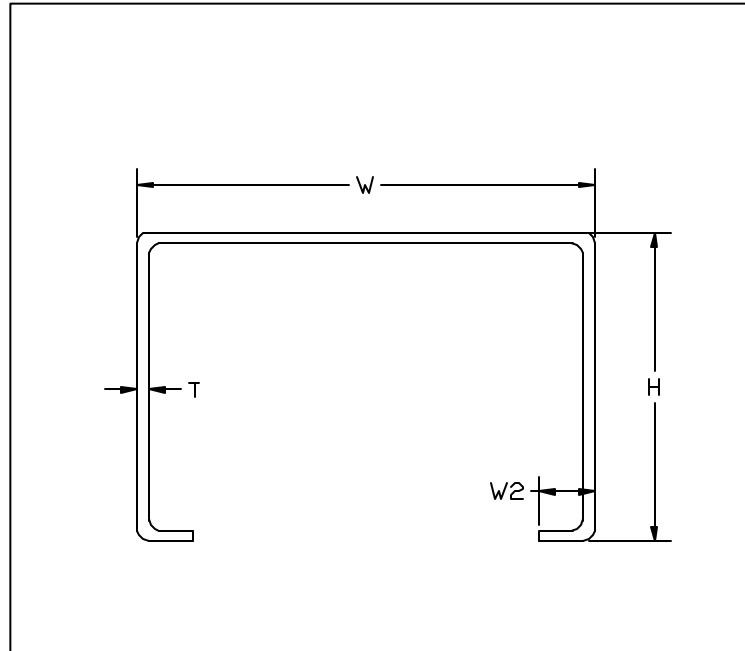


Figure 4.3 - Base Cross Section

4.1.2.2 Intermediate Cross Section

Design of the Intermediate cross section began through iteration of the developed deflection program while maintaining project specifications concerning size, robustness, and concentrated loading. Through extensive analysis and brainstorming, the Intermediate section was designed as shown in Figure 4.4. The design calls for a large thin wall U-shaped section around the top of the section which mates to a heavy short C-shaped section along the bottom. The edges of the heavy bottom structure were designed to handle the contact stresses from support rollers and provide a means of supporting the section against side loading. In addition, this overlap would allow for proper joining of the sections through a continuous resistance seam weld. In essence, the section was designed to have a large bending inertia, be lightweight, and direct all of the loading down to the thicker section base.

Specific dimensions for this section were determined through the beam deflection program such that the arm would meet the loading and end-deflection constraints. To meet these requirements, the minimum arm dimensions were as follows:

$$H=254 \text{ mm (10.0 in)}$$

$$H_2=25.4 \text{ mm (1.0 in)}$$

$$W=152.4 \text{ mm (6.0 in)}$$

$$t_2=4.77 \text{ mm (0.188 in)}$$

$$t=0.762 \text{ mm (0.030 in)}$$

4.1.2.3 Fly Cross Section

Design of the Fly section proceeded exactly as that of the Intermediate section with the exception of reduced loading. To accommodate for this reduced loading the section's bottom channel thickness and height were reduced in addition to the reduction in the overall height to fit into the Intermediate section. The wall thickness of the main beam section was kept constant with that of the Intermediate due to robustness constraints and concerns of localized sidewall buckling. The resulting dimensions for the Fly section were as follows:

$$\begin{aligned} H &= 226.10 \text{ mm (8.9 in)} & H_2 &= 14.99 \text{ mm (0.59 in)} \\ W &= 147.32 \text{ mm (5.8 in)} & t_2 &= 3.17 \text{ mm (0.125 in)} \\ t &= 0.762 \text{ mm (0.030 in)} \end{aligned}$$

where the variables were again defined as in Figure 4.4. These dimensions would produce a clearance between the Intermediate and Fly section sidewalls of 1.78 mm (0.070 in) and 0.89 mm (0.035 in) for the top and bottom edges. This clearance was kept small in order to maximize the stiffness to weight ratio of the arm.

The preceding analysis and design of the telescopic sections had been accomplished using ideal deflection calculations based on engineering assumptions that could be questioned for a telescopic beam unless the joints could be designed with adequate stiffness. Therefore, an extensive amount of work was necessary to ensure that the telescopic arm would emulate the deflection analysis.

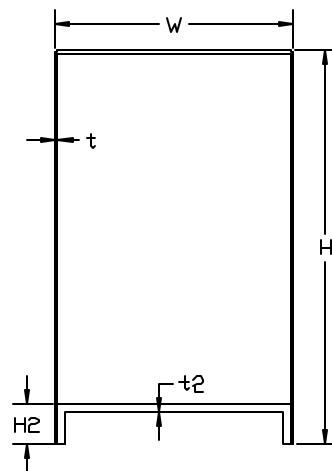


Figure 4.4 - Fly Cross Section

4.1.3 Vertical Support Systems

The joint connections were divided into two main support systems, the vertical support systems and the horizontal support systems. The vertical support systems were the most crucial in aligning the sections and ensuring that the arm would meet the deflection specifications. The first step in designing the vertical supports for the telescopic sections was to determine the loading at each of these joints. A complete analysis of this loading was performed at maximum extension of the arm to yield the largest joint loading. This loading was then used to design the primary support roller systems to handle loading at the end of the arm in the vertical down direction, and secondary support roller systems to handle loading in the vertical up direction. Due to the high loading, wear and necessary reliability of the vertical support systems, rollers were deemed necessary to ensure proper arm operation.

4.1.3.1 Primary Loading Rollers

The primary loading rollers are depicted in Figures 4.5-4.8 for both the Intermediate and Fly sections. These primary rollers were designed to handle the primary loading caused by the weight of the arm and the end load. High loading for these support rollers was distributed along the section using a series of rollers in an effort to reduce the localized contact stresses on the section. To ensure full contact between the rollers and sections, roller trucks were used wherever possible.

4.1.3.1.1 Intermediate and Fly Sections

The primary vertical support system for the Intermediate section was designed to use two pair of roller trucks, one located on the outer end of the base section, Figure 4.5, and the other pair located at the top back of the Intermediate section, Figure 4.6. The Fly section was designed to use a similar roller truck on the back of the section, Figure 4.8, with a set of fixed rollers for the outer support, see Figure 4.7. This was possible due to the reduced loading on the Fly section rollers. The roller trucks were designed to handle the specified arm loading with a factor of safety of about four based on the Maximum Shear Stress Theory. On the other hand, the rollers on the trucks were designed to carry up to five times the designed loading to allow for concentrated loading on a single roller due to misalignments.

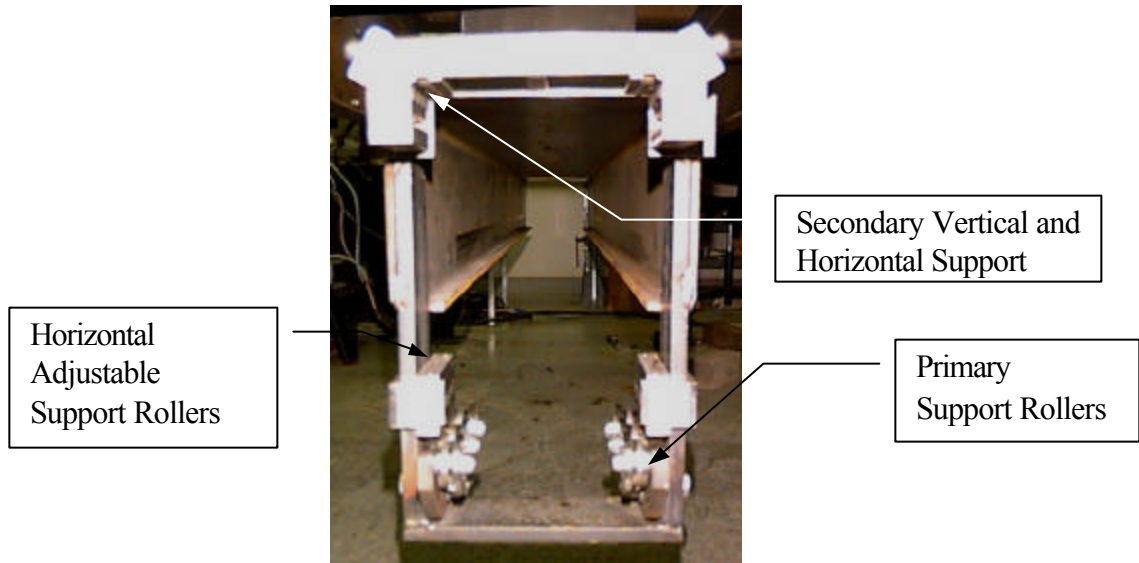


Figure 4.5 - Intermediate Section Outer Support System

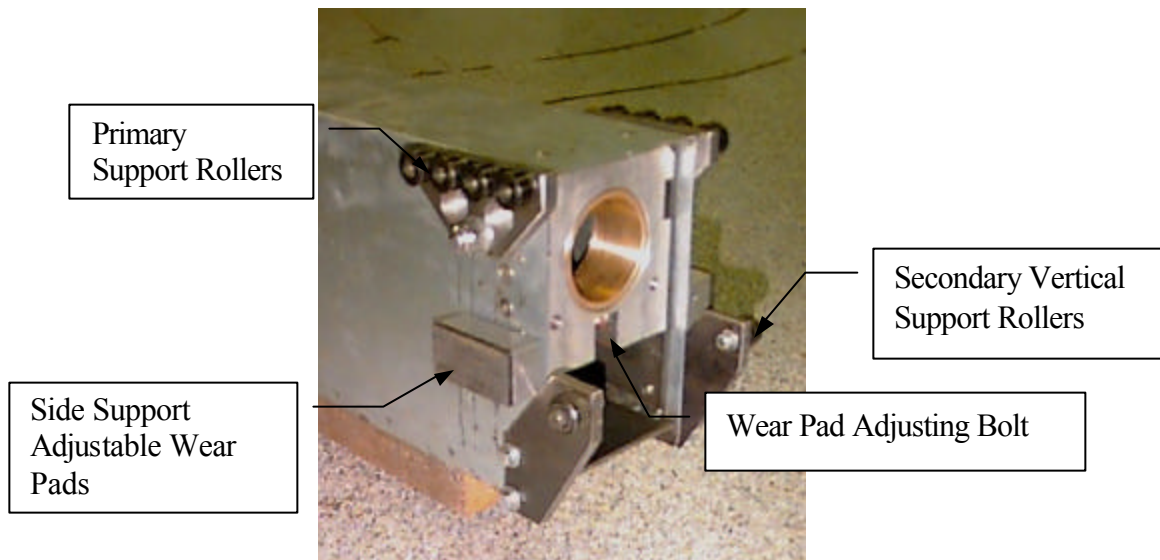


Figure 4.6 - Intermediate Section Rear Support System

A crucial part of the Fly section rear primary support was to design the roller truck such that the loading could be directed into the sidewall of the Intermediate section. This required that the roller truck be placed as close to the upper corner of the section as possible. To accomplish this, the side of the Fly section was notched out and the side support was integrated onto the roller truck, see Figure 4.8.

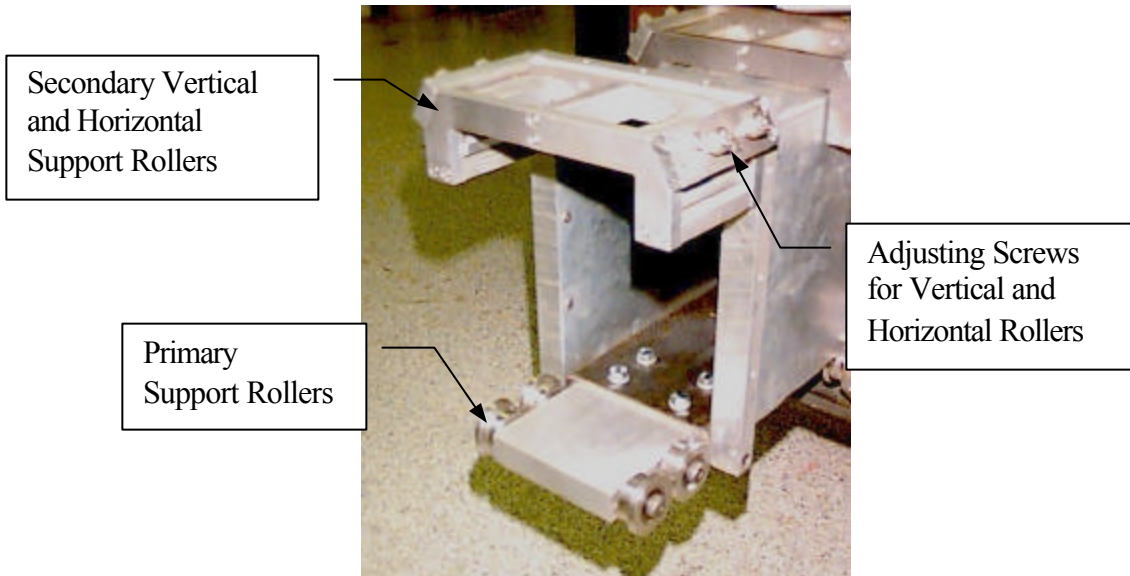


Figure 4.7 - Fly Section Outer Support System

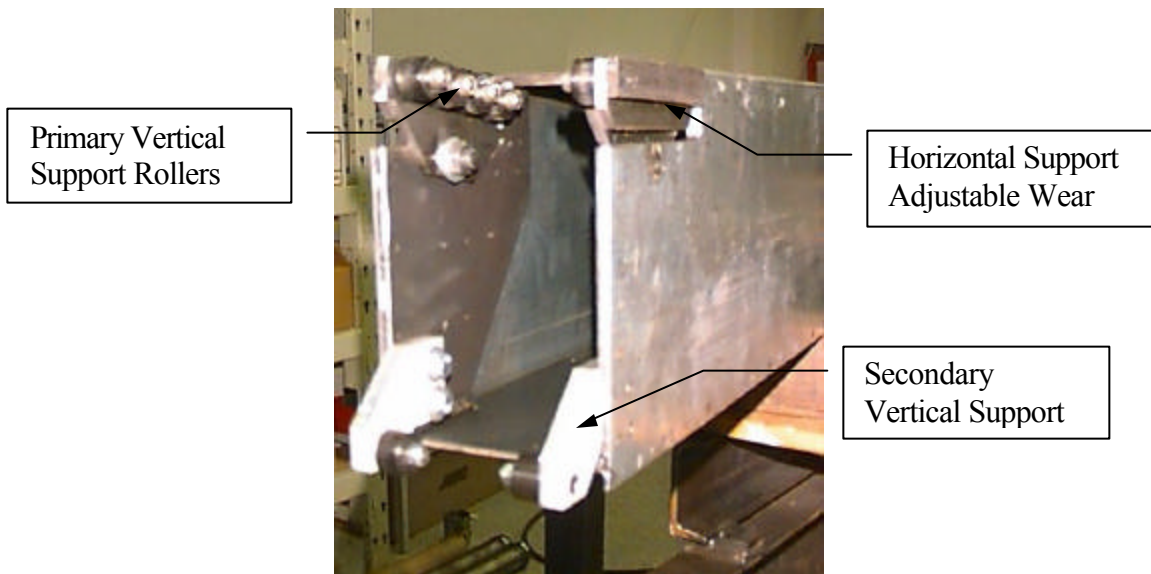


Figure 4.8 - Fly Section Rear Support System

4.1.3.2 Secondary Loading Rollers

The secondary loading rollers were far less crucial than the primary support rollers. Loading on these rollers would come from incidental upward loading on the end of the arm and from the weight of the arm sections upon retraction. The secondary support systems for each section are shown in Figures 4.5-4.8.

Lower loading requirements enabled each of these supports to be adjustable such that the arm sections could be preloaded to account for any misalignment. In addition, the outer supports for each section were designed to use the same adjustable part, with the Fly section support adjusted smaller.

4.1.4 Horizontal Support Systems

Horizontal supports for the telescopic arm are shown in Figures 4.5-4.8. These supports were designed by first analyzing the loading caused by friction between the sealant head and the road as well as acceleration loading caused during peak accelerations to the maximum velocity. As a worst case, the analysis was performed at maximum extension. These calculations yielded horizontal loading for the Intermediate section on the order of 4.45 KN (1000 lb), and on the order of 1.3 KN (300 lb) for the Fly section side supports. The designs for each section joint were then customized around the available clearances and loading to ensure a factor of safety of at least two. In addition, adjustable designs were used wherever possible.

4.1.5 Summary

The detailed design of the OCCSM telescopic arm structure began with a detailed deflection and loading analysis to ensure that the prototype arm would meet the project specifications. Through a detailed analysis of the arm cross sections and materials, it was determined that steel thin wall composite sections would be the most ideal design for the cantilevered sections. The base section included more flexibility since it remained under the vehicle where it could be rigidly supported. The resulting design of the Base section was designed around the Intermediate section constraints as well as arm deflection constraints. A program that enabled quick calculation of the end deflection for various cross sections and materials was developed and proved invaluable.

Once the sections were optimized, design began on the joint connections to ensure that the anticipated arm deflection and operation would evolve. Within this design, detailed analysis of the section loading under maximum operating parameters was performed. This analysis enabled the support systems to be designed safely and economically with factors of safety exceeding two in all components.

4.2 Telescopic Actuator System

The invention of the telescopic ball screw actuator offered large improvements over conventional linear actuation methods. As mentioned in the conceptual design phase, Chapter 3, the “controlled” ball screw actuator consisted of a series of two nested ball screws, each of different, prescribed leads, connected together with the small ball screw inside the larger ball screw. To prescribe rotation on the larger ball screw, a “split tube” was used which contained a slot down one side equal in length to the large ball screw stroke. The tube was sized to allow clearance for the large ball screw to pass within and a key was used to lock the rotation of the large screw to the split tube. The nut of the large ball screw was then connected to another shaft that enclosed the aforementioned split tube and large ball screw. To drive the two concentric shafts at different rates, a custom dual output planetary gearbox was designed. The gearbox used a single input shaft, a ninety-degree bevel reduction, and a conventional 3:1 planetary set to prescribe rotation of the actuator shafts to obtain constant velocity extension for each screw with respect to their ball nuts. The principle advantage of this design was the elimination of jamming and overrun during normal operation.

With the concept in hand, the next step was to determine the exact specifications of each of the components in order to achieve the desired actuator performance. Detailed calculations concerning the design of the Telescopic Actuation System may be found in Appendix A, pages A-25 through A-40.

4.2.1 Specifications

Numerous specifications were developed to guide the design of the telescopic actuator system. General stroke specifications required the actuator to have a stroke equal to 4.03 m (159.0 in) in order to reach the outer corner of a 3.6 m (12 ft) square workspace. On a performance level, the actuator was required to operate at a maximum speed of 0.91 m/s (36 in/s) with acceleration time of 0.5 seconds. In addition, the actuator was required to perform with sufficient accuracy to position the sealant head throughout the workspace within 3.1 mm (0.125 in) with minimal backlash. Once the design was started, more specific specifications were developed to ensure smooth motion of the arm. A major concern for the actuator of this long length was rotational vibrations associated with support misalignments. Adjustable supports were required to address these misalignment concerns.

4.2.2 Telescopic Ball Screw Actuator Design

4.2.2.1 Ball Screw Selection

The selection of the appropriate ball screws for this design began with analysis into the required performance specifications. The high velocity requirements and support misalignments necessitated ball screws of very high lead in order to avoid whip of the Intermediate screw. Additional geometry constraints imposed by the telescopic nature of the screws were used to size the diameters of the screws. To meet these specifications, the Intermediate ball screw was selected with a diameter of 50.8 mm (2.0 in) and a lead of 50.8 mm/rev (2.0 in/rev). The Fly ball screw was then selected with a diameter of 25.4 mm (1.0 in) and a lead of 25.4 mm/rev (1.0 in/rev). The ratio of the leads was arbitrary and was selected as a ratio of the Intermediate/Fly equal to two based on commercial availability.

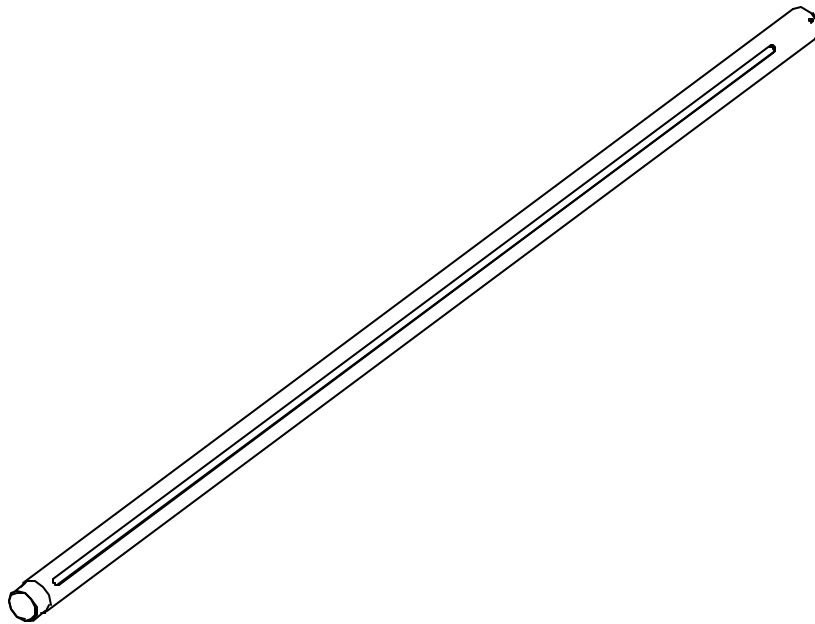


Figure 4.9 - Split Tube for Driving the Intermediate Ball Screw

4.2.2.2 Ball Screw Gun-Drilling

The telescopic nature of the actuator required a hole through the Intermediate ball screw to allow for the passage of the Fly ball screw. Concentricity of this hole was crucial to avoid

lowering the critical speed of the Intermediate ball screw. In order to fabricate the high lead ball screw with a 26.9 mm (1.062 in) hole, 2.4 m (96 in) long, through the entire screw, the screw was sent to a precision gun-drilling company. The hole was drilled to a maximum runout in concentricity of 0.381 mm (0.015 in) at the middle of the screw. In addition, the hole was drilled through the entire 2.4 m (96 in) length from one end in order to eliminate any ridges on the interior hole surface.

4.2.2.3 Drive Tube Design

With the ball screws specified, the focus shifted to the design of the two drive tubes that would cause rotation of the Intermediate ball screw and its nut. The crucial component in this design was the inner drive tube, split tube, shown in Figure 4.9, with a key slot down the length of one side to cause rotation of the Intermediate ball screw. The principle concern in this design was the torsional stress and deflection in the tube as the Intermediate screw would extend outward. A complete analysis was performed to determine the stress and deflection at the maximum driving torque. From this analysis, it was determined that deflection was more of a concern than wall thickness. However, this deflection would not result in a steady state error, rather it would result in torsional windup with a spring rate related to the stiffness of the tube. An acceptable torsional deflection of 0.0266 rad was achieved with a wall thickness of 6.35 mm (0.25 in). This torsional deflection would result in a linear windup of about 0.32 mm (0.012 in) at maximum acceleration.

The outer drive tube, see Figures 4.11a and 4.11b, was designed around the constraints of the split tube and the Intermediate ball nut. The size constraints necessitated by the split tube eliminated stress and deflection as a concern in the drive tube. This allowed the implementation of a thin wall tube with the wall thickness limited only by dimensional stability.

4.2.2.4 Actuator Supports

The actuator supports were designed to include four total supports, three of which were fully adjustable. The supports included the dual concentric output gearbox, a fixed bronze bearing in the rear of the Intermediate section, a rolling support attached to the end of the Intermediate ball screw, and a support at the end of the Fly section which restrained the Fly ball screw from

rotating. Figures 4.10 shows the fixed support in the Intermediate section and the fully adjustable Intermediate ball screw rolling support.

4.2.2.5 Actuator / Section Integration

The integration design of the actuator and sections concerned the actuation of each of the telescopic sections. The Fly screw end support was attached to the end of the Fly section to cause extension. However, a method of driving the Intermediate section still needed to be devised. It was determined that to ensure good controllability and performance, the sections should extend in a similar manner as the actuator such that each section would reach the end of its travel at the same time. This required the use of a connection plate between the end of the Intermediate ball screw and the rear of the Intermediate section. The plate was required to connect to the rear of the Intermediate due to the telescopic nature of the arm. In addition to good performance and controllability, this design optimized the strength of the arm throughout the workspace.

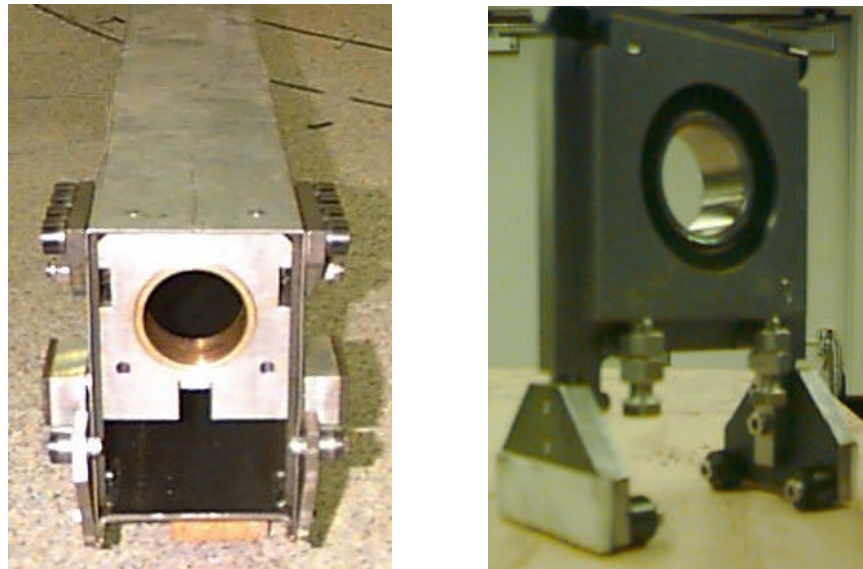


Figure 4.10 - Rear Intermediate Section Fixed Support (left) and Intermediate Ball Screw Rolling Support (right)

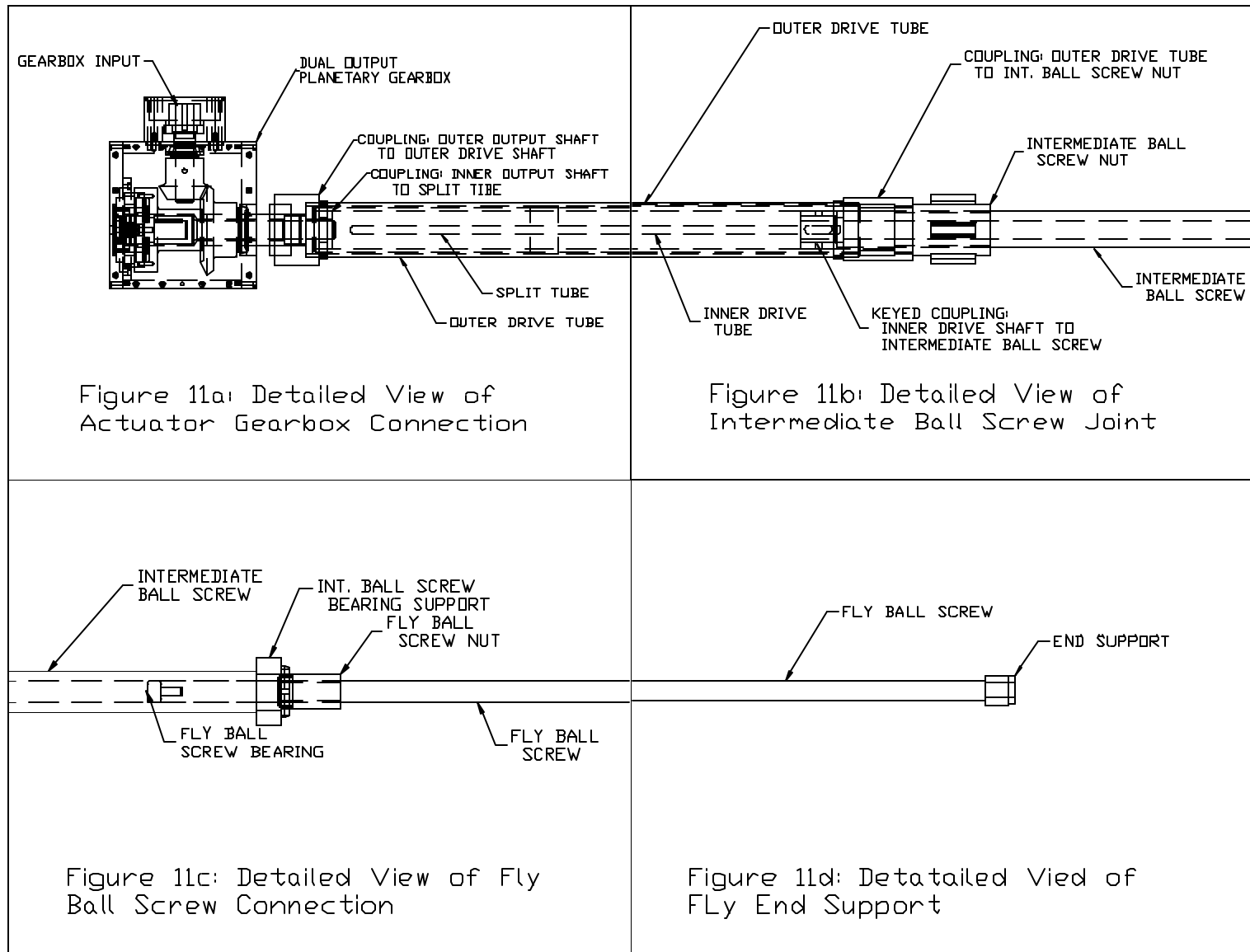


Figure 4.11 Detail Drawings of Telescopic Actuator System



Figure 4.12 - Apex 40 Servo Motor and Concentric Dual Output Planetary Gearbox Assembly

4.2.3 Concentric Output Planetary Gearbox Design

4.2.3.1 Kinematic Constraints

The detailed design of the gearbox began with specifications describing the required kinematic relationships between the input and output shafts as well as the means of achieving these relationships. From the detailed design of the telescopic actuator, it was decided to design the actuator with the smaller screw having a lead equal to one-half the lead of the larger screw. Through a simple calculation, it was shown that in order for each screw to travel out of its respective nut at the same rate, the gearbox outer output shaft should rotate at a rate of 3/2 that of the inner gearbox shaft or:

$$\frac{W_{outer}}{W_{inner}} = 1.5$$

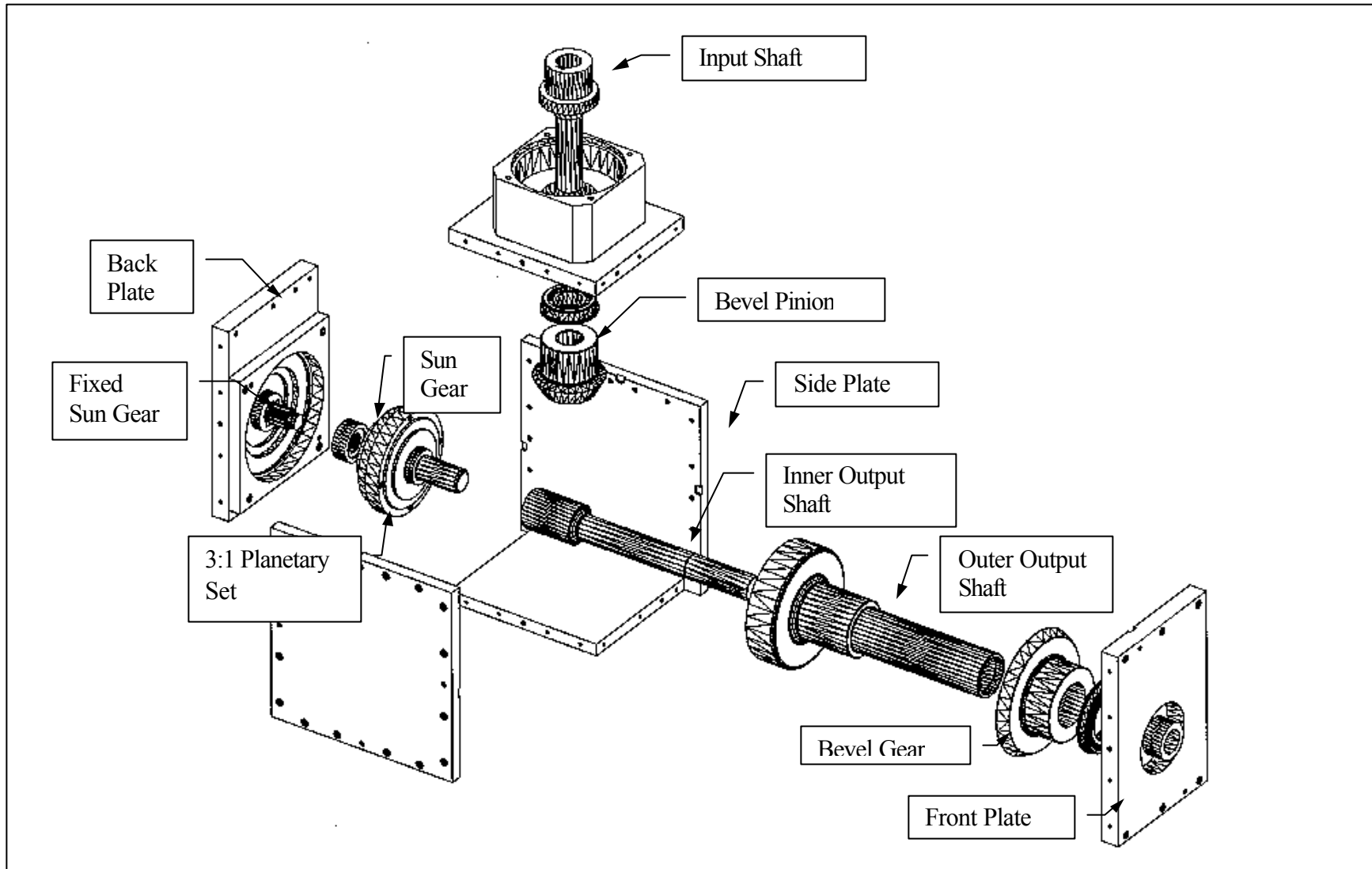


Figure 4.13 - Concentric Output Planetary Gearbox

With this constraint as a design specification, a method was to be developed to generate this relationship through concentric output shafts, with minimal backlash, and a single input.

The design selected, see Figures 4.12 and 4.13, included the use of a 3:1 (conventionally driven) planetary set, and a set of 2:1 reduction bevel gears. The input shaft entered in through the top of the gearbox and drove the pinion of the 2:1 bevel gear set. The gear of this bevel gear set was mounted directly onto the outer output shaft such that the outer output shaft is constrained by the relation $w_{out} = \frac{1}{2}w_{motor}$. The other end of this output shaft was then connected to the ring gear of the conventional 3:1 planetary set. The sun gear of this set was then fixed providing the inner output shaft to be driven by the planet carrier. Therefore, the inner output shaft was constrained according to the kinematic relation, $w_{inner} = \frac{1}{3}w_{motor}$. Therefore, the required kinematic constraints for the output shafts were satisfied.

4.2.3.2 Detailed Design

The kinematic analysis had yielded a general description of the gearbox components. However, the sizing of these components had yet to be determined. The first step was to calculate the required gearbox input torque and speed based on machine specifications and the previously developed gearbox kinematics. Through this analysis, it was determined that the required motor torque was 4.95 N-m (44 in-lb). The required input speed was then calculated to be 339 rad/sec (3240 rpm). These values were then used to select appropriate gear sets for the bevel gear reduction as well as the planetary set.

4.2.3.2.1 Bevel Gear Selection

The bevel gear set was chosen through use of manufacture's ratings as well as a detailed failure analysis based on tooth bending stresses and contact stresses. It was determined that a hardened 2:1 bevel gear set with a 127 mm (5.00 in) bevel gear would provide a factor of safety of about 2 for each of the two critical failure modes. For the tooth bending stress, the peak torque and speed were used to determine the factor of safety, while for the contact stresses (wear), the continuous duty torque and speed were used.

4.2.3.2.2 Planetary Gear Selection

Due to the limitation on fabrication of custom planetary gear sets, the gearbox was designed to use a 3:1 planetary set out of a commercially available Bayside® RA-115 gearhead. Strength and wear considerations were then derived from the manufacturer's specifications by examining the rated input torque and speeds.

4.2.3.2.3 Input Shaft

With the gear sets determined, the next step was to size the shafts that would connect them. The sizing of the input shaft was determined by the bore of the bevel pinion, torque and deflection considerations. Through a detailed calculation, it was determined that the critical design specification was not torque or deflection related. The only critical design factor was geometry. Therefore, the input shaft was sized to meet requirements of other connecting parts, such as the bevel pinion, the motor output shaft, input bearings, and the motor adapter plate.

4.2.3.2.4 Outer Output Shaft

The outer output shaft sizing proceeded in a similar manner as the input shaft with similar results. The fact that the outer output shaft had to contain the inner input shaft within, caused the dimensions to be large enough such that the stress and strain of the shaft became insignificant under the required gearbox loading. Therefore, the outer output shaft was optimized to allow for easy mating to the planetary ring gear, the bevel gear, bearings, as well as the actuator base tube. The ring gear was connected to the outer output shaft through a set of four 4.77 mm (0.188 in) diameter steel dowel pins. The bevel gear was then connected to the middle of the output shaft through a standard keyway and set screw configuration. Finally, the connection to the base tube of the actuator was attained through the application of a self-centering, tapered, locking bushing.

4.2.3.2.5 Inner Output Shaft

The final shaft within the gearbox was the inner output shaft. This shaft was simply an extender shaft for the original output shaft of the 3:1 Bayside® planetary set. The sizing of this shaft was based on a peak torque of 14.9 N-m (132 in-lb) and minimal angular deflections. Connections to the shaft included a keyed connection to the planetary set with a setscrew and a

taper pin connection to the actuator split tube. Both of these connections were designed to hold at maximum operating torque with a factor of safety of two.

4.2.3.2.6 Bearing Selections

The bearing selection became rather limited with the addition of a bevel gear reduction into the system. This created the need for axial as well as radial support in the shaft connections. To handle this combined loading, the gearbox was outfitted with a series of tapered roller bearings. The fact that the shafts were quite large eliminated the possibility of overloading the bearings and introduced a more crucial problem, underloading the bearings. If the bearings were to be loaded under the critical minimal loading, the rollers would begin to slide instead of rolling along the races. This would cause premature failure of the bearings due to wear. Therefore, the critical design specification for the bearings was to keep the loading above the minimal required loading through preloading and proper sizing. Through a detailed analysis, it was shown that the bearings would have a low enough load for virtually infinite life and were loaded enough to maintain rolling contact between the rollers and races.

4.2.3.2.7 Gearbox Housing Design

The design of the gearbox housing was centered around the two gear set arrangement and their corresponding supports. Due to the large size of the gearbox, it was decided to fabricate the box out of assembled aluminum plates. This would keep the cost and weight low. However, additional problems would need to be addressed to maintain proper gear alignment. To help ensure this proper alignment, the gearbox plates were machined from cast aluminum tool plate that is known for its great dimensional stability and flatness. On the other hand, this tool plate had disadvantages associated with weak threads on tapped holes, the inability to be anodized, and high malleability.

In addition to selecting a stable material to machine the plates, additional steps were taken in the design to ensure proper gear alignments. Dimensions for the prototype plates were all specified from a common edge as to eliminate the possibility of tolerance accumulation. Finally, alignment pins were provided to allow for proper reassembly to the original state.

Stresses in the gearbox housing exist only from the axial loading produced by the bevel gear set as well as the tapered roller bearings. These loads were calculated and were eliminated as a

critical design factor in the gearbox housing. Therefore, the gearbox housing wall thickness was determined by the bearing widths, seals, and other constraints associated with the internal gearbox components.

4.2.3.2.8 Lubrication

Lubrication specifications were derived by examining the operating speeds of the gearbox as well as maintenance considerations. Through this analysis, it was determined that the gearbox components would operate at a low enough speed as to allow for conventional grease. Grease was preferable to minimize leakage along the plate seams as well as ease the process of disassembly of the gearbox. The only question was whether the grease would work as well as oil in lubricating all of the components. There was concern that the grease would flow to the bottom of the gearbox away from the bevel gear areas. This would cause a shortage of grease for the bevel pinion.

Figure 4.14 shows an inside view of the gearbox after approximately 5 hours of use. From this picture, it was determined that the grease was remaining around the gears and that proper lubrication was achieved.

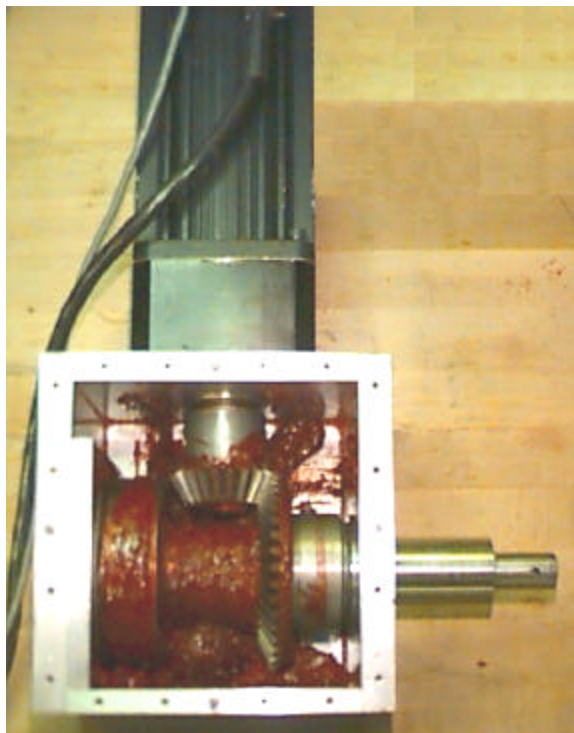


Figure 4.14 - Telescopic Gearbox after Five Hours of Operation

4.2.4 Summary

The design of the novel dual concentric output gearbox began from a specification of the required output kinematics and proceeded through detailed analysis and thought to form a complete working prototype. The key to the gearbox was the application of a conventional 3:1 planetary gearbox that was taken from a production gearhead. This gear set was driven through the ring gear, with the sun gear fixed to prescribe motion to the inner output shaft. On a detailed basis all gears, shafts and bearings were sized accordingly to ensure long life and high robustness.

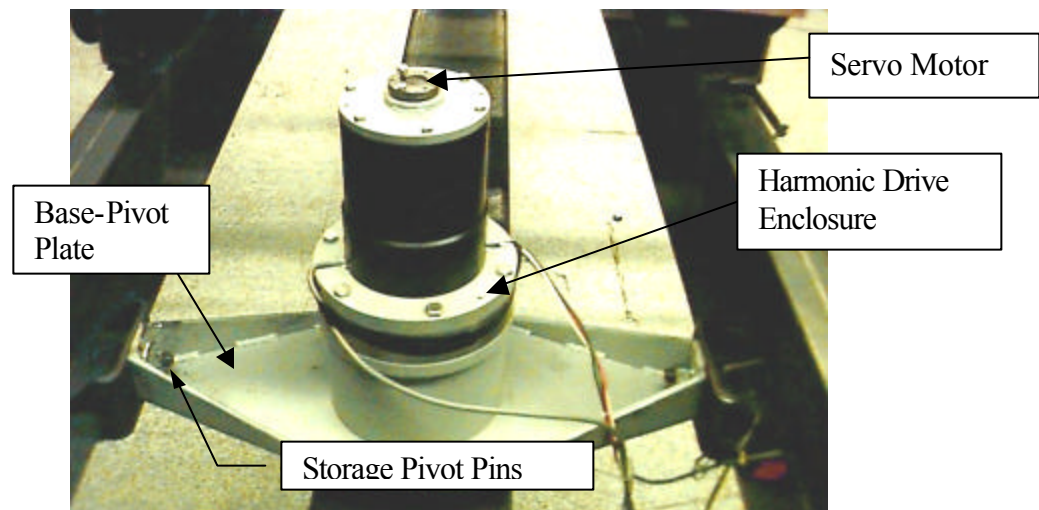


Figure 4.15 - Rotational Actuator System

4.3 Rotational Actuator System

Detailed calculations for the Rotational Actuation System can be found in Appendix A, pages A-19 through A-25.

4.3.1 Specifications

Design of the rotational actuation system, Figure 4.15, began with calculations of the necessary torque requirements to meet the machine specifications. Within these calculations, two critical operating scenarios were considered. The first scenario is at maximum extension where the rotational inertia of the arm is the largest but the angular acceleration is the lowest. The second scenario occurs at the minimum extension where the rotational inertia is lowest and the angular acceleration is highest. Through a detailed analysis, the first scenario at maximum

extension was proved to require the highest torque. The maximum required torque to actuate the arm to 0.91 m/s (3 ft/s) in 0.5 seconds was calculated to be 895 N-m (7951 in-lb).

In addition to handling the torque requirements of the arm, the rotational actuator must be capable of maintaining the required accuracy. To maintain this accuracy, two factors were considered, backlash and encoder resolution. Both of these factors affect the accuracy of the arm at maximum extension. Therefore, a large gear reduction should be used to increase the accuracy.

The final specifications used to design the rotational actuation system concerned robustness, size, weight, cost and commercial availability. Through the extensive trade-off analysis, it was shown that the harmonic drive gear reducer would best satisfy these specifications and be capable of attaining the required torque and accuracy.

4.3.2 Harmonic Drive Selection

The harmonic drive, Figure 3.8, was chosen because of its high gear reduction capabilities, compact space requirements and low backlash. This section presents the selection of the appropriate model for this application. The details of operation will not be discussed further here, the reader is referred to Chapter 3 for a detailed explanation.

4.3.2.1 Torque Requirements

The selection of the appropriate harmonic drive was performed concurrently with the selection of the motor. The torque calculations yielded a maximum required torque of 895 N-m (7951 in-lb). The harmonic drive was then selected such that the rated output torque would not exceed this value. The gear ratio of the harmonic drive was dependent on the torque requirements as well as the maximum output speed of the motor. It was desired to obtain the largest gear ratio possible while still maintaining the necessary speed in order to increase the stiffness of the arm and provide better workspace accuracy. Through a careful consideration of the motor and performance specifications, a gear ratio of 60:1 was selected.

4.3.2.2 Speed Requirements

The speed requirements for the rotational joint were defined from the project specifications and the rotational velocity at minimum extension. Through a simple calculation, the maximum rotational speed of the arm was calculated to be 0.348 rad/sec (3.3 rpm), which was then

translated to an input speed of 21 rad/sec (199 rpm). From a comparison against the manufacturers acceptable speeds, it was determined that this design was well within the design limits of the harmonic drive which is rated at speeds up to 3000 rpm.

4.3.2.3 Accuracy Requirements

To determine the effect of the harmonic drive backlash on the workspace, the input backlash was transferred through the harmonic drive gear reduction and translated into a x -deviation along the road surface at maximum extension. In order to meet the project specifications, the x -deviation must be within 3 mm (0.125 in). For the Harmonic Drive - model 65, the input backlash was given as 13 arc-min. The calculation was performed to yield a maximum x -deviation of 0.43 mm (0.017 in). Therefore, the harmonic drive backlash would satisfy the project specifications.

4.3.3 Servo Motor

Selection of the proper servomotor was constrained by two factors that separated this design from conventional servo motor applications. These factors included very low speed requirements and high torque requirements. To fit this application, a Dynaserv® DR-5030B Direct Drive Brushless motor was selected. The motor specifications include a rated speed of 240 rpm and a peak output torque of 30 N-m (22 ft-lb).

4.3.3.1 Torque Requirements

The torque requirements for the servomotor were defined as before by the performance specifications as well as the gear reduction ratio. Although the selections of the motor and gear reduction unit were performed in parallel, the details are given here with the assumption of a pre-selected gear ratio. With the gear reduction specified as 60:1, a quick calculation was performed to yield the required motor torque as 15 N-m (11 ft-lb). The motor specifications rate the peak torque output at 30 N-m (22 ft-lb) with the continuous torque ratings at two-thirds of the peak value, or 20 N-m (14.7 ft-lb). Therefore, the motor will have ample torque to meet the machine performance requirements.

4.3.3.2 Speed Requirements

To determine the maximum required speed of the motor, the arm maximum speed at minimum extension was converted through the pre-selected 60:1 ratio to attain a value of 20.9 rad/sec (3.32 rev/sec). This value was then compared to the rated speed of the motor, 25 rad/sec, to ensure that the motor would be adequate.

4.3.3.3 Accuracy Requirements

The final consideration in the selection of a motor was encoder resolution. As mentioned earlier, backlash and encoder resolution were the two factors that would combine to give position error at the end-effector. The motor's encoder resolution, 278,528 steps/rev, was translated through the gear reduction ratio and the maximum extension of the arm to determine the positioning capabilities of the motor. Assuming zero backlash, the calculation yielded a positioning resolution on the workspace of 389 steps/mm (10132 steps/in), or 0.0025 mm (9.9E-5 in).

4.3.4 Summary

The design of the rotational actuator system was directed through definition of the project specifications and rotational specifications. The servomotor and Harmonic Drive selections were performed in parallel in order to obtain the most ideal configuration. With the selection of a 60:1 gear reduction and a specialized servomotor, all of the required specifications were met and exceeded. The finished system specifications include a peak torque of 1800 N-m (1320 ft-lb), maximum arm angular velocity of 25 rad/sec, with mechanical workspace accuracy of ± 0.22 mm (0.009 in).

4.4 Vehicle Integration and Stowage System Design

Conceptual design of the vehicle integration and stowage system had led to the development of an idea to use a curved rail upon which a roller truck would run to track the radius formed by the end of the base section. The arm was then connected to the roller truck through a hinged linkage. The other component of the vehicle integration included the design of the rotational pivot mount. A key part of this mount was a compound joint that would allow the arm to rotate in the horizontal plane, as well as rotate in the vertical plane for stowage between the frame-rails.

The task at hand was to transfer these qualitative ideas into a detailed working design capable of meeting all specifications. Calculations for the Vehicle Integration and Stowage System can be found in Appendix A, pages A-42 through A-43.

4.4.1 Specifications

The specifications for the vehicle integration and stowage system were separated into two categories describing the end support and the rotational pivot discretely. The end support specifications required the support to hold the arm through the entire workspace. To accomplish this, the end support was required to track the radius formed by the end of the arm. In addition, the end support must allow for a simple stowage design that is highly reliable when in the unstowed position. In other words, the end support should not require active means to maintain the vertical position of the arm.

The pivot support specifications assured that the pivot was strong enough to handle the loading of the arm at all workspace locations, provided for easy mounting of the rotational actuator, and pivoted such that both horizontal and vertical motion of the arm is allowed.

4.4.2 Base-end Pivot Plate

The pivot plate, Figure 4.15, was designed according to calculations yielding the maximum reaction force at the pivot. This force varied for different extensions with the arm creating a maximum upward force of 2.1 KN (477 lb), from Figure 4.2, to a downward force of about 0.9 KN (200 lb) at full retraction, to support the weight of the arm. Horizontal motion was achieved by direct mounting of the rotational actuator system through a hole in the plate. Vertical motion of the arm was allowed through the two pivot bolts that connect the plate to the frame-rails.

4.4.3 Curved Rail Support System

The design of the curved rail, Figure 4.16, was derived through consideration of the project specifications and manufacturing considerations. From an early stage, it was realized that the end support would be highly critical in maintaining the height of the manipulator arm with respect to the workspace. The idea to use a curved rail would require that the radius of the rail exactly match the radius tracked by the arm or the result would be up and down motion in the arm. To solve this problem, the roller truck was designed to support the arm through a moment applied onto a curved support plate, see Figure 4.17. This design used a double row of rollers

inside the roller truck to support the moment imposed by the plates extending to support the arm. Axial support for the roller truck required only a single roller that tracked the edge of the support plate. This edge was known to be capable of being accurately manufactured to the proper radius either by flame cutting or machining.



Figure 4.16 - End Support System-Curved Rail

4.4.4 Stowage System

The key component to the stowage system, Figure 4.18, was the hinged plates which allowed the arm to be raised and eliminated the need for active support when in normal crack sealing operation. To raise the arm, a cable winch was provided onto the back of the roller truck. The cable from this winch extended down behind the plates to the bottom of the lower hinge plate. As the cable was raised, the hinged plates were forced to buckle out toward the end of the arm by the shortening of the cable. The arm was then allowed to rise until the top of the base section contacted the bottom of the winch mount. A rigid connection was then made between the arm and the truck frame through a simple pin connection to ensure safe transport.

Strength considerations were addressed through a detailed analysis of the end support loading. The critical components in the design were the hinged plates and the roller truck. The hinged plates were designed to force the connecting pins into direct shear through close alignment of the interconnecting joints. Through a quick calculation of the maximum shearing stress, it was determined that 9.5 mm (0.375 in) diameter rods would be sufficient to support the

maximum loading. A factor of safety of four was calculated based on material yield strength of 372 Mpa (54 ksi) and the Maximum Shear Stress Theory.

The roller truck was analyzed in a similar manner by transferring the moment of the plate loading force into radial loading on the bearings. This allowed the bearings, shafts and plate walls to be sized accordingly. Another critical section that was addressed was that of the backbone of the roller truck. The C-shape of the roller truck under moment loading will try to open up, thus bending the backbone of the roller truck. To prevent this, the backbone was designed with a factor of safety of 2.5 based on maximum loading.

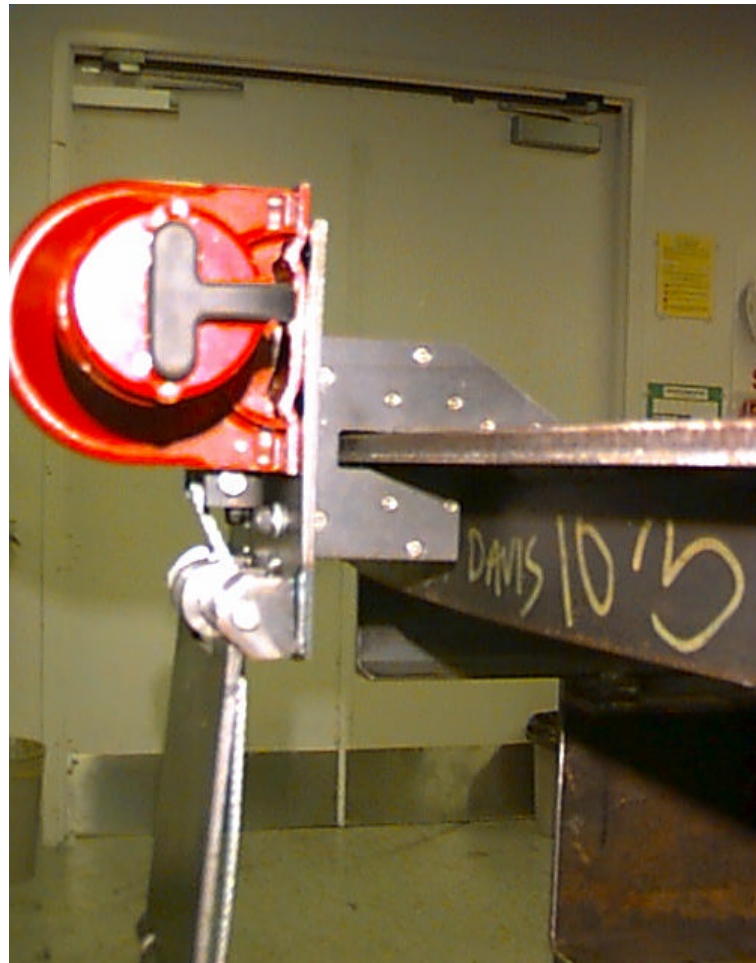


Figure 4.17 - Roller Truck Directing Loading into Curved Plate

4.4.5 Summary

The vehicle integration and stowage design had resulted in a clean and robust solution for supporting and stowing the OCCSM Telescopic R- θ Manipulator. Detailed design was initiated through a complete loading analysis to determine the maximum support loading. This loading

was then used along with the system specifications to ensure a safe design that would meet all specifications.

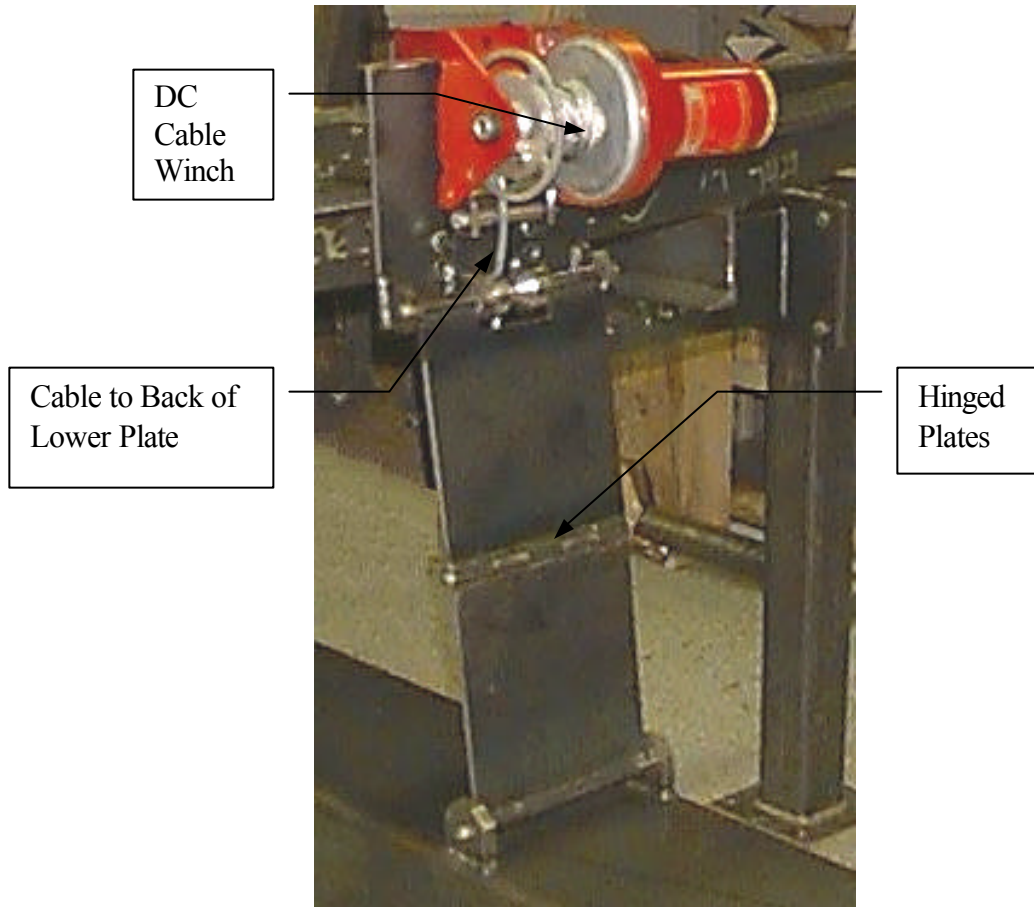


Figure 4.18 - OCCSM Stowage System

4.5 Summary

The detailed design of the OCCSM Telescopic $R-\theta$ Manipulator had been completed and the working prototype was ready for testing. The machine was designed through detailed analyses and brainstorming all in order to try to develop a machine that could perform up to specifications. From this point, Chapter 5 will be used to discuss the testing that was performed to evaluate the success of the first prototype Telescopic $R-\theta$ Manipulator. Furthermore, conclusions from these tests will be discussed on a subsystem specific level with a broader based project conclusions and recommendations presented in Chapter 6.

Chapter 5: EXPERIMENTAL VERIFICATION

5.1 Telescopic Arm Structure

The telescopic arm structure was evaluated through both qualitative and quantitative measurements. Qualitative measurements included observations based on dynamic actuation of the arm and static robustness considerations. On the other hand, quantitative testing was performed statically to determine the stiffness of the structure and the overall deflections under loading. Data from this quantitative analysis was then recorded and plotted to yield insight into the non-linear stiffness of the beam as a function of radial extension.

5.1.1 Qualitative Analysis

Qualitative analysis of the arm began at the beginning of fabrication and continued through the prototype assembly and operation. This analysis included testing of the robustness, quality, and performance of the various parts that comprised the telescopic arm including arm sections and joint connections.

5.1.1.1 Arm Sections

A major concern to be tested in the qualitative analysis was that of localized buckling in the sidewalls of the Intermediate and Fly sections. To address this concern, each of the sections was loaded in a test setup with up to three times the designed loading.

In addition to the concern of sidewall buckling, all sections were inspected to determine dimensional accuracy and integrity. Each section dimension was allowed 0.76 mm (0.030 in) deviance from nominal for the entire length. This strict tolerance was necessary to ensure that the section joints would remain in contact through the entire stroke of the arm and that the beam sections would extend out straight.

5.1.1.2 Joint Connections

The joint connections were another critical component of the telescopic arm. Qualitative analysis included inspection of the various support systems along the entire stroke of the telescopic arm. For this inspection, the aim was to ensure that the supports were contacting the sections for the entire length such that the sections had no “play” or movement in the joints.

5.1.1.3 Qualitative Conclusions

The qualitative analysis from an early stage in the project led to a major design change in the formation of the Intermediate and Fly steel composite sections. Through the localized buckling test, it was found that the 0.76 mm (0.030 in) wall thickness was too thin to support the concentrated loading at the primary support rollers. The result was localized buckling in the sidewalls directly above the center of the roller truck. This led to a revised design in which the wall thickness was increased to 1.52 mm (0.060 in). The test was successfully repeated with the improved sections with up to three times the design loading.

The other main concern was that of the welds which connected the bottom channel to the thin wall U-section for the composite beams. The original design called for a resistance seam weld along the bottom of each composite section. However, due to availability, this continuous seam weld was replaced by an array of spot welds spaced about 25 mm (1.0 in) apart. To test these welds, the sections were loaded with up to three times the designed loading. The only problems that occurred were in locations where there was poor penetration of the welds. As a result, these welds were reinforced and the testing was successfully repeated.

Finally, each section was inspected to determine dimensional accuracy. From this inspection, it was determined that great care must be taken in the manufacturing to ensure proper sizing. Each section was continuously remade until the desired tolerances were achieved.

5.1.2 Quantitative Analysis

5.1.2.1 Vertical Stiffness

The vertical stiffness at various extensions was measured by applying known loads to the end of the arm and measuring the corresponding deflection. The loading was applied through a pneumatic air cylinder for which the pressure could be varied to achieve precise force variations. To measure the corresponding deflection, a travel dial indicator was used. The results of these experiments were then recorded, see Table 5.1, for various extensions of the arm. This data was then plotted in force vs. deflection plots, see Figure 5.1, from which a linear line was fit to the data to yield the stiffness of the arm at each location. Figure 5.2 shows a plot of the arm stiffness vs. radial extension from which it is easy to depict the nonlinearity. Finally, in Figure 5.3, all force-deflection data was plotted on the same scale from which it becomes clear of the increasing stiffness as radial extension decreases due to the arm's telescopic construction.

Radial Extension(m)	Pressure (kPa)	Force (N)	Deflection (mm)
4.57	0.00	0.00	0.000
4.57	13.78	36.70	0.406
4.57	27.56	73.40	0.787
4.57	41.34	110.09	1.219
4.57	55.12	146.79	1.575
4.57	68.90	183.49	1.981
4.57	82.68	220.19	2.362
4.57	103.35	275.23	2.972
4.57	137.80	366.98	3.810
4.57	172.25	458.72	4.826
4.57	206.70	550.47	5.766
4.57	241.15	642.21	6.629
4.57	275.60	733.95	7.518
4.57	310.05	825.70	8.407
4.57	344.50	917.44	9.144
4.57	378.95	1009.19	9.982
4.57	413.40	1100.93	10.541

Table 5.1 - Force vs. Deflection Data for r=4.57m

5.1.2.2 Quantitative Conclusions

The results of the data clearly showed a nonlinear deflection characteristic for the telescopic arm. This nonlinearity is mainly attributed to the nested telescopic sections which become increasingly stiff as the arm is retracted. The data showed a slightly larger deflection at maximum extension than what was anticipated, about 135% of the predicted deflection. Possible sources of this discrepancy lie in the assumptions made for the calculations. The calculations assume infinitely stiff joints and zero support deflection, neither of which is true in the prototype arm. It was suspected that the majority of the error was occurring in deflection of the end support due to deflection of the mock-up truck frame. To quantify this, a dial indicator was placed under the end support, see Figure 5.4, and the arm was loaded at both the maximum and design loading cases at maximum extension (6.35 m (250 in)). The end support deflection for these two cases was found to be 3.2 mm (0.125 in) and 1.27 mm (.050 in), respectively. These values were then translated into vertical deflection at the end of the arm by assuming rotation about the rotational pivot point. The contribution of these deflections at the end of the arm were then calculated to be 9.7 mm (0.383 in) at maximum loading and 3.9 mm (0.150 in) for design loading. The data at this loading and extension was then corrected for the rotation and the measured deflection was found to only be 7% higher than calculated values.

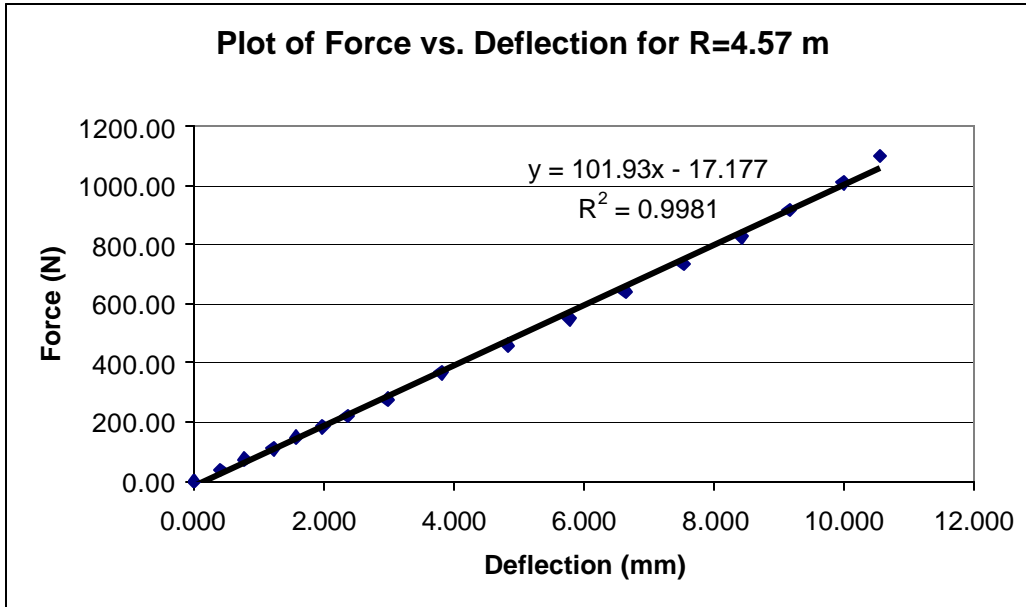


Figure 5.1 - Force vs. Deflection Plot for r=4.57m

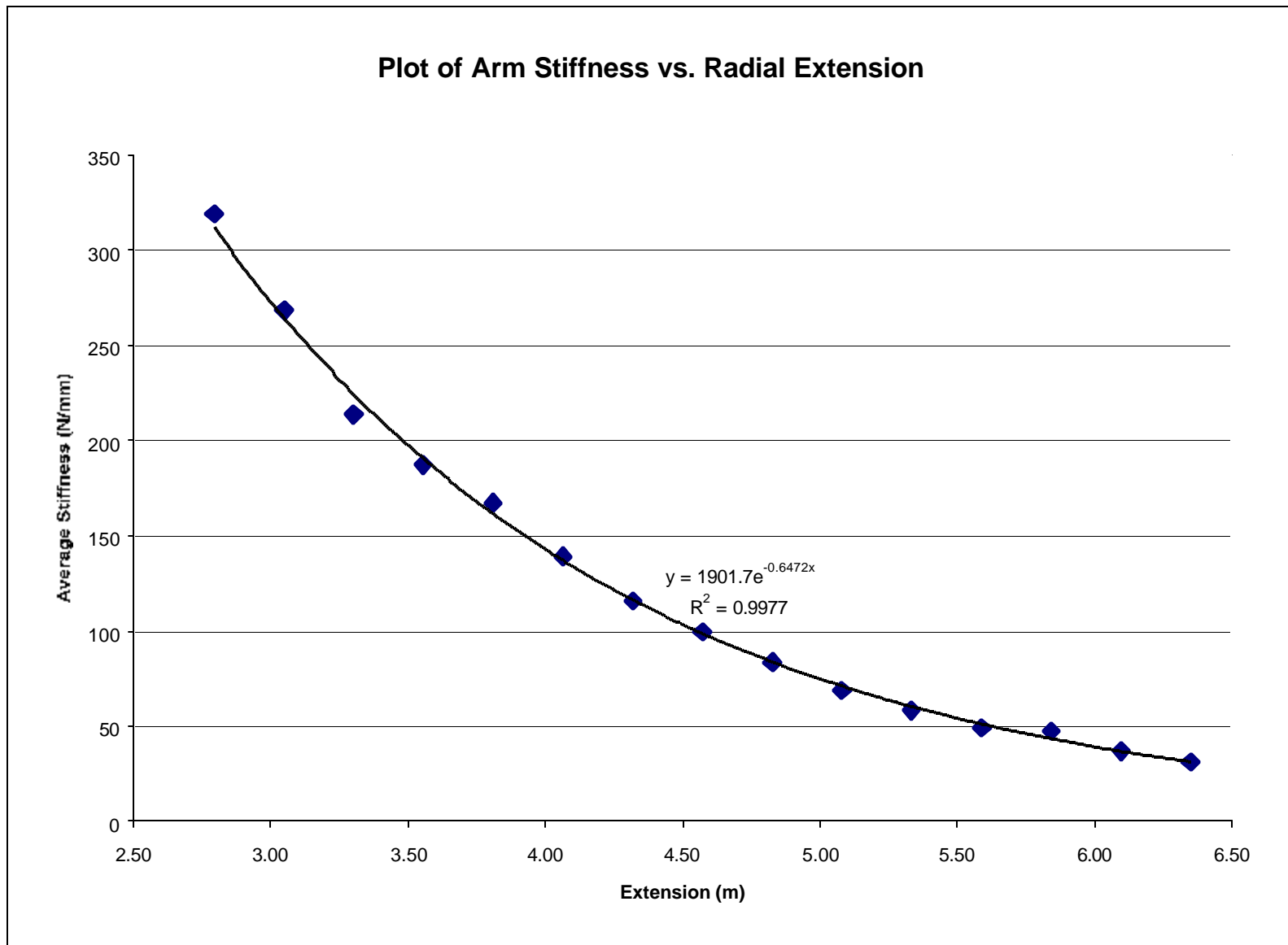


Figure 5.2 - Plot Depicting Nonlinear Stiffness of Arm

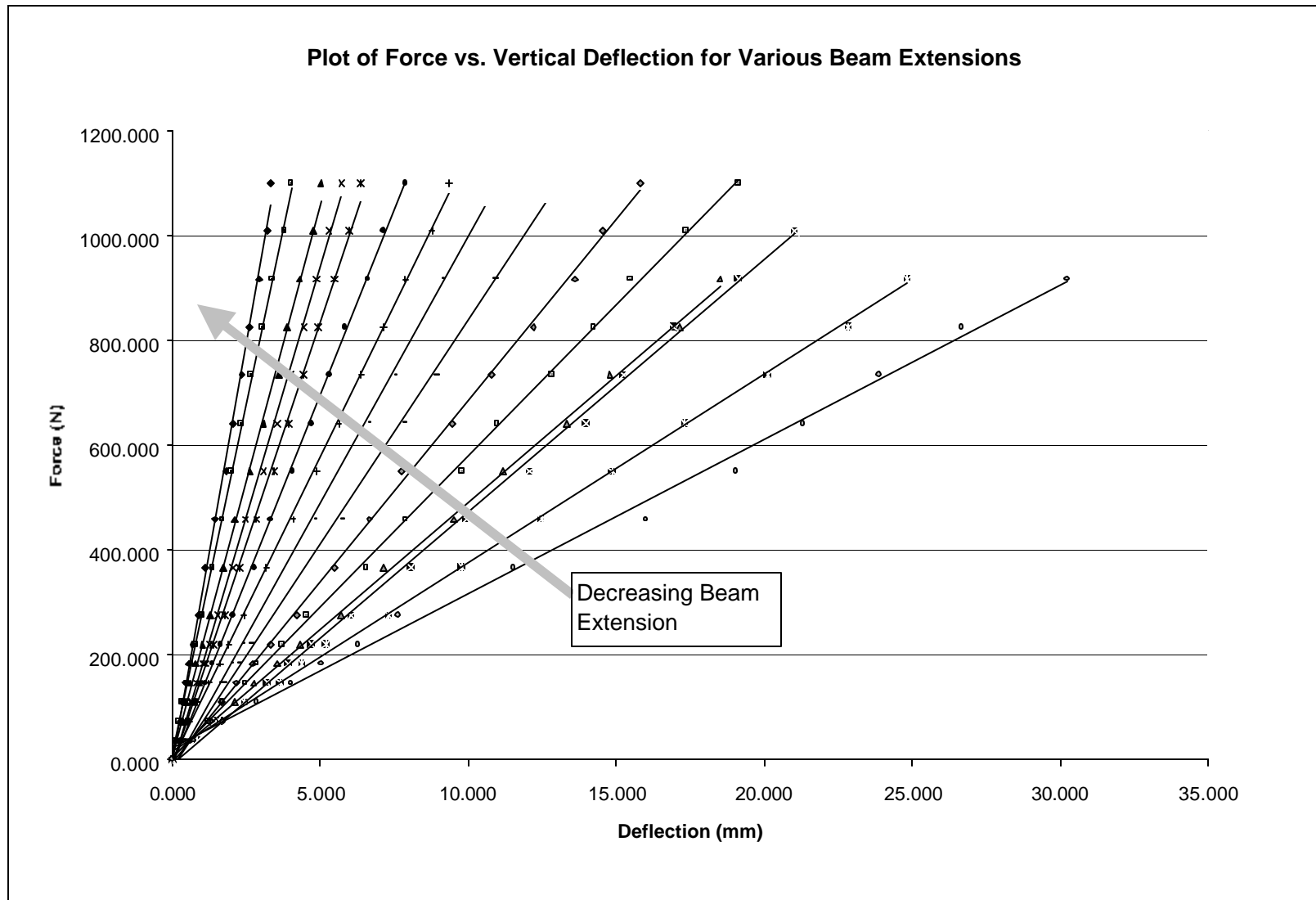


Figure 5.3 - Plot of Force vs. Deflection Data for Various Beam Extensions

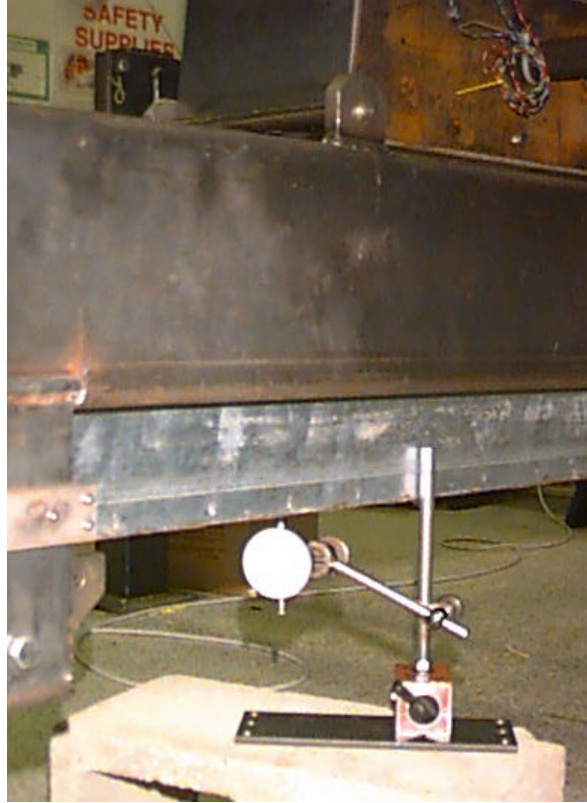


Figure 5.4 - End Support Deflection Measurement during Vertical End Deflection Test

5.2 Telescopic Ball Screw Actuator

5.2.1 Qualitative Analysis

5.2.1.1 Qualitative Observations

The telescopic actuator was evaluated qualitatively from the start of the assembly phase through its operation inside the telescopic arm. Qualitative observations such as noise, vibrations and misalignments were recorded.

5.2.1.2 Qualitative Conclusions

The telescopic ball screw actuator operated very well from a qualitative analysis. All of the components assembled with ease and fit well into the arm. The only major problem was due to misalignment of the actuator supports caused by poor assembly of the telescopic arm sections. This misalignment caused the actuator to bend at large extensions where the stiffness was reduced. To correct the problem, the sections will need to be readjusted to extend straight.

Another problem that was encountered due to misalignment and poor shaft concentricity was low amplitude vibrations in the arm. The vibration was of a higher frequency at smaller extensions and reduced as the arm was extended. This is consistent with the reduced stiffness in the actuator joints as it is extended. The problem was narrowed down to the curvature in the outer drive tube and support misalignment. Both of which are easily remedied.

5.2.2 Quantitative Analysis

5.2.2.1 Positioning Accuracy

The positioning accuracy for the telescopic actuator was evaluated through the use of a Cable Extension Transducer (CET) fixed at the base section as shown in Figure 5.5. The CET cable was then attached to the end of the arm to measure the extension concurrently with the drive motor's encoder. The arm was then commanded through the entire workspace to generate two sets of positioning data, one set for extension and another for retraction. The results are shown in Figure 5.6.

5.2.2.2 Actuator System Backlash

The data used above in the accuracy verification experiment was then used to determine the average actuator system backlash. Since the data was collected for both extension and retraction, the difference in the CET readings for each commanded position would represent the system backlash. The system backlash was evaluated from these seventy data points and averaged to yield an average linear system backlash of 0.381 mm (0.015 in).

5.2.2.3 Quantitative Conclusions

The data recorded for the accuracy validation of the telescopic actuator showed an increasing error as the arm was extended. The accuracy of these CET measurements is given by the manufacturer as 0.003% of the maximum extension capabilities of the CET. This calculates to an accuracy of ± 0.254 mm (0.010 in) for the CET used. This accuracy error was not enough to account for the over 2 mm (0.078 in) error measured by the CET.

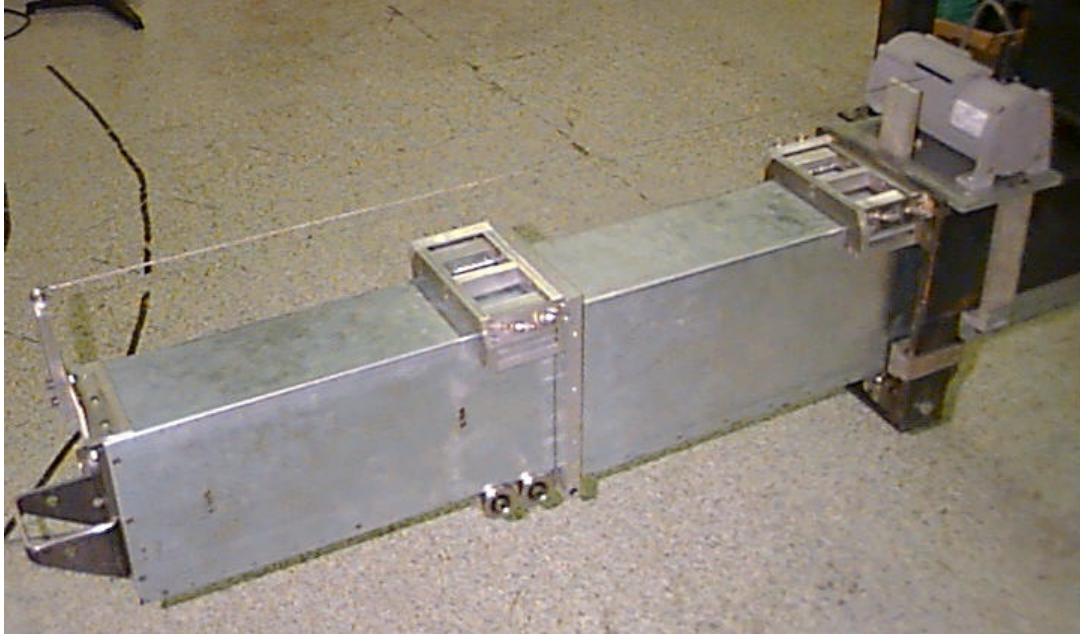


Figure 5.5 - CET Measuring Apparatus for Validation of Positioning Accuracy

One possible source of this error relates back to the misalignment in the ball screw actuator. If the ball screw was not traveling in a straight line, the measurement by the CET would be greater than the actual translate distance. This would account for some of the error present and is very plausible considering the misalignment in the telescopic sections.

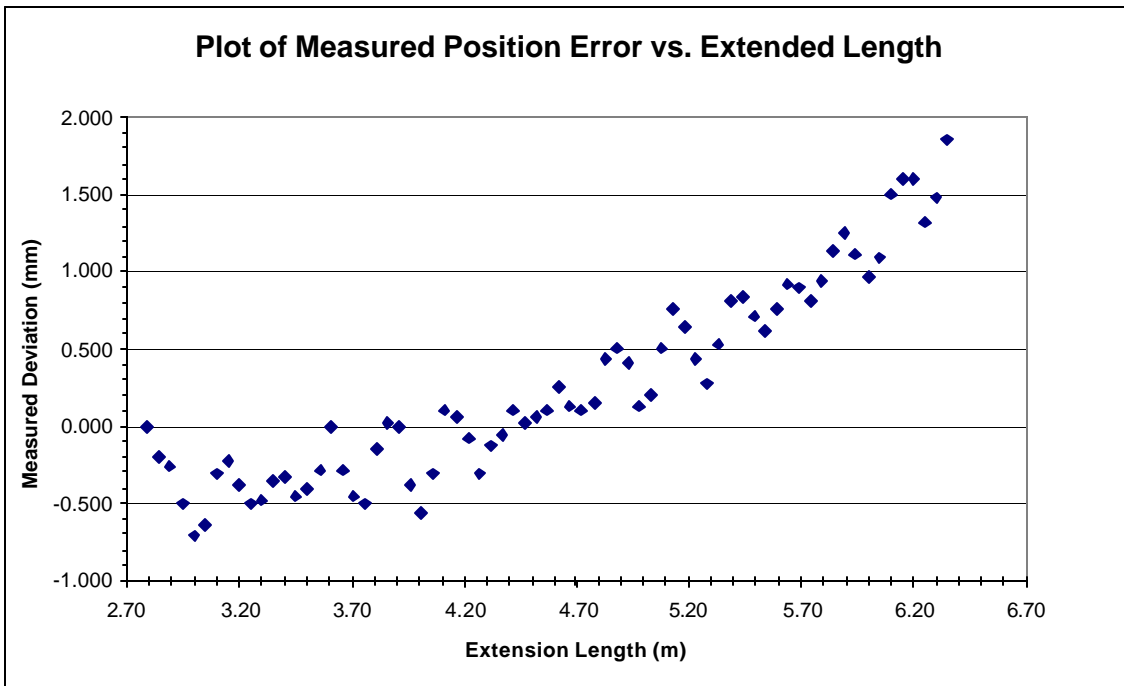
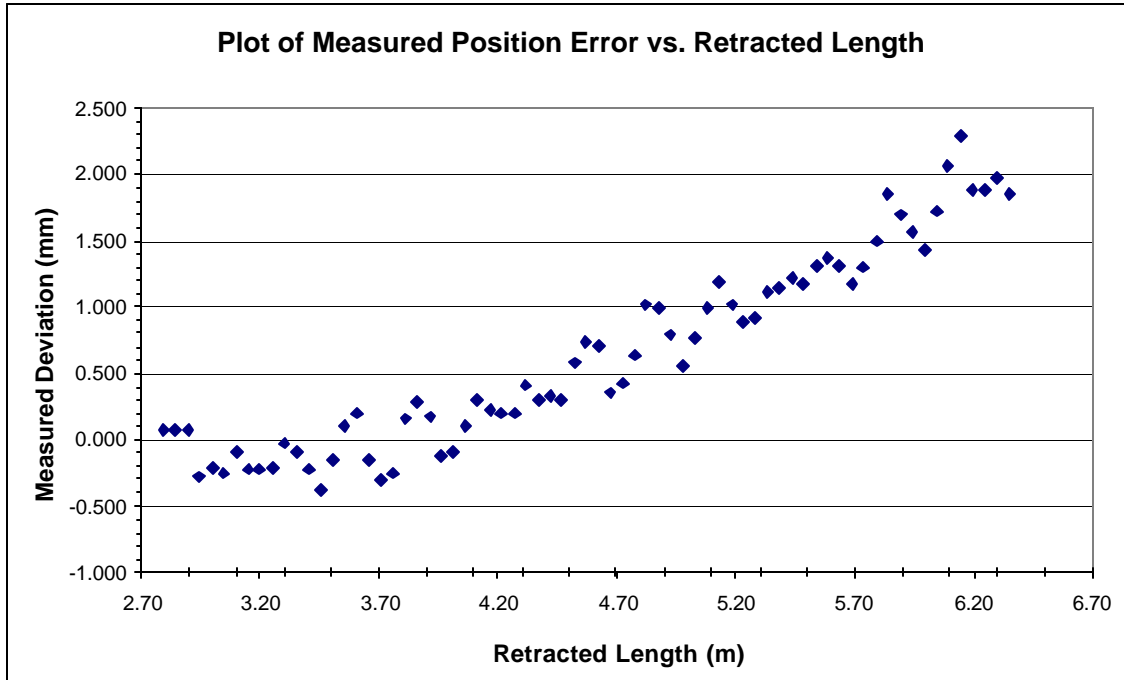


Figure 5.6 - Plots of Measured Error vs. Extended (Top) and Retracted (Bottom) Beam Length

5.3 Concentric Output Planetary Gearbox

5.3.1 Qualitative Analysis

Evaluation of the planetary gearbox began in the assembly phase and continued through operation. The evaluation concerned alignments, ease of assembly and fits in the assembly phase and included factors such as vibrations and noise in the operation phase.

5.3.1.1 Pre-Operation

Qualitatively, the assembly of the gearbox was very smooth. The setting of the center distances for the bevel gear reduction was an iterative and tedious process that was highly reliant on the machining tolerances of the gearbox plates. In addition, the support for the ring gear and outer output shaft had to be replaced with a tapered roller bearing that could support an axial load. With the radial bearing, as the front gearbox plate was tightened, the outer output shaft was forced towards the back of the gearbox, thus, locking the radial bearing (see Figure 4.13 for clarification).

5.3.1.2 Bevel Gear Noise

The dynamic testing of the gearbox was very successful except for the noise resulting from the bevel gear reduction. Due to the fact that the noise was louder in one direction than the other, it was assumed that there was some slight misalignment in the shafts. To remedy this, the gearbox was disassembled and readjusted until the noise was at an acceptable level.

5.3.1.3 Qualitative Conclusions

The qualitative analysis through the assembly and operation phases resulted in a number of modifications to the gearbox in both design and adjustments. Misalignment in the gearbox shafts was blamed for the high noise emission from the gearbox. However, this noise was reduced to an acceptable level by more closely setting the correct center distance of the bevel gears.

5.3.2 Quantitative Analysis

5.3.2.1 Gearbox Backlash

The gearbox backlash was measured directly off of the gearbox shafts using a dial indicator. In this method, the gearbox input shaft was fixed, while the two output shafts were allowed to

rotate. A thin plate was attached to each output shaft, from which horizontal deflection was measured. The measurement was repeated five times for each shaft and recorded. This data was then averaged and converted through trigonometry to find the output shafts' backlash. The measured outer output shaft had an average backlash of about 8 arc-min and the inner output shaft had an average backlash of about 11 arc-min. These values are in line with expectations assuming that the bevel gears are assembled correctly with 0.127 mm (0.005 in) backlash in the teeth. Translating this value to the outer output shaft yields a backlash of 6.8 arc-min.

5.3.2.2 Quantitative Conclusions

This measured backlash correlates well with the manufacturers prescribed backlash for the planetary set as well as the bevel gear set. It is slightly higher than these specifications, but well within acceptable limits.

5.4 Vehicle Integration and Stowage System

5.4.1 Qualitative Analysis

5.4.1.1 Curved Rail Support

Qualitative testing of the curved rail included visual inspections from a static loading as well as from dynamic operation of the arm. Statically, the rail support seemed to provide a reliable support for the end of the arm with no visible deflections at maximum loading. On the other hand, dynamic testing resulted in a stick-slip motion of the roller truck on the curved plate. This stick slip motion of the roller truck was then propagated into the arm to yield a jerking motion at the tip of the arm.

5.4.1.2 Stowage System

The stowage system was tested by raising and lowering the arm through the use of the DC winch system. The hinged plates folded as expected resulting in smooth lifting and lowering of the arm.

5.4.1.3 Rotational Pivot Plate

The rotational pivot plate was inspected by operating the arm throughout the workspace and into the storage position. The joint provided a rigid support throughout the workspace with

minor deflections detected around the pivot hole during the vertical deflection analysis. The only problem with this pivot plate was the lack of reinforcing of the frame rail around the connection points. However, this frame was merely a mock-up of the real truck that is expected to have reinforced frame rails.

5.4.1.4 Qualitative Conclusions

There was only one main problem that surfaced through the evaluation of the curved rail support. Stick-slip motion of the roller truck caused horizontal vibration at the tip of the arm. The rail and roller truck were inspected and the problem was determined to be the curved plates rough surface. The plate is made from hot rolled steel and as such has scale that is causing the roller truck to stick as the scale loosens on the plate. To solve this problem, it has been proposed to machine the curved plate on the top and bottom surface.

5.4.2 Quantitative Analysis

5.4.2.1 Stowage Time

The stowage time was measured using a hand crank through the winch as well as through DC power. The hand crank required minimal force through a significant number of rotations and took about 3 minutes to fully store the arm. Using the DC Winch, the arm was stowed in less than 1 minute with virtually no effort.

5.4.2.2 Quantitative Conclusions

The stowage system operated well through stowage system testing. It remains to be determined if the winch is required or if a simple hand crank should be used. The advantages of the winch in less effort, faster stowage and possible automatic control are virtually cancelled out by the wiring requirements necessary to power the winch.

5.5 Summary

Testing of the first prototype arm was based on qualitative evaluations as well as quantitative experiments. Each of the three main systems that comprise the arm was tested and in each case, either design changes or suggestions for changes were made. The major quantitative testing was limited to a vertical stiffness calculation for the arm and telescopic actuator accuracy verification due to time constraints. Future testing to include structural vibration analyses and dynamic end-

effector accelerations through operation would be of great value to future development of the OCCSM.

Chapter 6: THE OCCSM CAMERA BOOM

6.1 Introduction

The OCCSM uses a camera centered over the robotic arm's workspace to obtain an image of the roadway. The camera is mounted on the end of a boom that extends behind the truck and supplies pictures to the operator in the truck's cab. During operation, the camera boom positions the camera over the center of the workspace, but retracts once work is completed. A housing encloses the camera at the end of the boom and provides adjustments to align the camera with the workspace coordinates. This chapter focuses on the design of the camera boom, its retraction mechanism, and the camera housing. Vibration analysis of the camera boom and braces designed to minimize camera movement are also discussed.

6.2 The Camera Boom Requirements

The main purpose of the camera boom is to position the camera over the center of the workspace. Added to this purpose are several constraints and requirements that guide the boom's design. The frame members supporting the canopy over the truck bed also serve as mounts for the brackets that hold the camera boom. While the boom rests in the brackets below the canopy frame, it must not interfere with overhead clearance for workers on the truck bed. Furthermore, to allow the truck to enter garages or shops, the top of the canopy is restricted to a maximum of 3.6 m (12 ft) off the ground, leaving 2.3 m (7.5 ft) between the floor of the truck bed and the bottom of the canopy frame members. Mounting the boom just below the canopy places the camera high enough above the roadway to capture an image of the entire 366 x 366 cm (144 x 144 in) workspace.

The boom extension and retraction mechanism must be capable of moving the boom from its stowed position under the canopy, to the position that locates the camera in the center of the workspace, a distance of 2.3 m (7.5 ft). Because the boom moves between the two positions relatively infrequently, only at the start and completion of a job, a manually operated mechanism is suitable for the task. However, a single worker should be able to operate the mechanism while remaining in the truck bed.

A method of securing the camera boom in both the extended and retracted positions is necessary. Because the camera must line up accurately with the robotic arm's coordinates, the boom's position securing system must eliminate all movement as well as provide repeatability

for the extended configuration. Camera motion due to vibration must also be minimized to obtain as clear an image as possible.

6.3 The Camera Boom Supports

The camera boom receives support from the two rear canopy frame members that are 140 cm (54 in) apart. A bracket made from three pieces of steel angle and one steel bar welded into a box shape, hangs from each canopy frame member; see Figure 6.1. Delrin plastic fastened to the inner surfaces of the box acts as a bearing material between the boom and the bracket. A slot in one side of the plastic allows the chain, a component of the extension mechanism described in Section 5.3, to pass through the brackets as the boom extends and retracts.

To constrain the boom in the extended and retracted positions, bolts thread through the brackets and into the boom. To maximize the effectiveness of the bolts, the one on the rear support pulls the boom down against the bottom of the support, while the front one pushes the boom against the top of its support. Applying the bolt forces in this manner augments the loads naturally acting on the supports due to the boom's weight when in the extended position. To make the bolts easy to install and remove by hand, handles were welded onto the bolts, forming a "T" out of the assembly.

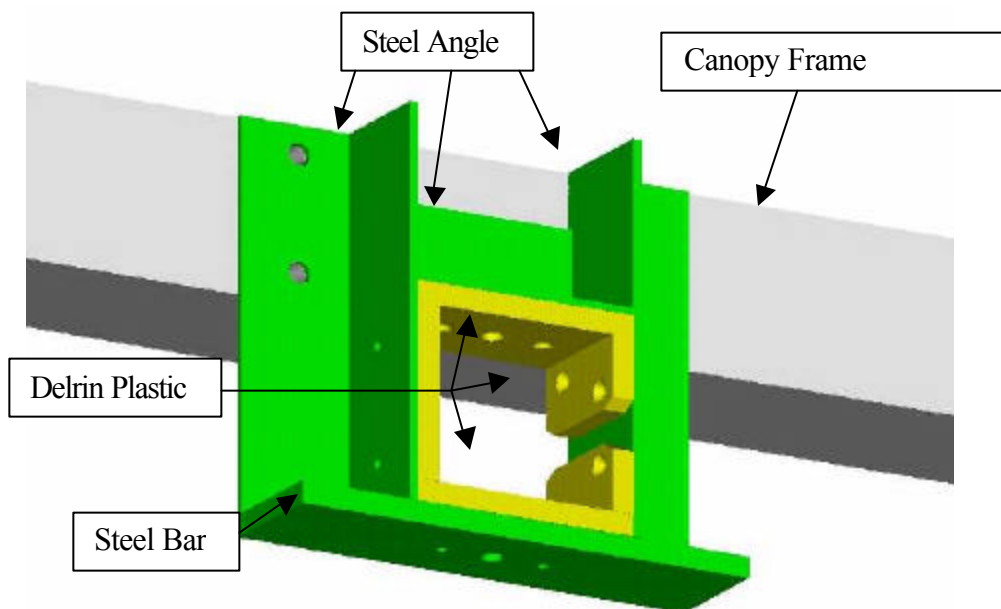


Figure 6.1 - Model of Camera Boom Bracket

6.4 Extension Mechanism

The extension and retraction mechanism must extend the boom out to the center of the workspace, 3.2 m (10.4 ft) behind the truck bed. Two options were considered to produce this motion: a pulley system and a rack and pinion mechanism. The rack and pinion mechanism was chosen because it required fewer parts and was simpler to integrate with the boom supports. The rack portion of the mechanism attaches to the side of the boom, while the pinion remains fixed and mounts to one of the boom brackets. A chain stretched alongside the boom is used as the rack and this approach keeps the design lightweight while providing ample strength. The pinion gear, simply a chain sprocket, attaches to a shaft with a handle that will be turned by the operator to move the boom.

The sizes of the mechanism's components were determined by a compromise between the force the operator needs to apply to the handle and the number of revolutions made by the pinion. Equation 6.1 relates the pinion's pitch diameter, d , to the number of pinion revolutions, t , necessary to extend the boom a distance l .

$$d = \frac{l}{\boldsymbol{p}t} \quad (6.1)$$

The boom needs to extend about 230 cm (90 in) to reach its working position, and should do so with a reasonable number of revolutions of the pinion gear. To achieve the required extension with 10 revolutions of the pinion gear requires a pitch diameter of just under 7.4 cm (2.9 in). A suitable chain sprocket was found with a pitch diameter of 6.510 cm (2.563 in), requiring 11.2 revolutions to fully extend the boom.

Next, an estimation of the force required to extend the boom was used to determine the length of handle needed to turn the shaft. Equation 6.2 describes the effect of the handle length, h , and the pinion's pitch diameter on the force required by the operator, P . The friction force, F , opposing the boom's motion, is approximated as shown in equation 6.3, using a coefficient of friction, \boldsymbol{m} , and the reaction forces at the boom's supports, F_1 and F_2 .

$$P = \frac{Fd}{2h} \quad (6.2)$$

$$F = \boldsymbol{m}(F_1 + F_2) \quad (6.3)$$

The reaction forces depend on the weight of the boom and its position relative to the supports. A simple analysis reveals that the reaction forces will be largest when the boom is

fully extended. Using the aluminum beam, whose selection is detailed in Section 6.5, the sum of the two reaction forces totals about 490 N (110 lb). With a relatively large estimated friction coefficient of 0.35, the maximum friction force opposing the beam's motion is calculated from Equation 6.3 to be nearly 180 N (40 lb). Applying Equation 6.2 with a handle length of 20 cm (8 in) and the sprocket mentioned above, results in a force of less than 31 N (7 lb) being required by the operator. This force lies well within the range that the operator should be able to exert on the overhead crank mechanism. The above analysis shows that the chosen chain sprocket size and handle length are acceptable in the design.

The parts of the crank assembly, shown in Figure 6.2, are fastened together using traditional methods. The sprocket slides on the shaft and is held in place by two set-screws. The shaft rotates in, and receives support from, two bronze bushings located on either side of the sprocket. A collar keeps the shaft from sliding out of the bushings by transferring the weight of the assembly to the flanged, lower bushing. The shaft extends far enough below the boom so that the handle welded to the end of the shaft clears the boom bracket. A handgrip screws into the end of the handle and may be folded up when not in use to provide more overhead clearance.

6.5 Selection of Boom Size and Material

The size of the boom and its material were key issues considered to minimize camera movement while keeping the design relatively lightweight. At full extension, the boom is essentially cantilevered 318 cm (125 in) off the back of the truck, with nearly an additional 180 cm (70 in) of the boom remaining between the boom support brackets. A square cross-section was chosen for the boom, as opposed to a circular cross-section, because it does not have to be constrained from rotating to keep the camera in alignment.

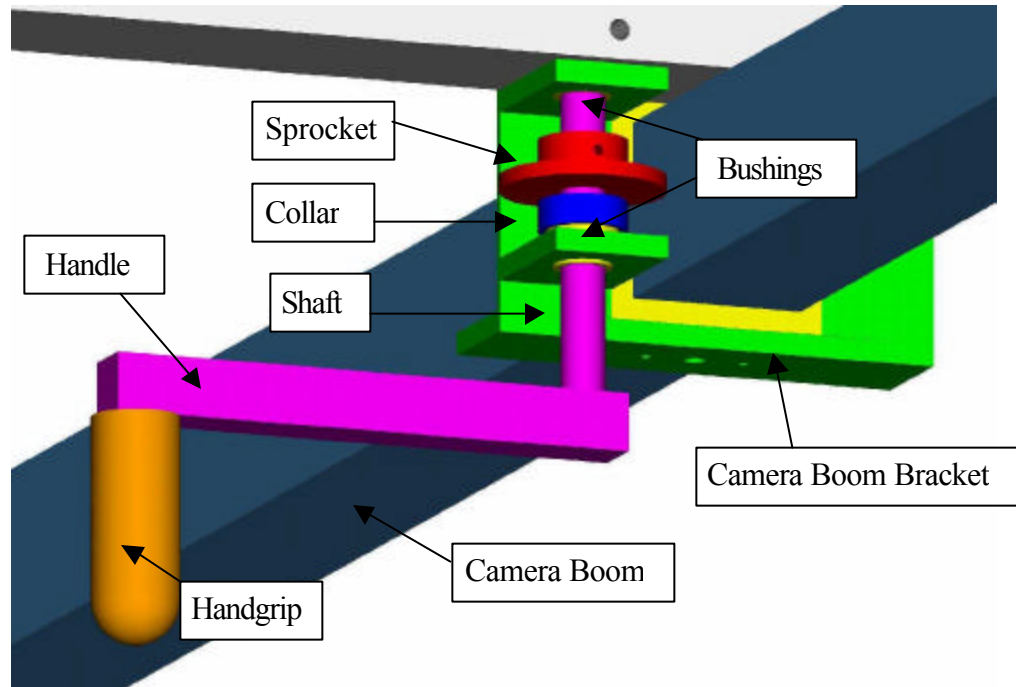


Figure 6.2 - Model of Camera Boom Crank Assembly

To begin the analysis of different materials and wall thicknesses, a boom with a 7.6 cm (3 in) square cross-section was chosen as a starting point. Throughout the design this size was deemed the most reasonable. A larger boom would begin to cut into the height clearance in the truck bed. Using a smaller boom would only further exaggerate problems encountered with vibration. Three different materials were compared: steel, aluminum, and a fiberglass composite. Each material was analyzed with varying wall thicknesses, ranging from 0.16 cm (0.063 in) to 0.953 cm (0.375 in). Table 5.1 lists the specific weight and Modulus of Elasticity for each of the materials. Four characteristics were examined to compare different materials and wall thicknesses: weight, static end deflection, vibration natural frequency, and maximum forced vibration amplitude.

6.5.1 Weight Analysis

The total weight of each prospective boom was obtained by multiplying the boom's volume by the specific weights listed in Table 6.1. To find the boom's volume, the cross-sectional area for each wall thickness was found, then the area was multiplied by the boom's total length. The graph in Figure 6.3 shows the results of this analysis, and provides an easy comparison for each combination of material and wall thickness.

Figure 6.3 shows that the use of steel becomes undesirable as wall thickness increases. The weight of both aluminum and fiberglass composite increase slowly with increased wall thickness when compared with steel. Being the lightest, the fiberglass boom is the preferred choice based on weight analysis. However, aluminum comes in a close second and should remain a possibility pending the results of the other analyses.

Material	Modulus of Elasticity	Specific Weight
Steel	200 GPa 29*10 ⁶ psi	0.077 N/cm ³ 0.284 lb _f /in ³
Aluminum	69 GPa 10*10 ⁶ psi	0.027 N/cm ³ 0.098 lb _f /in ³
Fiberglass Composite	21.7 GPa 3.15*10 ⁶ psi	0.014 N/cm ³ 0.053 lb _f /in ³

Note: All data was adapted from Hibbeler (1994); except for the Specific Weight of the Fiberglass obtained from the supplier's catalog and the Fiberglass Modulus of Elasticity, which was determined by experiment.

Table 6.1 - Properties of Possible Boom Materials

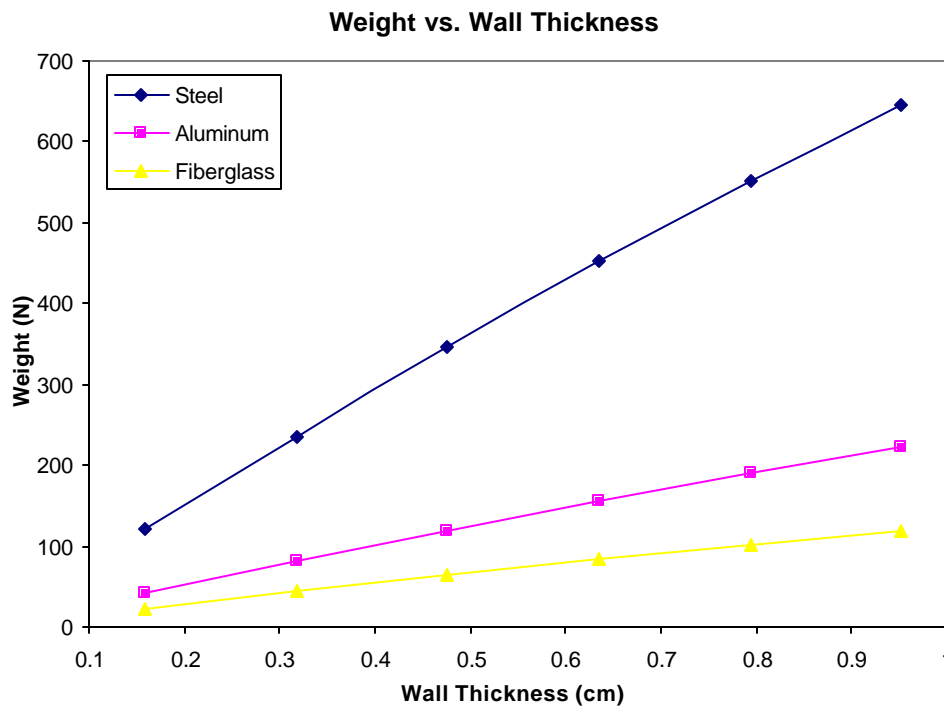


Figure 6.3 - Results of Boom Weight Analysis

6.5.2 Static End Deflection Analysis

The static deflection of the boom was determined using Mechanics of Materials methods, specifically Equation 6.4. Figure 6.4 shows the free body diagram of the boom and the two

coordinates required in formulating the deflection equations. Note that two deflection equations result from this analysis: one for the cantilevered section and the other for the section between the two supports. The force, F_c , on the end of the boom, includes the estimated weight of the camera and housing, about 22 N (5 lb), while the distributed load, w , is comprised of the boom's distributed weight and the distributed weight of the chain. Applying Equation 6.4, the moment expression, $M(x)$, was integrated twice to obtain the beam's deflection equation, $v(x)$.

$$EI \frac{\partial^2 \mathbf{u}}{\partial x^2} = M(x) \quad (6.4)$$

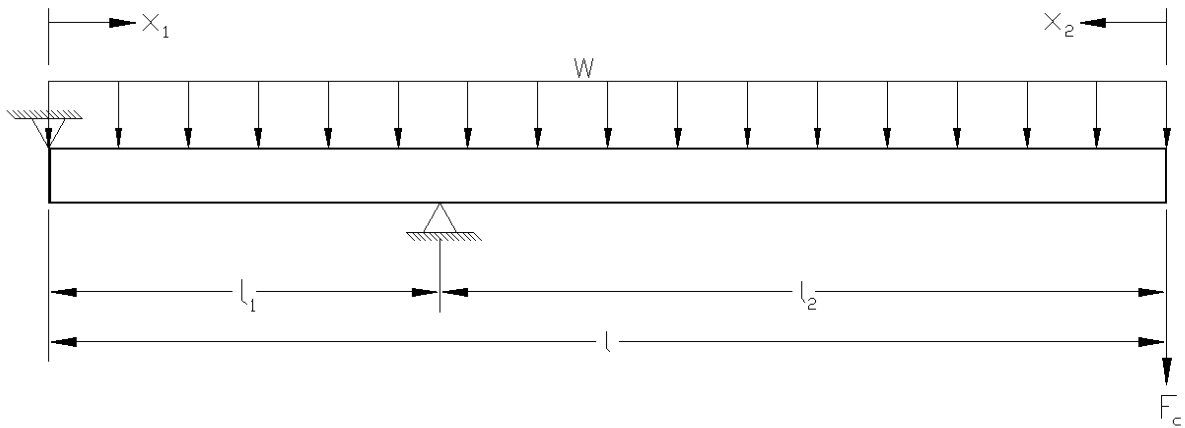


Figure 6.4 - Free Body Diagram of Camera Boom

Boundary conditions were used to solve for the constants of integration, giving final expressions for the boom's deflected shape. From these expressions, a simplified equation for the deflection at the end of the beam can be written as

$$\mathbf{u}_{end} = \frac{-1}{EI} \left(\frac{w}{24} l_2^3 l + \frac{w}{8} l_2^2 l^2 - \frac{w}{24} l_2 l^3 + \frac{F_c l_2^2 l}{3} \right). \quad (6.5)$$

The end deflections for the various beam materials and cross-sections may be compared by examining Figure 6.5.

Figure 6.5 shows the inadequacy of the fiberglass boom for supporting weight with minimal deflection. Although the deflection of the fiberglass boom improves with increased wall thickness, it remains nearly double the values obtained using either steel or aluminum. The deflection of both steel and aluminum booms are relatively close, especially with larger wall thicknesses, showing that these materials are preferred based on the deflection analysis.

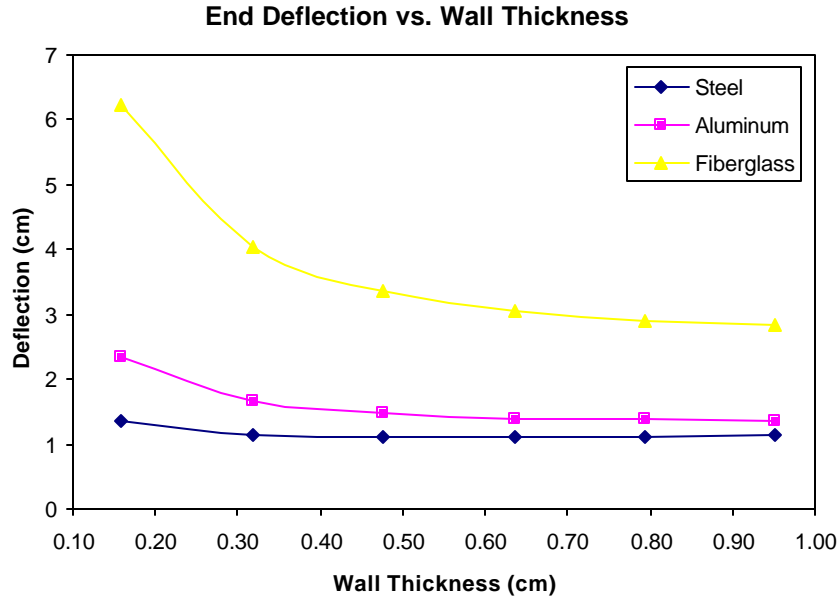


Figure 6.5 - Results of Camera Boom End Deflection Analysis

The joint connections were another critical component of the telescopic arm. Qualitative analysis included inspection of the various support systems along the entire stroke of the telescopic arm. For this inspection, the aim was to ensure that the supports were contacting the sections for the entire length such that the sections had no “play” or movement in the joints.

6.5.3 Natural Frequency Analysis

To obtain an estimate of the boom’s vibration natural frequency, Rayleigh’s Method was employed. Using Rayleigh’s Method, the familiar equation for natural frequency, shown in Equation 6.6, is used, but an equivalent mass, m_{eq} , must be found to approximate the continuous system as a point mass.

$$w_n = \sqrt{\frac{k}{m_{eq}}} \quad (6.6)$$

The equivalent mass is found by developing an expression for the maximum kinetic energy, T_{max} , in the system. The basic formulation of the solution is shown here, while the calculations for the analysis were performed in Matlab, using the program in Appendix B.

An essential assumption in finding the kinetic energy of the system is that the dynamic mode shape may be closely approximated by the static deflection shape, which was found in Section

6.5.2. Finding the maximum deflection, v_{max} , in each section of the boom allows the two equations for the static shape to be written in the form

$$\mathbf{u} = \frac{\mathbf{u}}{\mathbf{u}_{max}} \mathbf{u}_{max} \cdot (6.7)$$

Now, differentiating with respect to time gives an expression for the velocity profile, $\dot{\mathbf{u}}$, as

$$\dot{\mathbf{u}} = \frac{\mathbf{u}}{\mathbf{u}_{max}} \dot{\mathbf{u}}_{max} \cdot (6.8)$$

Using this result and applying Equation 6.9, a form of the kinetic energy equation where V represents velocity and w_m represents mass per unit length, to each section of the boom leads to Equation 6.10 for the boom's total kinetic energy.

$$T = \frac{1}{2} \int_0^l (w_m V^2) dx \quad (6.9)$$

$$T_{max} = \frac{w_m \dot{\mathbf{u}}_{1,max}^2}{2 \mathbf{u}_{1,max}^2} \int_0^{l_1} \mathbf{u}_1^2 dx_1 + \frac{w_m \dot{\mathbf{u}}_{2,max}^2}{2 \mathbf{u}_{2,max}^2} \int_0^{l_2} \mathbf{u}_2^2 dx_2 \quad (6.10)$$

In Equation 6.10, the numeric subscripts differentiate between the two sections of the boom and w_m represents the mass per unit length.

At this point, the only two unknowns on the right side of the equation are the two maximum velocities, $\dot{\mathbf{u}}_{1,max}$ and $\dot{\mathbf{u}}_{2,max}$. Before the equivalent mass can be found, one of these unknowns must be eliminated. Making the assumption that the ratio of the maximum velocities is equal to the ratio of maximum deflections, r , allows one of the unknowns to be eliminated, and we have

$$r = \frac{\mathbf{u}_{1,max}}{\mathbf{u}_{2,max}} = \frac{\dot{\mathbf{u}}_{1,max}}{\dot{\mathbf{u}}_{2,max}} \quad (6.11)$$

and

$$\dot{\mathbf{u}}_{1,max} = r \dot{\mathbf{u}}_{2,max} \cdot (6.12)$$

Using Equation 6.12, and letting I_1 and I_2 denote the numeric values of the integrals in Equation 6.10, the maximum kinetic energy of the boom becomes

$$T_{max} = \frac{1}{2} \left(\frac{w_m I_1 r^2}{\mathbf{u}_{1,max}^2} + \frac{w_m I_2}{\mathbf{u}_{2,max}^2} \right) \dot{\mathbf{u}}_{2,max}^2 = \frac{1}{2} m_{eq} \dot{\mathbf{u}}_{2,max}^2 \quad (6.13)$$

Equation 6.13 shows how the expression for the boom's equivalent mass is easily found by comparison to the standard expression for kinetic energy, shown on the far right side of the equation. Adding the mass of the camera and housing, C_m , the equivalent mass of the entire system can be represented as

$$m_{eq} = \frac{w_m I_1 r^2}{\mathbf{u}_{1,max}^2} + \frac{w_m I_2}{\mathbf{u}_{2,max}^2} + C_m. \quad (6.14)$$

The final piece of information needed to calculate the vibration natural frequency is the boom's stiffness, k . Because stiffness is simply force divided by distance, finding the deflection resulting from a force applied on the unsupported end of the beam gives the necessary information. Using Equation 6.5 and letting $w=0$, gives the following expression for the boom's stiffness.

$$k = \frac{F}{\mathbf{u}_{2,max}} = \frac{3EI}{l_2^2} \quad (6.15)$$

Finally, Equation 6.6 may be employed to calculate estimates of the beam's vibration natural frequency. The natural frequency of the boom was calculated for the three materials and varying wall thicknesses. The graph in Figure 6.6 shows the results of the natural frequency analysis for comparison.

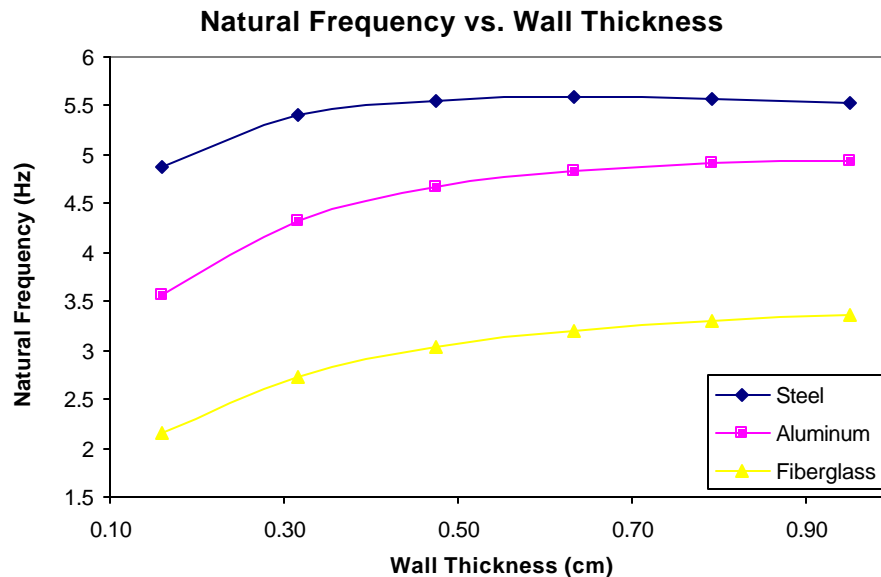


Figure 6.6 - Results of Camera Boom Natural Frequency Analysis

The validity of the solution was checked against the natural frequencies of two purely cantilevered beams using formulas also derived by Rayleigh's method (see Rao, 1995). The first beam was as long as the portion of the camera boom that extends off the back of the truck, while the second had a length equal to the entire camera boom. As expected, the natural frequency of these two cantilevered beams bracket the result from the detailed analysis described above, indicating the validity of the solution.

The boom can not be picked to avoid having its natural frequency near the frequency of the input, because of the undefinable nature of the vibration input. Therefore, a boom with a higher natural frequency is desired because, in general, a higher frequency corresponds to smaller amplitude vibrations. As with the deflection analysis results, the fiberglass boom lacks the natural frequency characteristics desired. A steel camera boom is clearly preferred, having a natural frequency about 1 Hz higher than aluminum and 3 Hz higher than the fiberglass boom. However, this advantage will have to be weighed carefully against the disadvantage in a steel boom's weight.

6.5.4 Forced Vibration Analysis

The final analysis used to determine the best camera boom material and size was the study of a forced, damped vibration response. Because the actual vibration input to the system is very complex, the analysis uses a sinusoidal force input applied on the free end of the boom. For each combination of boom material and wall thickness, the applied force had a magnitude of 4.4 N (1 lb). However, the forcing frequency, ω_f , is different for each combination since it was chosen to produce the maximum amplitude response.

The choice of a damping value was based on experiment and a couple of assumptions. Observations made of the vibrations of a beam equivalent in size to the camera boom revealed that the vibration amplitude decreased approximately ninety percent in a time span of ten seconds. From this observation, the logarithmic decrement, d , can be obtained from

$$d = \frac{1}{n} \ln \left(\frac{x_1}{x_{n+1}} \right) \quad (6.16)$$

where n represents the number of cycles observed and, x_1 and x_{n+1} are the amplitudes before and after n cycles, respectively. The number of cycles, n , occurring during the observation time, t , are calculated as

$$n = \frac{t w_n}{2 p} \sqrt{1 - x^2}. \quad (6.17)$$

Assuming a relatively small damping ratio, x , allows the radical in Equation 6.17 to be approximated as unity. The damping constant, c , is then expressed as

$$c = \frac{m_{eq} w_n d}{p}. \quad (6.18)$$

The sources of damping in the camera boom system may be split into two categories: internal damping in the boom itself and damping resulting from the boom mounts and the environment. Assuming that different boom materials have similar damping properties, allows the use of one damping value for all combinations of materials and wall thicknesses. Specifically, the damping value obtained using the data and procedure described in the previous paragraph will be used throughout the forced vibration analysis of the boom. While the damping value remains constant, the damping ratio differs from one combination of boom material and wall thickness to the next. The damping ratio, \mathbf{x} , is expressed as

$$\mathbf{x} = \frac{c}{2\sqrt{km_{eq}}} \quad (6.19)$$

and will be used to calculate the forced amplitude response and the forcing frequency.

The final parameter necessary to calculate the forced amplitude response is the forcing frequency, \mathbf{w}_f . As mentioned earlier, the forcing frequency is chosen to produce the maximum response and differs for each combination of boom material and wall thickness. The forcing frequency that will produce the maximum amplitude response in terms of the undamped natural frequency and the damping ratio is expressed as

$$\mathbf{w}_f = \mathbf{w}_n \sqrt{1 - 2\mathbf{x}^2}. \quad (6.20)$$

The amplitude response, X , is expressed as

$$X = \frac{F_0}{k \sqrt{\left[1 - \left(\frac{\mathbf{w}_f}{\mathbf{w}_n}\right)^2\right]^2 + \left[2\mathbf{x} \frac{\mathbf{w}_f}{\mathbf{w}_n}\right]^2}} \quad (6.21)$$

and using the forcing frequencies found from Equation 6.20 will ensure that this is the maximum vibration amplitude.

The results of the analysis appear in Figure 6.7 and clearly show that the fiberglass boom has a vibration amplitude nearly twice that of a steel boom. The amplitudes of the steel and aluminum booms are much closer, with the aluminum boom amplitude an average of about 20% greater than steel. Similar to the natural frequency analysis, the order of preference places steel first, aluminum second, and fiberglass last. Again, steel only shows minor advantages over aluminum, emphasizing the weight consideration.

6.5.5 Review of Analysis Results

Reviewing the results of the four characteristics analyzed, a fiberglass boom seems a poor choice since it exhibits significant disadvantages in three of the four analyses. However, the choice between steel and aluminum is not readily apparent. While steel appears better in all characteristics except for weight, the values for aluminum are usually within 20% of those for steel. Further comparisons reveal the similar characteristics of the two specific possibilities for boom material and size: steel with a 0.16 cm (0.063 in) wall thickness and aluminum with a 0.478 cm (0.188 in) wall thickness. Both of these combinations possess very similar qualities in the four characteristics analyzed, and either is a suitable choice from that standpoint. However, in other areas an aluminum boom has two advantages over a steel one. First, since the OCCSM will be subjected to weather, an aluminum boom has the property that it

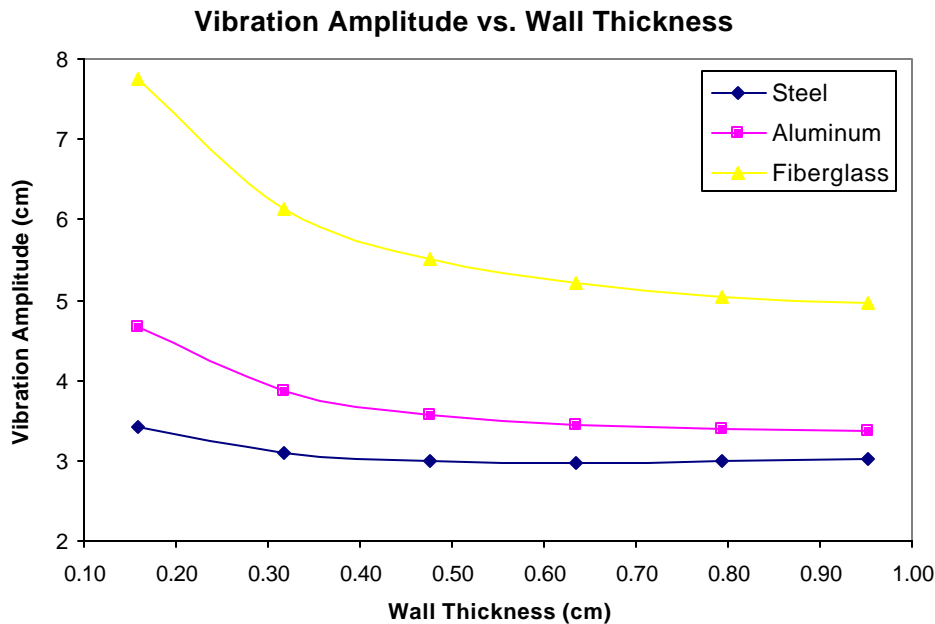


Figure 6.7 - Results of Maximum Vibration Amplitude Analysis

does not require extra weather protection. Second, fastening parts to an aluminum boom will be easier since the thicker wall allows the direct use of threaded fasteners. For these reasons the aluminum boom with a 0.478 cm (0.188 in) wall thickness was selected.

The forced vibration analysis discussed in Section 6.5.4 suggests that the camera boom will likely experience too much vibration. In the analysis, the excitation force was applied in a

manner to produce the largest response possible, on the very end of the boom and at the resonant frequency. Therefore, the results, which predict vibration amplitudes large enough to significantly reduce the quality of images taken by the camera, were not unexpected. However, even though the forcing function was applied to produce the worst case response, the magnitude of the force was only 4.4 N (1 lb). While the forcing function does not represent the real input, the boom will likely experience vibrations of this magnitude or greater at some time. Simple tests performed with the aluminum tube, acquired for use as the camera boom, supported the notion that vibrations would be above acceptable levels. A method of reducing the camera boom vibrations is needed to ensure the quality of images the camera supplies to the operator.

6.6 Camera Boom Braces

In addition to reducing camera movement to a reasonable level, the system used to reduce camera boom vibrations had to meet two other important requirements. First, the system must not require an additional worker besides the one who operates the camera boom crank mechanism. Second, any required assembly or adjustments should be accessible to the worker while remaining on the truck bed.

Two options were considered to provide the extra support to the camera boom. One option employed a cable attached to the end of the boom near the camera. The other end of the cable would attach to a removable post above the truck bed canopy, as shown in Figure 6.8. While this arrangement would reduce vibrations in the vertical direction, it would have minimal effect on horizontal vibrations. Also, the support post above the canopy would have to be removable or retractable in order to meet the overall truck height requirement. The extra complication involved in lowering the support post was not desirable, especially in the prototype machine, and can be avoided by using a simpler method to support the camera boom.

The second option that was considered to support the camera boom was chosen because it reduces vibration in all directions while remaining mechanically simple. The fundamental design involves two braces that attach to the cantilevered section of the camera boom and then extend to the two corner truck bed posts on the rear of the truck. The braces will be made from round steel tube with a 3.81 cm (1.5 in) diameter and a 0.318 cm (0.125 in) wall thickness to provide reasonable strength against buckling. Before further specifications could be made, a plan for how the braces would deploy and attach needed to be developed.

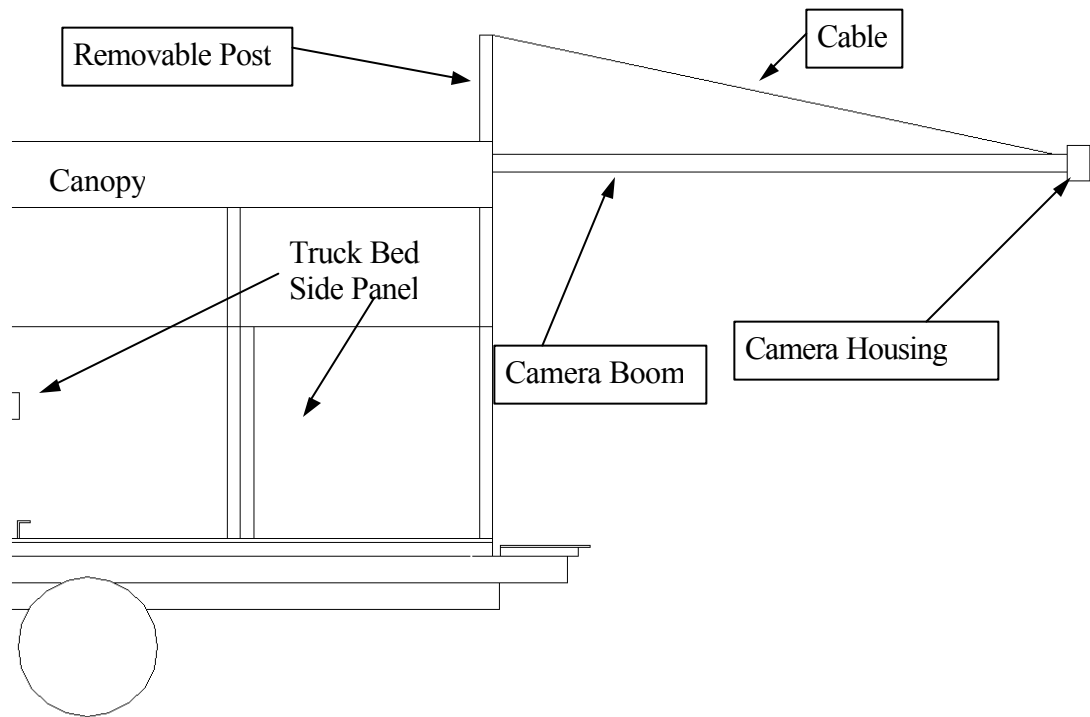


Figure 6.8 - Proposed Camera Boom Cable Support

6.6.1 Camera Boom Brace Arrangement

Two options were considered to provide the extra support to the camera boom. One option employed a cable attached to the end of the boom near the camera. The other end of the cable would attach to a removable post above the truck bed canopy, as shown in Figure 6.8. While this arrangement would reduce vibrations in the vertical direction, it would have minimal effect on horizontal vibrations. Also, the support post above the canopy would have to be removable or retractable in order to meet the overall truck height requirement. The extra complication involved in lowering the support post was not desirable, especially in the prototype machine, and can be avoided by using a simpler method to support the camera boom.

For convenience, the braces are stowed next to the camera boom, one brace on each side. To reach this stowage position, the braces disconnect from the truck bed posts and then swing up parallel to the boom, all while remaining attached to the boom. The connection between the boom and the braces uses a square bracket, similar to the two main boom support brackets that hang below the canopy. The braces connect to posts located far enough to the sides of the square bracket so that they clear the rest of the camera boom assembly, see Figure 6.9. This connection

forms a rotational joint designed to allow the braces to swing from the stowed position, parallel to the boom, to the connection on the truck bed posts. The square bracket is held in place lengthwise along the boom by a removable pin. For stowage, the pin is removed, and the bracket slides along the boom towards the camera housing, allowing the boom to be fully retracted. On deployment, when the boom is partially extended, the pin will be replaced, then the boom can be extended the rest of the way, and the braces can rotate down to connect with the truck bed posts.

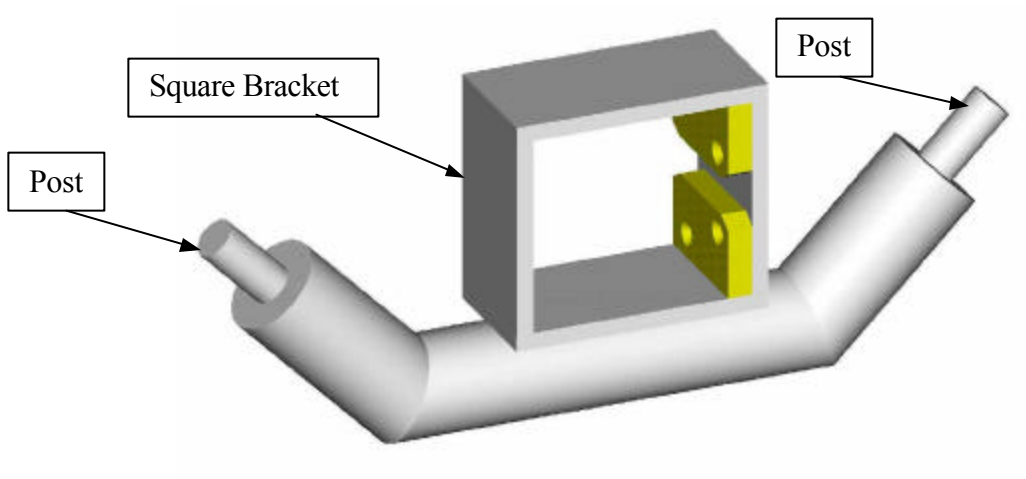


Figure 6.9 - Square Bracket with Brace Attachment Posts

Ideally, the braces would connect to the truck bed posts near the truck bed floor to create the largest angle possible between the braces and the boom. However, the rear panel of the truck bed prevents the braces from swinging to the bottom of the posts. Either the braces would have to be shortened to clear the panel and then be lengthened again to reach the post, or the boom would have to over-extend temporarily to allow the braces to clear the panel. To avoid either of these complications, the braces are designed to connect to the truck bed posts just above the rear panel, even though the arrangement reduces the angle between the braces and the camera boom. Either of the more complicated options may be employed if the current design does not provide enough rigidity.

6.6.2 Brace Bracket Location

The location on the camera boom where the square bracket attaches must also be considered. If the bracket attaches at the end near the camera, the angle between the braces and the boom will be relatively small, decreasing the effectiveness of the braces. As the bracket location

moves towards the truck, the noted angle increases. However, this is accompanied by the disadvantage of leaving a greater length of the boom cantilevered beyond the bracket.

Examining the vibration characteristics of the boom also provides insight to the problem. With the bracket near the camera, the primary mode shape will be similar to a fixed-pinned beam, with the pinned end being the end with the brace bracket. As the bracket location is moved towards the truck, the mode shape will change and the natural frequency will increase until it reaches a maximum. Moving the bracket further inward will cause the natural frequency to decrease as the cantilevered mode shape becomes dominant

Both of the above discussions indicate that an ideal location exists along the boom's length for the attachment of the square bracket. To determine the location where the bracket should be fixed, a vibration analysis was used. While a static deflection analysis was considered, the dynamic loads involved required the consideration of a vibration analysis. The following vibration analysis examines the lowest natural frequency of the boom for varying bracket locations. Again, since the vibration input is not defined, the analysis will focus on maximizing the natural frequency.

The analysis begins with the diagram shown in Figure 6.10, which considers only the section of the boom that extends beyond the back of the truck. The fixed support, on the right of the diagram, represents the end of the boom supported by the canopy brackets, while the pinned support, on the boom's midspan, represents the square brace bracket. Rather than using Rayleigh's Method, as with the previous vibration analysis, this analysis will use vibration methods for continuous systems. Again, the support at midspan makes it necessary to split the boom into two sections and use two coordinates, x_1 and x_2 , in the analysis. The weight of the camera and its housing is neglected to simplify the analysis. This simplification will not alter the trend of the results and should not change numerical results significantly.

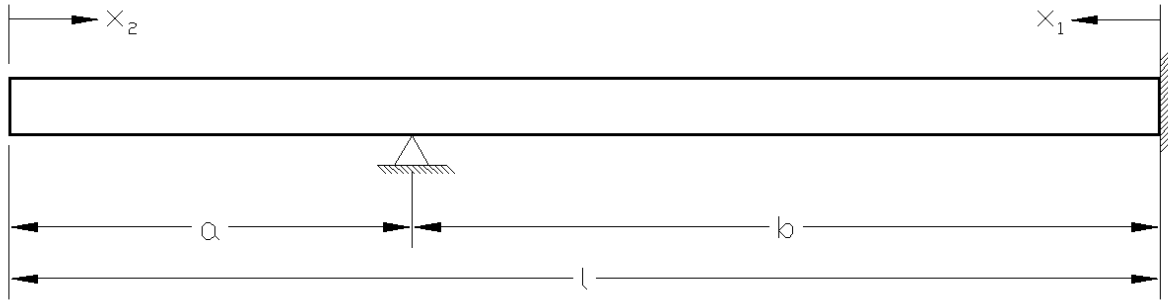


Figure 6.10 - Diagram of Camera Boom for Brace Location Analysis

The vibration mode shapes are described by Equations 6.22 and 6.23, where: C_1 through C_8 are constants to be determined, β is a constant containing boom properties and the unknown natural frequency, and W_1 and W_2 are the lateral displacements of the two sections of the boom.

$$W_1 = C_1 \cos(\beta x_1) + C_2 \sin(\beta x_1) + C_3 \cosh(\beta x_1) + C_4 \sinh(\beta x_1) \quad (6.22)$$

$$W_2 = C_5 \cos(\beta x_2) + C_6 \sin(\beta x_2) + C_7 \cosh(\beta x_2) + C_8 \sinh(\beta x_2) \quad (6.23)$$

Boundary conditions are used to solve for the constants, C_1 through C_8 . Applying the two boundary conditions on the fixed end, zero slope and zero deflection, yields

$$C_3 = -C_1 \quad (6.24)$$

and $C_4 = -C_2$. (6.25)

For the free end of the beam, the shear force and moment are zero, giving

$$C_7 = C_5 \quad (6.26)$$

and $C_8 = C_6$. (6.27)

The four remaining boundary conditions describe the pinned support: zero deflection, which gives one boundary condition for each section of the boom; the two section's slopes are equal; and the moments of the two sections are equal. These last four boundary conditions together with Equations 6.24-6.27 yield

$$0 = C_1 [\cos(\beta b) - \cosh(\beta b)] + C_2 [\sin(\beta b) - \sinh(\beta b)] \quad (6.28)$$

$$0 = C_5 [\cos(\beta a) + \cosh(\beta a)] + C_6 [\sin(\beta a) + \sinh(\beta a)] \quad (6.29)$$

$$\begin{aligned} C_1 [\sin(\beta b) + \sinh(\beta b)] - C_2 [\cos(\beta b) - \cosh(\beta b)] \\ = C_5 [\sinh(\beta a) - \sin(\beta a)] + C_6 [\cos(\beta a) + \cosh(\beta a)] \end{aligned} \quad (6.30)$$

$$C_1 [\cos(\mathbf{b}b) + \cosh(\mathbf{b}b)] + C_2 [\sin(\mathbf{b}b) + \sinh(\mathbf{b}b)] \\ = C_5 [\cos(\mathbf{b}a) - \cosh(\mathbf{b}a)] + C_6 [\sin(\mathbf{b}a) - \sinh(\mathbf{b}a)]. \quad (6.31)$$

A Matlab program, shown in Appendix C, was used to solve for the natural frequency using Equations 6.28-6.31. To find the natural frequency, the trigonometric coefficients of the four remaining constants, C_1 , C_2 , C_5 , and C_6 , are put in 4 x 4 matrix. The values of \mathbf{b} that make the determinant of this matrix equal to zero will return the natural frequencies of the system. Using the smallest value of \mathbf{b} satisfying the above condition, the lowest natural frequency is expressed as

$$\omega = \mathbf{b}^2 \sqrt{\frac{EI}{rA}} \quad (6.32)$$

where A denotes the cross-sectional area, I denotes the area moment of inertia, ρ denotes the density of the boom material, and E is the material's Modulus of Elasticity. Figure 6.11 shows the variation in the lowest natural frequency with the distance between the free end of the boom and the pinned support.

The graph shows that, based on the vibration analysis, the ideal location for the brace bracket is about 75 cm (30 in) from the free end. However, moving the bracket closer to the truck will increase the angle between the braces and the camera boom, effectively making the braces stiffer. For this reason, the brace bracket will be located about 50 cm (20 in) closer to the truck.

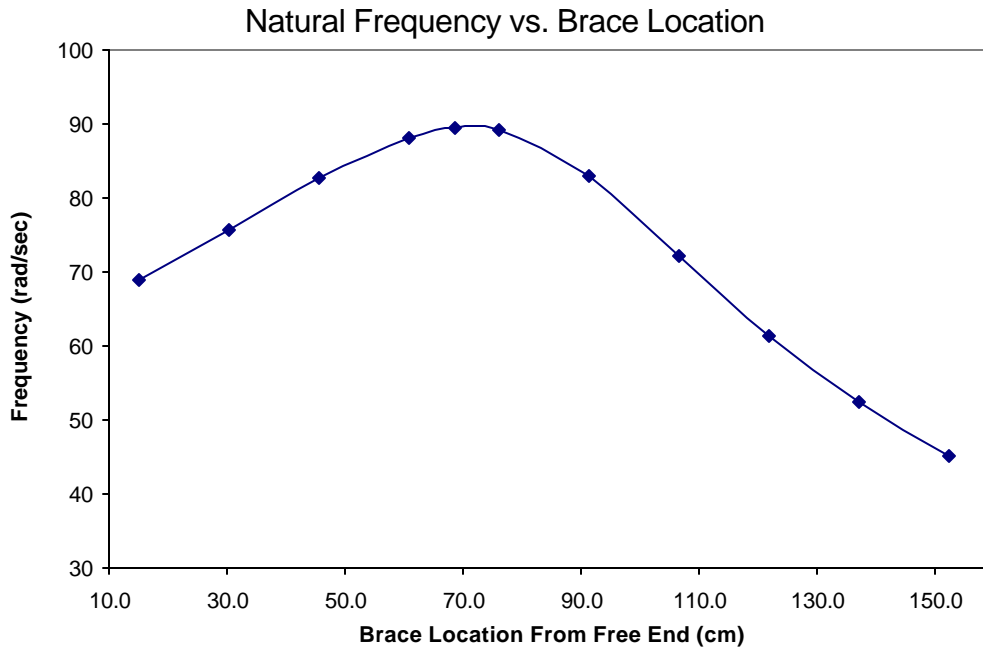


Figure 6.11 - Natural Frequency Results for Brace Analysis

6.7 The Camera Housing

A camera housing is needed to rigidly constrain the camera at the end of the boom and meet several other requirements. Besides providing a place to mount the camera, the design needs to completely enclose the camera to protect it from the weather. While the OCCSM will not be used in adverse weather, it will likely be stored outside when not in use. Also, because the camera needs to align with the coordinate system of the OCCSM's main robotic arm, camera adjustments are key features necessary in the camera housing. The camera boom sets the camera's physical location, but the camera housing must provide for the rotational orientation of the camera. Extra consideration was taken to ensure that the rotation adjustments would withstand the rough and possibly jarring environment. Additionally, since the weight of the camera and housing has a significant impact on camera boom vibration, the design must be lightweight.

A few basic elements will be present in a camera housing designed to meet the mentioned specifications. First, since the housing will completely enclose the camera, the bottom surface of the housing needs to incorporate a clear, colorless lens, through which the camera can view the road surface. An abrasion-resistant Polycarbonate plastic was chosen for the lens material. Second, including the lens surface, the housing effectively needs three horizontal surfaces. The

other two surfaces being the top of the housing and the mounting surface for the camera. Finally, the third important element in the camera housing design is an exit for the cable that connects the camera to the image processing computer.

Two designs were developed for the camera housing. The first uses a custom fabricated sheet metal box to cover an internal aluminum framework. While this design contains all the essential features, it is not considered as robust or as rigid as the second. The main component of the second design is an aluminum tube with an inner diameter large enough for the camera to fit inside. An aluminum cap covers the top of the tube, while the polycarbonate lens fits into the bottom of the tube, making an enclosed chamber for the camera. The camera body mounts to an aluminum ring, and the camera lens fits through a hole in the center of the ring. Once inside the main tube, the aluminum ring holding the camera rests on a ledge machined into the inner wall of the tube. Figure 6.12 shows a cross-section of the assembly.

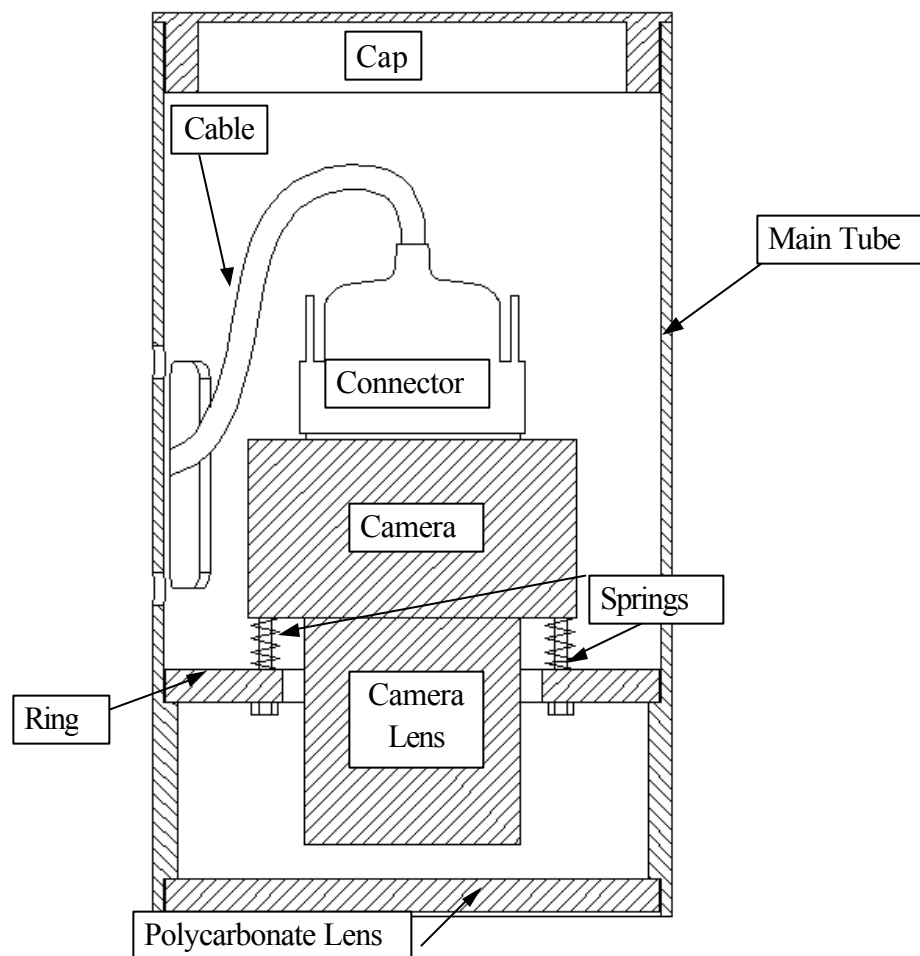


Figure 6.12 - Cross-Section of Camera Housing

The rotational adjustments for aligning the camera are provided by the connections between the tube, the ring, and the camera. To hold the camera on the ring, bolts protrude through holes on the ring and thread into the four corners of the camera body. Springs around each bolt keep the camera raised off the surface of the ring. Tightening or loosening the appropriate bolts will adjust the camera's tilt angle. The rotational orientation about the axis of the camera lens is set by rotating the ring inside the tube. Once the correct orientation is achieved, screws thread into the ring through slots in the wall of the tube. The slots are long enough to allow 20 degrees of adjustment about the axis.

To allow for a flush connection between the camera housing and the camera boom, a circular cut is machined in the end of the boom. The camera housing bolts to a 2.5 cm (1 in) wide aluminum bar fastened in the center of the camera boom's cross-section. The cable connecting the camera to the computer extends up the center of the camera boom from the computer and fits through a cut in the side of the camera housing, visible in Figure 6.12. The cut is made large enough to accommodate the 16-pin connector that plugs into the back of the camera.

6.8 Summary and Recommendations

This chapter has discussed the design of a mechanism used in obtaining an overhead image of the workspace of the OCCSM's robotic arm. First, the crank mechanism that extends and retracts the camera boom was described. Pending testing, this mechanism is expected to be reliable and easy to use. Next, the selection of the camera boom material was aided by several analyses, including vibration considerations. While the best option available was chosen, once the system has been assembled and used, a judgment can be made regarding whether enough room exists to use a boom with a larger cross-section for the next generation machine. A larger boom may preclude using the braces that were described in the section following the selection of the camera boom size. Finally, the camera housing design was discussed. The camera housing is expected to work well, and should require few, if any, modifications for future versions of the OCCSM.

Chapter 7: THE SEALANT HOSE RETRACTION SYSTEM

7.1 Introduction

Supplying sealant to the end of the OCCSM's robotic arm required two new systems to be developed. One of the new systems, the heated sealant hose connecting the melter in the truck bed to the sealant applicator on the end of the arm, has already been discussed in Chapter 3. The other system that needed to be developed is the hose retraction system that adjusts the effective length of the hose to compensate for the extension and retraction of the arm. During crack sealing, the arm on the OCCSM may extend as far as 4.03 m (13.3 ft) (Baker, 1998) to reach the far corners of the workspace. The hose retraction system must store the excess hose, allow the hose to be drawn out as the arm extends, and then bring the hose back into storage as the arm retracts. This chapter discusses the development of the system that manages the hose, allowing it to move with the arm. The system requirements and overall layout of the system are reviewed, options for powering the mechanism are analyzed, and details of the final design are discussed.

7.2 Design Requirements

As mentioned, the main requirement of the hose retraction system is to adjust the hose to match the length of the arm. Naturally, the system should achieve this requirement in the simplest manner, using parts that are reliable, commercially available or simple to make, and require minimal maintenance. Because the arm can supply power to pull the hose out as it extends, the hose retraction system does not need to do more than guide the hose during extension. However, the system must be able to pull the hose back into storage, since the hose cannot be pushed back in by the arm. To avoid extra complication involved in determining when the hose should be pulled back or left to extend, a system that keeps constant tension on the hose was sought. The tension applied to the hose should barely exceed the magnitude of the friction forces that restrict the hose's movement to avoid applying excess tension on the hose and unnecessary loads on the arm.

A location on the truck for the hose retraction system had to be determined before any design options could be considered. Since a great deal of space must be reserved for pallets of sealant material, the hose retraction system must not be placed on the truck bed. Accordingly, the best location puts the system below the truck bed, between the bed's frame rails. The frame rails are

15 cm (6 in) high, 74 cm (29 in) apart, and run the length of bed. In this location the hose retraction system is out of the way but may still be accessed by means of removable panels on the floor of the truck bed. This location also makes sense because the hose must enter the robotic arm below the truck bed just behind the rear axle.

7.3 Design Layout

A method was needed to store the hose in a manner that allows it to easily extend and retract with the arm. While hoses in general are typically stored on reels, this method requires a revolte joint between the reel and the supply line. A joint in the middle of the hose line complicates the matter of heating the hose. Extra steps would have to be taken to route the heater through the joint, and could possibly include designing a revolte joint for the heater. Furthermore, a reel would probably be too large to fit under the truck bed even though some additional space may be available between the truck's frame rails. Clearly, a reel would not satisfy the needs of this system.

The method that was chosen to store the hose consists of a pulley and track system running along the length of the truck bed. The hose wraps around the sheave once, so the sheave needs to move half the distance that the arm extends. In order to allow the sheave to move, it is mounted on a carriage that rides in tracks parallel to the frame rails, as shown in Figure 7.1. With this design, the hose coming from the melter will enter the area between the frame rails just beyond the point where the sheave stops when the arm is completely extended. Also, the system will be offset as shown in Figure 7.1 to locate the hose going to the arm as close as possible to the centerline of the truck. The 10 cm (4 in) EMT conduit, which routes the hose over the truck's differential, will also direct the hose the remaining distance to the centerline of the truck so the hose can enter the robotic arm.

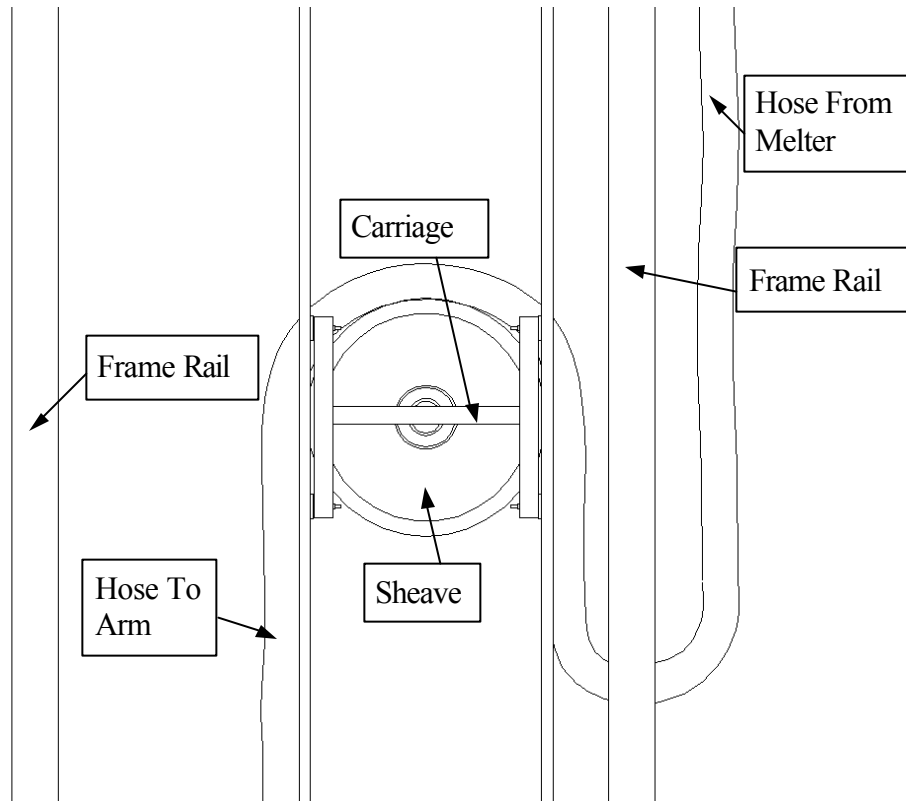


Figure 7.1 - Hose Retraction System Layout

7.4 Retraction Power System

Using the pulley and track design, the power system used to retract the hose will attach to the carriage that runs on the track. The system will constantly apply a force acting to pull the carriage and sheave towards the front of the truck bed. Because the hose wraps around the sheave, the force applied to the carriage must be double the force required to overcome friction forces opposing hose movement. All of the options considered to apply a force on the sheave employed a cable connecting the carriage to the power system. Using the cable, the power system will remain stationary allowing it to protrude below the bed frame rails into any space available between the truck's frame rails.

Several options were considered to supply power to keep the cable connected to the carriage under tension; all were powered by either electric, hydraulic, or spring devices. The majority of them employed a reel to wind the cable on, and they only differed in the method of applying torque to the reel. Both the torque required by the power device and the number of turns necessary to fully extend and retract the hose were varied by considering different size cable

reels. A gear reduction mechanism, using a series of chain sprockets and shafts, was also examined to adjust torque levels required by the power system.

7.4.1 Electric and Hydraulic Motor Options

While using an electric motor to provide torque is a possibility, it would require extra systems to prevent the motor from overheating when stalled. For example, power to the motor would need to be regulated based on whether the robotic arm was in motion or not. In order to avoid the problems associated with an electric motor, the use of a hydraulic motor was considered. While the hydraulic motor could supply constant torque, it also had a few disadvantages. First, it required routing hydraulic lines from the truck's PTO unit to the location under the truck bed. Also, to provide a constant torque, a constant flow of hydraulic fluid through the motor was required, making the system unnecessarily inefficient.

7.4.2 Hydraulic Cylinder Options

The use of hydraulic cylinders also required the installation hydraulic lines, but did not have the inefficiency associated with hydraulic motors. The first of two cylinder powered designs utilized the gear reduction mechanism described above. In addition to the cable connecting the carriage to the output of the gear mechanism, another cable and reel assembly connects the input of the gear mechanism to the cylinder rod. The configuration of the gear reduction allowed the cylinder to have a reasonable stroke length, but required it to produce higher forces. The main disadvantages of this system are the necessity for gearing, the additional parts needed to mount the gear mechanism, and the second reel and cable assembly.

The second design that utilized a hydraulic cylinder was based on a block and tackle. The cable connected to the carriage would be wound through the pulleys in the block and tackle, and the cylinder would simply provide a constant force to expand the mechanism. This design was mechanically simpler and easier to mount beneath the truck bed than the gear reduction design. However, this design still required a hydraulic supply, and a suitable block and tackle would have to be found or fabricated. Avoiding the hydraulics in either of these two designs would be possible by using gas springs. While this would eliminate the need for hydraulics, a simpler method is available where all the necessary parts, including the cable, are available as a single unit.

7.4.3 Spring Powered Tool Balancer

The use of a spring mechanism proved to be the simplest way to solve the hose retraction problem. A spring mechanism requires no electrical or hydraulic connections since it stores up energy as the arm extends. After examining several options of constant force and constant torque springs, a tool balancer, which uses a constant torque spring, was found that met all requirements.

A tool balancer is typically used to support a hand tool hanging above a manufacturing workstation, making the given operation more efficient and physically less stressful for the operator. The main body of the tool balancer encloses the spring and a reel for the cable. The spring is typically preloaded so it provides a nearly constant tension on the cable throughout its extension. The only significant disadvantages of the tool balancer design are the weight and cost of the tool balancer, and the spring's fatigue life. However, the weight and cost factors are likely very similar to the other options considered, which required more parts and involved more complication. The only data offered by the tool balancer manufacturer about the spring's fatigue life was that in typical operation they last for a few years. The spring's life is not a major concern because the OCCSM is expected to undergo limited use and the spring in the tool balancer can be replaced if failure occurs. The tool balancer used in this mechanism will provide about 330 N (75 lb) of tension on the cable with an extension length of 200 cm (78 in).

7.5 Detailed Design

With the conceptual design completed, the focus was shifted to the design of the individual parts. The track and rollers were the first items specified in detail since they work together and interact with a majority of the other parts. Several different configurations and track styles were considered. Commercially available track and roller combinations in general had high precision and tolerance, and were therefore also high in price. The best alternative was determined to be one using a standard 3.8 x 1.9 x 0.32 cm (1.5 x 0.75 x 0.125 in) C-channel for a track and having custom steel rollers made.

The rollers, which ride down the middle of the C-channel, were designed with a few features that were essential for their task. First, since the legs of the C-channel are slightly tapered, the roller surface in contact with the channel legs was machined with a matching taper, ensuring a maximum amount of contact area. Second, a lip was left on the roller that will come in contact

with the end of the channel legs to support any side loads. The middle of the roller was bored out to accommodate a bearing and a shoulder bolt that mounts the roller to the carriage.

The carriage is made from three pieces of 2.5 cm (1 in) square steel tubing welded together to form an “H”, as shown in Figure 7.2. The four rollers bolt to the ends of the two side tubes, and the shaft constraining the sheave is welded to the middle of crossbar that forms the center of the “H”. The size of the carriage places the wheels at the corners of a 30 cm (12 in) square, making the reaction forces on the rollers less than 156 N (35 lb) under the expected operating conditions. With the expected loads, the maximum bending stress in the carriage is 5.2 MPa (750 psi), providing a factor of safety against yield of 48.

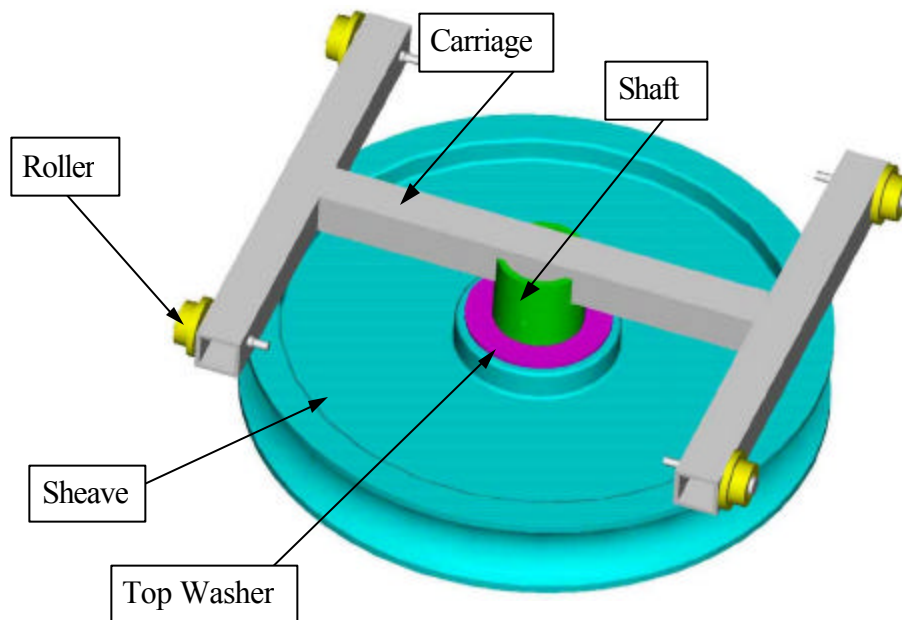


Figure 7.2 - Model of Carriage and Sheave

Finding something to function as a sheave required searching through several catalogs and contacting suppliers. Most of the difficulty resulted from the requirement for a relatively large diameter with a thin profile. Even though the hose was chosen because of its small bend radius, the minimum radius was still 18 cm (7 in), requiring a 36 cm (14 in) diameter sheave. The best solution found was a 41 cm (16 in) diameter textite wheel that was modified to fit the application. The main modifications include making the wheel thinner, cutting a round slot around the diameter of the wheel for the hose, and removing unnecessary material to reduce weight.

With the sheave design complete, its mounting shaft could be designed. As mentioned, the shaft attaches to the middle of the carriage and is made from a steel tube. The shaft's outer diameter is cut to match the 6.17 cm (2.43 in) inner diameter of the wheel. No bearing is used because the toughness of the wheel material and the relatively large wearing area provides a design life adequate for the prototype machine. To constrain the wheel in the axial direction, two custom flat washers are used, which contact flat surfaces near the wheel's hub. The top washer can be seen in Figure 7.2, and both are visible in the cross-section view shown in Figure 7.3. The lower washer bolts to the end of the shaft once the parts are assembled.

Brackets are used to connect all the components to the truck. These brackets are spaced along the length of the track and mounted to the crossbars that run across the width of the truck on top of the bed frame rails. The brackets are fabricated from 3.81 cm (1.5 in) steel angle, making it easy to connect the track to the crossbars, which run perpendicular to each other. Because the inside of the C-channel must be left clear for the rollers, the brackets are welded to the tracks, but are bolted to the crossbars so that the assembly is still removable.

While the design of the primary components of the hose retraction system was complete, a method of supporting the hose under the truck bed was still needed. There are two lengths of hose requiring support. The first length of hose stretches from where it enters the area under the truck bed to where it wraps around the sheave. The second stretch is between the sheave and the conduit that routes the hose around the truck's differential. Obviously, both of these lengths change as the hose extends and retracts with the robotic arm. To support the hose throughout its range of motion, a sheet metal tray hangs just far enough below the sheave for clearance, see Figure 7.3. The groove around the diameter of the sheave should slightly move the hose up and off the tray as the hose moves around the sheave. The same brackets used to mount the track to the truck bed are also used to hold the tray. The brackets' geometry accommodates the tray, which is about 15 cm (6 in) wider than the distance between the tracks

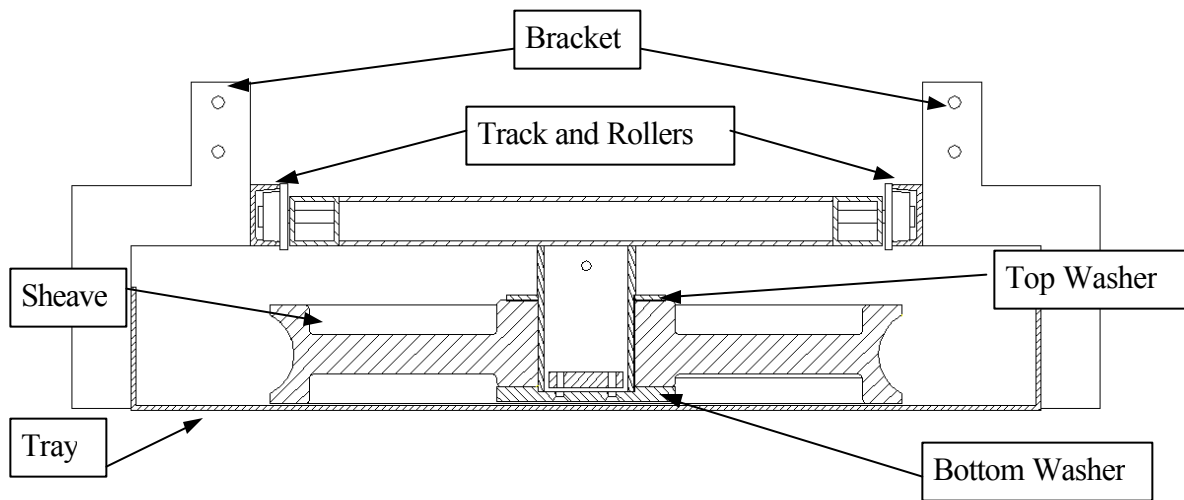


Figure 7.3 - Cross-Section of Hose Retraction Assembly

7.6 Summary and Recommendations

This chapter has presented the requirements and design of the hose retraction system on the OCCSM. The hose retraction system is needed to adjust the effective length of the sealant hose as the robotic arm extends and retracts. An important and challenging aspect of the design was placing the system in the limited space between the truck bed frame rails. Section 7.2 discussed the conceptual design and the reasons for using a pulley and track system. The several options for powering the mechanism were presented with the advantages and disadvantages of each discussed in Section 7.3. The power option using a tool balancer was chosen mainly because it did not need an additional supply of power since it stores up energy as the arm extends. Other factors influencing the decision were that the tool balancer required only parts used for mounting it to the truck bed and its availability commercially as a complete unit. Section 7.4 discussed the detailed design and important considerations associated with the individual parts.

Many of the system components have already been made or purchased, but they have not been assembled because of delays in receiving the vehicle. Once the truck arrives, the system will be assembled and the hose installed. However, the tool balancer will not be purchased until a measurement can be made of force required to move the hose, allowing the most suitable balancer to be chosen.

Once completed, the system is expected to operate smoothly. However, a few areas should be checked periodically for excessive wear or improper operation. One area of concern involves the hose cover's ability to withstand its interaction with the sheave while the hose is under up to 156 N (35 lb) of tension. Another issue is the effect, if any, that the hose tension will have on the

performance of the robotic arm. Most of the concerns result from the tension in the hose coming from friction forces opposing motion. If a problem does arise, adding rollers to specific portions of the hose path could reduce friction in the system. The hose retraction system designed here meets the requirements specified at the beginning of the chapter and should require few modifications for future versions of the OCCSM.

Chapter 8: THE CONTROL SYSTEM

8.1 Introduction

The control system of the OCCSM implements the most cutting-edge PC and information technologies including the Internet technology. It is the first highway construction and maintenance machine that utilizes the Internet. The embedded real-time control system is based on object-oriented software design and has the most sophisticated and easy-to-use man-machine user interface.

8.2 Control System Overview

The control system for OCCSM consists of five subsystems: imaging, motion control, operation control, user interface and main computer, as showing in Fig. 8.1. The imaging system provides the image of the 4 m by 4 m (12 ft x12 ft) workspace for the system. It scans the road surface and provides live images for the operator to detect cracks. Once a crack is identified, a high-resolution picture of the workspace is taken and mapped to the screen of the user-interface. The motion control subsystem controls the robotic arm within the workspace. It is a two-axis motion control system: one controls the rotation of the arm and the other the telescoping. Under

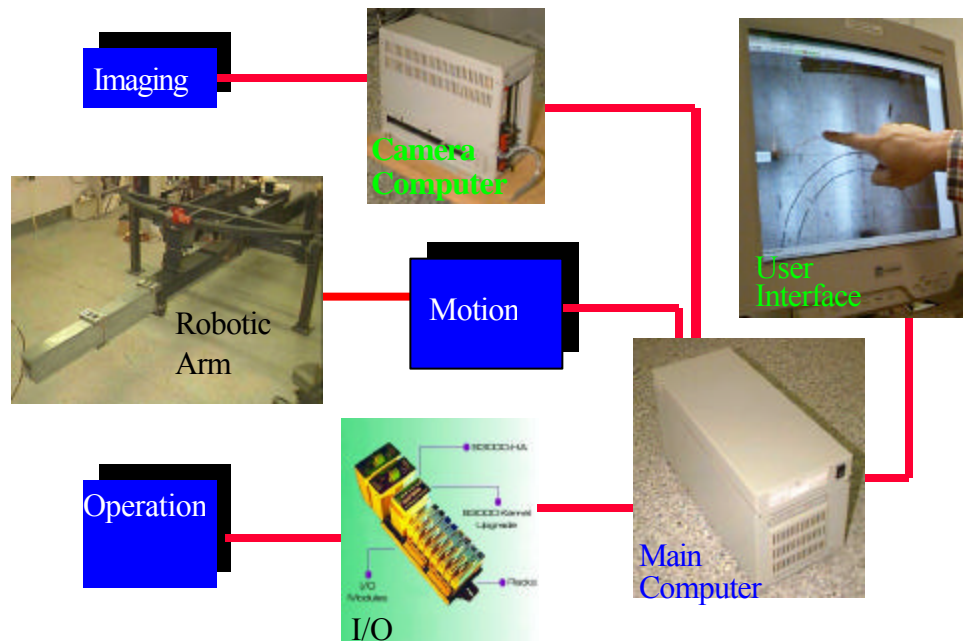


Figure 8.1 - Control System Overview

this control, the tip of the arm is able to move to any point within the workspace and follow a given path accurately at a controllable velocity. The operation control system controls the valves, switches and sensors of the sealing head, as well as the temperature and flow rate of the sealant. This subsystem must cooperate with the motion control system very well to perform a high quality sealing operation.

The user-interface provides a responsive and interactive control window for the operator to control the image processing, arm's movement, sealing operation and other tasks. In addition to all necessary control menus and buttons, the control window is mapped to the workspace with undistorted images. This allows the operator to interactively monitor and perform all the tasks in a straightforward manner.

Although the subsystems are distributed and separately accessible, a dedicated computer --- the main computer, is provided as a main platform for the operator. In order to handle concurrently the real-time control and user interface tasks, this platform must be reliable, multitasking, responsive and graphical with sufficient computing power.

8.3 Hardware

8.3.1 Robotic Arm and Servo Actuators

The robotic arm is the essential component of the OCCSM system, see Fig. 8.2. The manipulator system is comprised of a single revolute joint at its base and a telescopic arm. The telescoping motion is accomplished through a custom designed prismatic ball screw actuator which allows for extended reach, and provides this reach with constant velocity motion and high positioning accuracy. The actuator uses a dual, concentric output shaft gearbox, two drive tubes and two ball screws interconnected to obtain a stroke equal to the sum of the two screws. All components are connected in a prismatic manner similar to a telescopic hydraulic cylinder. The two ball screws are driven simultaneously with one input motor through a planetary gearbox. The ratio of the two outputs of the planetary system is inversely proportional to the ratio of the leads of the corresponding screws that they are driving. Accordingly, both ball screws extend at the same rate. The uniqueness of this actuator lies in its ability to translate at a constant velocity with high positional accuracy, but without the need for extraneous positioning devices (Baker, 1998).

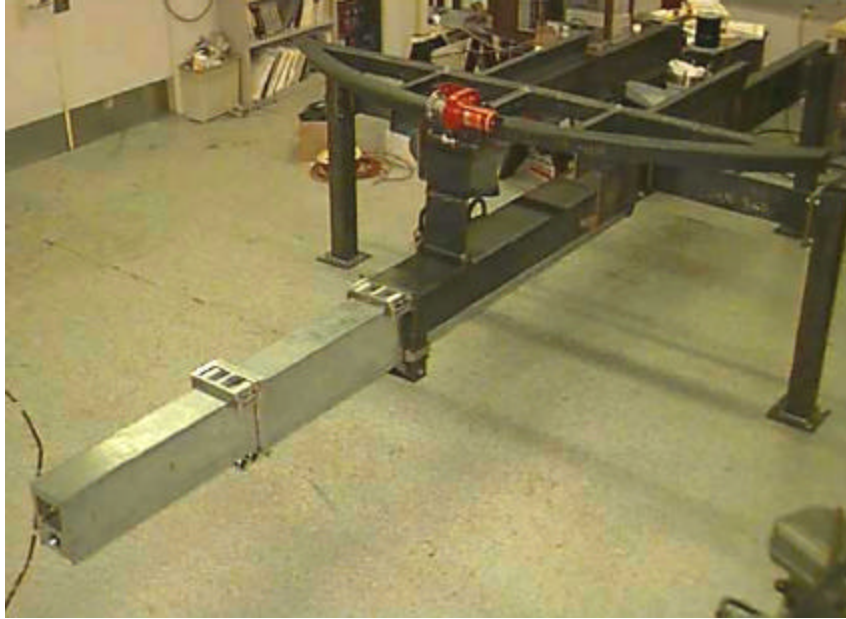


Figure 8.2 - Robotic Arm

Two brushless DC motors (Fig. 8.3) are used to drive the telescoping motion and the arm's rotation, which let the end-effector move within the 4 m by 4 m workspace. The telescoping motion is driven by an APEX620-MO-25 motor and the rotation by a Dynaserv-DR-5030B. Both are from Compumotor, Parker Hannifin Corporation. Some of the specifications of these two motors are listed in Table 8.1. For more details, please refer to the user guides.



Figure 8.3 - Motors controlling the two axes

	APEX620-MO-25	Dynaserv-DR-5030B
Torque, Nm	13.94	22
Speed, rps	62	4
Power, KVA	3.6	4.5

Table 8.1 - Specifications of the motors

Both Apex and Dynaserve motors come with their own servo drivers, APEX40 and SR5000, respectively. The primary function of those drivers is to seek and maintain a position command from an indexer or a velocity or torque command from a servo controller. In this case, the servo controller is the AT6250 motion controller that will be described later. These drivers are mounted into a power box showing in Fig. 8.4.

8.3.2 Motion Controller

The motion controller takes high-level instructions from the computer and sends commands to the motor drivers to reach the position, velocity or torque required by the instructions. It is both the programming and physical interface between the computer and the drivers.

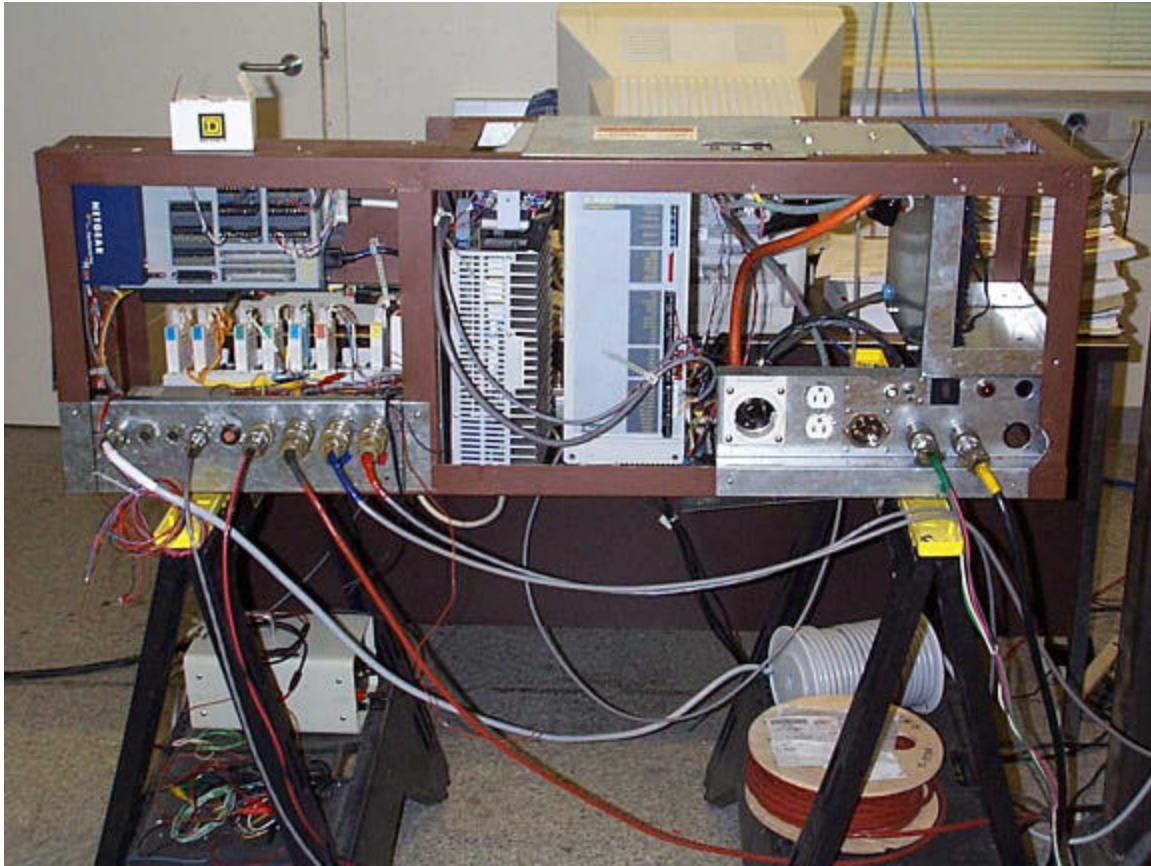


Figure 8.4 - Power box with motor drivers

The OCCSM system implements the AT6250 motion controller made by Compumotor. It is an ISA type card that fits in an ISA PC slot. This 2-axes motion controller has its own dual processor and operating system that can update each axis as fast as 200 microseconds. The dual processor board is comprised of a microprocessor for executing high-level motion programs and a digital signal processor (DSP) for high-speed sophisticated servo control. As such, the main computer, in which the AT6250 resides and will be described below, can be released from the real-time tasks and concentrate on the user interface and networking.

8.3.3 I/O Controller

The operation control subsystem deploys a B3000 brain board, from Opto 22, see Fig. 8.5. The so-called "brain board" is an external I/O board with a built-in microprocessor. Opto 22 I/O modules can be plugged into this board and the on-board microprocessor handles the A/D, D/A and even PID control tasks. The brain board created a truly distributed and scalable, intelligent I/O system. It communicates with the main controller in a command response mode as a slave

device and provides the local intelligence necessary to perform basic control functions such as on/off control, counting and latching, or complex tasks such as PID control, temperature conversion, time proportional output, and emergency shutdown.

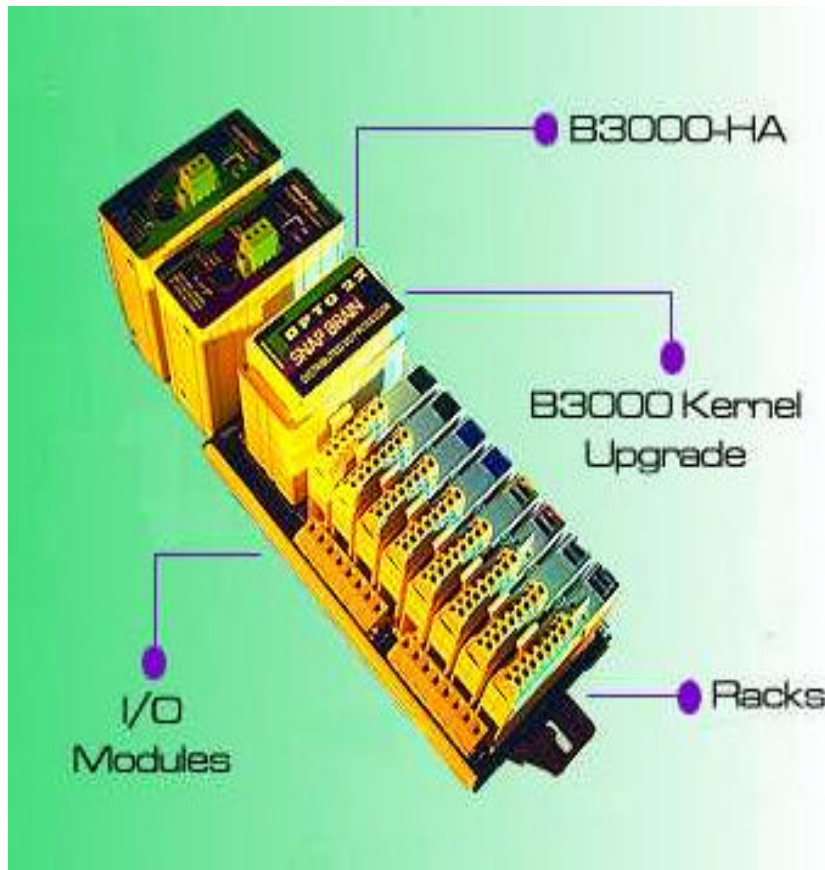


Figure 8.5 - Opto 22 brain board for analog/digital I/O control

Opto22 I/O units respond to Mystic, Optomux and Pamux protocols. Pamux uses a parallel interface. Mystic and Optomux use serial ports. The Mystic protocol is selected for its higher level of intelligence with PID control, event-reaction logic, pulse duration measurement, and much more, at speeds up to 2.5 MBaud. By performing most of the time-critical functions at the I/O unit level, system performance is optimized and is relatively independent of the main computer used for the user interface. A 16-bit processor dedicated to 16 or fewer I/O points performs digital functions such as latching, counting, and time delays or pulse generation. Analog PID loops, high/low limit monitoring, and engineering unit conversions are performed by the analog Mystic brain board. While it is possible to create code to talk directly to the Mystic

protocol brain board, the I/O control module uses the software driver provided by the vendor to control the temperatures and valves.

An AC37 high-speed communication adapter card, also from Opto22, is used for the communication between the brain board and the main computer. It is an ISA card that provides a RS-485 or 4-wire communications link. It is designed to allow any IBM AT or compatible computer access to the Opto22 Remote I/O Bus. The Remote I/O Bus is a standard RS-485 half-duplex (2-wire) serial communications link. The AC37 is primarily used to allow an AT to be the host on a Remote Bus link controlling a network of Opto 22 Remote I/O bricks, though it can also be used to monitor a link for redundant host applications. To user software, the AC37 appears as a standard IBM serial 'COM' port.

8.3.4 Digital Camera and its computer

The EDC-1000U computer camera, from Electrim Corporation, is the only one we could find that gives an 1134 x 972 resolution in the \$1000 price range. It uses an ISA interface card to control the camera and a PC is needed to control the camera.

The cable connecting the camera to the PC is limited to a maximum of 5 m (15 ft). Based on our early tests, using a cable longer than that will result in significantly degraded image quality. Other digital cameras with built-in microprocessors, which are usually 5-10 times more expensive, have similar limitations as they use a serial connection to the computer. Even though they use a fast RS-422 link, a long serial cable still decreases the image transfer speed to an unacceptable low baud rate.

Unfortunately, the main computer in the truck's cab is too far from the rear of the truck where the manipulator's workspace is located and the camera is mounted. Therefore it is impossible to use the main computer to handle the camera and a dedicated camera computer is necessary. As the PC price has dropped to the break-through \$500 level, the use of a dedicated computer for imaging is less expensive than using a high-end camera. There is another reason to use a dedicated camera computer: the image acquisition uses CPU time heavily. To get a full 1134 × 972 picture, for example, takes about 2 seconds. It is therefore apparently better to not use the main computer to handle this.



Figure 8.6 - The embedded camera computer

The advancements in embedded PC technology make it feasible to utilize a camera computer that's fast and small enough to be mounted near the camera. The camera computer uses a very small case (MBPC-641, from Advantech) as shown in Fig. 8.6. The back plane has three ISA slots inserted with a 3Com fast 10/100 network interface card, the camera interface card and a Pentium 133 single board CPU board with built-in video. A 1 GB notebook hard drive is mounted in the case and is installed with the Windows 98 operating system. By using a fast Ethernet network (100 Mbps) for the main controller and the camera controller, the image transfer is significantly faster than the 10 Mbps network. A full frame image (1134 x 972 x 256, about 1.1 MB), for example, takes about 1.5 seconds to be sent to the main computer over a 10 Mbps network and it takes only about 0.3 seconds over a fast network.

8.3.5 The Main Computer

The main computer is built in a compact embedding PC chassis, IPC-6806, from Advantech, see Fig. 8.7. It has 2 PICMG, 2 PCI and 2 ISA slots, a 3.5" hard drive bay and a floppy bay. The floppy drive bay is mounted with an LS-120 disk drive which uses both 1.44MB floppy disks and 120 MB Super Disks. A 4 GB hard drive is used to install the Windows NT 4.0 operating system and programming tools such as Microsoft Visual Studio 6.0. A Pentium 233 MMX single board computer (SBC), PBC-P5RV, from Recortec, is inserted in one of PICMG slots as the main control computer (this SBC is replaced with a dual-PIII board later). An Intel 10/100 fast network interface card is inserted in the other PCI slot. A high-resolution touch

screen monitor is set beside the driver and is used as the main interactive input/output device for the operator's convenience. The AT6250 motion control card described above is inserted in one of the ISA slots.

The main computer is networked to the I/O control subsystem and camera computer.



Figure 8.7 - The main embedded computer

8.4 Software

There are two parts of software: those running on the camera computer and those on the main computer. All the software is 32-bit, object-oriented, multithreaded and modular programmed in Visual C++ 6.0 (originally 5.0) and MFC (Microsoft Foundation Classes).

8.4.1 Camera Computer Software

The camera computer runs as both a real-time camera controller and an image server. Actually, it deploys a HTTP server. HTTP servers are those that are running all over the world and serving the WWW. By introducing the Internet technology, getting an image from the camera becomes as simple as opening a Web page within a Web browser.

The camera control and image acquisition program controls the camera through a 32-bit VXD driver for Windows 95/98 provided by Electrim Corp., the camera vender. By implementing the “virtual camera” concept, the same camera can be concurrently used for high-resolution still imaging, non-interlaced live imaging, and low resolution Web browsing. By making it Internet-enabled, the main computer can control the camera and acquire an image from the camera using the reliable and simple HTTP protocol. Furthermore, anyone can use a Web browser to monitor the workspace.

8.4.1.1 Camera Control

A “Virtual Camera” is actually an object of the CCamera class we built for handling the EDC-1000U camera. In order to make it easier to change the working mode and resolution of the camera for different purposes, we wrap the complexity of the functions provided by the VXD driver into a class, CCamera. A brief description of the CCamera class is shown as follows:

```
//camera.h : interface of the CCamera class
//Camera control functions to be wrapped into CCamera
extern "C" void __pascal __far
usubcam (unsigned int,int,int,int,unsigned int, field, int __far *);
extern "C" void __cdecl __far
InitDAC (unsigned int);
extern "C" void __cdecl __far
SetBiasValue (unsigned int, unsigned int);
extern "C" void __cdecl __far
SetGainValue (unsigned int, unsigned int);
//definition of camera class
//class CCamera;
class CCamera : public CObject
{
public:
    CCamera ( unsigned int nTop, unsigned int nBottom, unsigned int nWidth);
protected:
    CCamera();
    DECLARE_SERIAL( CCamera )
    ~CCamera();
// Attributes
protected:
    int m_nTop;
    int m_nBottom;
    int m_nWidth;
    unsigned int m_nExposureTime;
    int m_nBias;
    int m_nGain;
    int m_nABFlag;
    int m_nInterlaceFlag;
```

```

        int m_nFieldFlag;
        int m_nLineLength[V];
        pixel * m_pBuffer1[V];
        pixel * m_pBuffer2[V];
        pixel * m_pDisplayBuffer[V*2];
public:
//Operations
public:
    void InitCamera();
    void InitSettings();
    void SetBias(unsigned int nBias);
    void SetGain(unsigned int nGain);
    void ReadCamera();
    void WriteImage();
};

```

Each instance of the CCamera class is a virtual camera and all the virtual cameras, with different image sizes defined by the constructor, can share the same physical camera without confusion. For example, a virtual camera set as 1134 x 486 / non-interlaced, i.e., nTop=0, nBottom=486, nWidth=1134, and m_nInterlaceFlag=0, is used during the alignment of the camera to the workspace for its relatively fast and shadow-free updating. When the camera is taking images of moving objects, the interlaced image is degraded with shadows. Another virtual camera set as 1134 x 972 / interlaced is used to take the last picture for crack sealing due to its high resolution. A low-resolution virtual camera set as 72 x 72 / non-interlaced is used for the HTTP server to allow anyone to monitor the progress of the sealing process with a WWW browser.

8.4.1.2 HTTP Server

A simple HTTP server is built and runs on the camera computer. The server is based on an HTTP server example presented in the book "Inside Visual C++ for Version 5.0" (Kruglinsky, 1997) and trimmed to be as simple as possible for embedded systems. The main part of the HTTP server is a thread, the ServerThreadProc(LPVOID pParam), which listens on port 80 for some clients to connect and processes clients requests. If the request is an image, it will then create a CCamera object, i.e. a virtual camera described above, to get an image from the camera, and send it back to the client. So it works in the same way as a normal web server sending a GIF or JPG image to a client, except here the image is generated on-the-fly from the camera. The program is very simple, reliable and has a very small footprint of 51KB to fit embedded applications.

On the client side, the `CInternetSession`, one of the new Internet classes included in Visual C++ 4.2 or higher, makes HTTP client-side programming extremely simple. To get a file from a remote URL is as simple as opening a local file. The following few lines of code is all that is needed for the main computer to get an image from the camera through the HTTP server embedded on the camera computer:

```
#define MAXBUF 2000000
CInternetSession session;
CStdioFile* pFile = NULL;
Unsigned char buffer [MAXBUF]; //Store received file
CString sURL = "http://192.168.1.3 486 1134 ";

try {
pFile = session.OpenURL(sURL, 0, INTERNET_FLAG_TRANSFER_BINARY |
INTERNET_FLAG_KEEP_CONNECTION);

nBytesRead = pFile->Read(buffer, MAXBUF - 1);
}
```

where `http://192.168.1.3 486 1134` means the camera computer has a private IP address (192.168.1.3) and an 1134 (W) x 486 (H) image is requested. For more control of the camera, control parameters, such as interlaced mode, contrast, brightness and etc., can be appended to the URL address.

8.4.2 Main Computer Software

The three software modules that run on the main computer are:

1. User interface module
2. Motion control module
3. I/O control module.

The user interface module is at the highest level. While the motion control module provides a bridge between the user interface and the AT6250 motion controller, the I/O control module provides a bridge between the temperature/valves control and the user interface. Accordingly, the real-time control activities are hidden from the user interface. The user interface module is based on motion control and I/O control modules. Meanwhile, the motion control and I/O control modules themselves are independent Visual C++ classes that can be used by any Visual C++ programs, including the user interface module, to control the motion of the manipulator, the temperature of the sealant, and the valves and switches for the crack sealing operation. A major advantage of this architecture is that both of the real-time control modules, motion and I/O, can

be programmed and debugged separately, and they can be easily integrated into the user interface at a later time without any changes. The user interface can then simply use the objects constructed from those classes without having to deal with the low-level control routines. Such a modular and object-oriented architecture also means that the changes in one module and the corresponding hardware will not influence another module, which is very important for both development and future upgrading.

8.4.2.1 The Motion Control Module

AT6250 provides both the Dynamic Link Library (DLL) and the Dynamic Data Exchange (DDE) servers for Windows and Windows NT applications. Most of the DDE servers have their corresponding equivalent AT6250 commands or DLL call functions, but the DDE protocol automatically updates data to and from Windows applications. The motion control module mainly uses DLL calls to communicate with the AT6250 and encapsulates these calls for the motion control tasks.

There are mainly two classes in the motion control module: CServo and CMotion. CServo is the base classes of CMotion. CServo handles the very basic low-level and hardware-related functions needed for initialization, configuration and control of the motion control card. Some of the member functions of the CServo and their usages are listed in Table 8.2.

Function Name	Usage
InitializeControlCard()	Set port# & IRQ#, load OS for AT 6250
InitializeAxis()	Set axis scales, gains, hard limits, etc.
SetAxisPosition()	Set the target position
SetAxisVelocity()	Set the motion velocity
SetAxisSmoothAcceleration()	Set the motion acceleration
SetAxisDeceleration()	Set the motion deceleration
GetAxisPosition()	Read axis position
GetAxisVelocity()	Read axis velocity
GoMove()	Start the motion to target

Table 8.2 - CServo class

Derived from the base class CServo, the CMotion class provides high-level motion control functions and motion states data for the robotic arm control. All the functions are not hardware-related and one can use them, without knowing the hardware details, to conduct a two-axis motion, such as path following required by crack sealing operation. Table 8.3 listed some of the member variables and functions.

Class Members	Description
m_dLastR, m_dLastTheta, m_dCurrentR, m_dCurrentTheta, m_dNextR, m_dNextTheta	Last, current and next position
m_dNextRVelocity, m_dNextThetaVelocity	Next velocity
SetInitialConditions()	Set the initial conditions before a new motion
CalculateNextMove()	Calculate the radial and telescoping speeds for the next move.
InitiateNextMove()	Start a new move
WaitCurrentMoveDone()	Wait for the move to be done
StopMotion()	Stop the motion
HomeAngularAxis(), HomeRadialAxis()	Homing the two axis

Table 8.3 - CMotion class

8.4.2.2 The I/O Control Module

Similar to the motion control module, the I/O control module consists of two classes: the base class CSnap and the derived CSensor. The CSnap handles the hardware related functions and encapsulates the command sets included in the DLLs provided by Opto22, such as Digital Setup, Digital I/O Configuration, Digital Read/Write/Latch, Analog Setup, and Analog PID Loop. CSensor provides functions and states data for the crack sealing operations, such as setting the temperature of the sealant hose wall, setting the flow-rate of the sealant, etc. The user interface module and any other C++ code can use these functions and states data without having to deal with the hardware. This isolation between the hardware and software is highly desired in system development. These classes and some of their members are listed in Table 8.4.

Members	Description
CSensor	
EnergizeDriverRelay()	Turn on/off the power relay of the motor drivers
EnergizeHeadLiftRelay()	Turn on/off the power relay of the Sealant head
EnergizeFlasherRelay()	Turn on/off the power relay of the Flasher
GetHeadTemperature()	Read temperature of the sealant head
GetCartHeaterTemperature()	Read temperature of the cart heater
GetCupHeaterTemperature()	Read temperature of the cup heater
GetLoopHeaterTemperature()	Read temperature of the sealant loop heater
GetOilTemperature()	Read temperature of the oil
GetHoseHeaterTemperature()	Read temperature of sealant hose heater
GetSealantTemperature()	Read temperature of sealant
GetFloatPosition()	Read sealant reservoir level
SetFloatPressure()	Set the sealant reservoir pressure
SetSealantFlowrate()	Set the sealant flow rate
CSnap	
m_hPort	Port address
M_nErrorCode	Error code
M_nPosition[2]	Sealant head position
M_nSendData[16]	Data to be sent to Snap board
M_nReceData[16]	Data received from the Snap board
InitializeBus()	Initialize the communication bus
PortOpenAC37()	Open the serial port of AC37 board
PortCloseAC37()	Close the serial port of AC37 board
DigitalInputAC5A()	Read digital input
DigitalOutputDC5SNK()	Send digital putput
AnalogInputTM()	Read temperature
AnalogInputV()	Read voltage
AnalogOutputA23()	Send analog output on channel A23
AnalogOutputV25()	Send analog output on channel V25

Table 8.4 - CSnap and CSensor classes

8.4.2.3 The User Interface Module

When the truck is driving on a freeway at a speed of about 24 km/hr (15 mph), the digital camera working in the non-interlaced mode updates the road image every second, and the image is shown on the main display for the operator. Once a potential crack is identified, the truck will be stopped by the operator, and the camera will work in the interlaced mode in order to provide the highest resolution (1134 x 972) image of the workspace. The image will be mapped to the actual coordinates, and the distortion caused by the lens will be corrected. Thus, the image on

the screen will exactly map the workspace. To seal the crack, the operator simply uses his finger and follows the crack on the touch screen. The user interface program will then send the corresponding commands and path information to the motion control and I/O control programs. The motion control program will then control the manipulator to follow the crack while the I/O control program controls the sealant temperature and flow-rate to provide a high quality seal.

In order to handle all these tasks in an easy-to-use graphical user interface, many classes have been built into the user interface module, as shown in Fig. 8.8.

The CImage class handles the imaging tasks. It controls the camera, requests an image, corrects for distortion, stores the image in a device independent bitmap object --- an instance of CDib class, and draws the image on the screen. The image could be in any available size and resolution.

The CProcess class communicates with the motion and I/O modules and isolates the user interface from hardware. It provides, in a single class, all the functions that the user needs for motion and I/O control, such as turn on/off the power, start/pause a motion or queued motions. Since user interface should always not be blocked and remain responsive, all the time-consuming motion and I/O tasks are put in separated threads. However, multi-threaded programming is difficult and not so object friendly. The most important feature of CProcess is that it encapsulates the very complicated threads handling. The CControlThread works together with CProcess to handle all the real-time control tasks such as axis homing, path following and motion monitoring. The details will be given later.

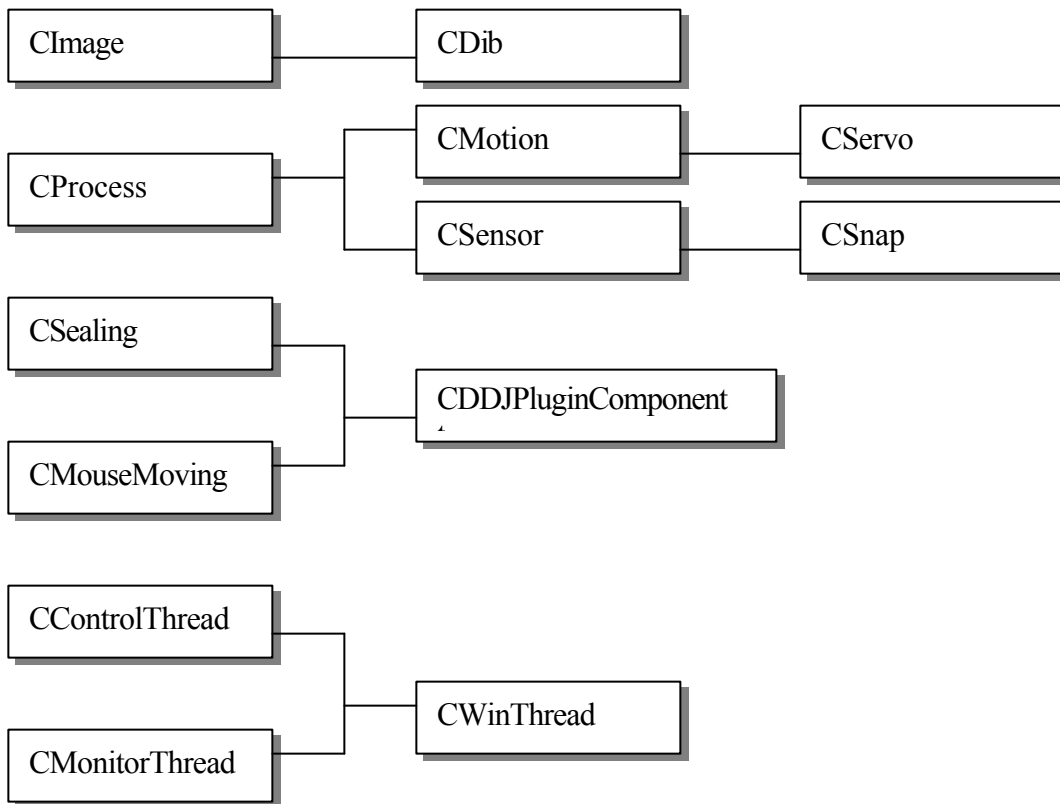


Figure 8.8 - User-interface classes architecture

The CSealing class handles the crack-sealing task, including path planning and smoothing. The CMouseMove is designed to handle the local zooming --- a tool helps the operator to see the crack image better in an amplified moving window. Both the CSealing and CMouseMove are derived from the CDDJPluginComponent class because they deal with the mouse events concurrently. One of MFC's limitations is that it cannot encapsulate different window functionality into separate objects. The CDDJPluginComponent, developed by Stefan Hoenig, provides a unique approach for this and hence is used here.

The CMonitoringThread class provides system-monitoring functionality in background. This thread is set to have a lower priority; so other time critical tasks like motion control have more CPU time. It requests periodically current states from the CProcess and refreshes the display with the newest status such as the position of the arm. It also uses the requested information to diagnose any possible abnormality and take prompt reactions. For example, if the arm runs away

from its suppose target more than, say, two seconds, this monitoring thread will stop the motion automatically.

8.5 Key Technologies

8.5.1 Embedded PC

The complexity of current embedded systems makes the adoption of PC technology highly attractive due to the wide availability of fast growing PC hardware and software support. A modern embedded control system often requires real-time machine vision, sensing, and motion-control as well as a graphic user interface. To realize these demanding functions, off-the-shelf PC hardware is easy to find, and highly adequate visual programming tools are readily available. While broadly applicable, the use of embedded PCs is most advantageous for products that are built in smaller quantities but require extensive development, such as the advanced highway maintenance and construction machines as well as such machines as industrial robots.

With the introduction of the PC104 and CompactPCI industrial standards, it is apparent that the value of PCs far exceeds the typical home and business desktop applications. That is, these industrial standards have opened up the possibility for embedded system application towards control, manufacturing, equipment, medical instruments, and telecommunications.

All the major core control units of the OCCSM deploy the newest embedded PCs. The main computer was a Pentium 200 SBC (Single Board Computer) and was found later not fast enough for motion control --- the arm ran away too often. The Pentium 200 SBC has been upgraded to a dual Pentium III 450 SBC that is now adequate to process the real-time motion control loops. The cost for the SBC and two Pentium III 450 MHz CPUs is merely over \$500. Nothing other than embedded PCs can give such a dual-processing power at such a low cost, needless to mention the advantages of mainstream software for PCs. The camera computer is a very compact embedded PC with a Pentium 133 CPU. The 133 MHz speed is adequate, because the speed bottleneck is the camera control interface card. Regardless the speed of the computer, it takes .2-2 seconds for the interface card to update an image, depending on the size of the image.

8.5.2 Object-oriented Software

Embedded systems are becoming more and more complex and software development has become the most important and costly part of an embedded system project. C++ and object-

oriented programming is replacing the simple and procedure-oriented coding (Auslander, 1996). Fortunately, by using embedded PC technology and the easy-to-use, 32-bit, event-driven and object-oriented languages like Visual Basic and Visual C++, developers can now focus more on the system level features instead of the programming techniques.

The software of OCCSM is totally object-oriented, as described above. Object-oriented programming brings many benefits to embedded systems, such as easy hardware encapsulation, features expansion and development dividing. Without an object-oriented architecture, the OCCSM system could never be a reality.

8.5.3 Programming with MFC

The embedded systems industry today is similar to the IC industry approximately 25 years ago when there were no 74xx series ICs to use. That is, developers have to find their own ways to implement systems within their time and resource constraints. Meanwhile, embedded systems are becoming more and more complex and software development has become the most costly part of an embedded system project. Fortunately, by using embedded PC technology, the Microsoft Foundation Classes (MFC) might play a similar role in software as the role of 74xx in the IC industry. Developers can now focus more on the system level features instead of the programming techniques.

The OCCSM project provides an example of integrating a real-time control system with an advanced user interface and Internet connectivity by using MFC. With MFC, adding a dialog box, a control button, a menu and other graphic interfaces into the OCCSM user interface is extremely easy. Building classes based on MFC other than from scratches allows inheriting the characters of the MFC, such as serialization and message mapping, which make data, I/O and user inputs handling significantly simplified. The new MFC has added classes for communication and Internet that's used by us in the distributed image processing and transferring.

8.5.4 Multithreaded Programming

The user interface should never be blocked by real-time tasks. For example, the homing procedure of the motion control takes few seconds. If the procedure is not running in a separate

thread, the operator cannot do anything else while homing. If something goes wrong, the operator has no control, except shutting down the power.

32-bit Windows platforms, such as Windows 95, 98 and NT, support multithreads. While the user interface is running in the front, real-time tasks can run in separated threads under the background. This way, the user interface remains responsive even in the middle of a real-time control task and the operator has control all the time. One can also run real-time tasks in another process, but two processes have separated memory space and therefore the programming is much more difficult and the communication between two process could cause unnecessary overhead.

Multithreaded programming used to be difficult, especially in the aspect of communication between threads. MFC changed that and wrapped the procedural threads and synchronization techniques into ready-to-use classes, such as the `CWinThread`, `CCriticalSection`, `CEvent`, `CSemaphore` and `CMutex`. By using these classes, multithreaded programming becomes more object-oriented.

Even though, multithreaded programming is still more complicated and needs special techniques. There are two types of threads: worker threads and user-interface threads. The user-interface threads can process user inputs but are too complicated to be implemented. However, in our case, user inputs are needed. For example, the homing procedure needs user to input the initial position and direction for both axes. A unique multithreaded scheme has been developed in the OCCSM project: the so-called CPD scheme --- Control-Process-Dialogue. In this scheme, there are three classes work together to handle the threads. The Process class (`CProcess`) provides all the functions and data required for real-time control tasks. The Control class (`CControlThread`) put these real-time control tasks into threads and hides these threads from the programmer. The dialogue class (`CprocessDlg`) handles the user input required by some of the real-time control threads. Thus, the user-interface programmer does not need to deal with the threads and the complicated synchronization. All he needs is the `CProcess` that appears as a normal class but multithreaded in nature. For example, to start the homing procedure, the programmer simply call the `Homing()` function of the `CProcess` and it will take care of the rest -- start a new thread for homing, pop out a dialogue for the initial position of the axis to be homed.

Multithreaded programming also provides an efficient method of system monitoring and that is done in the CMonitorThread class. System monitoring is critical to highway maintenance and construction machines, for the safety of both the operator and nearby traffic.

8.5.5 Real-time Control with Windows NT

Windows NT is a reliable, responsive and general-purpose 32-bit OS that is capable of pre-emptive, priority-based multitasking and networking and it has thorough memory protection and security mechanisms. NT restricts any direct access to I/O ports and, to do so, a driver is needed. NT currently supports about one-third of the devices supported by Windows 95/98 but increasingly more hardware vendors are providing drivers for NT. As a general-purpose OS, NT comes with some features for real-time applications, such as real-time priority class, virtual page locking into RAM, deferred procedure call (DPC) and interrupt masks. However, the number of available priorities in the real-time class (16 total) is too low and the DPC interrupt handler, while improving interrupt latency on average by preempting all tasks with any interrupt, is based on a FIFO (First In First Out) structure, without regard to priority and determinism. Moreover, although NT's very rich Win32 API allows easy creation of powerful multi-threaded applications, it lacks the ability to inherit the priority of another thread, which is required to solve the classic problem of priority inversion in a real-time system.

The challenge here is how will the system's real-time capability and stability be maintained while concurrently handling the demanding image processing and interactive graphical user interface? Commercial high-end real-time operating systems are expensive and proprietary, which detracts from their implementation in embedded PC systems. Freely distributed Linux has the potential to evolve into a sophisticated and reliable RTOS with the recent developments adding real-time facilities to the OS. Until the hardware and software support of Linux as well as its ease-of-use can rival that of Windows, Windows NT is still the preferred OS not only for the high performance 32-bit desktops, but also for reliable embedded systems as well. Real-time applications can take full advantage of Windows NT's standard user interface, network capabilities and off-the-shell development tools.

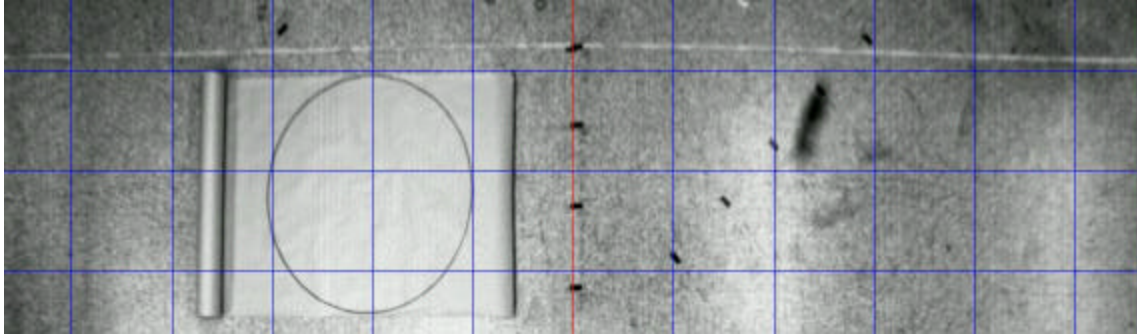


Figure 8.9 - Camera image with distortion

However, due to its business-oriented nature, Windows NT has some limitations related to determinism that are important for a real-time system (Kresta, 1998). There are mainly two approaches to address this issue. One is to complement the standard Windows NT kernel with a real-time one, whereas, the other is to dedicate one (or more) processor(s) for real-time control tasks and image processing while dedicating another processor for the operator's graphical user interface. The former is taken by some proprietary RTOS vendors. The latter is more cost-effective due to the low cost of PC microprocessors, and this approach usually results in a hybrid multiprocessor and/or distributed architecture that is modular and preferable. The OCCSM system is such a hybrid system, which has been proved to be able to handle concurrently the hard real-time tasks and graphical user interface.

8.5.6 Un-distortion of Camera Image

There are two types of distortion caused by the camera. First, the CCD of the camera has 7.8 x 6.8 pixels instead of square ones and that's why the circle looks taller than it actually is. This is easy to be corrected. Second, any lens causes distortion and that is why the straight line looks curved. See Fig. 8.9.

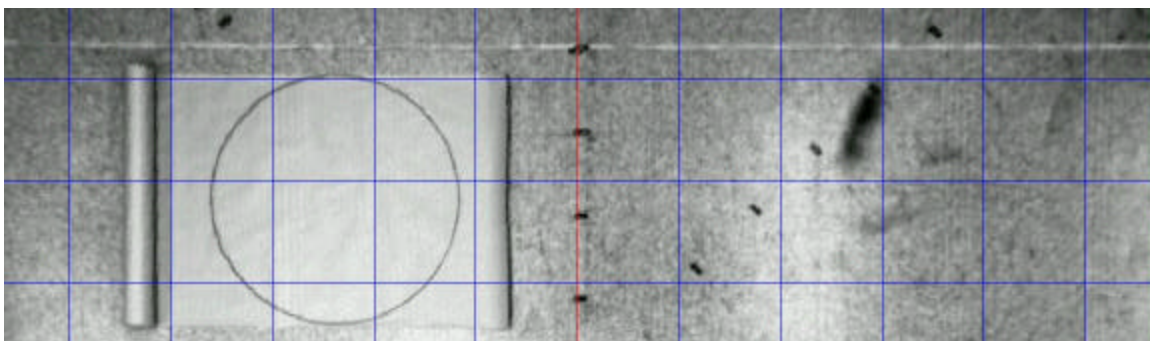


Figure 8.10 - Image after un-distortion

The lens distortion correction algorithm is based the following polynomial:

$$r_{undistortd} = a_1 + a_2 r_{dis} + a_3 r_{dis}^2 + \dots \quad (8.1)$$

where $r_{undistortd}$ is the actual location of the pixel, i.e. the distance between the pixel and the geometric center of the lens, r_{dis} the distorted location of the pixel and a_1, a_2 and $a_3 \dots$ are parameters to be determined by experiments. A program, DataFit, is developed to calculate these parameters. Based on our experiments, a second-order polynomial is accurate enough.

While all the distorted pixels will be converted using above polynomial, the new, un-distorted image, initialized to black, will still have some pixels that are not touched. These untouched black pixels must be assigned with proper brightness, or the new image looks funny. A simple way is to set them to the same brightness of the closest pixel. This simple method turns out very well in practice except that it generates some almost invisible artificial “feathers”. The developed un-distortion algorithm is extremely fast and accurate: both the circle and the straight line are recovered perfectly and the total mapping error is less than 1 pixel according to our measurements. See Fig. 8.10.

8.5.7 Motion Control Algorithm

Among all the control tasks, the motion control of the arm is the most important and challenging part. There are basically two problems involved in path following with the AT6250, the motion controller used here. First, the AT6250 can only follow a path that has been precompiled. For crack sealing, the path is dynamically taken from a random crack and it is not practical to be precompiled. Second, the path here is in pairs of (R, \mathbf{q}) instead of (X, Y) .

Therefore a path following algorithm is developed to allow (R, \mathbf{q}) path following. The algorithm is based on the continuous mode (on-the-fly), which allows constant movement of the load. Giving the next velocity v_s and position (x_2, y_2) , the required telescoping velocity v_r and rotational velocity v_q can then be calculated as:

$$s = \sqrt{(x_2 - x_1)^2 + (y_2 - y_1)^2}$$

$$r_1 = \sqrt{x_1^2 + y_1^2}$$

$$r_2 = \sqrt{x_2^2 + y_2^2}$$

$$\mathbf{q}_1 = a \tan(y_1 / x_1)$$

$$\mathbf{q}_2 = a \tan(y_2 / x_2)$$

$$v_r = v_s(r_2 - r_1) / s$$

$$v_q = v_s(q_2 - q_1) / s$$

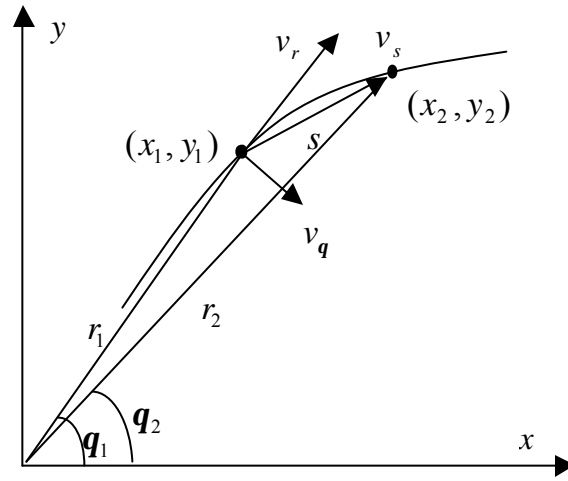


Figure 8.11 – Motion control coordinates

The control algorithm is then described in Fig. 8.12.

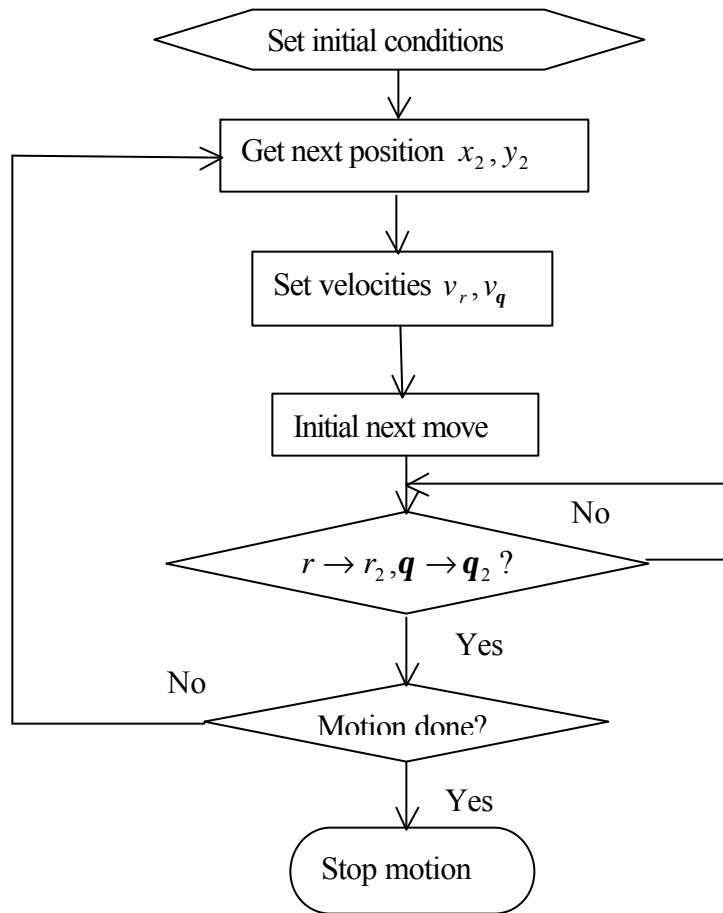


Figure 8.12 - Motion control algorithm

8.5.8 Integration of Highway and Information Highway

Today, embedded real-time control systems are evolving into information systems. To make it Internet enabled, an embedded control system can take advantage of the explosively growing Internet technology in many ways. If the control system comprises a network, TCP/IP is the favored protocol for connection. Not only does TCP/IP have universal connectivity between different platforms such as Windows, Unix, Macintosh, etc., but also even for an individual Windows network communication programming is made much easier than through the use of other protocols such as NetBEUI. Accordingly, TCP/IP programming tools are ubiquitous, and additionally, TCP/IP is more reliable and efficient.

The Internet also provides new ways to access an embedded system. A Web enabled embedded system allows the designers to leverage off the many existing protocols and software

that support the Internet. For example, by adding a small web (HTTP) server to an embedded system, a standard desktop Web browser can examine the system's status and even control it remotely. Furthermore, a Java applets or an ActiveX control can be linked on the web server of the embedded system. The applet or ActiveX control then provides a custom user interface to control the system, which can be upgraded by just changing the applet or ActiveX control on the server side.

Highway maintenance and construction activities can be viewed as a part of traffic information. Aside from radio and television forecasts, the WWW has become an increasingly more popular resource for traffic information. If all the machines working on the highways are Internet-aware, then they can be integrated into the WWW highway information system. For our machine, since the camera computer uses HTTP to communicate with the main computer, it is only one step away from allowing the camera image to be available on the WWW which would, in turn, allow remote sites (e.g., offices of the department of transportation) to watch the progress of the operation.

Security is one of the biggest concerns regarding the implementation of the Internet, and accordingly, it is a more important issue in the Internet-aware embedded systems. As embedded systems usually have neither a keyboard nor a monitor for the users to log on, it is not preferable to set a password for access control and security on a real-time control network. Improper access can not only allow the release of confidential information, but more importantly may allow damage to the system and its operation. At this time, it appears that the best protection approach is to set up a Proxy server as a firewall between the Internet and the real-time control subnets. A proxy server also removes the need to assign public IP addresses for all the embedded devices, as private IP addresses can be used under the subnet. The “robota.ahmct.ucdavis.edu” is the Proxy server for all the experimental real-time control networks including the one described in this paper and the Multiple Tethered Mobile Robot System (Feng and Velinsky, 1997) at the AHMCT Robotics Laboratory.

To control or monitor the embedded system through a Proxy server that runs an HTTP server and has access to the embedded systems behind, both CGI (common gateway interface) and ISAPI (Internet Server Application Programming Interface) can be used, if the server is a Windows NT or Windows 95. The ISAPI extension is more powerful and has much better performance than the CGI. The Visual C++ 5.0 has an ISAPI Extension Wizard that generates a

basic ISAPI DLL application to ease its programming. An ISAPI DLL can do virtually whatever an ordinary DLL can, which means it allows us to fully control an embedded system in a secure manner.

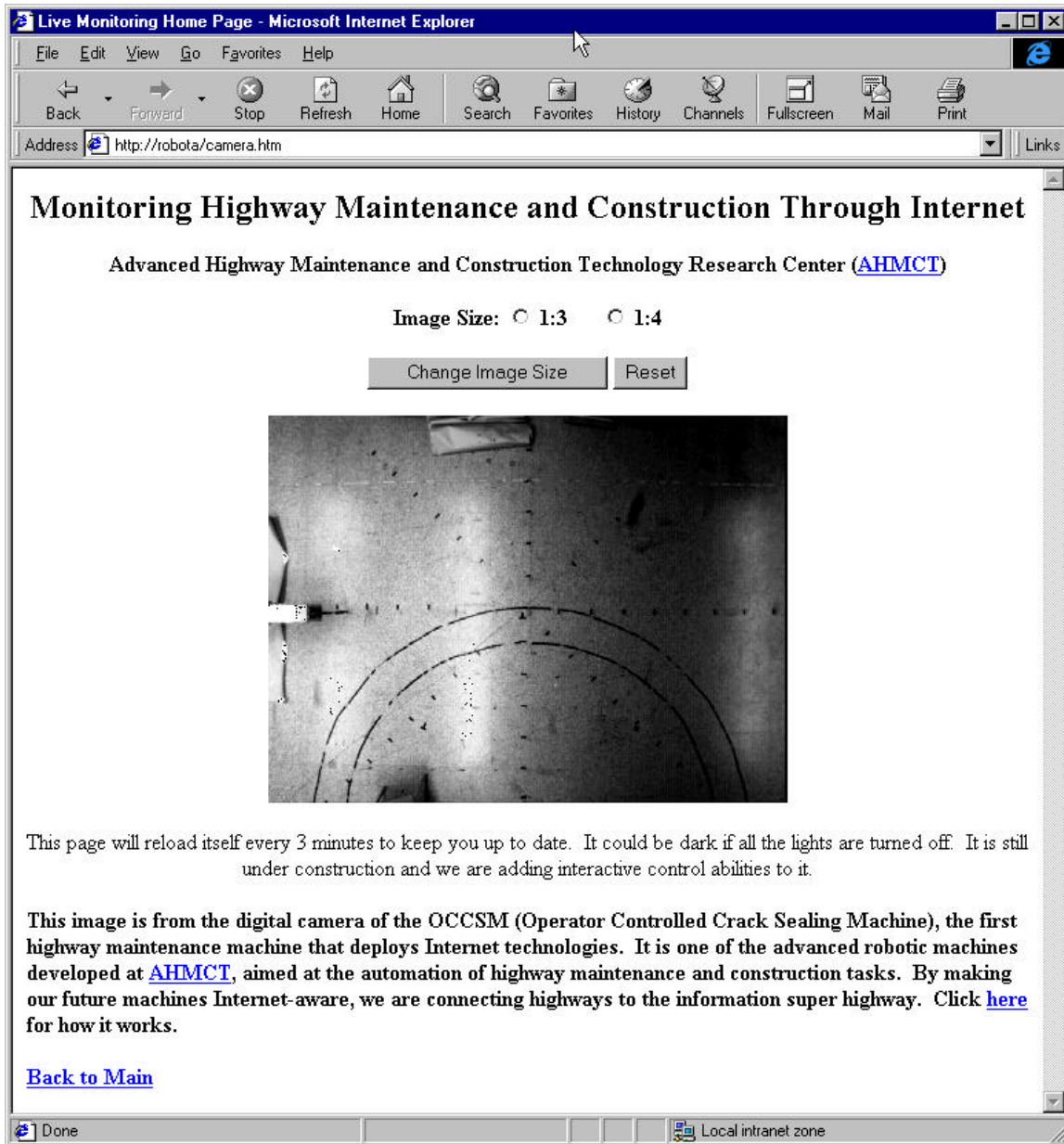


Figure 8.13 - Monitoring through Internet

An ISAPI DLL, "webdll.dll", has been built for the HTTP server running on robota.ahmct.ucdavis.edu and embedded in "camera.htm". This ISAPI is meanwhile a client to the embedded HTTP server of the camera and thus can get images from the camera in the same manner as the main computer. However the raw image pixels are further transferred into GIF

format to be output to the web browser that opened the “camera.htm” page. The interested reader can open:

<http://robota.ahmct.ucdavis.edu/camera.htm>

with a desktop browser to see the live image as shown in Fig. 8.13.

8.6 Experiments

The following pictures provide some of the experiment results conducted in the robotics lab of AHMCT.

The pictures in Fig. 14 and 15 shows that the arm follows an “8” and a square path respectively four times with very high accuracy and repeatability.

The pictures in Fig. 8.16, 8.17 and 8.18 present a simulation of a full crack sealing procedure. First, a path is drawn on the ground as a simulated highway crack and a picture of the workspace is taken and displayed on the screen. Second, the operator draws a path following the crack. Third, the motion starts and the tip of the arm follows the crack very well.

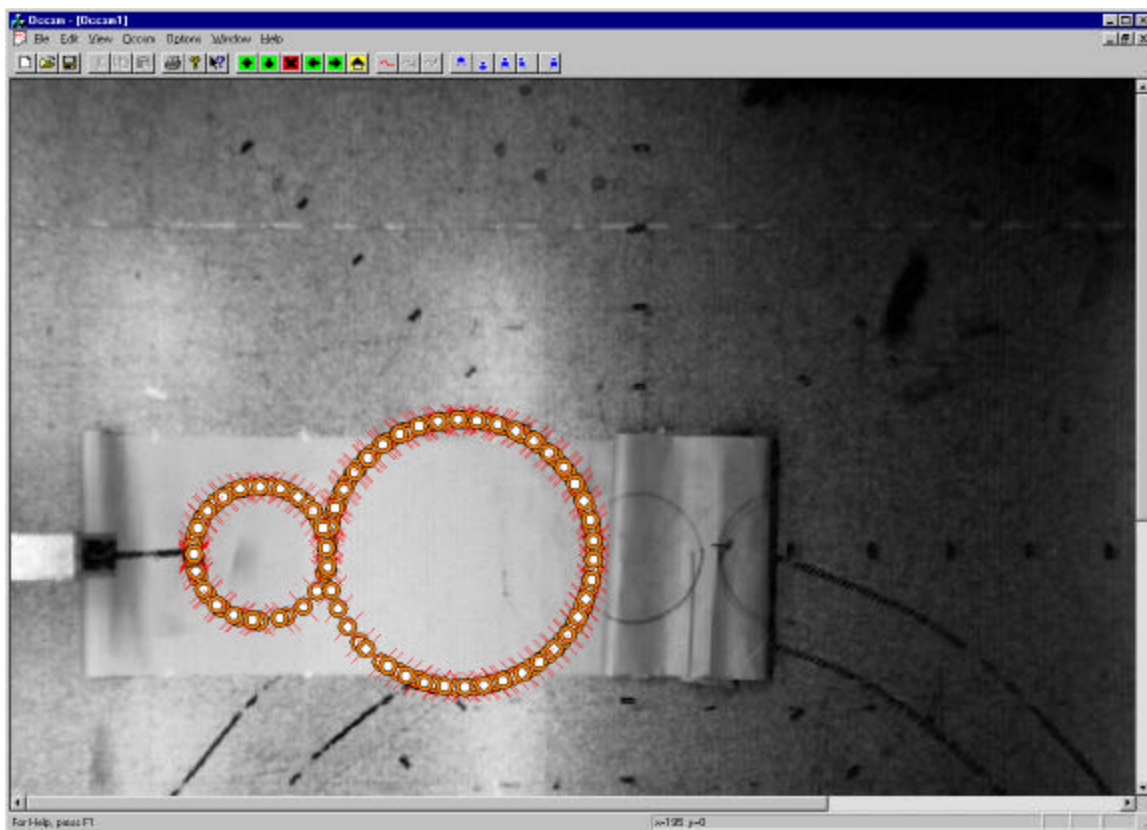


Figure 8.14 - “8” path following

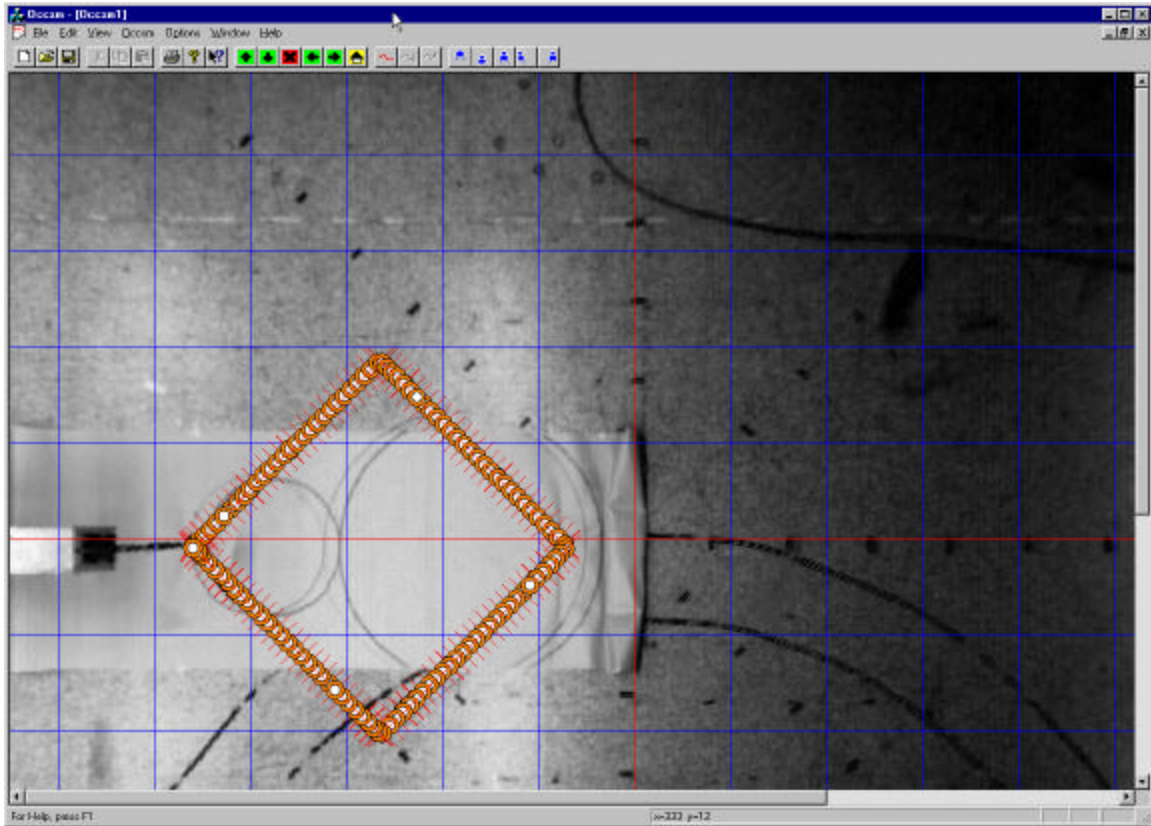


Figure 8.15 - Square path following

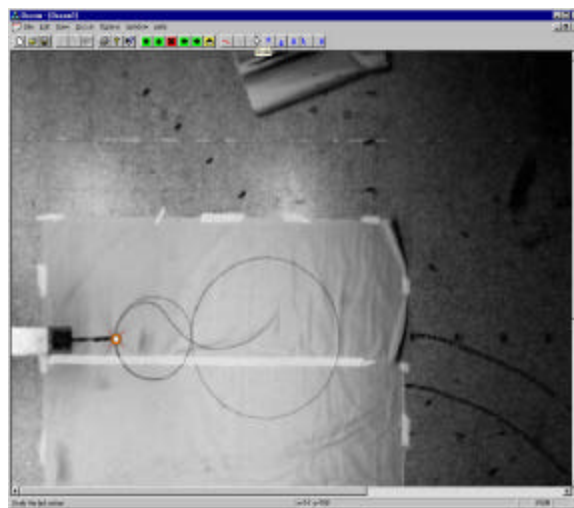


Figure 8.16 - An "S" curve simulating a crack

Chapter 9: CONCLUSIONS AND RECOMMENDATIONS

This report has presented work leading towards the development of the first prototype Operator Controlled Crack Sealing Machine (OCCSM). This has included component subsystems as well as numerous critical machine components. The R- θ telescopic manipulator arm has been discussed in detail from its concept phase through its detailed design, testing and test conclusions. Additionally, the camera boom system and the hose retraction systems' designs have been presented in detail. The machine's controller has also been presented in detail, and the R- θ telescopic manipulator arm has been integrated with the controller to provide a complete system operational in the AHMCT Robotics Laboratory. This system will be moved to the OCCSM support vehicle for use on actual highways in the next phase of the project. This Chapter presents project-wide conclusions of the total R- θ telescopic manipulator concept as well as the other systems, and proceeds with recommendations for future research into second-generation prototypes as well as enhanced testing of the current prototype.

9.1 Conclusions and Recommendations

9.1.1 Project Goals

The goal of this project was to produce an operator controlled crack sealing machine with the aim of increasing the productivity, quality, and safety of current crack sealing operations while maintaining affordability. The most important aspects of this phase in this quest was the design and fabrication of the R- θ Telescopic Manipulator, the development of the controller, and the integration of the two systems. Through extensive research, conceptual design, detailed design, and testing, the first-generation full-scale R- θ telescopic manipulator arm has been successfully lab tested and proven to meet or exceed all critical project specifications.

9.1.2 Telescopic Sections Design / Performance

Preliminary crack following has shown excellent arm response and tracking. The main drawback of this prototype is the lack of manufacturing precision in the telescopic sections and the complexity of the joint supports. The sections were conceptualized around the need for rapid prototyping to prove the concept. The next step in this progression is to reevaluate the conceptual design selection. It is recommended that aluminum open-form extrusions be

considered. Although these sections will not offer the high stiffness to weight ratio of steel, they can be held to far higher dimensional tolerances. In addition, these sections will allow the complexity of the joint connections to be reduced by breaking the corners of the section as shown in Figure 9.1. This would combine the horizontal and vertical support systems together to further reduce the weight and simplify the design.

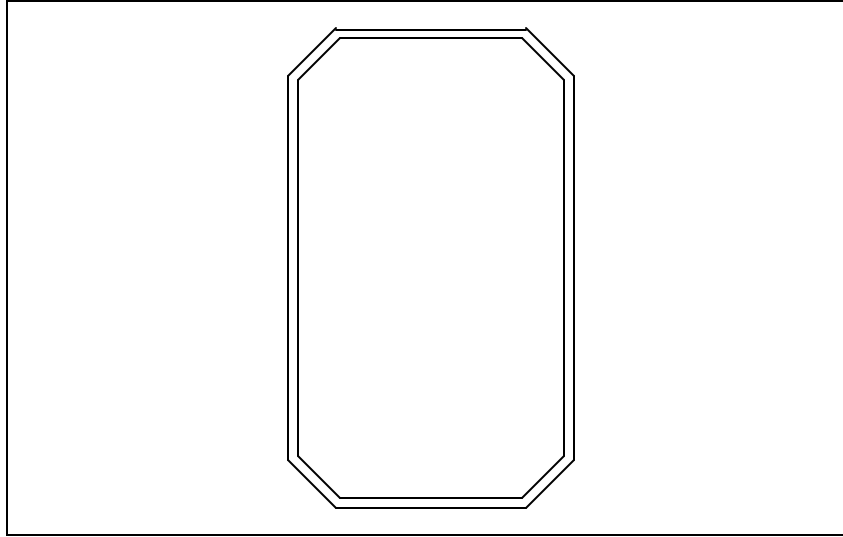


Figure 9.1 - Improved Telescopic Beam Cross Section

9.1.3 Actuation Systems/Performance

The actuator systems work very well in the prototype R- θ Telescopic Arm. The rotational actuation system exceeds all performance specifications and proves to be a clean and efficient design. The telescopic ball screw actuator has a few minor tuning problems that are related to the telescopic beam sections. Since the beam sections provide the support for the actuator components, it is very critical that they be aligned straight and true. The result of this misalignment is a whip type oscillation at larger extensions, corresponding to less joint stiffness in the sections as well as the actuator. With this exception, the actuator operates very well, meeting all performance specifications.

The only recommendation concerns the fabrication of the telescopic ball screw actuator. It is recommended that research be directed into reducing the cost of fabricating the hollow ball screw, possibly through grinding the threads onto a center-less ground tube. This would drastically reduce the cost of the actuator. In addition, V-thread screws can be substituted for the ball screws to reduce the cost. However, these screws will sacrifice positioning accuracy and

efficiency. In addition, at the time of this research, V-thread screws were not available in leads up to 51 mm/rev. This will require higher rotational velocities and thus more precise alignment of the supports.

9.1.4 Vehicle Integration / Performance

The vehicle integration system was found to be a very robust, economical and clean solution to supporting and stowing the telescopic arm. Preliminary operation has shown problems associated with the raw finish on the roller plate. The current roller plate, made from hot roll steel, has problems associated with pitting and a general bad surface finish that causes the roller truck to move in a stick-slip fashion at slow speeds. This induces a vibration in the arm and affects end-effector movement.

To alleviate this problem it is recommended that the surfaces of the support plate be machined. In addition, research should be directed into increasing the side stiffness of the hinged plates in an effort to provide more smooth motion. However, it is anticipated that the former suggestion will alleviate the problem.

9.1.5 Further Testing

Testing of the current R- θ telescopic manipulator presented in this report was limited. It is recommended that further testing be performed to quantify the static and dynamic behavior of the arm under varying conditions. It is recommended that the horizontal stiffness, vibrational responses / natural frequency, true actuator positioning accuracy, as well as frame deflection under loading all be researched to yield further insight into possible design improvements for the second generation R- θ Telescopic Manipulator.

9.1.6 Camera Boom and Hose Retraction Systems

Chapters 6 and 7 discussed the design of two additional systems for the OCCSM. The operation of the OCCSM requires an overhead image of the workspace behind the truck. The operator will use the image to trace a crack and create a path for the robotic arm holding the sealant applicator to follow. For this purpose, a camera boom was developed that holds a digital camera over the center of the workspace. When not in use, the camera boom is retracted by means of a hand operated crank mechanism that is also used to extend the boom. The camera boom and crank mechanism mount to the underside of the canopy that covers the OCCSM's

truck bed. Vibration characteristics of the camera boom were used to select a material and an appropriate wall thickness for the square tubular boom. To further minimize camera movement, braces were added between the boom and the rearmost truck bed posts. While the boom positions the camera directly over the center of the workspace, the camera's mount must provide rotational adjustments to align the camera with the workspace coordinates. An aluminum camera housing was developed to perform this task and to protect the camera from the weather. The main option available to improve the system developed here would be an increase in the cross sectional size of the boom. However, before a judgment on this option can be made, the overhead clearance in the truck bed must be evaluated.

Because the OCCSM's robotic arm may extend up to 4.03 m (13.3 ft), the sealant hose must also be able to extend this distance. The sealant hose retraction system discussed in Chapter 7 was designed to adjust the hose length to match the effective length of the arm. The hose runs through a sheave mounted to a carriage that rolls along a track, allowing the hose to extend and retract with the arm. A spring powered tool balancer stores energy as the arm pulls the hose out, then as the arm retracts, the tool balancer pulls the hose back in. A tool balancer was chosen because it does not require any electric or hydraulic power and was a single item that performed all the necessary functions. Testing of the hose retraction system will be performed in the next phase once the truck arrives and the system can be assembled on the truck.

9.1.7 Control System

Chapter 8 has discussed details of the OCCSM control system. This system implements the most cutting-edge PC and information technologies including the Internet technology. It is the first highway construction and maintenance machine that utilizes the Internet. The embedded real-time control system is based on object-oriented software design and has the most sophisticated and easy-to-use man-machine user interface. The system has been successfully integrated with the manipulator arm and tested in the AHMCT Robotics Laboratory.

Chapter 10: REFERENCES

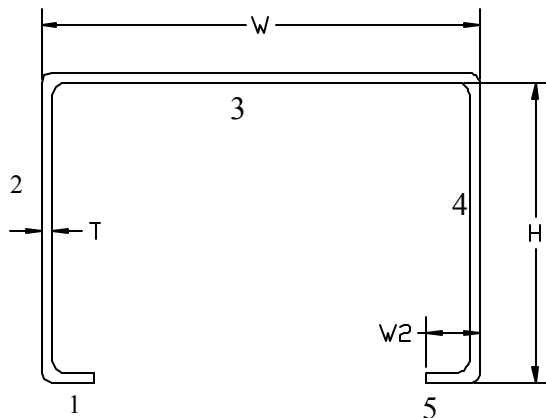
- Auslander, D.M., Ridgely, J.R. and Jones, J.C. (1996) "Real-Time Software for Implementation of Feedback Control." chapter in: *The Control Handbook*, edited by William S. Levine, CRC Press and IEEE Press, pp 323-344.
- Baker, Todd Lawrence (1998) "Development of a Telescopic Manipulator Arm for Highway Maintenance," M.S. Thesis, Univ. California, Davis.
- Feng, X., Baker, T.L., and Velinsky, S.A. (1998) "Long reach robotic manipulator for advanced highway maintenance and construction equipment." Romansy 12, *Theory and Practice of Robots and Manipulators*, the Twelfth CISM-IFTOMM Symposium, Paris.
- Feng, X., Bennett, D.A., and Velinsky, S.A. (1998) "Embedded PC control system for a highway crack sealing machine." Proc. of the ASME Design Technical Conferences, Paper #DETC98/CIE-5531.
- Feng, X., and Velinsky, S. A. (1997) "Distributed control of a multiple tethered mobile robot system for highway maintenance and construction." *Microcomputers in Civil Engineering* (12), 383-392.
- Hibbeler, R. C., Mechanics of Material, 2nd Ed. Prentice-Hall, 1994.
- Kresta, D. (1998) "Reliable control with Windows NT." Real-time computer show & conference, Santa Clara, California, USA.
- Kruglinsky, D. J. (1997) *Inside Visual C++*, Microsoft Press, Redmond, Washington.
- Kumar, S., et al. (1996) *The Codesign of Embedded Systems*, Kluwer Academic Publishers.
- Rao, S., Mechanical Vibrations, 3rd Ed., Addison-Wesley, 1995.
- Technology Development Center. Preliminary Market Report: Commercialization of Road Maintenance Technology, Crack/Joint Sealing Devices. Technology Development Center, 1993.
- Velinsky, S. A. (1993) "Fabrication and Testing of an Automated Crack Sealing Machine", SHRP-H-659, National Research Council Strategic Highway Research Program, Washington D.C.
- Velinsky, S. A. (1993) "Heavy Vehicle System for Automated Pavement Crack Sealing", *Heavy Vehicle Systems, International Journal of Vehicle Design*, Vol. 1, No. 1, pp. 114-128.

Appendix A. Calculations

Beam Cross Sectional Properties

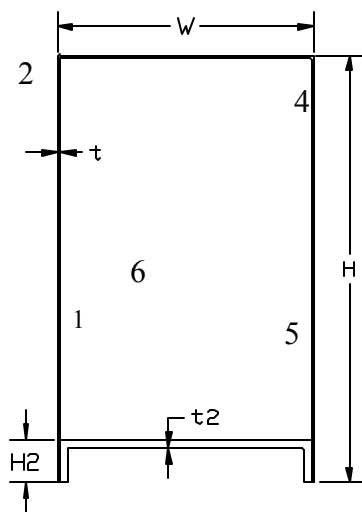
Formed Section Geometry

Base Section



Fly/Intermediate Sections

In order to calculate the beam section properties, each section was separated into i rectangular sections (1,2,3...). These i -sections were then used to determine the bending moments of inertia, centroid and other properties as shown in the following tables.



Base Section(w=9.375,t=.25,h=7,w2=1.25)

i	bi(in)	hi(in)	Ai(in ²)	Si(in)	Ai*Si(in ³)	di(from si*)	I0(in ⁴)	Ai*di ² (in ⁴)
1.000	1.250	0.250	0.313	0.125	0.039	-4.177	0.002	5.453
2.000	0.250	6.500	1.625	3.250	5.281	-1.052	5.721	1.799
3.000	9.375	0.250	2.344	6.875	16.113	2.573	0.012	15.515
4.000	0.250	6.500	1.625	3.250	5.281	-1.052	5.721	1.799
5.000	1.250	0.250	0.313	0.125	0.039	-4.177	0.002	5.453
Sum			6.219		26.754		11.458	30.018

Base Section Properties

si* (height to c.g.) 4.302 in
 Material Density 0.283 lb/in³
 Section Length 96.000 in
 Section Volume 597.000 in³
 Section Weight 168.951 lb
I section=I0+Ai*di²= 41.476 in⁴

Intermediate Section(w=6,t=.06,h=10,t2=.188,h2=1)

i	bi(in)	hi(in)	Ai(in ²)	Si(in)	Ai*Si(in ³)	di(from si*)	I0(in ⁴)	Ai*di ² (in ⁴)
1.000	0.188	0.812	0.153	0.406	0.062	-3.185	0.008	1.549
2.000	0.060	10.000	0.600	5.000	3.000	1.409	5.000	1.191
3.000	5.880	0.060	0.353	9.970	3.517	6.379	0.000	14.355
4.000	0.060	10.000	0.600	5.000	3.000	1.409	5.000	1.191
5.000	0.188	0.812	0.153	0.406	0.062	-3.185	0.008	1.549
6.000	5.880	0.188	1.105	0.906	1.002	-2.685	0.003	7.971
Sum			2.964		10.643		10.020	27.805

Intermediate Section Properties

si* (height to c.g.) 3.591 in
 Material Density 0.283 lb/in³
 Section Length 96.000 in
 Section Volume 284.501 in³
 Section Weight 80.514 lb
I section=I0+Ai*di²= 37.825 in⁴

Fly Section(w=5.75,t=.06,h=8.9,t2=.109,h2=.59)

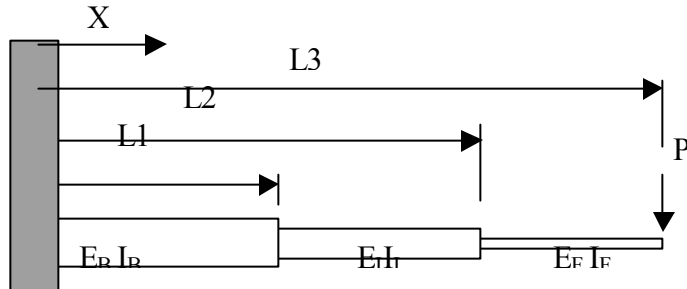
i	bi(in)	hi(in)	Ai(in ²)	Si(in)	Ai*Si(in ³)	di(from si*)	I0(in ⁴)	Ai*di ² (in ⁴)
1.000	0.109	0.481	0.052	0.241	0.013	-3.574	0.001	0.670
2.000	0.060	8.900	0.534	4.450	2.376	0.636	3.525	0.216
3.000	5.630	0.060	0.338	8.870	2.996	5.056	0.000	8.634
4.000	0.060	8.900	0.534	4.450	2.376	0.636	3.525	0.216
5.000	0.109	0.481	0.052	0.241	0.013	-3.574	0.001	0.670
6.000	5.630	0.109	0.614	0.536	0.329	-3.279	0.001	6.597
Sum			2.124		8.103		7.052	17.002

Fly Section Properties

si* (height to c.g.) 3.814 in
 Material Density 0.283 lb/in³
 Section Length 96.000 in
 Section Volume 203.935 in³
 Section Weight 57.714 lb
I section=I0+Ai*di²= 24.055 in⁴

Deflection Analysis – End Load

Deflection due to end load for varying cross sections and materials.



Engineering Assumptions

Infinitely stiff joints between cross sections.

Linear elastic deflections.

Sections remain plane, no localized buckling in side-walls.

Statics

$$\sum F_Y = 0 \Rightarrow R_1 = P$$

$$\sum M = M_1 = -PL_3$$

$$0 < x < L_1$$

$$E_B I_B v_1''(x) = M(x) = -PL_3 + Px$$

$$E_B I_B v_1'(x) = P \frac{x^2}{2} - PL_3 x + C_1$$

$$E_B I_B v_1(x) = P \frac{x^3}{6} - PL_3 \frac{x^2}{2} + C_1 x + C_2$$

B.C.

$$v_1'(0) = 0 \Rightarrow C_1 = 0$$

$$v_1(0) = 0 \Rightarrow C_2 = 0$$

$$L_1 < x < L_2$$

$$E_I I_I v_2''(x) = M(x) = -PL_3 + Px$$

$$E_I I_I v_2'(x) = P \frac{x^2}{2} - PL_3 x + C_{12}$$

$$E_I I_I v_2(x) = P \frac{x^3}{6} - PL_3 \frac{x^2}{2} + C_{12} x + C_{22}$$

B.C.

$$v_2'(L_1) = v_1'(L_1) \Rightarrow C_{12} = \frac{E_I I_I}{E_B I_B} \left(\frac{PL_1^2}{2} - PL_1 L_3 \right) - \frac{PL_1^2}{2} + PL_1 L_3$$

$$v_2(L_1) = v_1(L_1) \Rightarrow C_{22} = \frac{E_I I_I}{E_B I_B} \left(\frac{PL_3 L_1^2}{2} - \frac{PL_1^3}{3} \right) - \frac{PL_1^3}{3} + \frac{PL_3 L_1^3}{2}$$

$L_2 < x < L_3$

$$E_F I_F v_3''(x) = M(x) = -PL_3 + Px$$

$$E_F I_F v_3'(x) = P \frac{x^2}{2} - PL_3 x + C_{13}$$

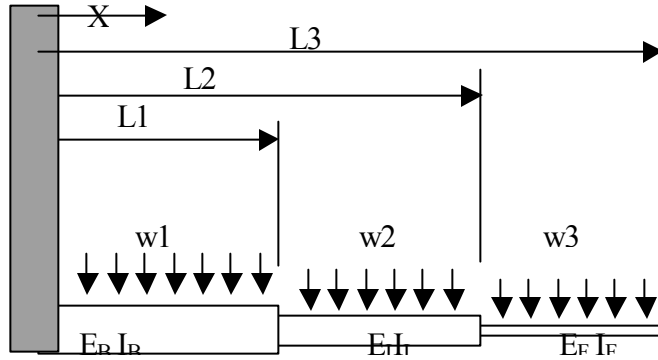
$$E_F I_F v_3(x) = P \frac{x^3}{6} - PL_3 \frac{x^2}{2} + C_{13} x + C_{23}$$

B.C.

$$v_3'(L_2) = v_2'(L_2) \Rightarrow C_{13} = \frac{E_F I_F}{E_I I_I} \left(\frac{PL_2^2}{2} - PL_2 L_3 + C_{12} \right) - \frac{PL_2^2}{2} + PL_2 L_3$$

$$v_2(L_2) = v_1(L_2) \Rightarrow C_{23} = \frac{E_F I_F}{E_I I_I} \left(\frac{PL_2^3}{6} - \frac{PL_3 L_2^2}{2} + C_{12} L_2 + C_{22} \right) - \frac{PL_2^3}{6} + \frac{PL_3 L_2^2}{2} - C_{13} L_2$$

Deflection due to distributed weight for varying cross sections and materials.



Engineering Assumptions

Infinitely stiff joints between cross sections.

Linear elastic deflections.

Sections remain plane, no localized buckling in side-walls.

Distributed loads act as point loads for static analysis.

Statics

$$\sum F_Y = 0 \Rightarrow R_1 = w_1 L_1 + w_2 (L_2 - L_1) + w_3 (L_3 - L_2)$$

$$\sum M = M_1 = \frac{-w_1 L_1^2}{2} - w_2 (L_2 - L_1) \left(\frac{L_1 + L_2}{2} \right) - w_3 (L_3 - L_2) \left(\frac{L_3 + L_2}{2} \right)$$

Deflection

$0 < x < L_1$

$$E_B I_B v^{IV} = -w_1$$

$$E_B I_B v^{III} = -w_1 x + C_1$$

$$E_B I_B v^{II} = -w_1 \frac{x^2}{2} + C_1 x + C_2$$

$$E_B I_B v^I = -w_1 \frac{x^3}{6} + C_1 \frac{x^2}{2} + C_2 x + C_3$$

$$E_B I_B v = -w_1 \frac{x^4}{24} + C_1 \frac{x^3}{6} + C_2 \frac{x^2}{2} + C_3 x + C_4$$

Boundary Conditions

$$E_B I_B v^{III}(0) = R_1 \Rightarrow C_1 = R_1$$

$$E_B I_B v^{II}(0) = M_1 \Rightarrow C_2 = M_1$$

$$v^I(0) = 0 \Rightarrow C_3 = 0$$

$$v(0) = 0 \Rightarrow C_4 = 0$$

Similarly for $L_1 < x < L_2$

$$E_i I_i v = -w_2 \frac{x^4}{24} + C_{12} \frac{x^3}{6} + C_{22} \frac{x^2}{2} + C_{32} x + C_{42}$$

Boundary Conditions

Applying continuity to all of the differential equations at the position $x=L_1$ will yield...

$$C_{12} = \frac{E_I I_I}{E_B I_B} (-w_1 L_1 + R_1) + w_2 L_1$$

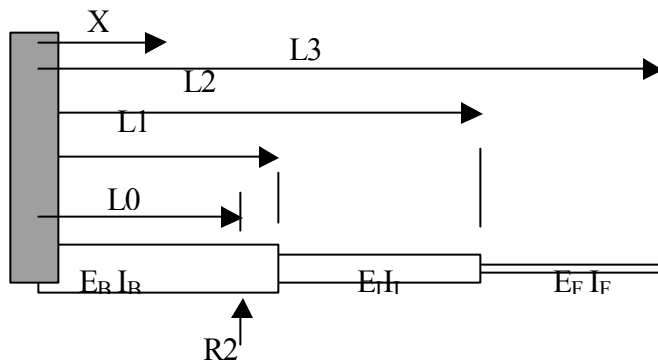
$$C_{22} = \frac{E_I I_I}{E_B I_B} \left(-w_1 \frac{L_1^2}{2} + R_1 L_1 + M_1 \right) + w_2 \frac{L_1^2}{2} - C_{12} L_1$$

$$C_{32} = \frac{E_I I_I}{E_B I_B} \left(-w_1 \frac{L_1^3}{6} + R_1 \frac{L_1^2}{2} + M_1 L_1 \right) + w_2 \frac{L_1^3}{6} - C_{12} \frac{L_1^2}{2} - C_{12} L_1$$

$$C_{42} = \frac{E_I I_I}{E_B I_B} \left(-w_1 \frac{L_1^4}{24} + R_1 \frac{L_1^3}{6} + M_1 \frac{L_1^2}{2} \right) + w_2 \frac{L_1^4}{24} - C_{12} \frac{L_1^3}{6} - C_{12} \frac{L_1^2}{2} - C_{32} L_1$$

Similar Equations will result for $L_2 < x < L_3$ and can be found by replacing all L_1 by L_2 and the beam subscripts for the intermediate (I) and the fly sections (F).

Determination of Reaction Force at Base End / Deflection due to R2



Note: The reaction force R_2 is determined by adding the deflections of the applied loads, P and the distributed weight, at the location L_0 and then applying the constraint that the deflection at L_0 must be zero.

Engineering Assumptions

Infinitely stiff joints between cross sections.

Linear elastic deflections.

Sections remain plane, no localized buckling in side-walls.

Statics

$$\sum F_Y = 0 \Rightarrow R_1 = -R_2$$

$$\sum M_1 = R_2 L_0$$

Deflections

$$0 < x < L_0$$

$$M = R_2 L_0 - R_2 x = E_B I_B v''$$

$$E_B I_B v' = R_2 L_0 x - \frac{R_2 x^2}{2} + C_1$$

$$E_B I_B v = \frac{R_2 L_0 x^2}{2} - \frac{R_2 x^3}{6} + C_1 x + C_2$$

Boundary Conditions

$$E_B I_B v'(0) = C_1 = 0 \Rightarrow C_1 = 0$$

$$E_B I_B v(0) = C_2 = 0 \Rightarrow C_2 = 0$$

$$L_0 < x < L_1$$

$$M = R_2 L_0 - R_2 x + R_2 (x - L_0) = E_B I_B v'' = 0$$

$$E_B I_B v_2' = C_1$$

$$E_B I_B v_2 = C_1 x + C_2$$

Boundary Conditions

$$v_2'(L_0) = v_1'(L_0) \Rightarrow C_1 = \frac{R_2 L_0^2}{2}$$

$$v_2(L_0) = v_1(L_0) \Rightarrow C_2 = -\frac{R_2 L_0^3}{6}$$

$L_1 < x < L_2$

$$E_I I_I v_3'' = 0$$

$$E_I I_I v_3' = C_1$$

$$E_I I_I v_3 = C_1 x + C_2$$

Boundary Conditions

$$v_3'(L_0) = v_2'(L_0) \Rightarrow C_1 = \frac{E_I I_I R_2 L_0^2}{2 E_B I_B}$$

$$v_3(L_0) = v_2(L_0) \Rightarrow C_2 = \frac{E_I I_I R_2 L_0^3}{6 E_B I_B}$$

$L_2 < x < L_3$

$$E_I I_I v_4'' = 0$$

$$E_I I_I v_4' = C_1$$

$$E_I I_I v_4 = C_1 x + C_2$$

Boundary Conditions

$$v_3'(L_0) = v_2'(L_0) \Rightarrow C_1 = \frac{E_I I_I R_2 L_0^2}{2 E_B I_B}$$

$$v_3(L_0) = v_2(L_0) \Rightarrow C_2 = \frac{E_I I_I R_2 L_0^3}{6 E_B I_B}$$

Solving for the reaction force R_2 as a function of the distributed load and the applied end load P .

From R_2 :

$$E_B I_B v = \frac{R_2 L_0 x^2}{2} - \frac{R_2 x^3}{6} \Rightarrow v(L_0) = \frac{R_2 L_0^3}{3 E_B I_B}$$

From the distributed loading:

$$E_B I_B v = -w_1 \frac{x^4}{24} + R_1 \frac{x^3}{6} + M_1 \frac{x^2}{2} \Rightarrow v(L_0) = \frac{-w_1 \frac{L_0^4}{24} + R_1 \frac{L_0^3}{6} + M_1 \frac{L_0^2}{2}}{E_B I_B}$$

where

$$R_1 = w_1 L_1 + w_2 (L_2 - L_1) + w_3 (L_3 - L_2)$$

$$M_1 = \frac{-w_1 L_1^2}{2} - w_2 (L_2 - L_1) \left(\frac{L_1 + L_2}{2} \right) - w_3 (L_3 - L_2) \left(\frac{L_3 + L_2}{2} \right)$$

Again, point loads were assumed for the distributed loading in determining the statics.

For the applied end load P:

$$E_B I_B v_1(x) = P \frac{x^3}{6} - PL_3 \frac{x^2}{2} \Rightarrow v_1(L_0) = \frac{P \frac{L_0^3}{6} - PL_3 \frac{L_0^2}{2}}{E_B I_B}$$

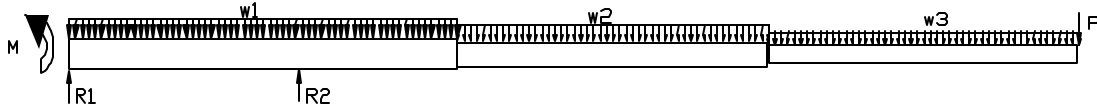
Finally, by applying the constraint that the deflection at L_0 be zero, we have

$$\frac{P \frac{L_0^3}{6} - PL_3 \frac{L_0^2}{2}}{E_B I_B} + \frac{-w_1 \frac{L_0^4}{24} + R_1 \frac{L_0^3}{6} + M_1 \frac{L_0^2}{2}}{E_B I_B} + \frac{R_2 L_0^3}{3 E_B I_B} = 0$$

where R_1 and M_1 are defined as in the distributed loading case. Therefore R_2 can be solved as:

$$R_2 = 3 \left(\frac{w_1 L_0}{24} - \frac{R_{1-DL}}{6} - \frac{M_{1-DL}}{2L_0} - \frac{P}{6} + \frac{PL_3}{2L_0} \right)$$

Telescopic Arm Stress Analysis



The critical stress location in the telescopic beams occurs at R2 and is found from the moment at R2:

$$\sum M_{R2} = M_1 - R_1 L_0 + w_1 L_1 \left(L_0 - \frac{L_1}{2} \right) - w_2 (L_2 - L_1) \left(\frac{L_2 + L_1}{2} - L_0 \right) - w_3 (L_3 - L_2) \dots$$

$$\dots \cdot \left(\frac{L_3 + L_2}{2} - L_0 \right)$$

where L_i are defined as in the deflection diagrams and M_1 , R_1 are found by superposition of the following equations for each loading condition.

End Load

$$\sum F_Y = 0 \Rightarrow R_{1-EL} = P$$

$$\sum M = M_{1-EL} = -PL_3$$

Distributed Load

$$\sum F_Y = 0 \Rightarrow R_{1-DL} = w_1 L_1 + w_2 (L_2 - L_1) + w_3 (L_3 - L_2)$$

$$\sum M = M_{1-DL} = \frac{-w_1 L_1^2}{2} - w_2 (L_2 - L_1) \left(\frac{L_1 + L_2}{2} \right) - w_3 (L_3 - L_2) \left(\frac{L_3 + L_2}{2} \right)$$

Reaction Force

$$\sum F_Y = 0 \Rightarrow R_{1-R2} = -R_2$$

$$\sum M_{1-R2} = R_2 L_0$$

where from before:

$$R_2 = 3 \left(\frac{w_1 L_0}{24} - \frac{R_{1-DL}}{6} - \frac{M_{1-DL}}{2L_0} - \frac{P}{6} + \frac{PL_3}{2L_0} \right)$$

and R_1 and M_1 are from the distributed loading as:

$$R_{1-DL} = w_1 L_1 + w_2 (L_2 - L_1) + w_3 (L_3 - L_2)$$

$$M_{1-DL} = \frac{-w_1 L_1^2}{2} - w_2 (L_2 - L_1) \left(\frac{L_1 + L_2}{2} \right) - w_3 (L_3 - L_2) \left(\frac{L_3 + L_2}{2} \right)$$

Therefore, using some careful bookkeeping the moment at R2 can be evaluated and used to evaluate the maximum bending stress in the beam through the following equation:

$$s_{xx} = \frac{Mc}{I_{xx}}$$

where M is the bending moment, c is the distance from the neutral axis to the outermost edge, and I is the bending inertia of the beam at this location.

The average shear stress in the section can be found by:

$$t_{xy} = \frac{V}{A}$$

Where V is the shear force in the section at R2, and A is the cross sectional area of the section at R2. *Note:* This shear stress vanishes at the edges of the section where the bending stress is maximum.

Using the maximum shear stress theory, the maximum shear stress in the section is found from:

$$t_{MAX} = \sqrt{\left(\frac{s_{xx}^2}{2} + t_{xy}^2\right)} \text{ where } t_{xy} \text{ and } s_{xx} \text{ are at the outer edge of the section } \therefore t_{xy} = 0.$$

And according to the theory, the maximum shear stress must be such that:

$$t_{MAX} \leq \frac{S_{yt}}{2n}$$

where S_{yt} is the tensile yield strength of the material and n is the factor of safety.

Numerical Evaluation

$$L_o = 81 \text{ in}$$

$$L_1 = 103.5 \text{ in}$$

$$L_2 = 183 \text{ in}$$

$$L_3 = 262.5 \text{ in}$$

$$P = 100 \text{ lb/in}$$

$$w1 = 2.54 \text{ lb/in}$$

$$w2 = 1.45 \text{ lb/in}$$

$$w3 = .80 \text{ lb/in}$$

using these values we find...

$$R_{1-EL} = -100\text{lb}$$

$$M_{1-EL} = -26250\text{lb}\cdot\text{in}$$

$$R_{1-DL} = 442\text{lb}$$

$$M_{1-DL} = -44284.60\text{lb}\cdot\text{in}$$

$$R_2 = 784\text{lb}$$

$$R_{1-R2} = -784\text{lb}$$

$$M_{1-R2} = 63512\text{lb}\cdot\text{in}$$

Therefore, we can find M1 and R1 as

$$M_1 = -7023\text{lb}\cdot\text{in}$$

$$R_1 = -242\text{lb}$$

Finally, substitution of these values into the equation for the Moment at R2 yields...

$$\sum M_{R2} = M_1 - R_1 L_0 + w_1 L_1 \left(L_0 - \frac{L_1}{2} \right) - w_2 (L_2 - L_1) \left(\frac{L_2 + L_1}{2} - L_0 \right) - w_3 (L_3 - L_2) \left(\frac{L_3 + L_2}{2} - L_0 \right)$$

$$M_{R2} = -7023 + 19602 + 7689 - 17723 - 14834.7 = -12289.7\text{lb}\cdot\text{in}$$

The corresponding bending stress is found using as:

$$s_{xx} = \frac{Mc}{I_{xx}} = \frac{(-12289.7\text{lb}\cdot\text{in})(4.3\text{in})}{41.476\text{in}^4} = -1.274\text{ksi}$$

where c is the distance from the neutral axis to the bottom of the base section.

The corresponding average shear stress is found as:

$$t_{xy} = \frac{V}{A} = \frac{784\text{lb}}{6.22\text{in}^2} = 0.126\text{ksi} \text{ which is significantly lower than the bending stress.}$$

And the maximum shear stress is then found as:

$$t_{MAX} = \sqrt{\left(\frac{s_{xx}}{2} \right)^2} = 0.637\text{ksi}$$

Using a yield strength for mild steel of 43ksi, the section has a calculated factor of safety of about 33.

Conclusion

This analysis has proven that the beam section stresses are very low and thus the beams should not fail under normal operation conditions. This analysis has also proven why the deflection was the major design consideration for the telescopic arm.

Joint Connections Loading Analysis

Assumptions:

Arm components act as point masses.

Infinitely stiff joint connections.

Beam deflection is small.

Procedure:

To determine the loading on the section joints, the arm parts were broken down into point masses that act over a distance to form a moment about the joint connection. This moment must be resolved through the two sets of primary support rollers.

Given:

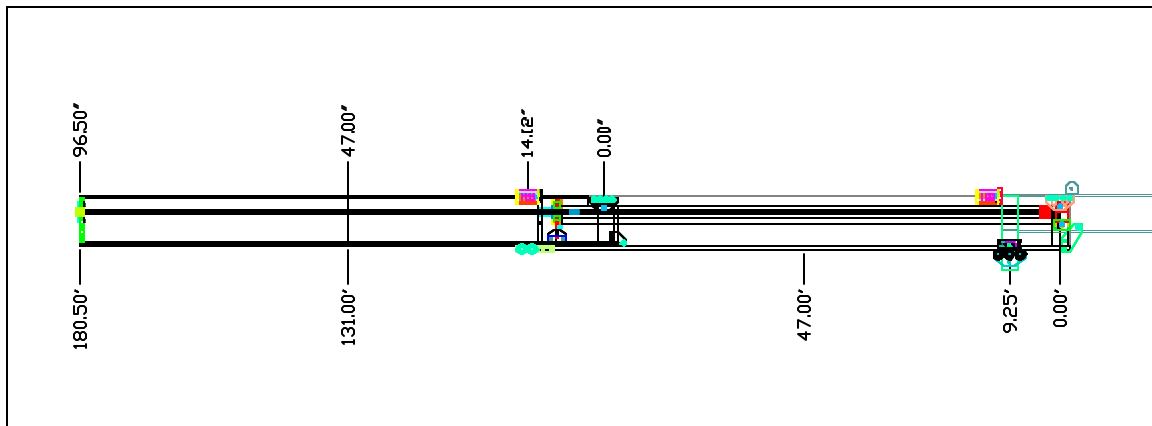


Figure 5-OCCSM Telescopic Arm c.g. / Support Dimensions

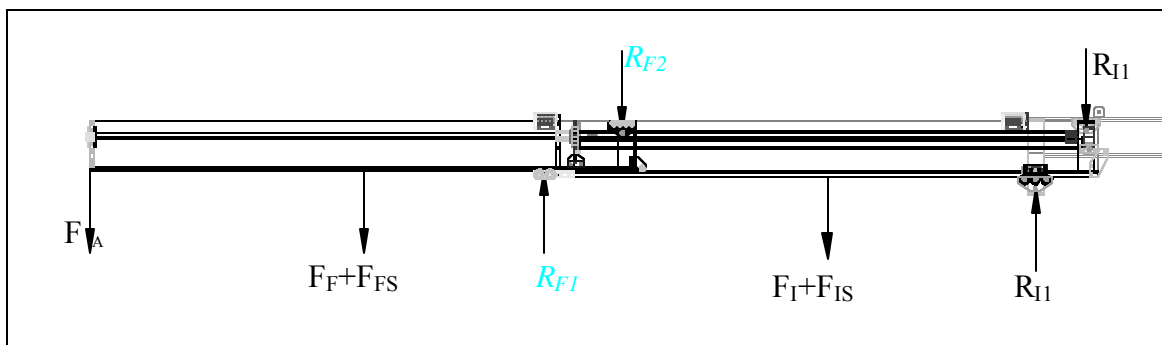


Figure 6-OCCSM Telescopic Arm FBD-Joint Analysis

Note: $R_{F1,2}$ do not represent external loads, rather act only on the fly section alone. They are provided here for the Fly joint analysis only.

$$m_B = 169lb$$

$$m_{BS} = 88lb$$

$$m_I = 80.5lb$$

$$m_{IS} = 62lb$$

$$m_F = 57.7lb$$

$$m_{FS} = 21lb$$

$$m_{SA} = 75lb$$

Where the subscripts are defined as follows:

B = base beam

I = intermediate beam

F = fly beam

BS = base screw

IS = intermediate screw

FS = fly screw

SA = sealant applicator

Statics: Intermediate Primary Loading Rollers

$$\sum M_{R12} = -R_{I1}(9.75) + (F_I + F_{IS})(47) + (F_F + F_{FS})(131) + F_{SA}(180.5)$$

$$\therefore R_{I1} = \frac{((F_I + F_{IS})(47) + (F_F + F_{FS})(131) + F_{SA}(180.5))}{9.75} = 3302 \text{ LB} = 14.69 \text{ KN}$$

$$\sum F_Y = 0 \Rightarrow R_{I2} = R_{I1} - F_I - F_{IS} - F_F - F_{FS} - F_{SA} = 3006 \text{ LB} = 13.35 \text{ KN}$$

Statics: Fly Primary Loading Rollers

$$\sum M_{RF2} = -R_{F1}(14.12) + (F_F + F_{FS})(47) + F_{SA}(96.5)$$

$$\therefore R_{F1} = \frac{(F_F + F_{FS})(47) + F_{SA}(96.5)}{14.12} = 774 \text{ LB} = 3.44 \text{ KN}$$

$$\sum F_Y = 0 \Rightarrow R_{F2} = R_{F1} - F_F - F_{FS} - F_{SA} = 620 \text{ LB} = 2.76 \text{ KN}$$

Statics: Horizontal Supports

Assume:

Sections can be modeled as point masses.

Inertia Forces will exist due to rotational acceleration, at max. extension ($\alpha=0.274$ rad/sec from previous calculation).

Same dimensions apply as in the vertical loading analysis.

FBD from before applies with forces and reactions substituted for the horizontal loading case.

Inertial Forces Sample Calculation

$$IF_{SA} = m_{SA}(\mathbf{ar}^2) = (100\text{lbm})(0.274\text{rad/sec})(269\text{in}) \bullet \frac{\text{lbf sec}^2}{386.4\text{lbm in}} = 19.1 \text{ lbf} = 84.9 \text{ N}$$

Therefore, the succeeding inertia forces can be calculated in a similar manner and statics can be performed to yield...

$$IF_{SA} = 19.1\text{lbf}$$

$$IF_I = 7.73\text{lbf}$$

$$IF_{IS} = 5.95\text{lbf}$$

$$IF_F = 8.98\text{lbf}$$

$$IF_{FS} = 3.26\text{lbf}$$

$$F_{FRIC} = 20\text{lbf}$$

Intermediate Horizontal Support Reactions

$$\sum M_{SI2} = -R_{SI1}(9.75) + (IF_I + IF_{IS})(47) + (IF_F + IF_{FS})(131) + (IF_{SA} + F_{FRIC})(180.5)$$

$$\therefore R_{SI1} = \frac{((IF_I + IF_{IS})(47) + (IF_F + IF_{FS})(131) + (IF_{SA} + F_{FRIC})(180.5))}{9.75} = 954 \text{ lbf} = 4.2 \text{ KN}$$

$$\sum F_Y = 0 \Rightarrow R_{I2} = R_{I1} - F_I - F_{IS} - F_F - F_{FS} - F_{SA} - F_{FRIC} = 889 \text{ lbf} = 3.9 \text{ KN}$$

Fly Horizontal Support Reactions

$$\sum M_{SI2} = -R_{SI1}(14) + (IF_F + IF_{FS})(47) + (IF_{SA} + F_{FRIC})(96.5)$$

$$\therefore R_{SI1} = \frac{((IF_F + IF_{FS})(47) + (IF_{SA} + F_{FRIC})(96.5))}{14} = 311 \text{ lbf} = 1.39 \text{ KN}$$

$$\sum F_Y = 0 \Rightarrow R_{I2} = R_{I1} - F_F - F_{FS} - F_{SA} - F_{FRIC} = 259.7 \text{ lbf} = 1.15 \text{ KN}$$

Sample Roller Truck Bolt Analysis

Intermediate Front Roller Truck

The pin has two failure possibilities, through bending stress or shear stress.

Bending Stress: (From Shigley)

$$F_{\text{max}} = 3302/2 = 1651 \text{ lbf}$$

$$M_{\text{max}} = 1651(0.25\text{in}) = 413 \text{ lbf-in}$$

$$D = 0.50 \text{ in}$$

$$C = 0.25 \text{ in}$$

$$I = \frac{pD^4}{64} = 3.07e^{-3} \text{ in}^4$$

$$s = \frac{Mc}{I} = \frac{(413)(0.25)}{3.07e^{-3}} = 33 \text{ ksi}$$

Using the Maximum Shear Stress Theory Yields...

$$t_{\text{MAX}} = \sqrt{\left(\frac{s_{xx}}{2}\right)^2 + (t_{xy})^2} = \frac{s_{xx}}{2} = 16.5 \text{ ksi}$$

$$S_y = 130 \text{ ksi (Grade 8 Bolt)}$$

$$\therefore n = \frac{S_y}{2t_{\text{MAX}}} = 3.9$$

Shear Stress: (From Shigley)

$$t_{\text{MAX}} = \frac{4V}{3A} = \frac{16(1651)}{3(p(0.5)^2)} = 11.2 \text{ ksi}$$

Using the Maximum Shear Stress Theory Yields...

$$t_{\text{MAX}} = \sqrt{\left(\frac{s_{xx}}{2}\right)^2 + (t_{xy})^2} = t_{\text{MAX}}$$

$$S_y = 130 \text{ ksi (Grade 8 Bolt)}$$

$$\therefore n = \frac{S_y}{2t_{\text{MAX}}} = 5.8$$

Torsional Analysis of Telescopic Arm

<i>Torsion of OCCSM Telescopic Arm (Roarke p156)</i>				
Theta=T*L/(K*G)	0.000498	rad	0.0031	deg
T=F*H	480	lbf*in		
F=	20	lbf		
H=	24	in		
L=	159	in		
G=	1.15E+07	psi		
t sides=	0.03	in		
Average t-top/btm	0.03	in		
Section Height=	10	in		
Section Width=	6	in		
K=	13.33527	in ⁴		
Sealant Head Error	0.011944	in		

<i>Torsion of OCCSM Telescopic Arm (Timoshenko)</i>				
Theta=T*L/(4*A²*G*t)	1.56E-05	rad	1E-04	deg
T=F*H	480	lbf*in		
F=	20	lbf		
H=	24	in		
L=	159	in		
G=	1.15E+07	psi		
t =	0.03	in		
Section Height=	10	in		
Section Width=	6	in		
A=	59.5218	in		
Sealant Head Error	0.000375	in		

Note: This formula assumes equal wall thicknesses

Note2: A= The mean of the areas enclosed by the inner and outer boundaries of the cross section of the tube.

Rotational Motor / Gearbox Specifications

Motor: *Dynaserv® DR5030B Brushless Servo Motor*

Peak Torque:	22 ftlb.
Rated Speed:	4 rev/sec
Resolution:	278528 steps/rev
Weight:	28.9 lb
Motor Inertia:	1420 oz-in ²
Max. Power Consumption:	3.6 KVA

Gearbox: *Harmonic Drive® - HDC65*

Gear Ratio:	60:1
Rated Output Torque:	7880 lbin @1750rpm
Maximum Output Torque:	10200 lbin
Static Torque Limit:	27750 lbin
Ratchet Torque Limit:	24000 lbin
Maximum Input Speed:	3500 rpm
Inertia:	15.54 lbm-in ²
Input Backlash	13 arc-min

Drive System Requirements:

Handle maximum torque requirements.

Capable of attaining maximum speed.

Capable of attaining required accuracy.

Calculations

Beam Inertia:	$J_b = 11.2E6 \text{ lbm-in}^2$
Gearbox Inertia:	$J_g = 15.54 \text{ lbm-in}^2$
Motor Inertia:	$J_m = 1420 \text{ oz-in}^2$
Vmax:	$V = 3 \text{ ft/sec}$
Time to Accelerate:	$t = .5 \text{ sec}$
Radial Extension:	$r = 262.5 \text{ in}$
Rated Motor Speed:	$n = 4 \text{ rev/sec}$
Gearbox Ratio:	$N = 60$
Motor Resolution:	$R = 278528 \text{ steps/rev}$

$$\text{Required Motor Torque} = t_R = \frac{1}{386.4} \left(\frac{J_b}{N^2} + \frac{J_m}{16} + J_g \right) \bullet \frac{VN}{rt} = 11.46 \text{ lbft}$$

Inertia Ratio(Jload/Jm):

$$\frac{J_{load}}{J_m} = \frac{\frac{J_b}{N^2} + J_g}{\frac{J_m}{16}} = 35.23$$

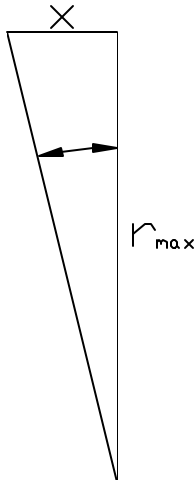
Required Motor Speed(at minimum extension)

$$n_r = N\dot{q} = (60)(0.3478\text{rad/sec}) = 20.868\text{rad/sec} = 3.32\text{rev/sec}$$

Arm Resolution(Steps/in(translation)) at max extension

$$R^* = \frac{NR}{2pr_{\max}} = \frac{(60)(278528\text{steps/rev})}{(2\text{prad/rev})(262.5\text{in})} = 10132\text{steps/in}$$

Transferred Backlash (at Maximum extension)



$$\tan \alpha = \frac{x}{r_{\max}} \approx \alpha$$
$$\therefore x = r_{\max} \cdot \alpha$$

where α is in radians.

Current Values

$$r_{\max} = 262.5 \text{ in}$$

$$\alpha = 13 \text{ arc-min/N} = 0.217\text{deg}/60 = 6.33\text{E-}5 \text{ rad}$$

$$\text{Therefore } x = 0.017 \text{ in}$$

Therefore, the calculations show that the specified gearbox and motor will meet and exceed all of the machine performance calculations.

Calculation for Rotational Inertia as a Function of Radial Extension

Variables:

r = radial distance to end of arm.

R_i = Radial distance from pivot to i 'th objects center of mass.

Constants:

I_{0_i} = Inertia of i 'th object about its own center of mass.

M_i = i 'th object mass

Subscripts:

B = base beam

I = intermediate beam

F = fly beam

BS = base screw

IS = intermediate screw

FS = fly screw

SA = sealant applicator

Equations:

For $103.5 < r < 262.5$

$$I(r) = (I_{0_B} + m_B r_B^2) + (I_{0_{BS}} + m_{BS} r_{BS}^2) + (I_{0_I} + m_I r_I^2) + (I_{0_F} + m_F r_F^2) + (I_{0_{IS}} + m_{IS} r_{IS}^2) + \dots$$

$$\dots + (I_{0_{FS}} + m_{FS} r_{FS}^2) + m_{SA} r^2$$

geometric constraints yield

$$r_B = 43.5$$

$$r_{BS} = 45$$

$$r_I = \frac{r - 105}{2} + 50.5$$

$$r_{IS} = \frac{r - 105}{2} + 52.5$$

$$r_F = r - 49.5$$

$$r_{FS} = r - 44.5$$

which yields

$$I(r) = (I_{0_B} + m_B (43.5)^2) + (I_{0_{BS}} + m_{BS} (43.5)^2) + (I_{0_I} + m_I \left(\frac{r - 105}{2} + 50.5\right)^2) + (I_{0_F} + m_F (r - 49.5)^2) + \dots$$

$$\dots + (I_{0_{IS}} + m_{IS} \left(\frac{r - 105}{2} + 52.5\right)^2) + (I_{0_{FS}} + m_{FS} (r - 44.5)^2) + m_{SA} r^2$$

which expands to

$$I(r) = (I_{0_B} + 189225m_B) + (I_{0_{BS}} + 2025m_{BS}) + (I_{0_I} + m_I(\frac{r^2}{4} - 29r + 841)) + (I_{0_F} + \dots$$

$$\dots + m_F(r^2 - 99r + 2450.25)) + (I_{0_{IS}} + m_{IS}(\frac{r^2}{4} - 27.25r + 742.56)) + \dots$$

$$\dots + (I_{0_{FS}} + m_{FS}(r^2 - 89r + 1980.25)) + m_{SA}r^2$$

and simplifies to

$$I(r) = (\frac{m_I + m_{IS}}{4} + m_F + m_{FS} + m_{SA})r^2 - (29m_I + 99m_F + 27.25m_{IS} + 89m_{FS})r + (I_{0_B} + \dots$$

$$\dots + I_{0_I} + I_{0_F} + I_{0_{BS}} + I_{0_{IS}} + I_{0_{FS}} + 1892.25m_B + 2025m_{BS} + 841m_I + 2450.25m_F + \dots$$

$$\dots + 742.56m_{IS} + 1980.25m_{FS})$$

Current Arm Values:

$$I_{0_B} = 253,429 \text{ lb}_m \text{ in}^2$$

$$I_{0_I} = 66,799 \text{ lb}_m \text{ in}^2$$

$$I_{0_F} = 41,750 \text{ lb}_m \text{ in}^2$$

$$I_{0_{BS}} = 92,602 \text{ lb}_m \text{ in}^2$$

$$I_{0_{IS}} = 48,113 \text{ lb}_m \text{ in}^2$$

$$I_{0_{FS}} = 15,695 \text{ lb}_m \text{ in}^2$$

$$m_B = 169 \text{ lb}_m$$

$$m_{BS} = 88 \text{ lb}_m$$

$$m_I = 80.5 \text{ lb}_m$$

$$m_{IS} = 62 \text{ lb}_m$$

$$m_F = 57.7 \text{ lb}_m$$

$$m_{FS} = 21 \text{ lb}_m$$

$$m_{SA} = 75 \text{ lb}_m$$

Substitution Yields

$$I(r) = 189.3r^2 - 11605r + 1267043 \text{ lb}_m \text{ in}^2$$

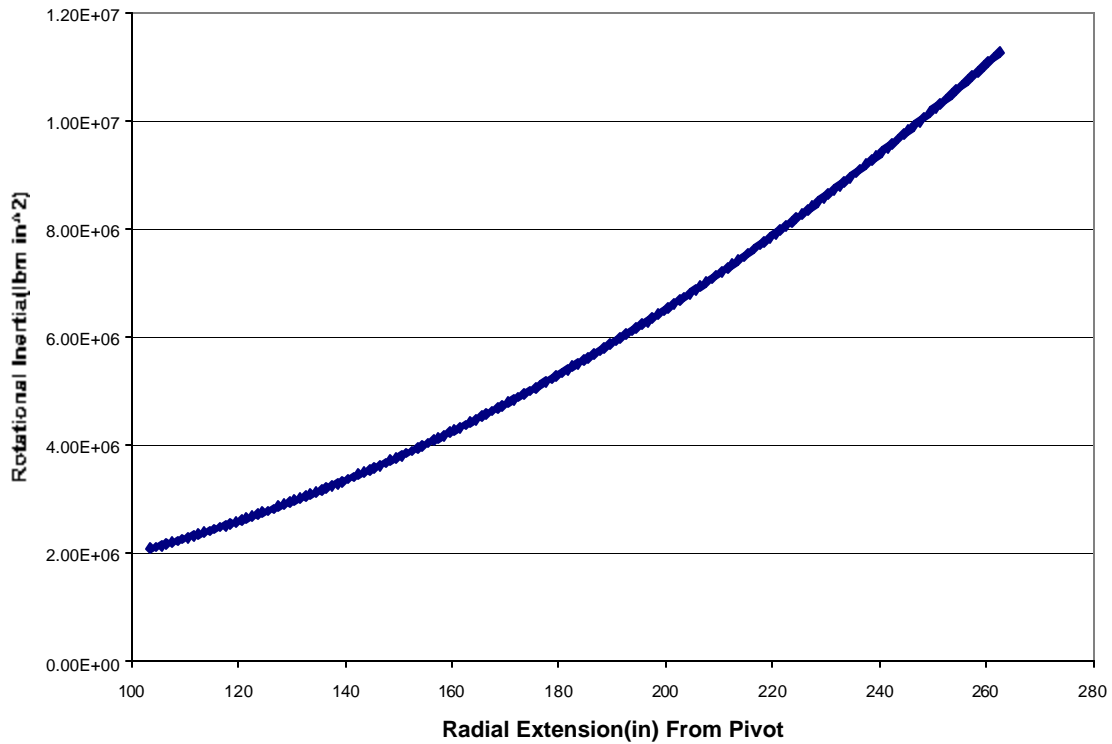
Therefore,

$$I_{min} = I(103.5) = 2.1E6 \text{ lb}_m \text{ in}^2$$

$$I_{max} = I(262.5) = 11.2E6 \text{ lb}_m \text{ in}^2$$

Graphical Representation

Rotational Inertia Vs. Radial Extension



This plot demonstrates the vast range of the rotational inertia values for the telescopic arm. These large deviations in the characteristics of the arm bring to question the rotational control system performance. The mechanical design of the OCCSM telescopic arm minimizes this deviance by using thin-wall light beam sections in an effort to maintain a stable control system.

Rotational Axis Torque Requirements

There are two possible design scenarios which will result in the maximum torque requirement due to the telescopic nature of the arm. The first is at minimum extension, where the rotational inertia is very low but the angular acceleration must be larger due to the arm's shorter length. The second is at maximum extension where the rotational inertia is very small and the angular acceleration is very low.

Minimum Extension

Radial Extension:	$r=103.5$ in
Rotational Inertia:	$I=2.1E6$ lbin ²
End Effector Velocity:	$V=36$ in/s
Time to Max Speed:	$t=0.5$ sec

Angular Velocity and Acceleration

$$\dot{q} = \frac{v}{r} = \frac{36}{103.5} = 0.3478 \text{ rad / sec}$$

$$a = \frac{\dot{J}}{t} = \frac{0.3478}{.5} = 0.6956 \text{ rad / sec}^2$$

Required Torque(Neglecting Motor Inertia)

$$t = J a \Rightarrow (2.1E6)(0.6956) \frac{\text{lb min}^2}{\text{sec}^2} \cdot \frac{\text{lbf}}{32.2 \frac{\text{lbmft}}{\text{sec}^2}} \cdot \frac{1 \text{ft}}{12 \text{in}} = 3780 \text{ lbf in}$$

Maximum Extension

Radial Extension:	$r=262.5$ in
Rotational Inertia:	$I=11.2E6$ lbin ²
End Effector Velocity:	$V=36$ in/s
Time to Max Speed:	$t=0.5$ sec

Angular Velocity and Acceleration

$$\dot{q} = \frac{v}{r} = \frac{36}{262.5} = 0.1371 \text{ rad / sec}$$

$$a = \frac{\dot{J}}{t} = \frac{0.1371}{.5} = 0.2743 \text{ rad / sec}^2$$

Required Torque(Neglecting Motor Inertia)

$$t = J a \Rightarrow (11.2E6)(0.2743) \frac{\text{lb min}^2}{\text{sec}^2} \cdot \frac{\text{lbf}}{32.2 \frac{\text{lbmft}}{\text{sec}^2}} \cdot \frac{1 \text{ft}}{12 \text{in}} = 795 \text{ lbf in}$$

Therefore, the design case to be used is at maximum extension where the required torque is about 7950 lbf in.

Telescopic Actuator System

Specifications

Motor: Compumotor® Apex 620

Peak Torque:	331 inlb.
Cont. Torque:	116 inlb
Rated Speed:	3700 rev/min
Resolution:	4096 steps/rev
Weight:	29.0 lb
Motor Inertia:	35.87 oz-in ²
Rated Power:	6 hp

Gearbox: Custom Dual Output Planetary System

Weight:	
Lubrication:	Grease
Casing:	Aluminum
Inertia (est.):	40 oz-in ²
Backlash(outer/inner):	8 / 11 arc-min
Input:	
Shaft (Dia.: Mount):	24mm: Keyed
Torque (Cont.):	116 inlb
Torque (Peak):	331 inlb
Speed (Peak):	3600 rev/min

Outer Output:	
Shaft (Dia.: Mount):	25mm: No. 6 Taper Pin
Ratio(I/O):	1/2
Torque (Cont.):	232 inlb
Torque (Peak):	662 inlb
Speed (Peak):	1800 rev/min

Inner Output:	
Shaft (Dia.: Mount):	1.75in: Clamp-on Coupling
Ratio(I/O):	1/3
Torque (Cont.):	348 inlb
Torque (Peak):	993 inlb
Speed (rpm):	1200 rev/min

Prismatic Ball Screw Actuator

Retracted Length:	107 in
Stroke:	159 in
Effective Lead:	0.667 in/motor rev
Peak Translational Speed:	40 in/sec (Motor Limited)

Outer Drive Tube:
 Clearance Diameter: 4.0 in
 Diameter: 3.0 in
 Wall Thickness: 0.125 in
 Length: 96 in
 Rotational Inertia: 1016 oz in²
 Approx. Weight: 46 lb

Split Tube:
 Outer Diameter: 2.563 in
 Inside Diameter: 2.060 in
 Length: 94.40 in
 Slot Length: 88 in
 Rotational Inertia: 1047 oz in²
 Approx. Weight: 40 lb

Intermediate Ball Screw
 Lead: 2.000 in/rev
 Diameter: 2.000 in
 # of starts: 2 start
 Lead Accuracy: 0.0005 in/ft.
 Length: 92 in
 Through Hole Diameter: 1.062 in
 Rotational Inertia: 603 oz in²
 Approx. Weight: 62 lb

Fly Ball Screw
 Lead: 1.000 in/rev
 Diameter: 1.000 in
 # of Starts: 2 start
 Lead Accuracy: 0.0005 in/ft
 Length: 96 in
 Weight: 21 lb

Ball Screw Actuator: Kinematic Analysis

Notation:

w_i = Angular Speed of the i^{th} object.

v_i = Translational Speed of the i^{th} object.

L_i = Screw Lead of the i^{th} object. ($L = 1/\text{Pitch}$)

Subscripts:

I = Gearbox input

BT = Base tube

IS = Intermediate screw

FS = Fly screw

Gearbox Equations:

$$w_{BT} = \frac{1}{2} w_I$$

$$w_{IS} = \frac{1}{3} w_I$$

Ball Screw Equations:

$$(w_{BT} - w_{IS})L_{IS} = v_{IS}$$

$$(w_{IS} - w_{FS})L_{FS} + v_{IS} = v_{FS}$$

$$w_{FS} = 0$$

$$\frac{L_{IS}}{L_{FS}} = 2$$

Relation of Motor Input Velocity to End Translation:

$$(w_{IS} - w_{FS})L_{FS} + v_{IS} = (w_{IS})L_{FS} + (w_{BT} - w_{IS})L_{IS} = v_{FS}$$

$$\left(\frac{w_{IS}}{2} + (w_{BT} - w_{IS}) \right) = v_{FS}$$

Substitute for w_{BT} , w_{IS} as functions of w_I .

$$\left(\frac{1}{2} w_I - \frac{1}{6} w_I \right) L_{IS} = \frac{1}{3} w_I L_{IS} = v_{FS}$$

Note:

All w_i are in [rev/sec], L_i are in [in/rev] and v_i are in [in/sec].

Current Ball Screw Values:

$$L_{IS} = 2 \text{ in / rev}$$

$$L_{FS} = 1 \text{ in / rev}$$

Therefore, the relational equation is:

$$v_{FS} = \frac{2}{3} \mathbf{w}_I$$

with $\mathbf{w}_I(\text{Max}) = 61 \text{ rev / sec}$

$$v_{FS}(\text{Max}) = \frac{2}{3} \mathbf{w}_I = 40 \text{ in / sec}$$

Required Gearbox Inner Output Torque Calculation

$$t_{Motor} = \frac{1}{386.4} \left(\left(\frac{J_{Load} + J_{IS}}{e} \right) + J_{Motor} + J_{Gearbox} \right) \frac{\mathbf{w}N}{t} + \frac{T_F}{N}$$

where:

t_i = Torque [ozin]

J_i = Rotational Inertia [ozin²]

\mathbf{w} = Angular Velocity [rad / s]

t = Time [sec]

e = efficiency [%x100]

Ball Screw Rotational Inertia, J_{IS}

$$J_{IST} = J_{ST} + J_{IS}$$

$$J_i = \frac{1}{2} M_o r_o^2 - \frac{1}{2} M_i r_i^2$$

$$J_i = \frac{1}{2} M_o r_o^2 - \frac{1}{2} M_i r_i^2 = \frac{1}{2} (\mathbf{rpr}_o^2 L) r_o^2 - \frac{1}{2} (\mathbf{rpr}_i^2 L) r_i^2 = \frac{1}{2} \mathbf{rpl} (r_o^4 - r_i^4)$$

For the split tube, $r_o=1.28\text{in}$, $r_i=1.03\text{in}$, $L=94.4\text{in}$:

$$J_{ST} = \frac{1}{2} \mathbf{rpl} (r_o^4 - r_i^4) = \frac{1}{2} \mathbf{p} (94.4) (1.28^4 - 1.03^4) (0.283) = 65.42 \text{ lb}_m \text{ in}^2$$

For the Intermediate Ball Screw, $r_o=1.0\text{in}$, $r_i=0.53\text{in}$, $L=92\text{in}$:

$$J_{IS} = \frac{1}{2} \mathbf{rpl} (r_o^4 - r_i^4) = \frac{1}{2} \mathbf{p} (92) (1^4 - 0.53^4) (0.283) = 37.67 \text{ lb}_m \text{ in}^2$$

Therefore. ..

$$J_{IST} = 65.42 + 37.67 = 102.89 \text{ lb}_m \text{ in}^2$$

Equivalent Load Rotational Inertia

$$J_{Load} = \frac{W}{(2pP)^2} = \frac{WL_{IS}^2}{39.47}$$

where W is the weight of all of the moving masses. In this case...

$$W = m_{IS} + m_I + m_F + m_{FS} + m_{SA} = 62 + 81 + 58 + 21 + 75 = 297lb$$

Therefore...

$$J_{Load} = \frac{WL_{IS}^2}{39.47} = \frac{(297)(4)}{39.47} = 30.09lbin$$

Frictional Equivalent Torque:

$$T_F = \frac{F_f L_{IS}}{2pe} = \frac{mF_n L_{IS}}{2pe} = \frac{(0.15)(200)(2)}{2p(0.81)} = 11.78lbin$$

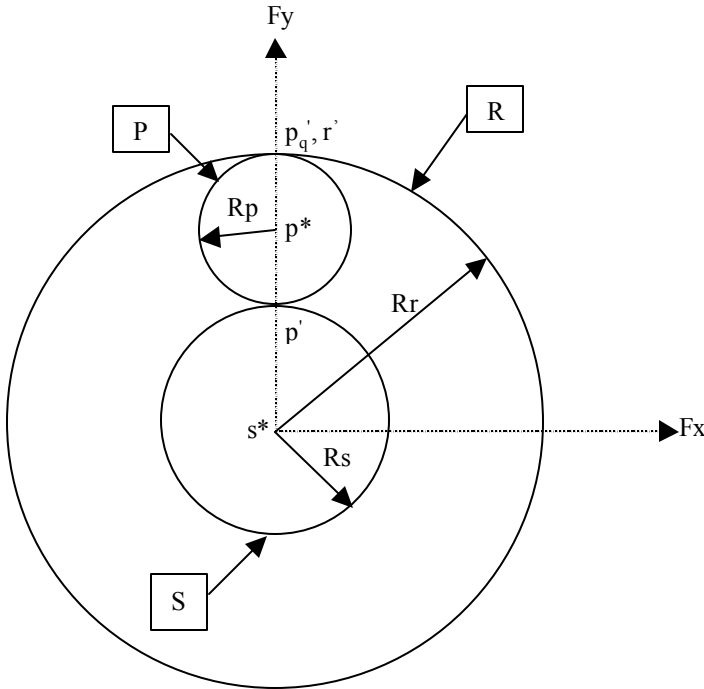
Assuming that the frictional forces in the section arise from the wearpads and that the normal forces on these wear pads total 200lb.

Therefore, the Required Motor Torque is:

$$t_{Motor} = \frac{1}{386.4} \left(\frac{\left(\frac{J_{Load} + J_{IS}}{e} \right)}{N^2} + J_{Motor} + J_{Gearbox} \right) \frac{wN}{t} + \frac{T_F}{N}$$

$$t_{Motor} = \frac{1}{386.4} \left(\frac{\frac{30.09(16)}{0.81} + 102.89(16)}{9} + 35.87 + 40 \right) \frac{127(3)}{0.5} + \frac{(11.78)(16)}{3} = 703ozin$$

Gearbox Calculations
Planetary Kinematic Analysis



Given:

$$** \quad {}^F \tilde{\mathbf{w}}^R = \Omega \bar{f}_Z$$

$$** \quad {}^F \tilde{\mathbf{w}}^S = 0$$

** Object P rolls on S and R

Desire:

$$N = \frac{\Omega}{\mathbf{w}_A}$$

Solution:

$${}^F \tilde{\mathbf{v}}^{p^*} = {}^F \tilde{\mathbf{v}}^{p_1} + {}^F \tilde{\mathbf{w}}^P \times \mathbf{r}^{p_1^* p^*} \quad (1)$$

$${}^F \tilde{\mathbf{v}}^{p_2} = {}^F \tilde{\mathbf{v}}^{R'} = {}^F \tilde{\mathbf{v}}^{S^*} + {}^F \tilde{\mathbf{w}}^R \times \mathbf{r}^{S^* R'} = \Omega \bar{f}_Z \times \mathbf{r}_r \bar{f}_y = -\Omega r_r \bar{f}_x \quad (2)$$

$${}^F \tilde{\mathbf{v}}^{P^*} = {}^F \tilde{\mathbf{v}}^{P_2} + {}^F \tilde{\mathbf{w}}^P \times \mathbf{r}^{P_2 P^*}$$

$${}^F \tilde{\mathbf{v}}^{P^*} = -\Omega r_r \bar{f}_x + \mathbf{w}_P \bar{f}_Z \times -r_P \bar{f}_y = -\Omega r_r \bar{f}_x + \mathbf{w}_P r_P \bar{f}_x = (-\Omega r_r + \mathbf{w}_P r_P) \bar{f}_x \quad (3)$$

From 1, 3

$$\mathbf{w}_P \bar{f}_Z \times r_P \bar{f}_y = -\mathbf{w}_P r_P = -\Omega r_r + \mathbf{w}_P r_P \Rightarrow \mathbf{w}_P = \frac{\Omega r_r}{2 r_P} \quad (4)$$

Then from 3,4

$${}^F \tilde{v}^{P*} = \left(-\Omega r_r + \frac{\Omega r_r}{2 r_p} r_p \right) \bar{f}_x = \frac{\Omega r_r}{2} \bar{f}_x \quad (5)$$

Then, by connecting an arm from s* to p* we can determine the angular velocity of this arm as...

$$\begin{aligned} {}^F \tilde{v}^{P*} &= {}^F \tilde{v}^{S*} + {}^F \tilde{\omega}^A \times r^{S*P*} \\ -\frac{\Omega r_r}{2} \bar{f}_x &= \mathbf{w}_A \bar{f}_z \times (r_p + r_s) \bar{f}_y \\ -\frac{\Omega r_r}{2} \bar{f}_x &= -\mathbf{w}_A (r_p + r_s) \bar{f}_x \Rightarrow \mathbf{w}_A = \frac{\Omega r_r}{2(r_p + r_s)} \quad (6) \end{aligned}$$

From geometry, the following equation arises...

$$2r_p + r_s = r_r \Rightarrow r_p + r_s = r_r - r_p \quad (7)$$

Substitution of (7) into (6) yields...

$$\mathbf{w}_A = \frac{\Omega r_r}{2(r_r - r_p)} \Rightarrow \frac{\mathbf{w}_A}{\Omega} = \frac{r_r}{2(r_r - r_p)} \quad (8)$$

∴ given a desired ratio of output \mathbf{w}_A to Input Ω a relationship between r_r and r_p can be found as...

$$r_r = 2 \frac{\mathbf{w}_A}{\Omega} (r_r - r_p) \Rightarrow r_p = r_r \left(1 - \frac{N}{2} \right) \text{ where } N = \frac{\Omega}{\mathbf{w}_A} \quad (10)$$

Gearbox Input/Output Kinematics

$$N = \frac{3}{2} \Rightarrow \mathbf{w}_A = \frac{2\Omega}{3}$$

Ω is the angular velocity of the ring gear which is derived from...

$$\Omega = \frac{\mathbf{w}_1}{2}, \text{ where } \mathbf{w}_1 \text{ is the input angular velocity.}$$

Therefore, the outer output shaft is related to the input by a ratio of 1/2 :

$$\Omega = \frac{\mathbf{w}_1}{2}$$

The inner output shaft is connected to the arm and has the relationship...

$$\mathbf{w}_A = \frac{2\Omega}{3} = \frac{\mathbf{w}_1}{3} \text{ (a gear reduction of 1/3.)}$$

Gearbox Bevel Gear Analysis

Peak Input Torque: 350 inlb

Bevel Gear Stress Analysis:

Gear Bending Stresses/Contact Stresses

Assumptions:

Bending stresses are maximum at peak transmitted torque

Contact stresses (wear), will occur under continuous transmitted torque

Centrifugal forces on geartrain are small

Sun gear stresses are identical to planet stresses

Equations:

From Shigley,

Gear Bending Strength

$$s = \frac{W_t K_a P_s K_s K_m}{K_v F J}$$

where σ =bending stress in gear tooth

W_t =transmitted load

K_a =application factor

P_s =diametral pitch

K_s =size factor

K_m =load distribution factor

K_v =dynamic Factor

F =face width

J =geometry factor

$$s_{all} = \frac{S_t K_L}{K_T K_R}$$

where σ_{all} =maximum allowable stress in gear tooth

S_t = AGMA bending stress

K_L =life factor

K_T =temperature factor

K_R =reliability factor

Gear Contact Stresses

$$s = C_p \left(\frac{W_t C_a C_s C_f C_m}{C_v F d I} \right)^{1/2}$$

where σ =contact stress on gear

C_p =elastic coefficient

W_t =transmitted load

C_a =application factor

C_f =surface factor

C_s =size factor

C_m =load distribution factor

C_v =dynamic Factor

F =face width

d =pitch diameter

I =geometry factor

$$\mathbf{s}_{all} = \frac{S_c C_L C_H}{C_T C_R}$$

where σ_{all} =maximum allowable contact stress in gear

S_c = AGMA contact stress

C_L =life factor

C_T =temperature factor

C_R =reliability factor

C_H =hardness factor

Calculations/Results: See following page

Bevel Gear Analysis

Gearbox Details

Torque Input (in lb)	332	Desired F.S.	2
Continuous Torque(in lb)	166	n-motor(rpm)	3700
Gear Ratio	2	Material Properties	E v
	Pinion Gear	Steel	3.00E+07 0.3
Peak Wt (lb.)	265.6	132.8	
Continuous Wt(lb)	132.8	66.4	

Stress Analysis:Bevel Gears

	Phi	Diameter	p(teeth/in)	Teeth	E	v	Qv	V(ft/min)	F(in)
Bevel Pinion	20	2.5	8	20	3.00E+07	0.3	9	2421.644	0.83
Bevel Gear	20	5	8	40	3.00E+07	0.3	9	2421.644	0.83

Surface Contact Correction Factors

Cp	2.29E+03
Ca	1.5
Cv(pinion)	0.780845
Cv(gear)	0.780845
A(pinion)	76.87883
B(pinion)	0.520021
A(gear)	76.87883
B(gear)	0.520021
Cs	1
Cm	1.3
Cf	1
I	0.078
Mn	1
Mg	2
Sc(pinion)	200000
Sc(gear)	200000
Cl	1
Ch(pinion)	1
Ch(gear)	1.00069
A	0.00069
BHNp	360
BHNg	360
Ct	1
Cr	1

Strength Correction Factors

Ka	1.5
Kv(pinion)	0.780845
Kv(gear)	0.780845
Ks	1
Km	1
J(pinion)	0.23
J(gear)	0.21
St(pinion)	60000
St(gear)	60000
Kl	1
Kt	1
Kr	1

Pinion Contact Stress	103687.8
Allowable Stress	200000
Gear Contact Stress	73318.34
Allowable Stress	200138

Pinion Bending Stress	21381.52
Pinion Allowable Stress	60000
Gear Bending Stress	11708.93
Gear Allowable Stress	60000

Surface Contact Factor of Safety

Gear	2.729713
Pinion	1.928867

Strength Based Factor of Safety

Gear	5.124294
Pinion	2.806161

Shaft Reactions (FBD)

Assumptions:

All forces are point forces, not distributed

Reaction load points from tapered roller bearings are at $a=0$

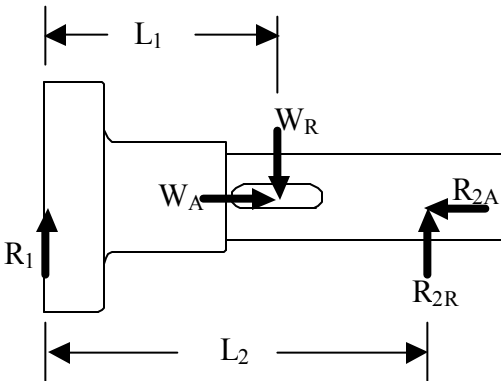
Bearings cannot support moments

Equations:

$$\sum F = 0 \quad \text{where } F = \text{applied forces, } M = \text{applied moments}$$

$$\sum M = 0$$

Calculations/Results: (NOTE: The analysis of only the outer output shaft is shown here for simplicity. All other shaft calculations were performed in a similar manner.



Outer Output Shaft:FBD-Vertical Plane

Shaft Loading: 5" Bevel Gear-

$$W_r = W_t \tan j \cos g = 140(\tan 20^\circ)(\cos 45^\circ) = 36.0lb$$

$$W_a = W_t \tan j \sin g = 140(\tan 20^\circ)(\sin 45^\circ) = 36.0lb$$

$$L_1 = 4.75in$$

$$L_2 = 6.75in$$

Statics(Vertical Plane)

$$\sum F_y = 0 = -W_r + R_{2R} + R_1 : \text{Eq. 1}$$

$$\sum F_x = 0 = W_a - R_{2A} : \text{Eq. 2}$$

$$\sum M_{R1} = 0 = W_r(L_1) - R_{2R}(L_2) : \text{Eq. 3}$$

From Eq. 3:
 $R_{2R} = 25.3LB$

From Eq. 2:
 $R_1 = 10.7LB$

From Eq. 1:
 $R_{2A} = 36.0LB$

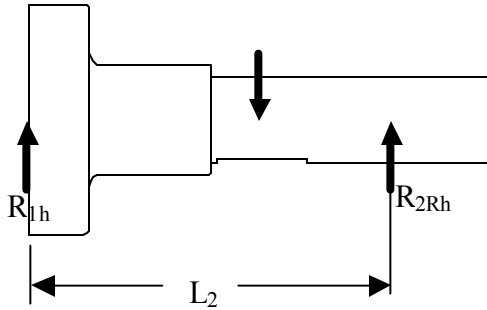


Figure 9-Outer Output Shaft:FBD-Horizontal Plane

Statics(Horizontal Plane)

$$\sum F_y = 0 = -W_t + R_{2Rh} + R_{1h} : \text{Eq. 1h}$$

$$\sum M_{R1} = 0 = W_t(L_1) - R_{2Rh}(L_2) : \text{Eq. 2h}$$

From eq.3h:

$$R_{2Rh} = 98.5lb$$

From eq.1h:

$$R_{1h} = 41.5lb$$

Shaft Strengths

Assumptions:

Maximum shear stress theory is adequate

Failure will occur under peak torque loading

Equations:

From Shigley

$$s_{xx} = \frac{F}{A} + \frac{Mc}{I} = \frac{4K_{fa}F}{pd^2} + \frac{16K_fM}{pd^3}$$

$$t_{xy} = \frac{Tr}{J} = \frac{32K_{fs}T}{pd^3}$$

$$t_{\max} = \left(\left(\frac{s_{xx}}{2} \right)^2 + (t_{xy})^2 \right)^{1/2} = \frac{S_y}{2n}$$

where σ_{xx} =stress due to axial and bending

τ_{xy} = stress due to torsion

F=axial applied load

d=diameter of shaft

c=radius of shaft

I=bending inertia of shaft

T=torque applied to shaft

J=polar moment of inertia

K_{fa} =axial stress concentration factor

K_f =bending stress concentration factor

K_{fs} =torsional stress concentration factor

τ_{\max} =maximum shear stress

S_y = material yield stress

n= factor of safety

Calculations/Results:

Outer Output Shaft(see FBD)

Given:

T(peak) input=331 in-lb

F= W_a

D_o =1.75in

D_i =1.125in

$$A = \frac{\pi}{4} (D_o^2 - D_i^2) = 2.148 \text{ in}^2$$

$$M_{\max} = \frac{(W_R^2 + W_t^2)^{0.5} L_1}{4} = 171.7 \text{ lb-in}$$

$$I = \frac{\mathbf{p}(D_o^4 - D_I^4)}{64} = 0.707in^4$$

$$J = \frac{\mathbf{p}(D_o^4 - D_I^4)}{32} = 1.413in^4$$

$$c = \frac{D}{2}$$

$$\therefore \mathbf{s}_{xx} = \frac{F}{A} + \frac{Mc}{I} = \frac{36}{2.148} + \frac{171.7(0.875)}{0.707} = 229.26\text{psi}$$

$$\mathbf{t}_{xy} = \frac{Tr}{J} = \frac{(662)(0.875)}{1.413} = 409.9\text{psi}$$

$$\mathbf{t}_{\max} = \left(\left(\frac{\mathbf{s}_{xx}}{2} \right)^2 + (\mathbf{t}_{xy})^2 \right)^{1/2} = 425\text{psi} = \frac{S_y}{2n} = \frac{54000\text{psi}}{2n}$$

$$n = FS = 63.5$$

Planetary Analysis

Peak inputs to Bayside® RA115 - 3 : 1 planetary system :

$$\text{Torque} : \frac{5.0}{2.5}(T_{input}) = 700\text{lb}\cdot\text{in}$$

$$\text{Speed} : \frac{2.5}{5.0}(w_{input}) = 1850 \text{ rev/min}$$

Peak Planetary Outputs :

Torque : 993 inlb

Speed : 1200 rev/min

Bayside® RA115 - 3 : 1 Planetary *Rated Loading* :

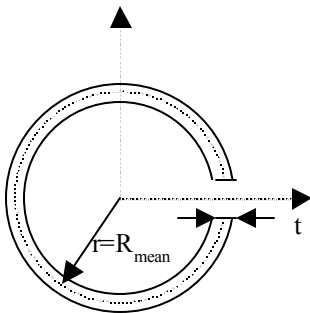
Rated Output Torque : 1600 inlb

Peak Output Torque : 2656 inlb

Input Speed : 5000 rev/min

Therefore, the Bayside® planetary set is operating within the manufacturer's specifications.

Split Tube Analysis



From Roarke, Formulas for Stress & Strain

$$q = \frac{TL}{KG} \quad K = \frac{2}{3}prt^3$$

$$t_{\max} = \frac{T(6pr + 1.8t)}{4p^2r^2t^2}$$

From the gearbox and motor specifications, the maximum torque applied to the split tube is 132 lbin.

Split Tube Specifications

Outer Diameter:	2.563 in
Inside Diameter:	2.060 in
Length:	94.40 in
Slot Length:	88 in
Rotational Inertia:	1047 oz in ²
Approx. Weight:	40 lb

Applying Roarke's equations yields...

Stress

$$t_{\max} = \frac{T(6pr + 1.8t)}{4p^2r^2t^2} = \frac{132\text{lbin}(6p(1.15\text{in}) + 1.8(0.25\text{in}))}{4p^2(1.15\text{in})^2(0.25\text{in})^2} = 0.878\text{ksi}$$

Using the maximum shear stress theory

$$t_{\max} \leq \frac{S_{sy}}{2n} = \frac{44}{4} = 11\text{ksi}$$

where n is a factor of safety of 2 and S_{sy} is the tensile yield strength of hot roll steel. Therefore, the tube is well below the safe stress limits.

Deflection

$$q = \frac{TL}{KG} \quad K = \frac{2}{3}prt^3 = \frac{2}{3}p(1.15)(0.25)^3 = 0.03763in^4$$

$$q = \frac{TL}{KG} = \frac{132lbin(88in)}{(0.03763in^4)(11.6E6psi)} = 0.0266rad$$

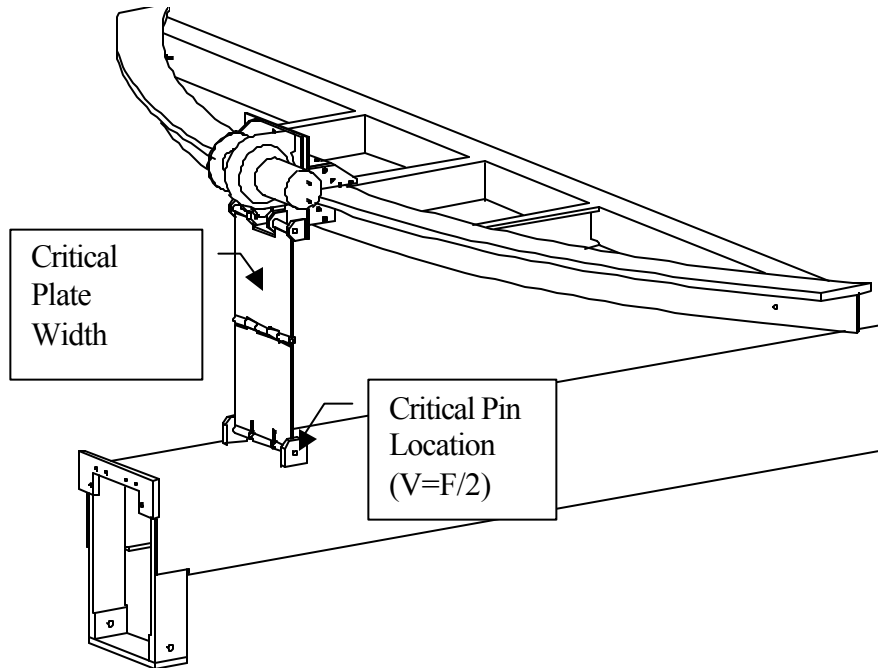
Conclusion

This value is acceptable since it is not a steady state error. Rather it represents torsional windup that will disappear as motion stops. This will represent the lag in the translation of the ball screw under acceleration and deceleration to maximum speeds. During normal operation at slower speeds, this deflection will be negligible.

Hinged Plate Analysis

Assumptions:

hinge pins are forced into direct shear through close tolerances
loading in plates in purely axial



Given Dimensions:

Plate width(nominal)-	7.0 in
Plate width at critical section-	4.5in
Plate Thickness-	0.25 in
Pin diameter-	0.375in

Maximum Loading(Axial)- 1100 lb

Calculations:

Plate Stress:

$$s = \frac{F}{A} = \frac{1100}{(4.5)(.25)} = 977 \text{ psi}$$

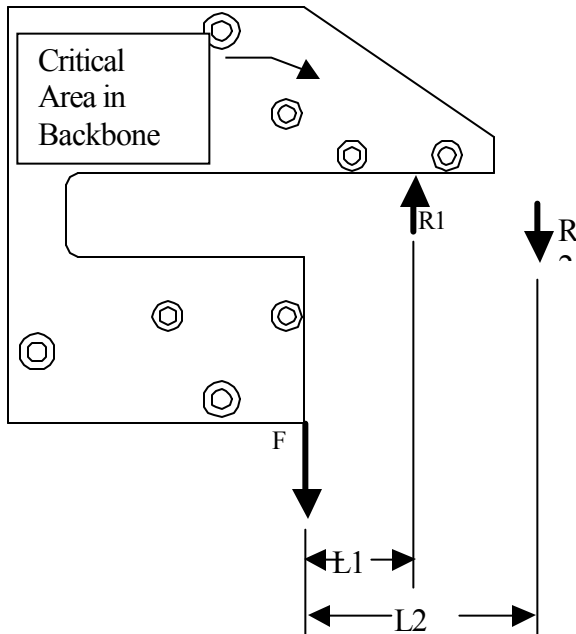
$$t_{\max} = \frac{s}{2} = \frac{S_y}{2n} \Rightarrow n \approx 64 \text{ (based on } S_y = 32\text{ksi)}$$

Pin shear:

$$t_{\max} = \frac{4V}{3A} = \frac{16(550\text{lb})}{3(\pi(0.375)^2)} = 6.6\text{ksi}$$

$$t_{\max} = 6.6\text{ksi} = \frac{S_y}{2n} \Rightarrow n = 4.8 \text{ (based on a } S_y \text{ for steel of 32ksi)}$$

Support Truck Analysis
Support Truck FBD



Given:

$$F=1100 \text{ lb}$$

$$L1=1.31 \text{ in}$$

$$L2=2.56 \text{ in}$$

$$\text{Backbone Thickness}=0.625 \text{ in}$$

$$\text{Backbone Width}=6.0 \text{ in}$$

Statics:

$$\sum M_{R2} = R1(L2 - L1) - F(L2) = 0 \Rightarrow R1 = \frac{F(L2)}{L2 - L1} = 2253 \text{ lb}$$

$$\sum F_y = R1 - R2 - F = 0 \Rightarrow R2 = R1 - F = 1153 \text{ lb}$$

Stress Analysis:

$$s = \frac{Mc}{I} = \frac{12(R1(L1 - .625))}{(6)(.625)^3} = 12.7 \text{ ksi}$$

$$t_{\max} = \frac{s}{2} = \frac{S_y}{2n} \Rightarrow n = 2.5$$

Appendix B. MATLAB Program for Camera Boom Size Selection

```

***vib.m***
%This MATLAB file calculates the weight, maximum deflection, natural
%frequency and forced vibration amplitude of the camera boom. Discussion
%of the analysis maybe found in Chapter 5 of this thesis.

clear all
close all

F=5; %end load (lb)
l=182; %total length (in)
l2=125; %cantilevered length (in)
b=3; %beam width, OD (in)
h=3; %beam height, OD (in)
t=.125; %beam wall thickness (in)
E=29*10^6; %modulus of elasticity (lb/in^2)
dns=.0088145; %beam material density (slug/in^3)
    %note: g/cm^3 * 1.12287e-3 = slug/in^3
xA=b*h-(b-2*t)*(h-2*t); %cross section area (in^2)
Wt=dns*xA*1*32.2 %total beam weight (lbf)
wl=dns*xA + 6/(32.2*1); %mass per length (slug/in)(includes chain)
w=wl*32.2; %distributed load (lb/in)
I=(b*h^3-(b-2*t)*(h-2*t)^3)/12; %moment of inertia (in^4)
I1 = I2;

%%COEFFICIENTS OF THE DEFLECTION EQUATIONS%%
%The a terms are the coefficients of x1 and x2 in the deflection equations.
%The first 'subscript' refers to deflection equation 1 or 2, and the second
%'subscript' corresponds to the power of x the coefficient multiplies.
a14 = -w/24;
a13 = -((-w*1^2 + 2*w*1*12 + 2*F*12)/(I2))/12;
a12 = 0;
a11 = -(w*1^3)/24 + (w*12*1^2)/8 - (w*1*12^2)/24 - (w*12^3)/24 + F*(1*12-12^2)/6;
a10 = 0;
a24 = -w/24;
a23 = -F/6;
a22 = 0;
a21 = -(w*1^3)/24 + (w*12*1^2)/8 + (w*1*12^2)/24 + (w*12^3)/24 + F*(2*1*12+12^2)/6;
a20 = (w*12*1^3)/24 - w*(1^2)*(12^2)/8 - (w*1*12^3)/24 - (F*1*12^2)/3;

%%MAXIMUM DEFLECTIONS - and the ratio r%%
v2max = a20/(E*I) %maximum deflection for the cantilevered section

slope1eq = [a14*4 a13*3 0 a11]; %coefficients of the slope eq for section 1
x1maxs = roots(slope1eq); %one of these roots will be the value of x1 at v1max

for i = 1:3 %this for loop determines the correct root
if 0 < x1maxs(i) < l1

```

```

x1max = x1maxs(i);
end
end

v1max = (a14*x1max^4 + a13*x1max^3 + a11*x1max)/(E*I);    %max defl of section 1 OK

r = abs(v1max/v2max);          %ratio of the maximum deflections of the two sections

%%squaring v1 and v2 and evaluating the integrals I1 and I2 in the Tmax expression%%

a1 = [a14 a13 a12 a11 a10]*(1/(E*I));    %vector of poly coeff of v1
a2 = [a24 a23 a22 a21 a20]*(1/(E*I));    %vector of poly coeff of v2

c1 = conv(a1,a1);                %vector of poly coeff of v1^2
c2 = conv(a2,a2);                %vector of poly coeff of v2^2

I1 = (c1(1)*I1^9)/9 + (c1(2)*I1^8)/8 + (c1(3)*I1^7)/7 + (c1(4)*I1^6)/6 + (c1(5)*I1^5)/5 +
(c1(6)*I1^4)/4 + (c1(7)*I1^3)/3 + (c1(8)*I1^2)/2 + (c1(9)*I1);
I2 = (c2(1)*I2^9)/9 + (c2(2)*I2^8)/8 + (c2(3)*I2^7)/7 + (c2(4)*I2^6)/6 + (c2(5)*I2^5)/5 +
(c2(6)*I2^4)/4 + (c2(7)*I2^3)/3 + (c2(8)*I2^2)/2 + (c2(9)*I2);

%%finally, the equivalent mass!!!%%
meqb = (w1*I1*r^2)/v1max^2 + (w1*I2)/v2max^2;          %equiv mass of beam (slug)
mF = F/32.2;                                          %mass of end weight (slug)
meq = meqb + mF;                                     %total equivalent mass (slug)

%%the beam stiffness%%
k = 3*E*I/(l*I2^2);                                  %the beam stiffness (lb/in)

%%the natural frequency%%
Wn = sqrt(k*I2/meq);                                  %(rad/s)
Hz = Wn/(2*pi)                                       %(hz)

%%Forced Vibration Amplitude%%
c=.291;                                               %damping value (lb*s/ft)
z=c/(2*sqrt(12*k*meq));                               %damping ratio
Fo=1;                                                 %magnitude of harmonic force (lb)
Wf=Wn*sqrt(1-2*z^2);                                 %forcing freq for max amp (rad/s)

den1=(1-(Wf/Wn)^2)^2;
den2=(2*z*Wf/Wn)^2;
amp=Fo/(k*sqrt(den1 + den2)) %maximum vibration amplitude (in)

```

Appendix C. MATLAB Program for Camera Boom Brace Location

This appendix contains two MATLAB programs. The first program is the main program, brace.m, shown on this page. The second program, deter.m, shown on the following page, is a function that is called by the main program.

```
***brace.m***

clear all
clear global
close all
global dens area I E a b
height=3;
width=3;
thick=.0625;
area=width*height-(width-2*thick)*(height-2*thick);
I=(width*height^3-(width-2*thick)*(height-2*thick)^3)/12;

l=130;           %length of beam (in)

%These are for the Fiberglass Composite beam
%E=3.15*10^6;    %modulus of elasticity (psi)
%dens=.0525/32.2; %density (slugs/in^3)
%These are for a steel beam
%E=29*10^6;     %modulus of elasticity (psi)
%dens=.0088145; %density (slugs/in^3)
%These are for an aluminum beam
E=10*10^6;     %modulus of elasticity (psi)
dens=.0030430; %density (slugs/in^3)
aa=[6 12 18 24 27 30 36 42 48 54 60];
lwrs=ones(size(aa,2));
uprs=100*ones(size(aa,2));

for ainc=1:size(aa,2)
    a=aa(1,ainc);
    b=l-a;
    lwr=lwrs(1,ainc);
    upr=uprs(1,ainc);

    ww(ainc)=fzero('deter',50);
end

figure(1)
plot(aa,ww,'+')

***deter.m***

function [detr] = deter(w)

global dens area E I a b
```

```

beta=(((dens*area)/(E*I))^0.25)*sqrt(w);
sa=sin(beta*a);
sha=sinh(beta*a);
sb=sin(beta*b);
shb=sinh(beta*b);
ca=cos(beta*a);
cha=cosh(beta*a);
cb=cos(beta*b);
chb=cosh(beta*b);

matrx=[[ (cb-chb) (sb-shb) 0 0]
        [0 0 (ca+cha) (sa+sha)]
        [(-sb-shb) (cb-chb) (sha-sa) (ca+cha)]
        [(-cb-chb) (-sb-shb) (ca-cha) (sa-sha)]];

detr=det(matrx)

```